Mononuclear Zinc(II) Complexes with Intramolecular Hydrogen Bonding Interactions: Towards More Efficient Synthetic Nucleases

A Thesis Submitted for the Degree of

Doctor of Philosophy

by

Rafael Torres Martin de Rosales

School of Chemistry
University of Edinburgh
King's Buildings
West Mains Road
Edinburgh, EH9 3JJ

January 2005

Abstract

Nucleases are important enzymes responsible for catalysing the otherwise very slow hydrolytic cleavage of phosphodiester bonds of DNA and RNA. Many of these enzymes require one or more (typically two) metal co-factors, with zinc(II) being one of the most frequently employed. In addition to the metal(s), the participation of specific second sphere active site residues in proton transfer events, substrate activation and positioning and transition state stabilisation appear to be essential, but these aspects are not fully elucidated.

A series of mononuclear zinc(II) complexes of tris-pyridylmethyl-amine (**tpa**)-based tripodal ligands containing the unit (6-NHR-2-pyridylmethyl)amine (R = CO^tBut, H, $CH_2{}^tBut$) resembling the catalytic zinc sites of nucleases have been synthesised and fully characterised. Some of these complexes were used to explore strategies to induce the hydrogen bond interactions that influence the catalytic performance of nucleases, and to investigate the factors that affect their strength. X-ray diffraction, NMR and IR studies revealed the formation of hydrogen bonding interactions between amide/amine groups and other zinc-bound ligands both in solution and in the solid state. The energies of these hydrogen bonds have been estimated by IR and VT ^1H NMR coalescence studies. From this work, it appears that metal-ligand bonding may be as important as the nature of the hydrogen bond donors and acceptors towards defining the geometry and strength of the hydrogen bond formed.

The effect of different hydrogen bonding microenvironments on structural features of trigonal bipyramidal $[(\mathbf{L})Zn(Cl)]^+$ (**L** = **tpa** derivatives) cations has been investigated. Among the implications of introducing hydrogen bonding groups is the lengthening of the axial Zn-Cl and equatorial L-Zn bonds. This structural study may facilitate future structure-function relationships. We have also investigated the effect of these hydrogen bonding microenvironments in the acidity of a zinc(II)-bound water molecule, which is a key parameter of catalytic zinc sites. Thus, from potentiometric titrations it appears that amino hydrogen bonding groups adjacent to a zinc(II)-bound water molecule enhance the acidity of this water molecule as much as 1 pK_a unit per hydrogen bonding group. The effect of hydrogen bonding groups in the affinity of phosphate esters to zinc(II) complexes was also investigated. It has been established that hydrogen bonding increases the affinity of phosphates to zinc(II) centres in neutral aqueous solution.

The results presented in this work provide important insights into the possible role(s) of the active site microenvironment in modulating the zinc(II)-promoted hydrolysis of nucleic acids and may contribute to the development of more efficient synthetic nucleases.

To Esther

Acknowledgements

I wish to express my sincere gratitude and appreciation to my supervisor Dr. Juan Mareque for his guidance, understanding, patience and specially for giving me the opportunity of pursuing doctoral studies in this interesting field. His enthusiasm and dedication to chemistry has been a great source of motivation for the completion of this thesis and my future career in research.

I also wish to thank Dr. Eduardo Cabrera and Dr. Jose Antonio Giménez, from the University of Granada, Spain. Without their advice and support during my undergraduate studies, I would have never got that far.

I would also like to thank all the members of Mareque's group, past and present. Above all Emiliano Salvagni and Laurent Metteau, my labmates and friends, for the good times inside and outside the lab. My gratitude also goes to Dr. Ravi Prabaharan for the potentiometric titrations included in this thesis.

I also want to thank the people who made the inorganic corridor a friendly environment to work, especially my friends Michele Melchionna, Alejandro Sánchez Perucha, Dr. Pedro Pinho and Dr. Robert Pfeifer. I would also like to extend my gratitude to the School of Chemistry for financial support during these years and to all the technical staff. In particular, Mr. John Millar from the NMR services for his help when things went wrong with the spectrometer and enjoyable conversations.

I also wish to thank Esther, my other half, who contributed with her wonderful smile and endless love among many other things.

Finally, I am extremely grateful to my parents, Juan Miguel and María Paz, for their unconditional support and love and for giving me and my brother and sister the best education possible.

Declaration

I hereby declare that, except where specific reference is made to other sources, the work contained in this thesis is the original work of my own research since the registration of the PhD degree in October 2001, and any collaboration has been clearly indicated. This thesis has been composed by myself and has not been submitted, in whole or part, for any other degree, diploma or other qualification.

Abbreviations

AIBN	2,2'-azobis(2-methyl-propionitrile)
AMP	adenosine monophosphate
AP	alkaline phosphatase
ApA	adenylyl(3'-5')phosphoadenine
BNPP	bis(4-nitrophenyl)phosphate
CA	carbonic anhydrase
ca.	circa
CCDC	Cambridge Crystallographic Data Centre
CPA	carboxypeptidase A
CSD	Cambridge Structural Database
DBP	dibenzyl phosphate
DCM	dichloromethane
DMF	dimethylformamide
DMSO	dimethylsulfoxide
DNA	deoxyribonucleic acid
ENPP	ethyl(4-nitrophenyl)phosphate
ESI-MS	electrospray ionisation mass spectroscopy
et al.	and others
FT	Fourier transform
h	Planck´s constant
HEPES	4-(2-hydroxyethyl)-1-piperazineethanesulfonic acid
HPLC	high performance liquid chromatography
HPNP	2-hydroxypropyl(4-nitrophenyl)phosphate
HSAB	hard and soft acid-base theory
i. e.	that is
IR	infrared
IUBMB	International Union of Biochemistry & Molecular Biology
L	ligand
N	Avogadro´s number
NBS	*N*-bromosuccinimide
NMR	nuclear magnetic resonance
NPP	*p*-nitrophenyl phosphate
PP	phenyl phosphate
R	universal gas constant
RNA	ribonucleic acid
SN	staphylococcal nuclease
T_c	coalescence temperature
tpa	tris-pyridylmethyl-amine
TS	transition state
vide infra	see below
vide supra	see above
vs.	in contrast to
VT	variable temperature

Table of Contents

Chapter 1. Introduction

1.1 Introduction and thesis outline

An important area of bio-mimetic chemistry is the study of synthetic analogues of important bio-molecules such as enzymes. This thesis work is concerned with the chemistry of nucleases, which are hydrolytic enzymes responsible of cleaving phosphodiester bonds of nucleic acids. This task is essential for nucleic acid modification/repair.

The aim of this thesis work is to mimic the structure and function of nucleases with a view to better understanding their catalytic mechanisms. These enzyme mimics could also be of great utility and importance for their potential medicinal and biotechnological applications.[1]

Nucleases achieve highly efficient catalysis by cooperation of metal ions and functional amino acid side chains at the active site. The focus of this thesis work is set in elucidating the ways in which these amino acid residues present in the active site, but not directly bound to the metal, participate in the catalytic activity of nucleases. At present, this important mechanistic aspect is not fully understood and more work is required. By synthesising carefully chosen ligands, binding them to zinc and reacting these complexes with suitable substrates, it should be possible to gain an insight into the roles of several of the interactions between the nucleic acids and the active site of nucleases.

First, a brief introduction about enzyme catalysis will be provided along with an overview of the roles of zinc in biocatalysis. Secondly, a concise summary of the most relevant work that has been done so far to elucidate the structures and mechanisms of some nucleases will be provided. This will illustrate why this study is relevant. Finally, the work during my PhD will be discussed.

1.2 Enzyme catalysis

Enzymes are macromolecules that catalyse most biochemical reactions with great efficiency and high chemical and chiral selectivity, and they are capable of enhancing reaction rates by several billion times.[2, 3]

Most enzymes are large proteins, but it is in a smaller region, known as the active site where the substrate is bound and converted to the product. Enzymes derive their catalytic activity from the precise three-dimensional structure of the entire protein, but when considering the mechanism of catalysis it is often useful to focus on the active site.

1.2.1 Enzymes and biocatalysis

Enzymes enhance reaction rates by binding, and thus stabilising, selectively the transition state.[4] This gives an alternative reaction pathway with lower activation energy.

Figure 1.1 shows an energy profile diagram and illustrates the relative activation energies of a catalysed and un-catalysed reaction.[5] The two transition states of interest for the un-catalysed and catalysed reactions are represented by $TS_{(uncat)}$ and $TS_{(cat)}$, respectively. As mentioned before, binding of the enzyme to the TS lowers its free energy by binding more strongly the transition state (TS) than to the substrate (S). Since binding of the enzyme to the substrate ($\Delta G^{o}_{(S)}$) is smaller than $\Delta G^{o}_{(TS)}$, the activation energy of the catalysed reaction ($\Delta G^{+}_{(cat)}$) is smaller than for the uncatalysed reaction.

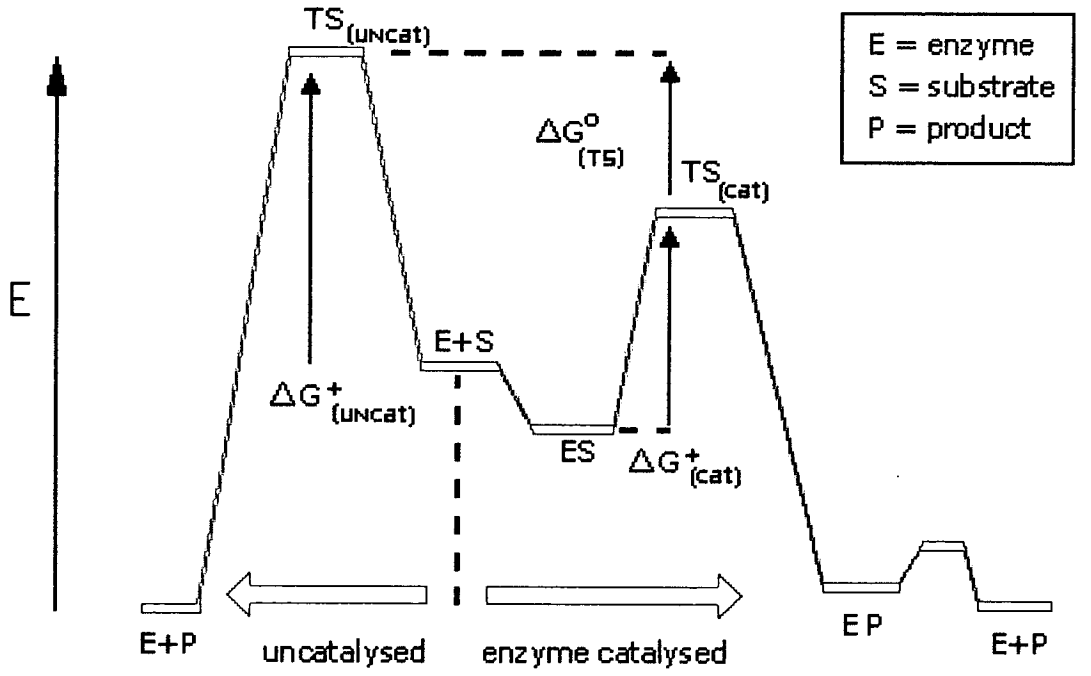

Fig. 1.1 *Energy profile diagram for a catalysed (red) and uncatalysed (blue) reaction.*

Early studies on enzyme mechanisms led to the suggestion that the enzyme active site and substrate fit together due to their complimentary molecular surfaces.

This analogy is known as the 'lock and key' theory. This analogy could, however, lead to misunderstandings, as an enzyme tightly bound to a substrate would not facilitate its transformation to products. Thus, some interactions must take place only when the transition state is reached resulting in a stronger binding. This is known as the 'Induced Fit Theory' and was originally postulated by Daniel Koshland in 1958.[3] Thus, enzymes are able to lower the activation energy of a given reaction through precise fitting of the substrate/transition state and the active site of the enzyme (Figure 1.2).

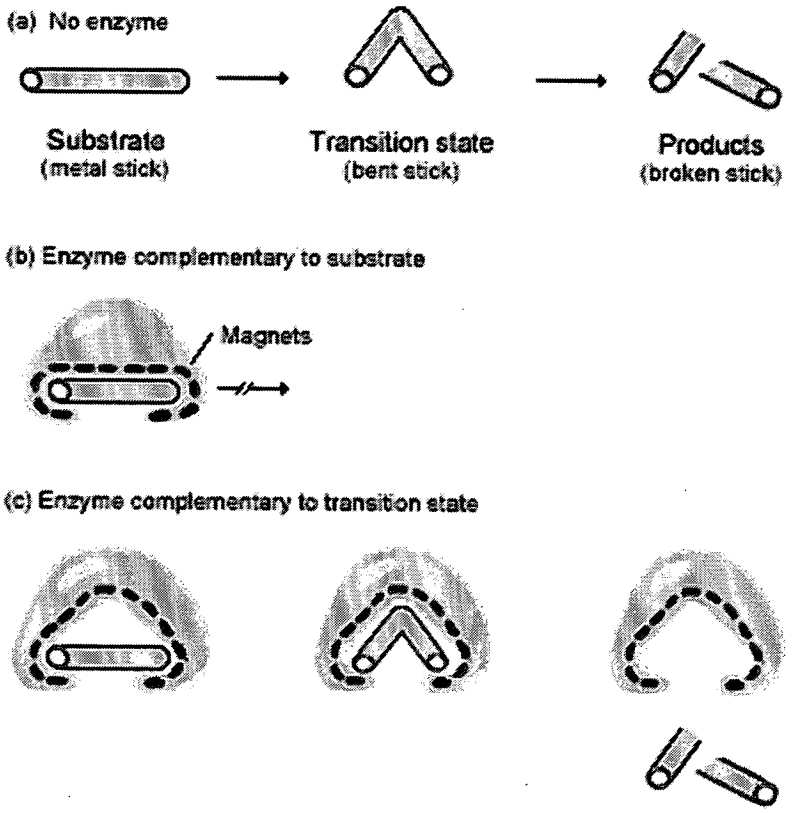

Fig. 1.2 *Schematic representation of the 'induced fit theory' of enzyme catalysis.*

Several specific strategies for achieving the preferential binding of the enzyme to the TS over the ground state (GS) have been proposed:[6]

1) Increased chemical contacts to the transition state

S_N1 reactions are known to proceed faster in high dielectric solvents, presumably due to better solvation of the charged transition states and intermediates. Likewise, enzymes and artificial enzymes preorganise and converge hydrogen bonding groups, point charges, dipoles, and hydrophobic groups to best solvate and stabilise the transition state and high-energy intermediates.

2) Introduction of strain into the substrate

The introduction of strain into a substrate upon binding is often cited as a way of lowering the energy of activation of a reaction.[4] Upon binding to a substrate, a conformational or electronic strain toward the structure is introduced because the cavity fits best the shape of the TS.

3) *Reducing the kinetic order of a reaction*

In second-order processes, such as the collision of two molecules to yield products, it is required the loss of translational and rotational entropy upon achieving the transition state. Since the transition state has partially the translational and rotational entropy of the product, any catalyst that binds the product better than the

two separate substrates should increase the rate of reaction, as the TS has product character.[7] This strategy, however, can be plagued by severe product inhibition.

4) Proximity of functional groups

In any natural or artificial catalyst, molecular recognition contacts and catalytic functional groups are used to bind the substrate and facilitate a chemical transformation. Presumably, all the individual catalytic functional groups, if free in solution, could perform the same catalysis on the condition that all these groups achieve the correct spatial conformation in solution.

1.2.2 Hydrogen bonding

As mentioned above, enzymes need to bind strongly the transition state of the reaction to achieve catalysis.[8] Therefore bonding between the enzyme and the substrate is very important in biocatalysis. It must have two characteristics, it must be strong enough to recognise the substrate and, at the same time weak enough to allow rapid release of the product. This might sound contradictory, but natural enzymes achieve this difficult balance by providing functional groups for ionic, hydrogen bonding, and hydrophobic interactions. Of these, hydrogen bonding is arguably one of the most important types of interactions in Nature.

A hydrogen bond (D-H···A) is commonly described as the interaction of a hydrogen atom covalently bonded to an electron rich atom (D, hydrogen bond donor) with another electron rich atom (A, hydrogen bond acceptor). However, since it was first described by Linus Pauling in his paper on the nature of the chemical bond,[9] the hydrogen bond concept has proven to be more complex. For example, although the hydrogen bond donor (D) is usually an electronegative atom (N, O, S or halide) it has been shown that C or even metals can act as hydrogen bond donors resulting in C-H···A and M-H···A bonds respectively.[10-15] Similarly, the hydrogen bond acceptor (A) does not necessarily needs to be a electronegative main group element bearing a lone pair. For example, areas of excess electron density of an aromatic ring or a multiple bond and even metals can also be hydrogen bond acceptors.[16-21]

Thus, a hydrogen bond is probably best described as a bond between an electron-poor hydrogen and a region of electron density. A common feature of all types of hydrogen bonds is the weakening of the D-H bond, which is reflected in a decrease of the D-H stretch vibration frequency. This characteristic makes IR spectroscopy a suitable technique to study hydrogen bonding.

Hydrogen bonds are much weaker than covalent bonds but are the strongest of the non-covalent interactions, with strengths ranging from 5-20 kJ/mol. Unlike other intermolecular forces these bonds are directional, so multiple hydrogen bonds can be aligned in such a way to complement each other. This is often the case in enzyme active sites and results in the weaker binding of a 'less complementary' substrate than the 'more complementary' transition state.

As well as hydrogen bonding sites offered by amino acid residues, many enzymes contain a metal ion at the active site. This metal cofactor often binds directly to the substrate and is essential for catalysis. Nature utilises several metals in biocatalysis, some of the most common ones include iron, copper, manganese. In this discussion, however, only the role of zinc in biology will be considered.

1.3 The role of zinc in biology

Until recently, very little research had been carried out to investigate biological roles of zinc. This limited research on zinc was in part due to its 'invisibility' to most spectroscopic techniques. In fact, just 9 years ago zinc did not have an element-related section among less abundant metals in biology at the seventh International Conference on Bioinorganic Chemistry (ICBIC'95) in Lübeck, Germany.[22] Zinc has even been referred to as a 'boring element'.[23]

But the truth is that zinc is the second most abundant transition metal in biology and is essential in all forms of life, from bacteria to humans.[22, 24-28] In humans, the adult body contains about 1.5 to 2.5 grams of zinc and it is present in all organs, tissues, fluids and secretions.[27] Physiologically, zinc is vital for many biological processes such as sexual maturation and reproduction, growth and development, dark vision adaptation, olfactory and gustatory activity, insulin storage and release and for a variety of host immune defences. Moreover, it is now known

that zinc enzymes monitor the replication, transcription and translation of the genetic code of all species.[24, 29]

Over 95% of total body zinc is bound to proteins within cells and cell membranes. To support this, just to mention that more than three hundred enzymes are now known to contain at least one atom of zinc and that zinc is the only metal that is essential in the six enzyme classes established by the International Union of Biochemistry & Molecular Biology (IUBMB).[30]

In these enzymes the role of zinc can be divided into four categories: non-catalytic, structural, regulatory and catalytic:[29]

Non-catalytic: In certain metalloenzymes, a fraction of zinc is neither involved in catalysis nor essential for the maintenance of the tertiary structure of the enzyme. In those cases zinc is said to play a non-catalytic role.

Structural: Zinc plays a structural role when it is required solely for the structural stability of the enzyme, being necessary for activity only to the extent that the overall conformation of the enzyme affects its action. A structural zinc(II) ion is also found in non-enzyme proteins such as the zinc fingers and metallothioneins.[22]

Regulatory: If an enzyme is able to catalyse a reaction without zinc, but the presence of zinc either enhances or inhibits the enzymatic activity then zinc is

considered to have a regulatory role. Regulatory zinc may then act as an activator or as an inhibitor.

Catalytic: Zinc is said to have a catalytic role when it is essential for and is directly involved in catalysis by the enzyme. Its removal leads to a total loss of enzymatic activity.

A given metalloenzyme may contain multiple numbers and types of zinc atoms and these may play different roles. Of these four categories, however, only the catalytic role of zinc will be examined more closely in this discussion. There are several physical and chemical properties of zinc that make zinc an attractive element and extremely useful in catalysis.

1.3.1 Physical properties of zinc relevant to catalysis

There are five areas to consider when discussing the usefulness of a transition metal as an enzyme cofactor: redox activity, coordination geometry, binding properties, ligand exchange and Lewis acidity.

Redox activity: Zinc exists as a divalent cation in all enzymes. Zinc(II) has a d^{10} electron configuration and consequently does not take part in any process that involves electron transfer. The diamagnetism of zinc(II) represents a major

advantage when studying reaction mechanisms, as they can be studied in great detail by NMR.

Coordination geometry: The coordination number of zinc has been analysed on the basis of crystal structures of small molecules and can vary between four and six.[31] The filled d-shell of zinc indicates that zinc complexes are not subject to ligand field stabilisation effects and so the coordination number and geometry adopted is largely dictated by ligand size and charge.[32-34]

The coordination geometry of catalytic zinc is highly distorted and can fluctuate and have unusual bond lengths and odd number of ligands. This situation of energetic stress at the active site has been termed with the Greek word *entasis,* meaning tension.[35] As a result, the zinc centre is considered to be energetically primed for catalytic activity.

Binding properties: Zinc is a borderline acid according to Pearson's hard and soft acid-base (HSAB) theory and therefore shows great affinity and can accommodate elements like nitrogen, oxygen and sulphur atoms in its coordination polyhedron.[36, 37] Hence, zinc binds strongly to many proteins.[38]

Ligand exchange: Fast ligand exchange is essential for high turnover rates in catalysis. The flexibility in coordination geometry of zinc complexes makes ligand exchange more facile than for Ni(II) or Mg(II), thus enhancing the ability of zinc to effect a catalytic cycle.

Lewis acidity: Zinc(II) is a good Lewis acid. Many of the important roles of zinc in enzyme catalysis involve the activation of water as a nucleophile. This activation results from the ability of zinc(II) ions to lower the pK_a of a bound water molecule from 14 to as low as 7. Only Mn(II), Fe(III), and Cu(II) are better in this regard, but these ions are redox active and could be involved in unwanted electron transfer reactions.[39] Zinc(II) can also activate electrophiles such as carboxy- and phosphoesters, making the carbon and phosphorus centres even more electrophilic and hence more susceptible to nucleophilic attack.

1.3.2 Proposed mechanisms for zinc-mediated enzyme catalysis

Despite intensive research, the precise mode of action of zinc is still not fully understood.[24] In this regard, enzyme mimics have been very helpful (*vide infra*). Two types of mechanisms are thought to account for the way in which zinc directs catalysis: the *zinc-substrate mechanism* and the *zinc-hydroxide mechanism.*

In the *zinc-substrate mechanism*, it is proposed that the substrate binds directly to zinc and displaces the metal-bound H_2O molecule. In this process, the zinc acts as a Lewis acid activating the substrate, thereby facilitating nucleophilic attack. According to this hypothesis, the function of zinc is to activate the electrophile.

In the *zinc-hydroxide mechanism,* the substrate does not bind directly to the metal and zinc mediates its function through the metal-bound water molecule. In this case, zinc exerts its catalytic role by lowering the pK_a of the bound-water molecule from ~ 14 to as low as ~ 7. The resulting metal-bound hydroxide is then believed to act as the nucleophile. Thus, the function of zinc is then to activate the nucleophile.

These two mechanisms do not need to be mutually exclusive, as it is believed that in some enzymes these two mechanisms operate together. In this third case, the substrate binds to the metal but does not displace the metal-bound water molecule. As a result, substrate and nucleophile are simultaneously coordinated to the zinc centre. The function of zinc in this case is to polarise the substrate and the water molecule and to arrange them in close proximity.

Now that an overview of the catalytic role of zinc within enzymes has been provided, the discussion will be focused on metallonucleases, the class of enzymes concerned with this thesis work.

1.4 Nucleases

1.4.1 Roles of nucleases

The human genome consists of 23 chromosomes and approximately three billion base pairs of deoxyribonucleic acid (DNA).[40] In this DNA are coded 100,000 genes, of which most are transcribed into messenger ribonucleic acid (mRNA) before

the corresponding protein can be synthesised. The relevance of these linkages is obvious if we take into account the importance of maintaining the integrity of the genetic code. The truth is that Nature could hardly devise more suitable links than phosphodiester bonds to join nucleosides in RNA and DNA.[41]

In terms of kinetic stability, these bonds are extremely stable due to the repulsion between the negatively charged backbone and any potential nucleophiles.[41] Half lives are estimated to be 200 million years for DNA[42] and 100 years for RNA[43] at pH 7 and 25°C. The higher reactivity of RNA compared with DNA is due to the presence of the ribose 2'-OH group, which acts as an intramolecular nucleophile.

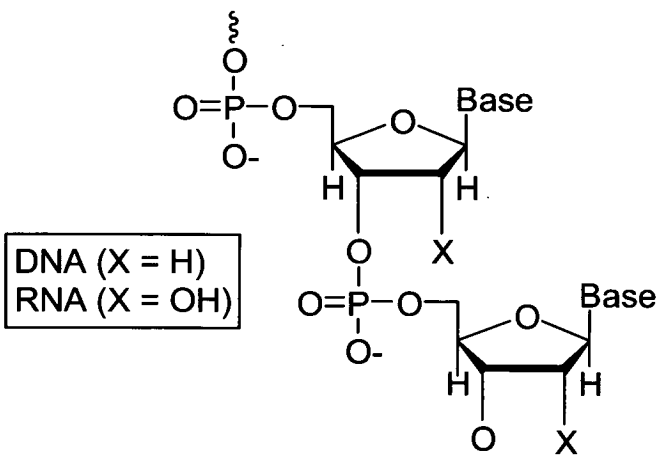

Fig. 1.3 *Structure of nucleic acids.*

This remarkable kinetic stability, however, can also be a problem. Mutations of DNA can occur, and these need to be repaired. Also, foreign DNA and proteins need to be destroyed. A single mutation in any one of these genes, loss of the mRNA, or degradation of an essential protein could potentially lead to serious consequences. To perform this task Nature has developed a class of enzymes called nucleases.

Nucleases are hydrolytic enzymes that cleave the phosphodiester bonds of DNA and RNA backbones. These enzymes commonly achieve highly efficient catalysis by active site cooperation of metal ions, typically zinc, and functional amino acid side chains.

1.4.2 Mechanisms of nucleases

Metal ions and functional groups in nucleases can promote hydrolytic cleavage of phosphodiester bonds in one or several of the following ways:

- Electrostatic activation of the substrate (ground state effect) or stabilisation of the transition state by metal ion coordination, hydrogen bonding and/or proton transfer.

- Nucleophilic attack on the substrate by a functional group or by a metal-coordinated hydroxide, which are generated by Lewis-acid activation of a metal-coordinated water molecule.

We are interested in elucidating the importance of the cooperative mechanisms between zinc ions and second sphere residues in the efficiency of nucleases, the reason being that several of these enzymes contain active sites with second sphere amino acid side chains that seem be implicated in catalysis. Three examples of metallonucleases are briefly discussed below.

Nuclease S1 is an important trinuclear Zn(II) enzyme present in *Aspergillus oryzae.*[44] The proposed mechanism[45] involves the interaction of a Zn(II) ion and a Lys-ammonium group with the phosphodiester group, facilitating the attack of a nucleophile, possibly a carboxylate group of a Glu residue (Scheme 1.1). The mixed anhydride is then cleaved by a Zn(II)-coordinated hydroxide, yielding a phosphate monoester and regenerating the carboxylate group.

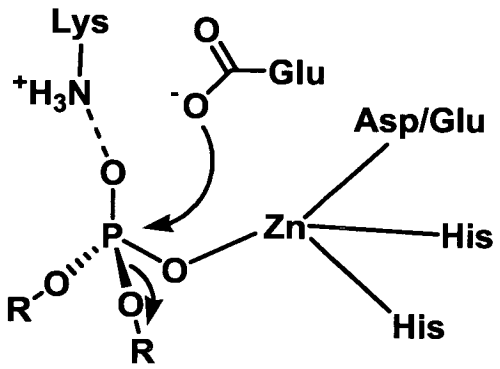

Scheme 1.1 *Proposed mechanism of Nuclease S1.*[45]

Alkaline phosphatase (AP) contains two Zn(II) ions with different coordination environments. This enzyme hydrolyses phosphate monoesters by using the two cooperative Zn(II) ions and specific second sphere amino acid residues (Scheme 1.2). Two of these residues are Ser-102 and Arg-166. Thus, it is now considered that the phosphate ester, coordinated by the zinc(II) ions, is initially attacked by the deprotonated serine to give a phosphoserine intermediate, which is subsequently attacked by an adjacent Zn-OH. The guanidinium group of Arg-166 is hydrogen bonded to the phosphoserine intermediate. Thus, Arg-166 could contribute

to the activation of the P-centre or be involved in proton transfer to the leaving group.

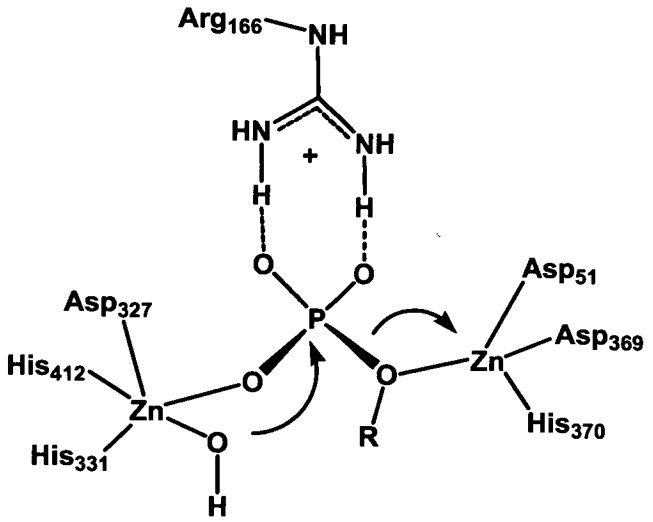

Scheme 1.2 *Proposed mechanism of alkaline phosphatase.*

Staphylococcal nuclease (SN) cleaves the phosphodiester backbone of DNA and RNA to yield 3'-mononucleotides. It is a digestive enzyme without sequence specificity but with enormous catalytic efficiency. Thus, DNA hydrolysis by SN is accelerated 10^{16}-fold compared to the uncatalysed reaction. This is probably the highest rate enhancement for enzymatic phosphodiester cleavage.

The structure of the active site of SN with a bound nucleotide 3'-5'-diphosphate has been obtained by X-ray crystallography.[46] In terms of the mechanism of hydrolysis of SN, there is evidence to suggest that the phosphodiester group is activated for nucleophilic attack by coordination to the M^{2+} (M = Ca, Cd) ion and perhaps even hydrogen bonding to the guanidinium group of Arg-35[47, 48] (Scheme 1.3). The nucleophile seems to be either a calcium-bound or a free water

molecule, which is deprotonated by a carboxylate group of Glu-43. A second guanidinium group belonging to Arg-87 could be responsible for stabilising the trigonal-bipyramidal transition state (Scheme 1.3).

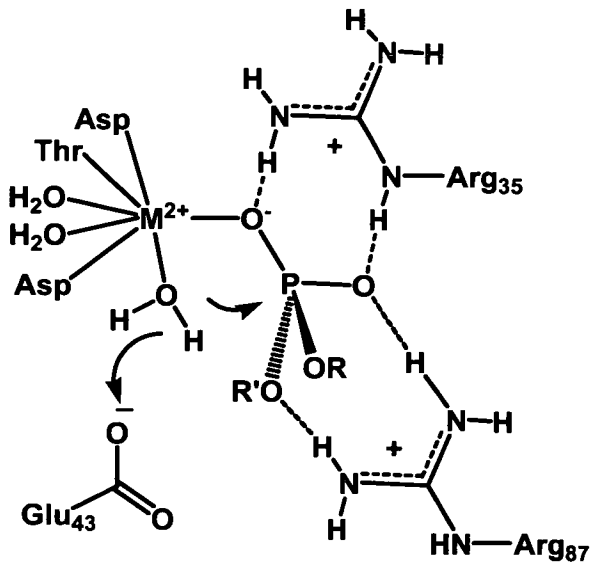

Scheme 1.3 *Proposed mechanism of Staphylococcal nuclease.*[47-48]

A common feature of these three different types of metallonucleases is neither the metal nor their first coordination sphere, but the believed functionally-important participation of second coordination sphere amino acid residues.

1.5 Synthetic models of nucleases

By synthesising complexes that mimic the active site of an enzyme and studying their chemistry, it has been proven possible to gain new insights into the mechanisms of enzyme catalysis.[47-49] Thus, an alternative approach to investigate

enzyme mechanisms is to model the active site using carefully chosen synthetic analogues. Another potential application of a synthetic nuclease would be as an artificial site-specific restriction enzyme.[8] In that respect, it would be very useful to build an artificial restriction enzyme that, while retaining the efficiency of natural nucleases towards phosphate ester cleavage, it has sequence specificity. Such molecule would allow molecular biologists to cut DNA at sites perhaps not recognised by current restriction enzymes.[49]

In this section the main focus will be on briefly reviewing transition metal-based artificial nucleases, specially Zn(II) complexes, and 'organic' hydrogen bonding supramolecular systems for phosphate ester hydrolysis. However, it is important to mention that lanthanide(III) complexes and ions have also proven extraordinarily effective at promoting the hydrolysis of phosphodiesters; although with somewhat less well-understood mechanisms. Despite some disadvantages, such as toxicity and relatively poorly understood coordination chemistry which makes mechanistic studies more challenging, the exploitation of lanthanides in synthetic nucleases appears quite promising. Important contributions in this area can be found in recent reports from Morrow *et al.*,[50-52], Scheineder *et al.*,[53, 54] Gunnlaugsson *et al.*,[55, 56] and Chin *et al.*[57].

1.5.1 Modelling the active site of zinc nucleases

There are several challenges associated with modelling the active site of a zinc enzyme. The same properties of zinc that make it useful in biocatalysis, such as

its intermediate hardness and fast ligand exchange, make it difficult to synthesise stable synthetic analogues of the active site. Furthermore, whereas *pseudo*-tetrahedral coordination geometry is prevalent in zinc enzymes, higher coordination numbers are common for simple zinc complexes in both the solid state and solution. A rational approach to minimise these problems involves the use of carefully designed poly-dentate ligands. In terms of the nature of the coordinating groups, the most common first coordination sphere amino acid residue in the active site of zinc(II) nucleases and hydrolases is histidine (*vide supra*), hence ligands that provide nitrogen donors should be particularly appropriate.

The presence of second sphere hydrogen bonding interactions to metal bound substrates in the active site in nucleases is also common. This represents perhaps the most challenging problem, and until very recently it has been largely neglected. The zinc(II) ion(s) must be firmly bound within a suitable primary co-ordination sphere and there must be also other groups attached to the ligand framework to mimic the secondary sphere hydrogen bonding groups (Scheme 1.4). These must be positioned in such a way as to avoid metal coordination and to interact with the substrate in a similar way as the second sphere amino acid residues do in the active sites of nucleases. For this, properly functionalised rigid poly-dentate ligands are most suitable. This is the approach used in this thesis for the construction of more precise synthetic models of zinc enzymes, and more efficient synthetic nucleases.

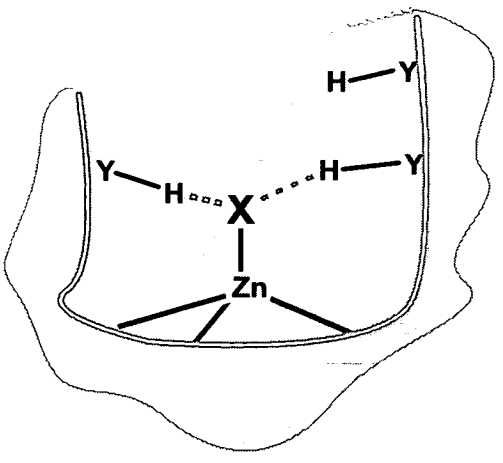

Y = N, O; **X** = H_2O, OH, substrate

Scheme 1.4

Another important aspect regarding the modelling of nucleases has to do with the selection of a suitable substrate to carry out the functional studies. The natural substrates of nuclease enzymes, RNA and in particular DNA are very resistant to hydrolysis. Therefore, most model studies use *p*-nitrophenyl esters, which are far more reactive (Figure 1.4).

Whereas ethyl(4-nitrophenyl)phosphate (**ENPP**) and bis(4-nitrophenyl)phosphate (**BNPP**) are reactive models for DNA hydrolysis, 2-hydroxypropyl(4-nitrophenyl)phosphate (**HPNP**) is used as a model for RNA hydrolysis. In addition to their reactivity, hydrolysis of these species affords *p*-nitrophenol, the conjugate base of which, *p*-nitrophenolate, absorbs intensely at 400 nm. Hence, the kinetics of hydrolysis can be conveniently monitored. The kinetics of hydrolysis is often investigated under different conditions including, pH, temperature and ionic strength. ^{31}P NMR and HPLC are commonly used for product analysis.

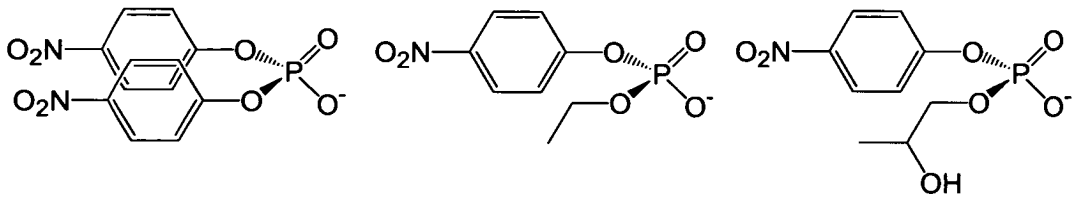

Fig. 1.4 *Activated nucleic acids analogues.*

1.5.2 Relevant synthetic modelling work

1.5.2.1 Transition metal-based synthetic nucleases

The development of transition metal-based synthetic nucleases has been attracting much attention recently. However, there is not a unified general strategy to create effective metal complexes for phosphate ester hydrolysis. The three main strategies used so far are discussed below.

- Monometallic models:

Some of the most active enzymes in Nature are metalloenzymes containing only one catalytic metal in the active site,[2] therefore many synthetic models of nucleases are monometallic complexes and have provided fundamental information about the role of metal ions in nucleases.

Important mechanistic studies of metal-promoted hydrolysis of activated phosphodiesters have been carried out using substitutionally inert complexes. In a

series of very interesting studies in the late 1980s using monometallic LM(III) complexes (M = Ir, Co; L = polydentade amine *eg.* en, tren, etc.) it was proposed that following substrate binding to the metal centre, the phosphodiester is attacked by a metal-coordinated hydroxide, generated from deprotonation of the metal-bound water molecule.[42, 58, 59] These mechanistic studies together with the information gained with natural nucleases provided further evidence of the important roles of the catalytic metal in the active site of nucleases by activation of the substrate towards nucleophilic attack and/or activation of the nucleophile.

However, it is well recognised that the use of strong Lewis acids like Cu(II) and Zn(II) has a number of advantages, importantly biological relevance. Most of the mechanistic studies on phosphodiester hydrolysis by biologically relevant labile metals have been carried out using LCu(II) complexes (L = bipy, terpy and derivatives and macrocyclic polyamines) and important contributors include Burstyn *et al.*[60-64]and Chin *et al.* [65, 66]. Meticulous studies, however, have also shown that mononuclear zinc(II) complexes promote hydrolysis of phosphodiesters. These studies were mainly carried out using LZn(II) complexes (L = macrocyclic polyamines and tris(pyrazolyl)hydroborates) by Kimura *et al.*[67-69], Kitajima *et al.*[70] and Vahrenkamp *et al.*. [71, 72]

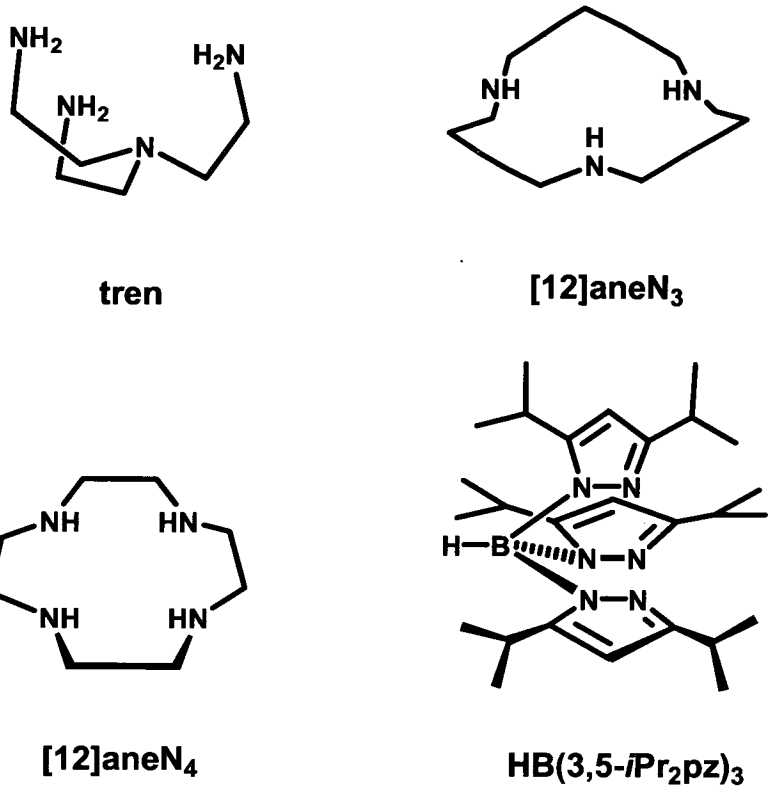

Fig. 1.5 *Illustration of some of the most commonly used ligands for hydrolysis of phosphodiesters.*

Interestingly, using a series of zinc(II) complexes with macrocyclic polyamines offering different numbers of nitrogen donors Kimura *et al.*[73] demonstrated that the Lewis acidity of the Zn(II) atom is related to the rate of hydrolysis of phosphodiesters and that the mechanism involves a metal-bound hydroxide as the nucleophile. Thus, the tridentate complex $Zn[12]aneN_3^{2+}$ was significantly more active than the tetradentate complex $Zn[12]aneN_4^{2+}$ and correlates with the lower pK_a value of the metal-bound water molecule in $Zn[12]aneN_3^{2+}$. Similarly, in a recent study it was reported that there is a correlation between the pK_a value of the metal-bound water molecule and the rate constant for cleavage of HPNP at optimal pH for a series of mononuclear Zn(II) complexes of polydentate and macrocyclic amines.[74] The authors show that the lower the pK_a value for the metal

bound water molecule the most active the catalyst is, in agreement with Kimura's work, and highlighting the important effect that the first coordination sphere has on the hydrolytic cleavage of phosphodiesters. There are, however, disadvantages and/or deficiencies associated with the use of some of these ligands, these include insuficient stability and water solubility.

- Cooperation of multiple metals:

A number of multimetallic complexes,[75-80] have been made to mimic the active sites of alkaline phosphatase (*vide supra*), kidney bean purple acid phosphatase (a dinuclear Zn(II)/Fe(III) enzyme) and nuclease P1 (a trinuclear zinc(II) enzyme) among others.[81, 82] These complexes generally show faster rates of phosphate ester hydrolysis than their corresponding mononuclear counterparts, presumably due to cooperativity between the metals towards activation of nucleophile and/or substrate species. Moreover, multiple metals could also help in the stabilisation of the highly negative transition state (a pentacoordinated phosphorus) and the release of the leaving group.

It has been shown that the best bimetallic artificial catalysts are those in which the metals are separated by a distance near to that of bimetallic enzymes, which is *ca.* 4 Å. To achieve this metal-metal distance is a difficult part in the design as they will tend to repel each other. A suitable strategy is to incorporate a bridging ligand between the metal centres such as phenolates and alkoxides (Fig. 1.6(a-d)). These groups will draw the metals together in an optimal orientation for cooperative

catalysis and have the advantage that one can predict the distances between the metals. Alternatively, the phosphate ester could also act as the bridging ligand.[83] Another approach, recently reported by Anslyn *et al.*[84] is to use steric gearing strategies to maintain the two metals in close proximity (Fig. 1.6(e)).

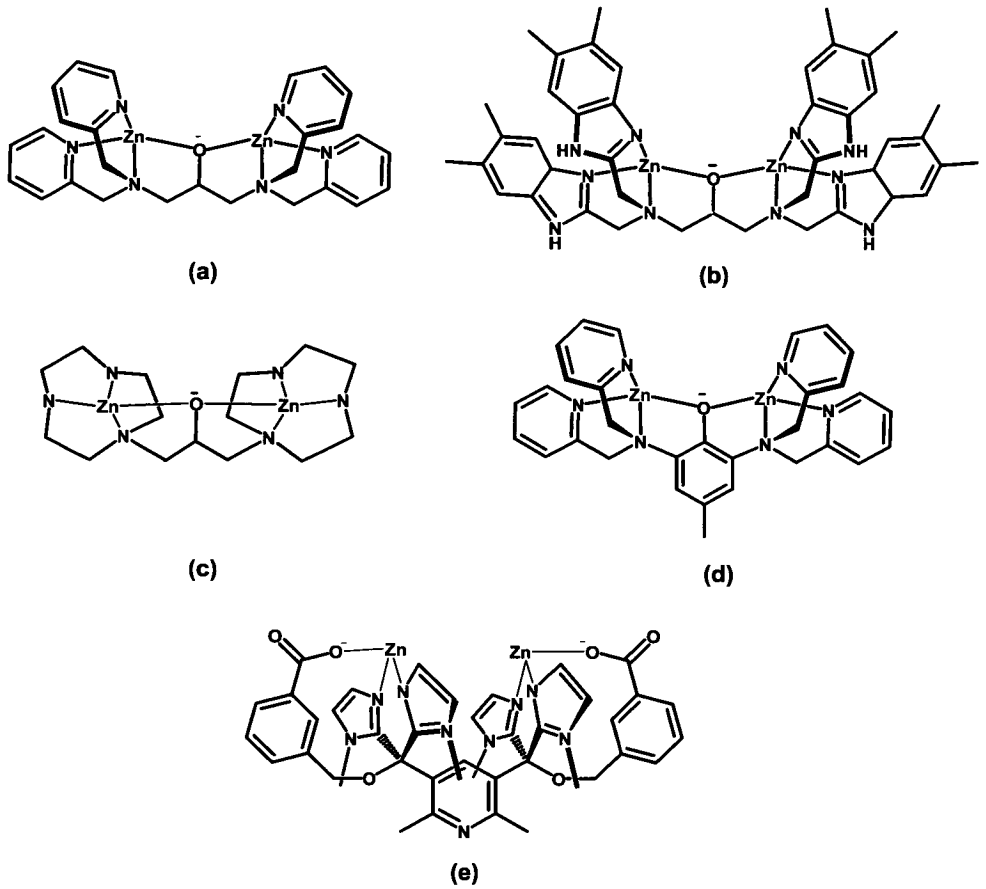

Fig. 1.6. *Illustration of some bimetallic zinc complexes that hydrolyse phosphodiesters.*[84-88]

Rate ratios (rate enhancements provided by the catalysts, k_{cat}/k_{uncat}) by these multimetallic catalysts for the cleavage of activated phosphodiesters such as HPNP have been reported.[85] For example, the dinuclear Zn(II) complex shown in Figure 1.6(b) is able to hydrolyse HPNP with a rate ratio of 3.9×10^4 in aqueous solution and physiological conditions.[86] A detailed kinetic study of the hydrolysis of HPNP at

neutral pH by the compound shown in Fig. 6(c) in comparison to a related mononuclear complex Zn(**LOH**) (below) was reported by Morrow *et al.*[87] This study suggested that the higher 1.2 x 10^5-fold acceleration achieved by the dinuclear catalyst compared to 3.4 x 10^3-fold acceleration by the mononuclear catalyst at neutral pH was due to the lowering of the pK_a of the metal-bound water, an enhancement in substrate binding and additional transition state stabilisation. Similarly, the compound shown in Figure 6(e) exhibits a 80-fold rate enhancement compared with a mononuclear complex for the cleavage of HPNP.[84]

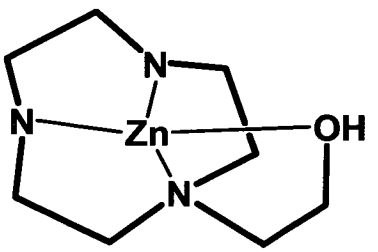

Zn(LOH)

Some of these compounds are also able to hydrolyse diribonucleotides. For example, the dinuclear Zn(II) complex shown in Fig. 1.6(a) has been reported to hydrolyse the RNA dimer adenylyl (3'-5')phosphoadenine (ApA) with rate enhancements of *ca.* 7 x 10^3 in water and 50 °C.[88]

One of the most active catalysts that make use of the cooperation between two metals was reported by Chin *et al.*[89] The dinuclear Cu(II) complex (Figure 1.7) reported hydrolyses ApA and 2'-3'-cyclic adenosine monophosphate (2'-3'-cAMP) with rate enhancements as high as 10^5 (at 50 °C) and 10^8 (at 25 °C), respectively, over the uncatalysed reaction in aqueous solution and pH 7.3 .

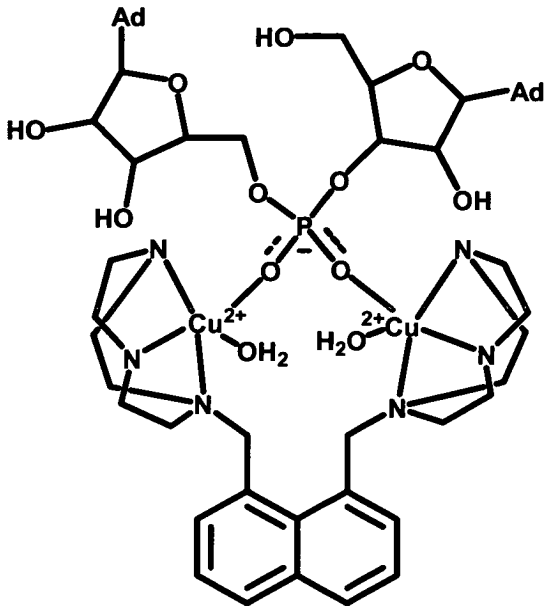

Fig. 1.7 Dinuclear Cu(II) complex that catalyses the hydrolysis of ApA using the two cooperative metal centres.[89]

In this system the cooperativity was suggested to be due to the bridging of the phosphate ester. In fact, this complex is about 500 times more reactive per metal centre than a related mononuclear Cu(II) complex for cleaving ApA. In terms of mechanism the authors proposed that a metal-bound hydroxide acted as the nucleophile on the phosphorus centre.

- Cooperation of metals and non-coordinating groups

Metal-base cooperation: In 1990, an interesting study by Breslow *et al.*[90] investigated the effect of a non-coordinating imidazole group (Figure 1.8(a)) in a macrocyclic zinc(II) complex in the cleavage of HPNP. The rate of hydrolysis was enhanced by a factor of 20 relative to the unfunctionalised complex presumably by

generating an intramolecular alcoholate nucleophile by proton abstraction from the substrate alcohol group. Based on pH-rate profiles, it was suggested that the imidazole group was acting as a general base catalyst.

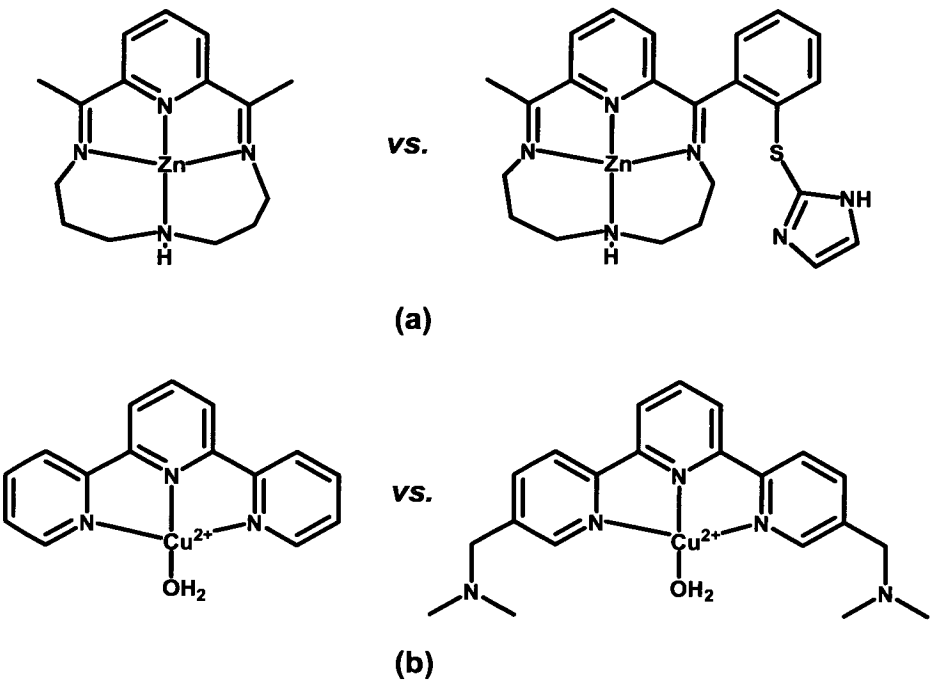

Fig. 1.8 *Macrocyclic Zn(II) complexes (a) and terpyridine Cu(II) complexes (b) used to study the participation of second coordination sphere basic groups in the hydrolysis of HPNP.*[90-91]

In a similar work by Hamilton *et al.*[91] the tertiary amino groups of a Cu(II) terpyridine complex (Figure 1.8(b)) were proposed to act as an auxiliary base in the hydrolysis of HPNP based on pH-rate profiles. This compound hydrolyses HPNP seven times faster than its unfunctionalised counter-part complex. The proposed mechanism involves deprotonation of the substrate hydroxyl group by the amino groups.

Metal-acid cooperation: The role of non-coordinating NH-acidic groups in the hydrolysis of phosphodiester bonds was investigated by Krämer *et al.*[92] in 1996 using LCu(II) complexes (L = bipy derivative) (Figure 1.9)

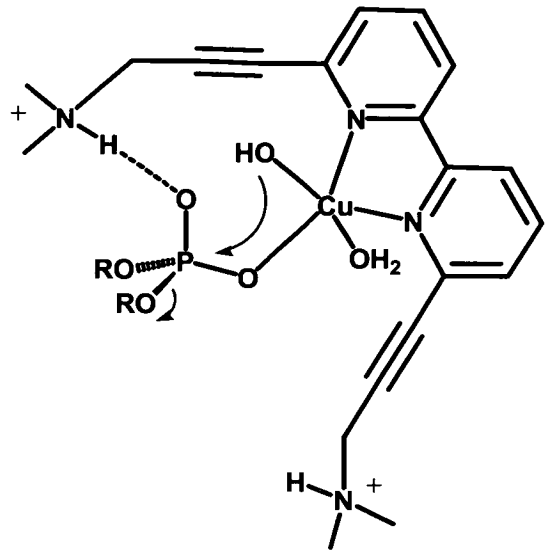

Fig. 1.9 *Proposed reaction mechanism for the hydrolysis of BNPP by LCu(II) (L = bipy derivative).*[92]

In this important study, the authors elegantly attached the ammonium groups using rigid propyne spacers to avoid coordination of the pendant group and facilitate interaction with the metal-bound phosphate. In fact, it was shown that the presence of these quaternary ammonium groups resulted in a remarkable rate increase of the hydrolysis of the metal-bound phosphodiester (BNPP) of 2900-fold over the control unfunctionalised complex. This enhancement in reactivity was explained in terms of the additional electrostatic activation provided by N-H···O-P hydrogen bonding. The relative rate constant was calculated to be 4×10^7.

Similarly, Chin *et al.*[93] investigated the role of amino groups in the proximity of a Cu(II) centre in the hydrolysis of 2'-3'-cAMP. In this study it was proposed that

the two amino groups acted as hydrogen bond donors to the metal-bound phosphodiester and hydroxide group (Figure 1.10).

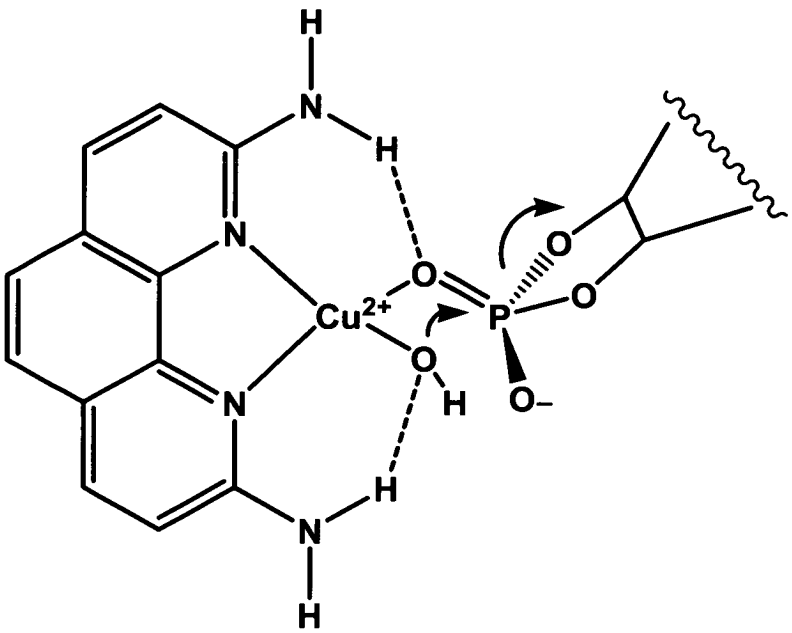

Fig 1.10 *Proposed reaction mechanism for the hydrolysis of 2'-3'-cAMP by LCu(II) (L = phenantroline derivative).*[93]

In fact, it was shown that this compound hydrolyses 2'-3'-cAMP much faster (625-fold) than the control complex lacking the primary amino groups. The rate ratio over the uncatalysed reaction was calculated to be 3.5×10^4.

Very recently, Anslyn *et al.*[94] have reported a series of zinc(II) complexes containing guanidinium/ammonium groups that hydrolyse ApA with rate enhancements relative to the related unfunctionalised complex as high as 3300-fold.

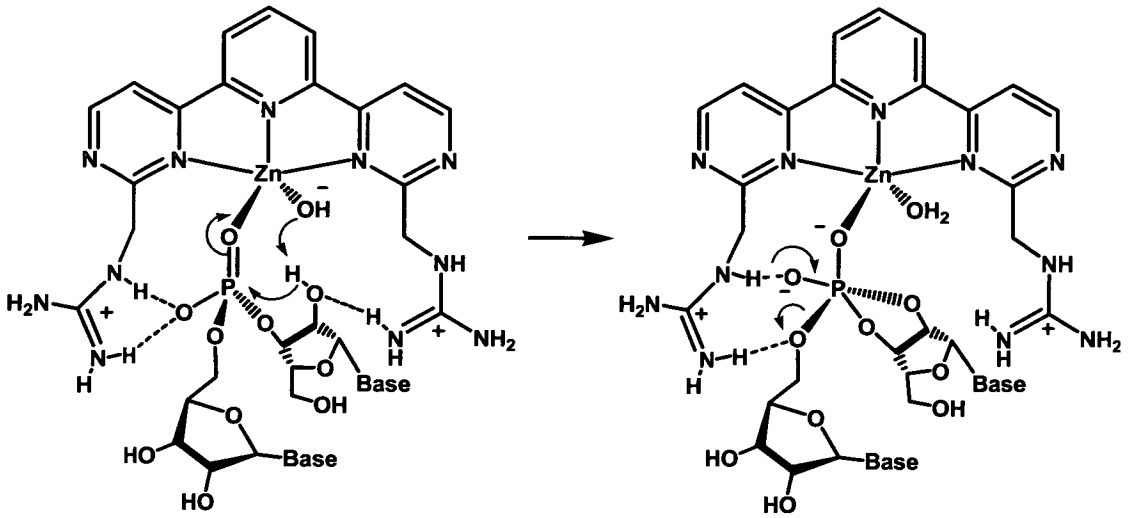

Fig. 1.11 *Proposed reaction mechanism for the hydrolysis of ApA by LZn(II) (L=bisguanidinium derivative).*[94]

In the proposed mechanism (Figure 1.11) the metal-bound hydroxide acts as a general base, deprotonating the 2′-OH of the ribose which in turn attacks the phosphorus centre. Remarkably, the rate constant for the hydrolysis of ApA is only 25 times less than the very active dinuclear copper(II) complex reported by Chin *et al.* (Figure 1.7) and the enhancement is only one order of magnitude less than the enhancement attributed to the guanidinium groups of Staphylococcal Nuclease.[48] Furthermore, the fact that the metal-free ligand alone does not hydrolyse ApA at a measurable rate and the remarkable enhancement from the guanidinium groups demonstrated cooperativity.

1.5.2.2 Hydrogen-bonding 'organic' synthetic nucleases

Since organic groups are believed to play an important functional role metallonucleases, in this section a brief review of 'organic' synthetic nucleases is given.

Early work by Springs and Haake[95] demonstrated that guanidinium groups are able to accelerate by as much as 27-fold the rate of attack of nucleophiles such as F^- on BNPP in water solution as the result of electrostatic stabilisation of the reaction transition state (Figure 1.12). This result proved that the positive charge on guanidinium groups makes them effective electrostatic catalysts, as well as potential proton donors.[96]

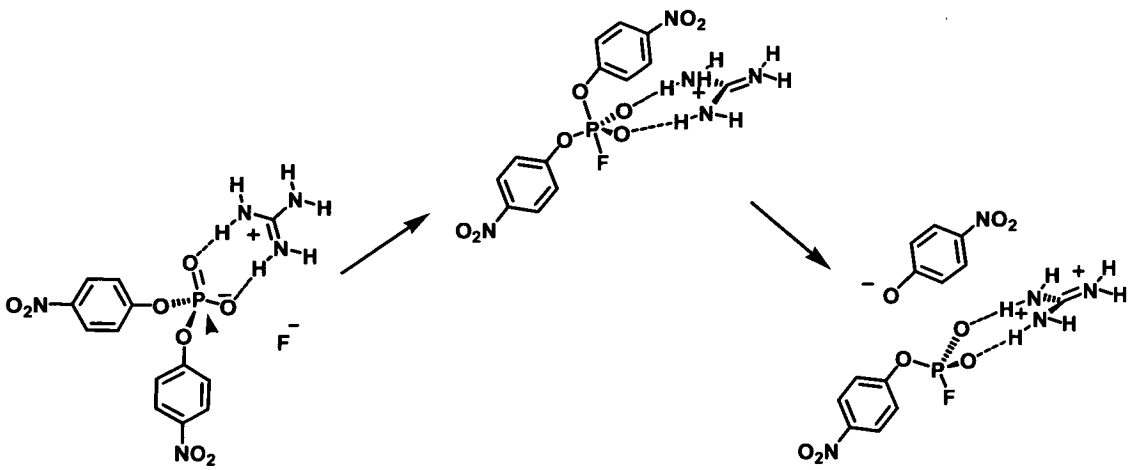

Fig. 1.12 *Proposed mechanism for the guanidinum-accelerated F^- attack on phosphodiesters.*[95]

Hamilton *et al.*[97] have also reported acceleration of in this case hydrolysis of HPNP with a bis(acylguanidinium) receptor (Figure 1.13). The rate of release of *p*-

nitrophenol is accelerated near 1000-fold over identical conditions without the addition of the catalyst.

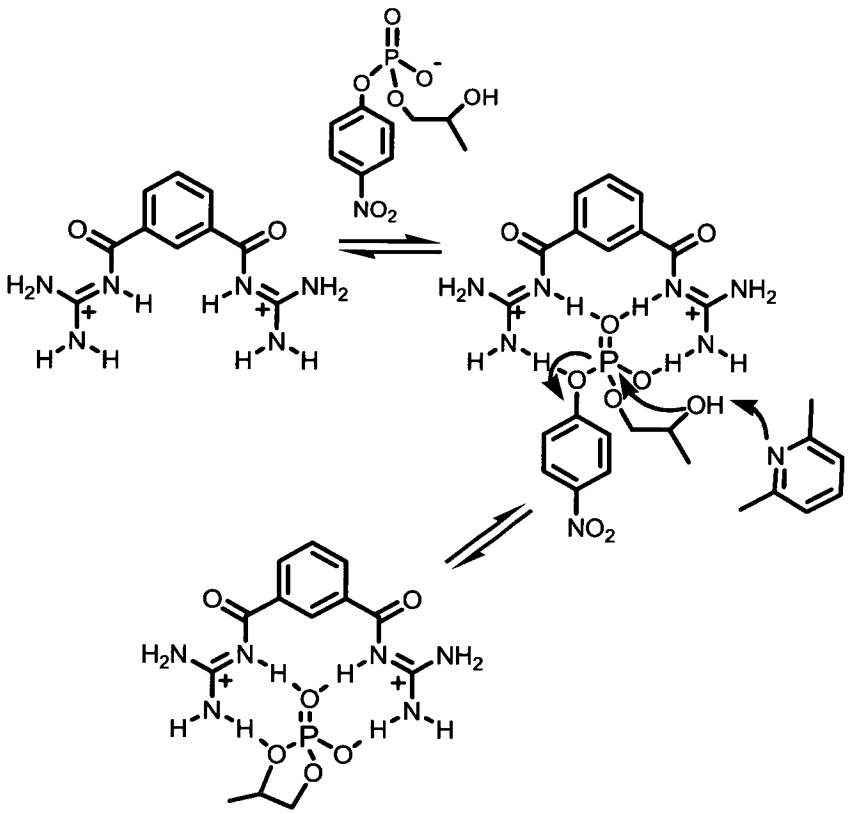

Fig. 1.13 *Proposed mechanism for the hydrolysis of HPNP by a bis(acylguanidinium) receptor.*[97]

In the proposed mechanism shown in figure 1.13 the bis(acylguanidinium) receptor acts in a similar manner to that proposed for the guanidinium residues of staphylococcal nuclease (SN), and lutidine acts as a general base. In comparison with metal-based artificial catalysts that hydrolyse HPNP, the rate enhancement provided by this compound (10^3) is 1-2 orders of magnitude lower. It is also important to note that the solvent used for the kinetic studies of this bis(acylguanidinium) receptor was acetonitrile due to solubility problems. Furthermore, the kinetic studies were run with a high excess of receptor and base (lutidine) which makes the medium highly polar, facilitating the formation of the receptor-HPNP complex.

Using a more rigid receptor, Anslyn *et al.* reported the hydrolysis of RNA in water at physiological conditions using micromolar receptor concentrations and imidazole as a general base.[98] The proposed mechanism for the hydrolysis of RNA by this bis-alkylguanidinium receptor is shown in Figure 1.14.

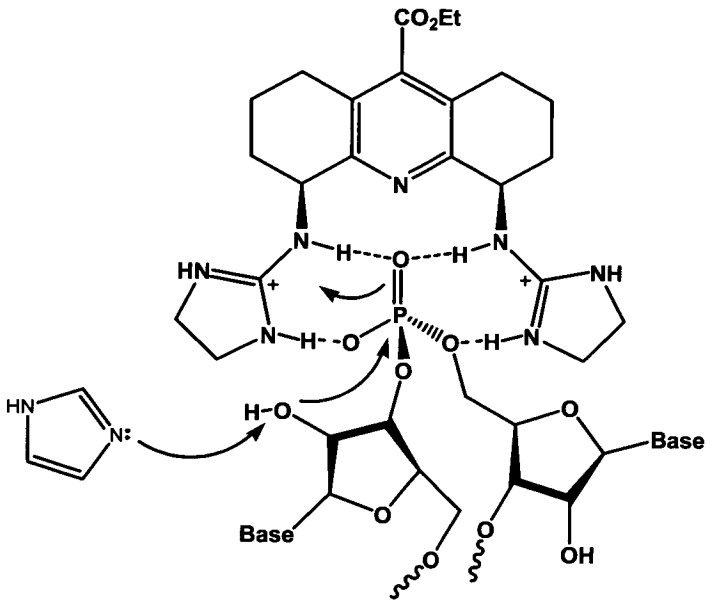

Fig. 1.14 *Proposed mechanism for the hydrolysis of RNA by the bis(alkylguanidinium) receptor.*[98]

The authors propose that imidazole acts as a general base to deliver the 2'-OH to the phosphodiester linkage. The phosphorane transition state is then stabilised by ion pairing and/or guanidinium general-acid proton transfer from the receptor. The hydrolysis of RNA in the presence of the receptor is enhanced by a factor of 20-fold which further demonstrates that mimicking the arginine functionalities of SN is a successful approach for catalysing phosphodiester cleavage.

1.6 Project Aims

The involvement of well positioned XH groups (X = N, O) of arginine, lysine, histidine, tyrosine and/or serine residues in hydrogen bonding interactions to water and/or substrate groups is an ubiquitous feature in nucleases. Many of these interactions/amino acid residues are thought to be functionally important, but the mechanistic details regarding their precise roles remain unclear.[22, 99]

The main objective of this thesis was set on obtaining a better understanding of the roles of these amino acid residues present in the secondary coordination sphere of zinc in the active site of nucleases. Current hypotheses suggest that these second sphere active site residues can participate in one or several of the following catalytically-important events: substrate activation and positioning, nucleophile generation/activation, proton transfer events, and transition state stabilisation. The exact mechanistic details, however, remain to be elucidated. Moreover, in these enzymes, the cooperation between metals and non-coordinating active site residues may be necessary for the efficient activation, recognition and/or stabilisation mechanisms but the relative contributions of metals and second sphere residues has not been quantified yet.

Thus, the specific aims of this thesis are:

1. To design and synthesise a series of ligands capable of binding zinc and hydrogen bonding to metal-bound ligands.

2. To investigate strategies to induce and manipulate the formation and strength of hydrogen bonding to metal-bound ligands.

3. To investigate the effect(s) of hydrogen bonding groups in Zn(II) complexes of these ligands in properties relevant to phosphate ester hydrolysis.

1.7 References

(1) C. A. Stein and J. S. Cohen, *Cancer Res.*, 1998, **48**, 2659.

(2) R. Wolfenden and M. J. Snider, *Acc. Chem. Res.*, 2001, **34**, 938.

(3) D. L. Nelson and M. M. Cox, '*Principles of Biochemistry*', Worth Publishers, New York, 2000.

(4) A. Fersht, '*Enzyme Structure and Mechanism*', WH Freeman & Co., New York, 1985.

(5) A. J. Kirby, *Angew. Chem. Int. Ed.*, 1996, **35**, 707.

(6) D. A. Bell and E. V. Anslyn, *Compr. Supramol. Chem.*, 1996, **2**, 439.

(7) M. I. Page and W. P. Jencks, *Proc. Natl. Acad. Sci. U. S. A.*, 1971, **68**, 1678.

(8) A. Radzicka and R. Wolfenden, *Science*, 1995, **267**, 90.

(9) L. Pauling, *J. Am. Chem. Soc.*, 1931, **53**, 1367.

(10) G. R. Desiraju and T. Steiner, '*The Weak Hydrogen Bond*', Oxford University Press, Oxford, 1999.

(11) M. A. Adams, K. Folting, J. C. Huffman and K. G. Caulton, *Inorg. Chem.*, 1979, **18**, 3020.

(12) L. M. Epstein, E. S. Shubina, A. N. Krylov, A. Z. Kreindlin and M. I. Ribinskaya, *J. Organomet. Chem.*, 1993, **447**, 277.

(13) S. A. Fairhurst, R. A. Henderson, D. L. Hughes, S. K. Ibrahim and C. J. Pickett, *Chem. Commun.*, 1995, 1569.

(14) E. Peris and R. H. Crabtree, *Chem. Commun.*, 1995, 2179.

(15) D. Braga, F. Grepioni, E. Tedesco, K. Biradha and G. R. Desiraju, *Organometallics*, 1996, **15**, 2692.

(16) S. Suzuki, P. G. Green, R. E. Bumgarner, S. Dasgupta, W. A. Goddard, III and G. A. Blake, *Science*, 1992, **257**, 942.

(17) D. S. Trifan and R. Bacskai, *J. Am. Chem. Soc.*, 1960, **82**, 5010.

(18) D. M. Roe, P. M. Bailey, K. Mosely and P. M. Maitlis, *Chem. Commun.*, 1972, 1273.

(19) R. S. Drago, M. S. Norazi, R. J. Klinger and C. S. Chamberlain, *Inorg. Chem.*, 1979, **18**, 1254.

(20) L. Brammer, J. M. Charnock, P. L. Goggin, R. J. Goodfellow, A. G. Orpen and T. F. Koetzle, *J. Chem. Soc., Dalton Trans.*, 1991, 1789.

(21) L. Brammer, J. C. Mareque-Rivas and D. Zhao, *Inorg. Chem.*, 1998, **37**, 5512.

(22) W. N. Lipscomb and N. Sträter, *Chem. Rev.*, 1996, **96**, 2375.

(23) H. Vahrenkamp, *Chem. Unserer Zeit*, 1988, **22**, 73.

(24) B. L. Vallee and D. S. Auld, *Proc. Natl. Acad. Sci. U. S. A.*, 1990, **87**, 220.

(25) B. L. Vallee and D. S. Auld, *Biochemistry*, 1990, **29**, 5647.

(26) J. E. Coleman, *Ann. Rev. Biochem.*, 1992, **61**, 897.

(27) C. F. Mills, '*Zinc in human biology*', Springer-Verlag, New York, 1989.

(28) D. H. Nies, *Appl. Microbiol. Biotechnol.*, 1999, **31**, 730.

(29) T. G. Spiro, '*Zinc Enzymes*', John Wiley & Sons, New York, 1983.

(30) To visit the homepage of the IUBMB: www.iubmb.unibe.ch

(31) C. W. Bock, A. K. Katz and J. P. Glusker, *J. Am. Chem. Soc.*, 1995, **117**, 3754.

(32) J. A. Tainer, V. A. Roberts and E. D. Getzoff, *Curr. Opinion Biotechnolo.*, 1991, **2**, 582.

(33) D. Christianson, *Adv. Protein Chem.*, 1991, **42**, 281.

(34) J. M. Berg and D. L. Merkle, *J. Am. Chem. Soc.*, 1989, **111**, 3759.

(35) B. L. Vallee and R. J. Williams, *Proc. Natl. Acad. Sci. USA*, 1968, **59**, 498.

(36) R. G. Pearson, *J. Am. Chem. Soc.*, 1963, **85**, 3533.

(37) R. G. Pearson, *Science*, 1966, **151**, 172.

(38) F. A. Cotton, G. Wilkinson, C. A. Murillo and M. Bochmann, '*Advanced Inorganic Chemistry*', John Wiley & Sons, New York, 1999.

(39) E. Ochiai, *J. Chem. Educ.*, 1988, **65**, 943.

(40) 'DOE Human Genome Program: Primer on molecular genetics', Oak Ridge National Laboratory, Oak Ridge, TN, 1992.

(41) F. H. Westheimer, *Science*, 1987, **235**, 1173.

(42) J. Chin, M. Banaszczyk, V. Jubian and X. Zou, *J. Am. Chem. Soc.*, 1989, **111**, 186.

(43) N. H. Williams and J. Chin, *Chem. Commun.*, 1996, 131.

(44) K. Shishido and N. Habuka, *Biochim. Biophys. Acta*, 1986, **884**, 215.

(45) H. Witzel, W. Berg, O. Creutzenberg and A. Karreh, '*Zinc Enzymes*', Boston, 1986.

(46) F. A. Cotton, J. E. E. Hazen and M. J. Legg, *Proc. Natl. Acad. Sci. U. S. A.*, 1979, **76**, 2551.

(47) D. J. Weber, A. K. Meeker and A. S. Mildvan, *Biochemistry*, 1991, **30**, 6103.

(48) E. H. Serpersu, D. Shortle and A. S. Mildvan, *Biochemistry*, 1987, **26**, 1289.

(49) T. D. Tullius, '*Metal-DNA Chemistry*', ed. T. D. Tullius, Oxford University Press, 1989.

(50) J. R. Morrow, K. Aures and D. Epstein, *Chem. Commun.*, 1995, 2431.

(51) J. R. Morrow, V. M. Buttrey, K. A. Shelton and J. Berback, *J. Am. Chem. Soc*, 1992, **114**, 1903.

(52) S. Amin, J. R. Morrow, C. H. Lake and M. R. Churchill, *Angew. Chem. Int. Ed.*, 1994, **33**, 773.

(53) J. Rammo, H. Rettich and H.-J. Scheineder, *Chem. Commun.*, 1996, 105.

(54) A. Roigh and H.-J. Scheineder, *Eur. J. Org. Chem.*, 2001, 205.

(55) T. Gunnlaugsson, R. J. H. Davies, M. Nieuwenhuyzen, C. S. Stevenson, R. Viguier and S. Mulready, *Chem. Commun.*, 2002, 2136.

(56) T. Gunnlaugsson, R. J. H. Davies, M. Nieuwenhuyzen, J. E. O'Brien, C. S. Stevenson and S. Mulready, *Polyhedron*, 2003, **22**, 711.

(57) N. H. Williams, B. Takasaki, M. Wall and J. Chin, *Acc. Chem. Res.*, 1999, **32**, 485.

(58) P. Hendry and A. M. Sargeson, *J. Am. Chem. Soc*, 1989, **111**, 1989.

(59) J. Chin and X. Zou, *J. Am. Chem. Soc*, 1988, **1988**, 223.

(60) J. N. Burstyn and K. A. Deal, *Inorg. Chem.*, 1993, **32**, 3585.

(61) K. A. Deal and J. N. Burstyn, *Inorg. Chem.*, 1996, **35**, 2792.

(62) K. A. Deal, A. C. Hengge and J. N. Burstyn, *J. Am. Chem. Soc*, 1996, **118**, 1713.

(63) E. L. Hegg and J. N. Burstyn, *Coord. Chem. Rev.*, 1998, **173**, 133.

(64) K. M. Deck, T. A. Tseng and J. N. Burstyn, *Inorg. Chem.*, 2002, **41**, 669.

(65) J. A. Connolly, J. H. Kim, M. Banaszczyk, M. Drouin and J. Chin, *Inorg. Chem.*, 1995, 1094.

(66) M. J. Young, D. Wahnon, R. C. Hynes and J. Chin, *J. Am. Chem. Soc*, 1995, **117**, 9441.

(67) E. Kimura and T. Koike, *Chem. Commun.*, 1998, 1495.

(68) E. Kimura, Y. Kodama, T. Koike and M. Shiro, *J. Am. Chem. Soc.*, 1995, **117**, 8304.

(69) E. Kimura, I. Nakamura, T. Koike, M. Shionoya, Y. Kodama, T. Ikeda and M. Shiro, *J. Am. Chem. Soc.*, 1994, **116**, 4764.

(70) S. Hikichi, M. Tanaka, Y. Morooka and N. Kitajima, *Chem. Commun.*, 1992, 814.

(71) M. Ruf, K. Weis and H. Vahrenkamp, *Chem. Commun.*, 1994, 135.

(72) M. Rombach, C. Maurer, K. Weis, E. Keller and H. Vahrenkamp, *Chem. Eur. J.*, 1999, **5**, 1013.

(73) T. Koike and E. Kimura, *J. Am. Chem. Soc*, 1991, **113**, 8935.

(74) L. Bonfa, M. Gatos, F. Mancin, P. Tecilla and U. Tonellato, *Inorg. Chem.*, 2003, **42**, 3943.

(75) N. V. Kaminskaia, C. He and S. J. Lippard, *Inorg. Chem.*, 2000, **39**, 3365.

(76) T. Humphry, M. Forconi, N. H. Williams and A. C. Hengge, *J. Am. Chem. Soc.*, 2002, **124**, 14860.

(77) E. Bernard, S. Chardon-Noblat, A. Deronzier and J.-M. Latour, *Inorg. Chem.*, 1999, **38**, 190.

(78) P. Molenveld, W. M. G. Stikvoort, H. Koojiman, A. L. Spek, J. F. J. Engbersen and D. N. Reinhoudt, *J. Org. Chem*, 1999, **64**, 3896.

(79) N. H. Williams, A.-M. Lebuis and J. Chin, *J. Am. Chem. Soc*, 1999, **121**, 3341.

(80) S. Liu and A. D. Hamilton, *Chem. Commun.*, 1999, 587.

(81) D. E. Wilcox, *Chem. Rev.*, 1996, **96**, 2435.

(82) N. L. Strater, T. Klabunde and B.Krebs, *Angew. Chem. Int. Ed. Engl.*, 1996, **35**, 2024.

(83) D. Wahnon, A.-M. Lebuis and J. Chin, *Angew. Chem. Int. Ed.*, 1995, **34**, 2412.

(84) K. Worm, F. Chu, K. Matsumoto, M. D. Best, V. Lynch and E. V. Anslyn, *Chem. Eur. J.*, 2003, **9**, 741.

(85) J. R. Morrow and O. Iranzo, *Curr. Opinion in Chem. Biology*, 2004, **8**, 192.

(86) S. Albedyhl, D. Schnieders, A. Jancsó, T. Gajda and B. Krebs, *Eur. J. Inorg. Chem.*, 2002, **6**, 1400.

(87) O. Iranzo, A. Y. Kovalevsky, J. R. Morrow and J. P. Richard, *J. Am. Chem. Soc*, 2003, **125**, 1988.

(88) M. Yashiro, A. Ishikubo and M. Komiyama, *Chem. Commun.*, 1997, 83.

(89) M. J. Young and J. Chin, *J. Am. Chem. Soc*, 1995, **117**, 10577.

(90) R. Breslow, D. Berger and D. L. Huang, *J. Am. Chem. Soc*, 1990, **112**, 3686.

(91) S. Liu and A. D. Hamilton, *Tetrahedron Lett.*, 1997, **38**, 1107.

(92) E. Kövári and R. Krämer, *J. Am. Chem. Soc.*, 1996, **118**, 12704.

(93) M. Wall, B. Linkletter, D. Williams, A.-M. Lebuis, R. C. Hynes and J. Chin, *J. Am. Chem. Soc.*, 1999, **121**, 4710.

(94) H. Aït-Haddou, J. Sumaoka, S. L. Wiskur, J. F. Folmer-Andersen and E. V. Anslyn, *Angew. Chem. Int. Ed.*, 2002, **41**, 4014.

(95) B. Springs and P. Haake, *Tetrahedron Lett.*, 1977, 3223.

(96) C. L. Hannon and E. V. Anslyn, '*The Guanidinium Group. Its Biological Role and Synthetic Analogs, Bioorganic Chemistry Frontiers*', Springer-Verlag, Berlin, 1993.

(97) V. Jubian, R. P. Dixon and A. D. Hamilton, *J. Am. Chem. Soc.*, 1992, **114**, 1120.

(98) J. Smith, K. Ariga and E. V. Anslyn, *J. Am. Chem. Soc*, 1993, **115**, 362.

(99) R. Krämer, *Coord. Chem. Rev.*, 1999, **182**, 243.

Chapter 2. Inducing Internal N-H···Cl-Zn Hydrogen Bonding in Complexes of Ligands Derived From Tris-Pyridylmethyl-Amine (tpa)

2.1 INTRODUCTION

The design of ligands that provide a second coordination sphere to interact with exogenous metal-bound ligands in synthetic analogues of nucleases is nontrivial, primarily due to the relative weakness of these interactions. Therefore, as a first step, this thesis work explored strategies to induce and establish the formation of hydrogen bonding to metal-bound ligands.

In this chapter, we investigate the use of the unit (6-NHR-2-pyridylmethyl)amine in zinc(II) complexes of tris-pyridylmethyl-amine (**tpa**)-based ligands as a strategy to induce the formation of internal hydrogen bonding to metal-bound ligands. Structural features, including hydrogen bonding interactions found in the solid state by X-ray diffraction studies, are contrasted and correlated with NMR and/or IR studies in solution.

2.2 RESULTS AND DISCUSSION

2.2.1 LIGAND SELECTION AND SYNTHESIS

We decided to use the ligand tris-pyridylmethyl-amine (**tpa**)[1] (Scheme 2.1) as the ligand framework for the following reasons. First, the rigidity of the metal complex formed is an important characteristic to take into account. If the ligand provides the metal with a flexible coordination geometry, the desired second sphere

interaction (hydrogen bonding) might be difficult to form or even not formed at all. In that respect, **tpa** is an excellent ligand framework as it is a rigid tripodal ligand providing a N4 binding site for the metal that can be used as a source of stability for the resulting zinc(II) complexes, while it leaves available coordination sites to exogenous ligands. Secondly, it offers the possibility to incorporate substituents to create a second sphere microenvironment that could influence the chemistry at the metal centre. In particular, the ligand fragment (6-NHR-2-pyridylmethyl)amine seemed to us a perfect candidate as it provides a N-H group in a suitable stereochemistry to participate in an internal hydrogen bond to an adjacent metal-bound ligand (Scheme 2.1).

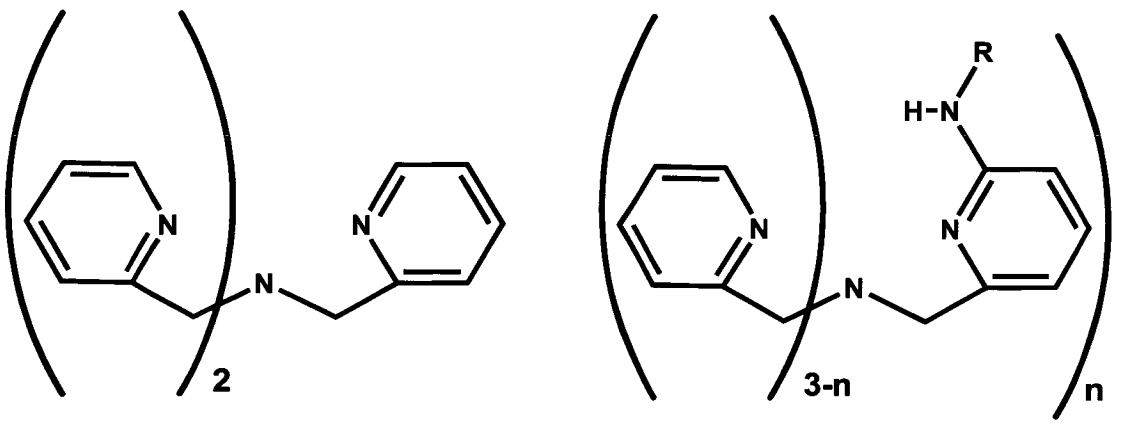

Scheme 2.1

In this chapter we investigate zinc(II) coordination and hydrogen bonding of two ligands, *N,N*-bis(2-pyridylmethyl)-*N*-(6-pivaloylamido-2-pyridylmethyl)amine ($\mathbf{L_1}^1$; superscript 1 refers to R = CO^{t}Bu, subscript 1 refers to **one** H-bonding group)

and *N,N*-bis(2-pyridylmethyl)-*N*-(6-amino-2-pyridylmethyl)amine ($\mathbf{L_1}^2$; superscript 1 refers to R = H, subscript 1 refers to **one** H-bonding group). $\mathbf{L_1}^1$ offers one electron withdrawing amide N-H group as a potential hydrogen bond donor. $\mathbf{L_1}^2$ offers one electron donating amino NH_2 unit which can act both as a hydrogen bond donor and/or acceptor, and offers less impediment than $\mathbf{L_1}^1$ to the approach of an external substrate.

2.2.1.1 Synthesis of *N,N*-bis(2-pyridylmethyl)-*N*-(6-pivaloylamido-2-pyridylmethyl)amine ($\mathbf{L_1}^1$)

The synthesis of $\mathbf{L_1}^1$ can be accomplished in 5 steps.[2, 3]

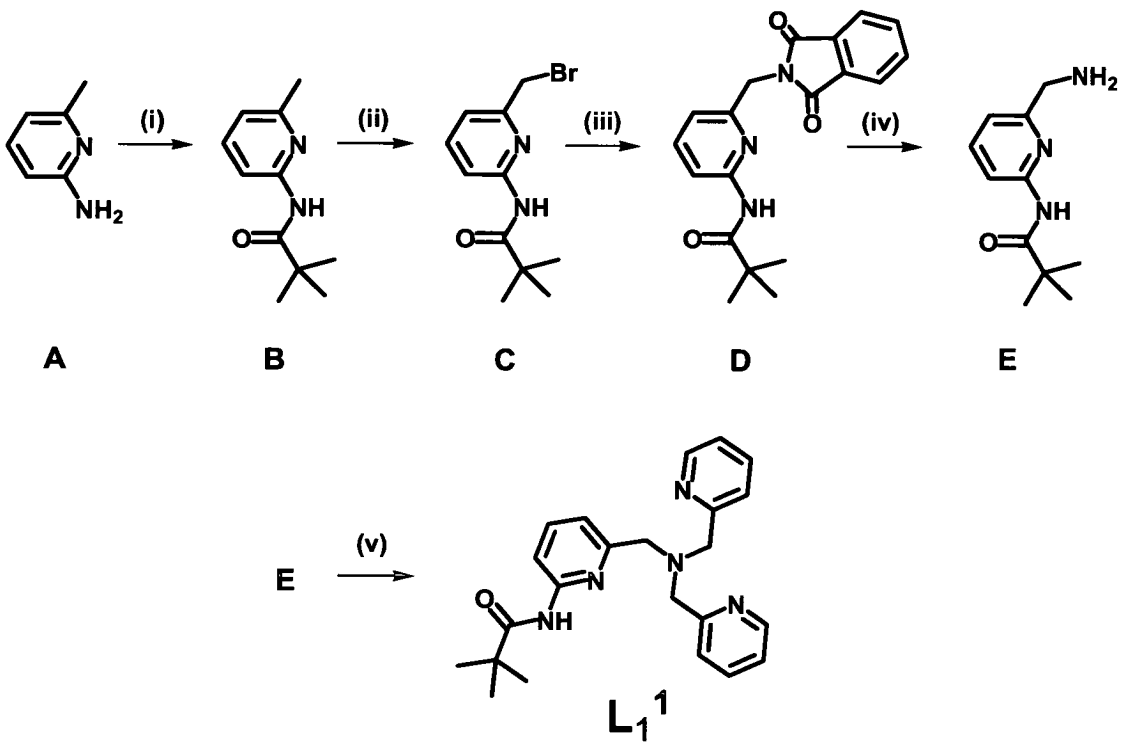

Scheme 2.2 Reagents and conditions used for the synthesis of compounds **A-E** and $\mathbf{L_1}^1$; (i) ^{t}BuCOCl (1.5 equiv.), CH_2Cl_2, NEt_3, 22 h; (ii) NBS (1.5 equiv.) AIBN (0.1 equiv.), CCl_4, 80 °C, 3.5 h; (iii) potassium phthalamide (1 equiv.), DMF, 120 °C, 3 h; (iv) $N_2H_4 \cdot H_2O$ (1 equiv.), EtOH, 60 °C, 3 h; (v) $PyCH_2Cl$ (2 equiv.), Na_2CO_3, CH_3CN, 44°C, 48 h.

The strategy for the synthesis of the ligands is shown in Scheme 2.2. The first step of the synthesis involves the protection of the amino group of 2-amino-6-methylpyridine (**A**) with trimethylacetyl chloride using triethylamine as a base. This reaction yields the desired product in high purity after using flash chromatography. The second step is the bromination of the picoline methyl group of **A** using *N*-bromosuccinimide (**NBS**) as bromination agent and a catalytic amount of 2,2'-azobis(2-methyl-propionitrile) (**AIBN**) as radical initiator in refluxing carbon tetrachloride. This reaction proceeds in low yield and requires flash chromatography to separate the mono- (**C**) from the bis- and the non-brominated products. Despite this fact, reasonably good yields were obtained (*ca.* 43 %) by optimising the reaction conditions. **C** can be quantitatively converted into *N*-[6-(aminomethyl)-2-pyridyl]pivalamide (**E**) using the Gabriel synthesis of primary amines.

The asymmetric tripodal ligand $\mathbf{L_1}^1$ was then prepared by coupling 2 equivalents of 2-picolyl chloride with 1 equivalent of **E** in acetonitrile using 10 equivalents of sodium carbonate. This reaction proceeds in good yields and the crude product can be purified to yield the pure free ligand by recrystallisation from diethyl ether.

2.2.1.2 Synthesis of *N,N*-bis(2-pyridylmethyl)-*N*-(6-amino-2-pyridylmethyl)amine (L_1^2)

The synthesis of $\mathbf{L_1}^2$ can be accomplished in one step as shown in Scheme 2.3.

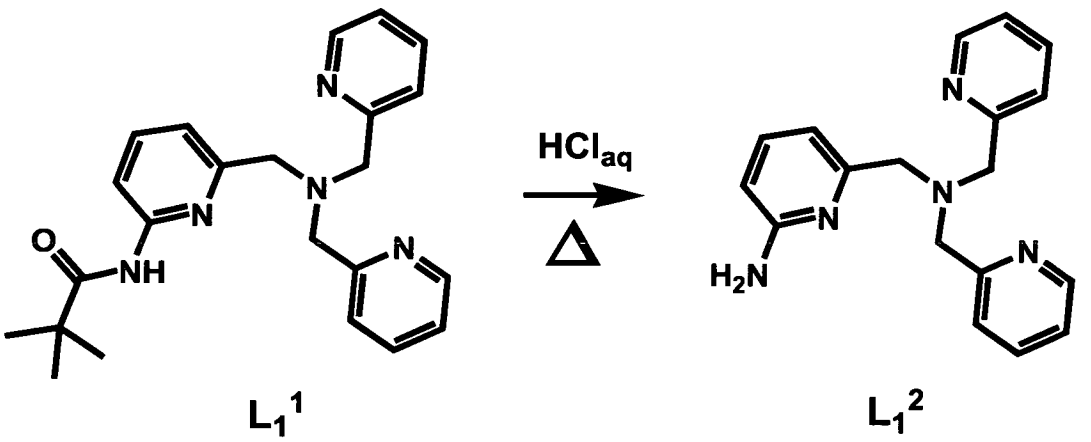

Scheme 2.3

The synthesis of $\mathbf{L_1}^2$ was carried out starting from the corresponding tripodal ligand $\mathbf{L_1}^1$ with the (6-pivaloylamido-2-pyridylmethyl)amine fragment upon hydrolysis. The trimethylacetyl protecting group of $\mathbf{L_1}^1$ was cleaved by refluxing in 2M $HCl_{(aq)}$ for 48 h to yield the unprotected amine $\mathbf{L_1}^2$. This reaction proceeds in excellent yields (96 %) after basifying the reaction solution and extracting the desired product with dichloromethane.

2.2.2 SYNTHESIS OF Zn(II) COMPLEXES

The synthesis of the zinc(II) complexes of $\mathbf{L_1}^1$, $[(\mathbf{L_1}^1)Zn](PF_6)_2$ and $[(\mathbf{L_1}^1)Zn(Cl)](X)$ (X = Cl, BPh_4), was accomplished using $ZnCl_2$ as common precursor. Thus, the reaction of $ZnCl_2$ with two equivalents of $AgPF_6$ in dry acetonitrile affords the complex $[Zn(NCCH_3)_4](PF_6)_2$, which after removal of the AgCl precipitate by filtration and addition of one equivalent of $\mathbf{L_1}^1$ affords $[(\mathbf{L_1}^1)Zn](PF_6)_2$. The $[(\mathbf{L_1}^1)Zn]^{2+}$ cation can be quantitatively converted to the

$[(\mathbf{L_1}^1)Zn(Cl)]^+$ cation in the presence of Cl^- ions. Alternatively, the $[(\mathbf{L_1}^1)Zn(Cl)]^+$ cation can be prepared mixing equimolar amounts of $\mathbf{L_1}^1$ and $ZnCl_2$ in acetonitrile (Scheme 2.4).

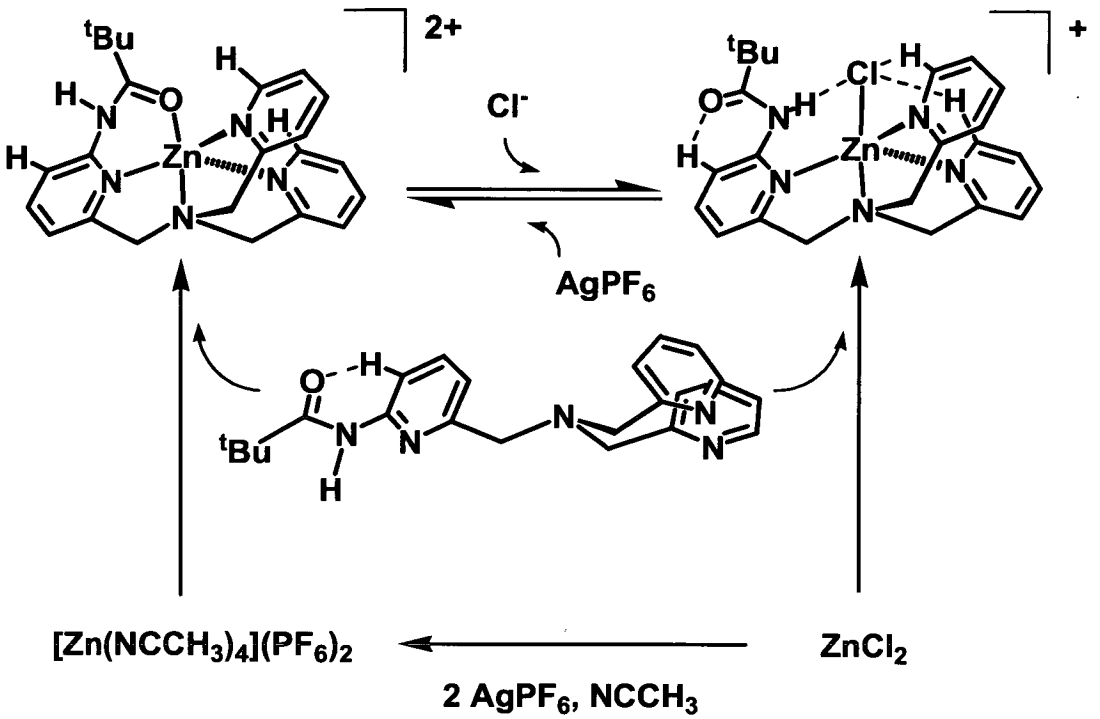

Scheme 2.4

The synthesis of Zn(II) complexes of $\mathbf{L_1}^2$, $[(\mathbf{L_1}^2)Zn(Cl)](X)$ (X = Cl, BPh_4) was also achieved using $ZnCl_2$ as common precursor. Thus, mixing equimolar amounts of $\mathbf{L_1}^2$ and $ZnCl_2$ yields $[(\mathbf{L_1}^2)Zn(Cl)](Cl)$ from which $[(\mathbf{L_1}^2)Zn(Cl)](BPh_4)$ was prepared by metathesis reaction with $NaBPh_4$.

Interestingly, in the presence of Cl^- the Zn(II) ion prefers trigonal bipyramidal N_4Cl ligation over N_4O (in $\mathbf{L_1}^1$) and octahedral N_4Cl_2 coordination environments

(Scheme 2.5), despite the fact that chelate effects and the possibility of coordinating an additional group to the Zn(II) centre could be considered sources of stability.

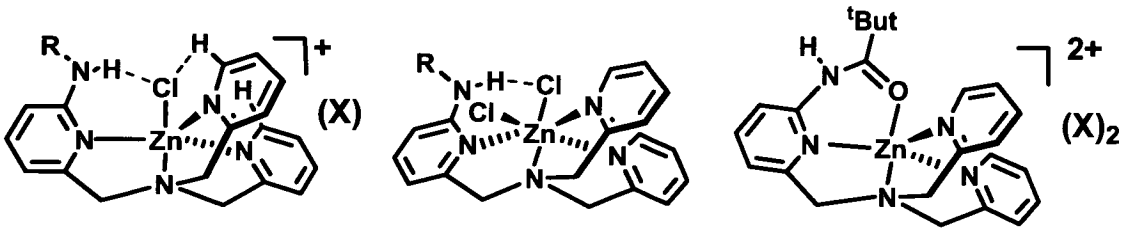

R = CO^tBu (L_1^1); X =Cl, BPh_4
R = H (L_1^2); X = Cl, BPh_4

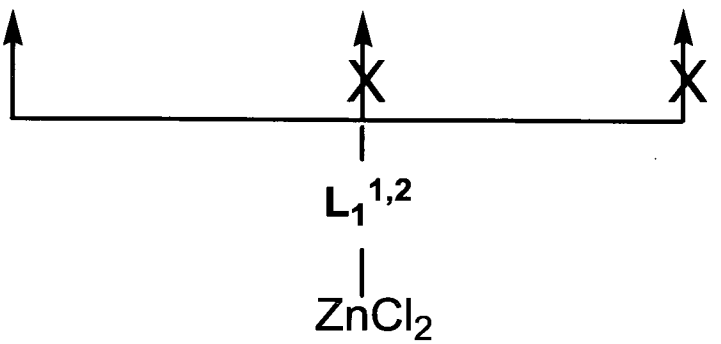

Scheme 2.5

2.2.3 X-RAY CRYSTALLOGRAPHY

Crystal data for $\mathbf{L_1}^1$, $[(\mathbf{L_1}^1)Zn](PF_6)_2 \cdot 0.5CH_3OH$, $[(\mathbf{L_1}^1)Zn(Cl)](BPh_4) \cdot CH_3CN$, $[(\mathbf{L_1}^2)Zn(Cl)](BPh_4) \cdot 0.5CH_3CN$ are listed in Table 2.1.

Table 2.1 Crystallographic data and structure refinement details for $\mathbf{L_1}^1$ and complexes $[(\mathbf{L_1}^1)Zn](PF_6)_2 \cdot 0.5CH_3OH$, $[(\mathbf{L_1}^1)Zn(Cl)](BPh_4) \cdot CH_3CN$ and $[(\mathbf{L_1}^2)Zn(Cl)](BPh_4) \cdot 0.5CH_3CN$.

	$\mathbf{L_1}^1$	$[(\mathbf{L_1}^1)Zn](PF_6)_2 \cdot 0.5CH_3OH$	$[(\mathbf{L_1}^1)Zn(Cl)](BPh_4) \cdot CH_3CN$	$[(\mathbf{L_1}^2)Zn(Cl)](BPh_4) \cdot 0.5CH_3CN$
Empirical Formula	$C_{23}H_{27}N_5O$	$C_{23.50}H_{29}F_{12}N_5O_{1.50}P_2Zn$	$C_{49}H_{50}BClN_6OZn$	$C_{43}H_{40.5}BClN_{5.5}Zn$
M_r	389.50	760.83	850.58	745.94
T/ K	150	150	150	150(2)
Crystal system	Monoclinic	Monoclinic	Triclinic	Monoclinic
Space group	$P2_1/c$	$P2_1/c$	P-1	$P2_1/n$
Crystal size/mm	0.63 × 0.34 × 0.27	0.5 × 0.29 × 0.12	0.86 × 0.42 × 0.26	0.91 × 0.6 × 0.58
a /Å	10.9702(9)	14.424(2)	10.295(3)	9.9482(13)
b /Å	9.7048(8)	11.3946(19)	14.243(4)	16.374(2)
c /Å	19.1103(15)	19.420(2)	15.328(4)	23.249(3)
α / °	90.00	90.00	73.973(5)	90
β / °	90.555(2)	106.072(11)	86.034(5)	101.631(2)
γ / °	90.00	90.00	84.577(5)	90
V / Å^3	2034.5(3)	3067.0(8)	2148.4(11)	3709.2(8)
Z	4	4	2	4
D_c / g cm^{-3}	1.272	1.648	1.315	1.336
μ / mm^{-1}	0.081	3.062	0.679	0.773
R_{int}	0.0259	0.0256	0.0247	0.0321
$R_1(F)^a$	0.0566	0.0419	0.0502	0.0470
$wR_2(F^2)^a$ (all data)	0.1221	0.0770	0.0983	0.0995
$S(F^2)^a$ (all data)	1.018	1.028	0.953	1.047
Largest difference peak, hole/e Å^3	0.365, -0.228	0.423, -0.327	0.544, -0.304	0.606, –0.327

$^a R_1(F) = \Sigma(|F_o| - |F_c|)/ \Sigma(|F_o|$; $wR_2(F^2) = [\Sigma w(F_o^2 - F_c^2)^2/\Sigma wF_0^4]^{1/2}$; $S(F^2) = [\Sigma w(F_o^2 - F_c^2)^2/(n-p)]^{1/2}$.

2.2.3.1 Structure of L_1^1

Single crystals suitable for X-ray diffraction were grown by slow evaporation of a solution of $\mathbf{L_1}^1$ in diethyl ether. An ORTEP plot[5] of the X-ray crystal structure of $\mathbf{L_1}^1$ is shown in Fig. 2.1. In this structure the three pyridine nitrogens (N(2), N(12) and N(22)) are located on the same side of the molecule, and opposed to the bridgehead amine nitrogen (N(1)) of the tripodal ligand (Fig. 2.1). Presumably this arrangement allows a weak interaction between the H-atoms in the 3-position (labelling scheme given in Scheme 2.6) of each pyridine ring and the lone pair of the bridgehead nitrogen. It allows also the amide N–H to be engaged in hydrogen bonding with a pyridine nitrogen of a symmetry related molecule in the crystal structure (Table 2.2, Fig. 2.2). In this arrangement, however, a substantial re-organisation needs to take place to allow metal co-ordination to the three pyridine (N_{py}) and one amine (N_{amine}) nitrogen atoms.

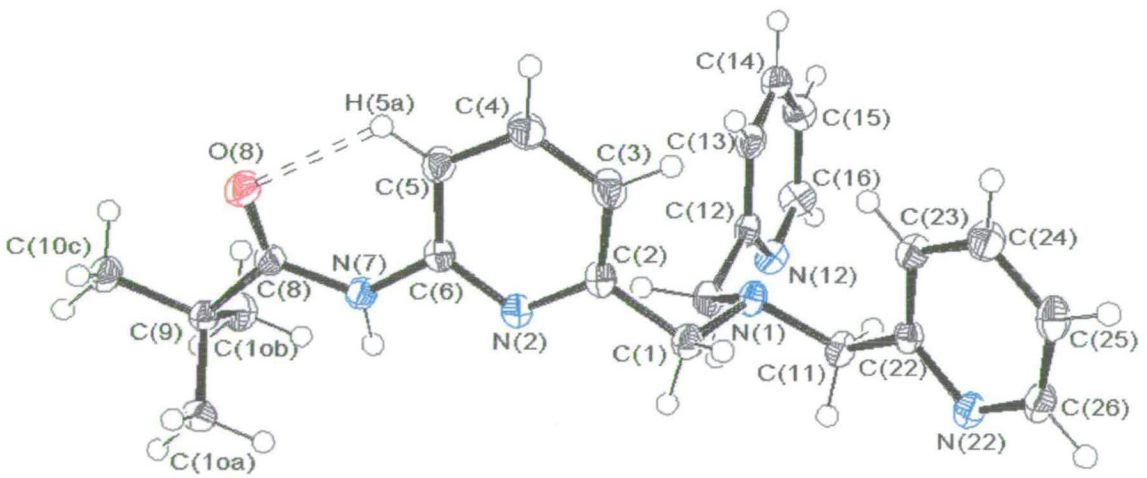

Fig. 2.1 An ORTEP plot drawn with 50% probability thermal ellipsoids of the ligand $\mathbf{L_1}^1$.

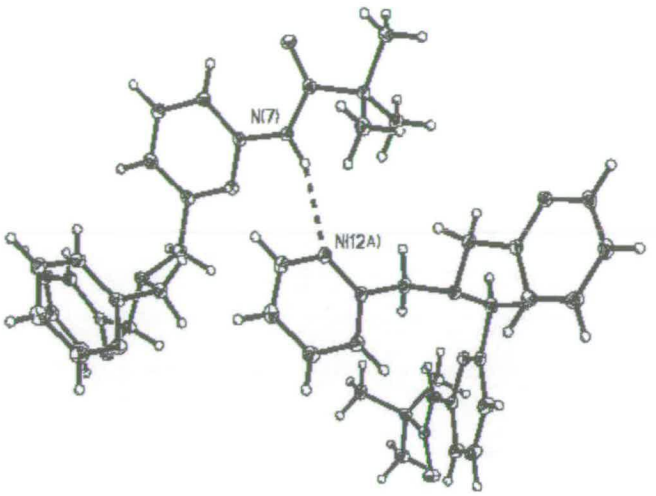

Fig. 2.2 An ORTEP plot drawn with 30 % probability thermal ellipsoids showing intermolecular N(7)-H(7N)···N(12) hydrogen bonding in the crystal structure of $\mathbf{L_1}^1$.

The amide plane of the pivaloylamido unit in $\mathbf{L_1}^1$ is oriented in such a way as to optimise the interaction of its oxygen with the hydrogen atom in the adjacent position of the same pyridine ring, namely H5 (C(5)···O(8) 2.8174(16) Å, H(5A)···O(8) 2.22 Å, C(5)–H(5A)···O(8) 120° with C(5)–H(5A) fixed to 0.95 Å). In agreement with this suggestion is the small angle between the pyridine (N(2)C(2)C(3)C(4)C(5)C(6)) and amide (N(7)C(8)O(8)) planes, 11.4°. In this arrangement, the amide N-H is optimally pre-organised for the interaction with molecules '*cis*' to the pyridine N-atom once bound to a metal (*vide infra*).

2.2.3.2 Structure of $[(L_1{}^1)Zn](PF_6)_2 \cdot 0.5CH_3OH$

Single crystals suitable for X-ray diffraction were grown by slow evaporation of a solution of $[(\mathbf{L_1}^1)Zn](PF_6)_2$ in methanol/chloroform (1:1). The structure of the

cation is shown in Fig. 2.3 and selected distances and angles are given in Table 2.3. The zinc(II) centre is in a trigonal bipyramidal N4O environment with the three pyridine nitrogen atoms occupying the equatorial positions and the bridgehead nitrogen and amide oxygen in the axial positions. A related structure with the zinc(II) centre in a N2S2O co-ordination environment was reported recently.[6]

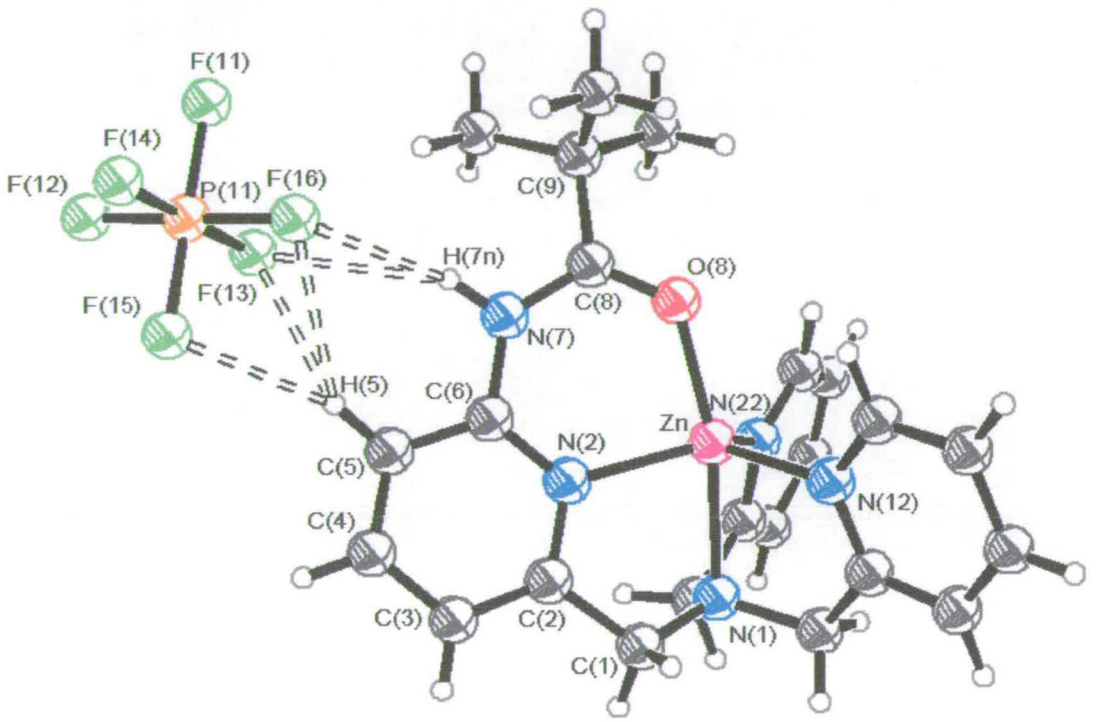

Fig. 2.3 An ORTEP plot drawn with 50 % probability thermal ellipsoids showing hydrogen bonding between the $[(\mathbf{L_1}^1)Zn]^{2+}$ cation and one of the PF_6^- anions in the crystal structure of $[(\mathbf{L_1}^1)Zn](PF_6)_2 \cdot 0.5CH_3OH$.

In $[(\mathbf{L_1}^1)Zn](PF_6)_2$, the zinc(II) ion sits slightly above the trigonal 'plane' resulting in acute N_{axial}–Zn–$N_{equatorial}$ angles of 80.12(7)°, 81.09(7)° and 80.01(7)°. The Zn–N_{py} distances are 2.060(2) Å, 2.023(2) Å and 2.027(2) Å, the longest corresponding to the substituted pyridine, presumably due to the electron-withdrawing effect of the pivaloylamido unit. The Zn–N_{amine} distance of 2.175(2) Å

is significantly longer than the Zn–N_{py} distances. The angle between the atoms located at the axial positions, N(1)–Zn–O(8) is 167.75(6)° and bent towards the substituted pyridine. This deviation from linearity and orientation presumably optimises co-ordination of the carbonyl group. The amide NH and the adjacent aromatic CH hydrogen bond to one of the PF_6^- molecules in a polyfurcated mode (Table 2.2, Fig. 2.3).

2.2.3.3 Structure of $[(L_1^1)Zn(Cl)](BPh_4)\cdot CH_3CN$

Single crystals suitable for X-ray diffraction were grown by slow evaporation of a solution of $[(L_1^1)Zn(Cl)](BPh_4)$ in CH_3CN/H_2O (1:1). The structure of the $[(L_1^1)Zn(Cl)]^+$ cation is shown in Fig. 2.4; selected distances and angles are given in Table 2.3.

As in $[(L_1^1)Zn](PF_6)_2$, the zinc(II) centre is in a trigonal bipyramidal environment ligated to the three pyridine nitrogen atoms in the trigonal plane, and to the bridgehead nitrogen of the tripodal ligand and a chloride ion in the axial positions. Coordination of the chloride dictates the positioning of the pivaloylamido group, which seeks to optimise N–H···Cl hydrogen bonding (N(7)···Cl 3.2127(19) Å; H(7N)···Cl 2.22 Å; N(7)–H(7N)···Cl 168° for a N(7)–H(7N) bond extended to 1.01 Å).[7] As a result of this, the angle between the pyridine plane (N(2)C(2)C(3)C(4)C(5)C(6)) and the plane containing the amide group (N(7)C(8)O(8)) is 31.5°. This arrangement of the amide group, however, still allows

some interaction between the carbonyl O-atom and H5, (C(5)···O(8) 2.83(3) Å, H(5A)···O(8) 2.34 Å, C(5)–H(5A)···O8 112° with C(5)–H(5A) fixed to 0.95 Å) although this is slightly weaker than in 'free' $\mathbf{L_1}^1$. As in $[(\mathbf{L_1}^1)Zn](PF_6)_2$, the longest $Zn–N_{equatorial}$ bond is made to the substituted pyridine. All Zn–N distances are longer than the corresponding ones in $[(\mathbf{L_1}^1)Zn](PF_6)_2$ and are in accordance with other $[(L)Zn(Cl)]^+$ cations,[8] which may reflect a combination of electronic and steric effects associated with coordinating the chloride ion at the axial position and the different arrangement of the pivaloylamido group. Thus, the zinc(II) centre in $[(\mathbf{L_1}^1)Zn(Cl)](BPh_4)$, which is part of a 1+ cation, should be more electron rich than in $[(\mathbf{L_1}^1)Zn](PF_6)_2$, in which it is part of a 2+ cation. Also, the fact that all $N_{axial}–Zn–N_{equatorial}$ angles, 78.02(5)°, 77.51(6)° and 77.75(6)°, are smaller than in $[(\mathbf{L_1}^1)Zn](PF_6)_2$ may be an indication of a more sterically demanding arrangement of the pivaloylamido group.

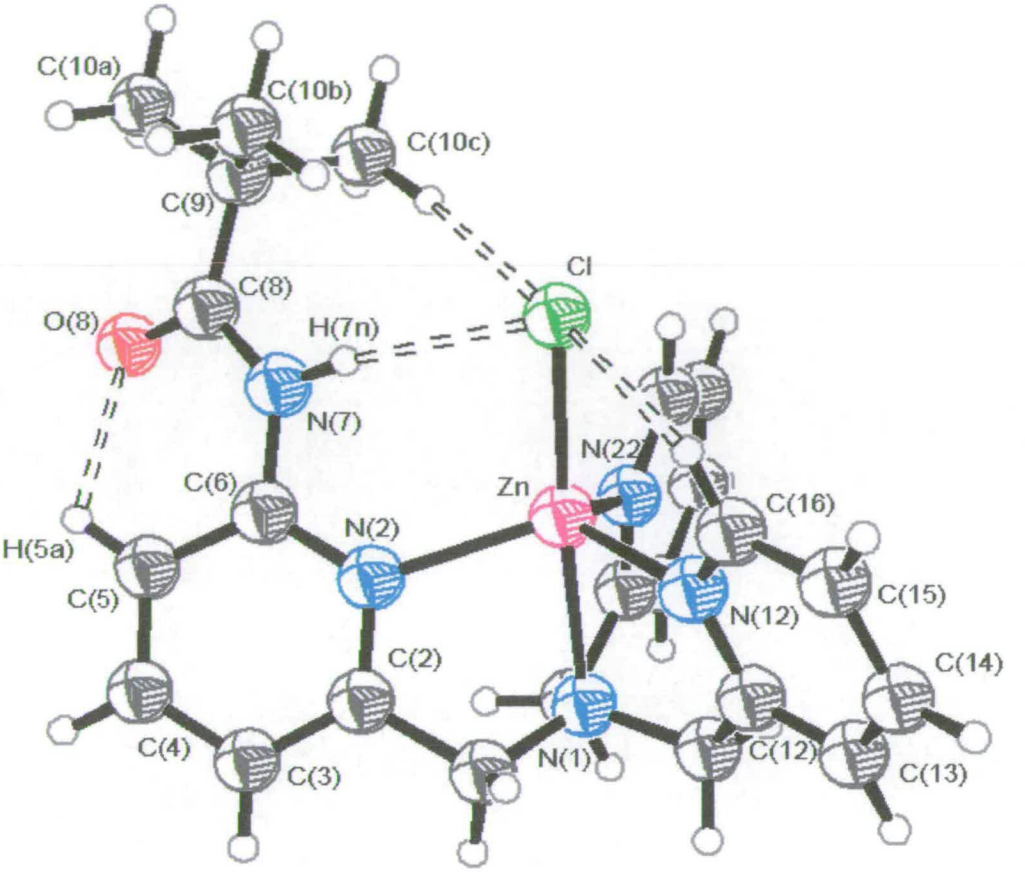

Fig. 2.4 An ORTEP plot drawn with 50% probability ellipsoids of the molecular structure of the $[(\mathbf{L_1}^1)Zn(Cl)]^+$ cation of $[(\mathbf{L_1}^1)Zn(Cl)](BPh_4)\cdot CH_3CN$.

Another interesting feature of the X-ray crystal structure of $[(\mathbf{L_1}^1)Zn(Cl)](BPh_4)$ is intramolecular C–H···Cl hydrogen bonding. The zinc-bound chloride interacts weakly with hydrogen atoms of the *tert*-butyl group and the *ortho* position (6-position) of the one of the pyridines (Table 2.2, Fig. 2.4). Interaction with the pyridine hydrogen atoms may be facilitated by the N_{amine}–Zn–Cl angle of 174.09(4)°, which is significantly more linear than the N_{amine}–Zn–O angle in $[(\mathbf{L_1}^1)Zn]^{2+}$ (167.75(6)°), bringing the coordinated chloride closer to the *ortho* (6-position) pyridine hydrogen atoms.

Thus, in $[(\mathbf{L_1}^1)Zn(Cl)](BPh_4)$, N-H···Cl, C-H···Cl and C-H···O hydrogen bonding seem to be in balance and in which N-H···Cl hydrogen bonding is the strongest. The subtle balance or competition of intermolecular interactions determines their relative strength.[9, 10]

2.2.3.4 Structure of $[(L_1^2)Zn(Cl)](BPh_4)\cdot 0.5CH_3CN$

A thermal ellipsoid plot of the X-ray crystal structure of $[(\mathbf{L_1}^2)Zn(Cl)](BPh_4)$ is shown in Fig. 2.5 and selected distances and angles are given in Table 2.3.

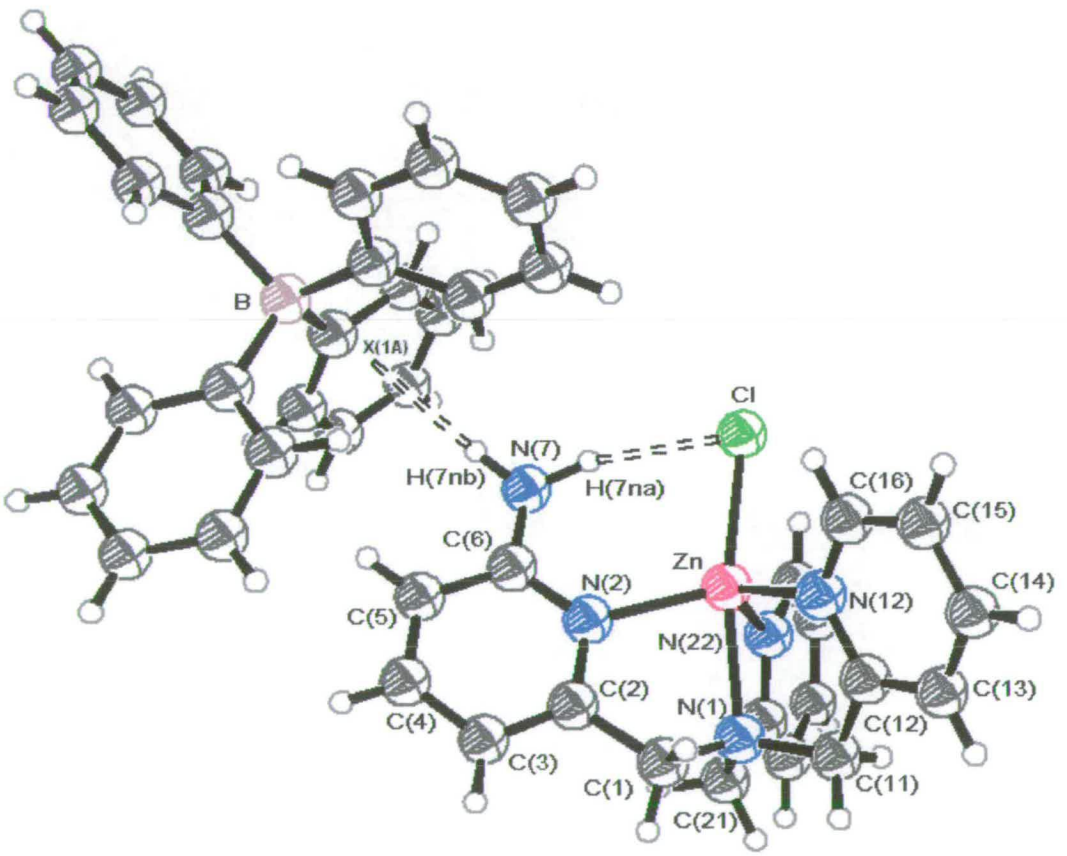

Fig. 2.5 Thermal ellipsoid plot drawn with 50% probability ellipsoids of $[(L_1^2)Zn(Cl)](BPh_4)$ of $[(L_1^2)Zn(Cl)](BPh_4)\cdot 0.5CH_3CN$ showing the internal N–H···Cl–Zn and external N–H···π hydrogen bonding.

As in $[(\mathbf{L_1}^1)Zn(Cl)](BPh_4)\cdot CH_3CN$, in $[(\mathbf{L_1}^2)Zn(Cl)](BPh_4)\cdot 0.5CH_3CN$ the zinc(II) centre is in a trigonal bipyramidal environment ligated to the three pyridine nitrogen atoms in the trigonal plane, and to the bridgehead nitrogen of the tripodal ligand and a chloride ion in the axial positions. The Zn–N distances are in accordance with other $[(L)Zn(Cl)]^+$ cations.[8, 11] In $[(\mathbf{L_1}^1)Zn(Cl)](BPh_4)\cdot CH_3CN$ the longest $Zn–N_{equatorial}$ bond was made to the substituted pyridine (Zn–N(2) 2.1351(15) Å) presumably due to the electron withdrawing donating effects of the pivaloylamido group. In contrast, in the case of $[(\mathbf{L_1}^2)Zn(Cl)](BPh_4)\cdot 0.5CH_3CN$ the shortest $Zn–N_{equatorial}$ distance corresponds to the substituted pyridine (Zn–N(2) 2.0704(19) Å) probably due to the electron donating effect of the amino groups. Another interesting feature of $[(\mathbf{L_1}^2)Zn(Cl)](BPh_4)\cdot 0.5CH_3CN$ is the participation of the amino group in internal N–H···Cl–Zn hydrogen bonding (Table 2.2) (N(7)···Cl 3.213(3) Å; H(7N)···Cl 2.24 Å; N(7)–H(7N)···Cl 160° for a N(7)–H(7N) bond extended to 1.01 Å) and external N–H···π hydrogen bonding (N(7)···X(1A) 3.26 Å, H(7NB)···X(1A) 2.26 Å, N(7)–H(7NB)···X(1A) 168°; Fig. 2.5) with a phenyl group of the BPh_4^- anion (X(1A) = Centroid of the phenyl ring) (Table 2.2).

Table 2.2 Geometric features of the main hydrogen bonding interactions in $\mathbf{L_1}^1$, $[(\mathbf{L_1}^1)Zn](PF_6)_2 \cdot 0.5CH_3OH$, $[(\mathbf{L_1}^1)Zn(Cl)](BPh_4)\cdot CH_3CN$ and $[(\mathbf{L_1}^2)Zn(Cl)](BPh_4)\cdot 0.5CH_3CN$.

	Interaction	D–H/Å	D···A/Å	H···A/Å	D–H···A/ °
$\mathbf{L_1}^1$					
	N(7)–H7N···N12^c	1.01^a	3.2720(15)	2.33	154.4
$[(\mathbf{L_1}^1)Zn](PF_6)_2\cdot 0.5CH_3OH$					
	N(7)–H(7N)···F(13)	1.01^a	3.472(3)	2.56	149.7
	N(7)–H(7N)···F(16)	1.01^a	3.310(2)	2.46	141.7
	C(5)–H(5)···F(13)	0.95^a	3.391(3)	2.59	142.2
	C(5)–H(5)···F(15)	0.95^a	3.257(3)	2.34	161.0
	C(5)–H(5)···F(16)	0.95^a	3.433(3)	2.65	140.1
$[(\mathbf{L_1}^1)Zn(Cl)](BPh_4)\cdot CH_3CN$					
	N(7)–H(7N)···Cl	1.01^b	3.2127(19)	2.22	167.7
	C(16)–H(16A)···Cl	0.95^a	3.348(2)	2.77	119.8
	C(26)–H(26A)···Cl	0.95^a	3.566(3)	2.98	120.9
	C(10C)–H(10H)···Cl	0.95^a	3.716(2)	2.80	156.0
$[(\mathbf{L_1}^2)Zn(Cl)](BPh_4)\cdot 0.5CH_3CN$					
	N(7)–H(7NA)···Cl	1.01^b	3.213(3)	2.24	160.4
	N(7)-H(7NB)···X(1A)	1.01^b	3.26	2.26	168.0

^{a} Fixed distance and calculated position. ^{b} Extended distance. ^{c} Generated applying the symmetry operation $-x$, $0.5 + y$, $0.5 - z$.

Table 2.3 Selected bond lengths (Å) and angles (°) for zinc(II) complexes $[(L_1^1)Zn](PF_6)_2 \cdot 0.5CH_3OH$, $[(L_1^1)Zn(Cl)](BPh_4) \cdot CH_3CN$ and $[(L_1^2)Zn(Cl)](BPh_4) \cdot 0.5CH_3CN$.

	$[(L_1^1)Zn](PF_6)_2 \cdot 0.5CH_3OH$	$[(L_1^1)Zn(Cl)](BPh_4) \cdot CH_3CN$	$[(L_1^2)Zn(Cl)](BPh_4) \cdot 0.5CH3CN$
Zn–N(2)	2.0590(18)	2.1351(15)	2.0704(19)
Zn–N(12)	2.0227(19)	2.0885(16)	2.1021(19)
Zn–N(22)	2.0272(19)	2.0651(17)	2.081(2)
Zn–N(1)	2.1750(18)	2.1990(15)	2.2247(18)
Zn–O(8)	2.0005(16)	N/A	N/A
Zn–Cl	N/A	2.2812(7)	2.2959(7)
N(2)–Zn–N(12)	118.08(8)	121.11(6)	113.26(7)
N(2)–Zn–N(22)	123.53(7)	109.84(6)	113.34(7)
N(12)–Zn–N(22)	110.12(8)	115.84(6)	120.25(7)
N(1)–Zn–N(2)	80.12(7)	78.02(5)	79.11(7)
N(1)–Zn–N(12)	81.09(7)	77.51(6)	76.54(7)
N(1)–Zn–N(22)	80.01(7)	77.75(6)	77.75(7)
N(1)–Zn–O(8)	167.75(6)	N/A	N/A
N(1)–Zn–Cl	N/A	174.09(4)	170.00(5)
O(8)–Zn–N(2)	88.59(7)	N/A	N/A
O(8)–Zn–N(12)	108.69(7)	N/A	N/A
O(8)–Zn–N(22)	102.67(7)	N/A	N/A
Cl–Zn–N(2)	N/A	106.20(4)	110.50(5)
Cl–Zn–N(12)	N/A	96.66(5)	96.55(6)
Cl–Zn–N(22)	N/A	104.24(5)	100.10(6)

2.2.4 NMR AND IR STUDIES

NMR and IR studies were used to probe the solution structures of L_1^1 and L_1^2 and the zinc(II) complexes ($[(L_1^1)Zn](PF_6)_2$, $[(L_1^1)Zn(Cl)](BPh_4)$ and $[(L_1^2)Zn(Cl)](BPh_4)$) in acetonitrile, and to correlate with the X-ray crystal structures.

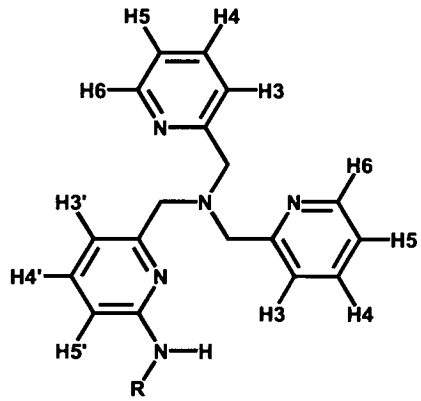

R = CO ^{t}But (L_1^1); H (L_1^2)

Scheme 2.6. Labelling scheme for L_1^1 and L_1^2.

2.2.4.1 6-Pivaloylamido-2-pyridylmethyl derivatives (L_1^1, $[(L_1^1)Zn](PF_6)_2$ and $[(L_1^1)Zn(Cl)](BPh_4)$)

^{1}H NMR studies of L_1^1 in CD_3CN reveal a downfield shift of the H5' resonance relative to H3', which is consistent with the retention of the C–H···O interaction in solution. In $[(L_1^1)Zn](PF_6)_2$ all the ^{1}H NMR resonances undergo a downfield shift relative to L_1^1, consistent with metal binding. A notable exception is the shift by 0.55 ppm upfield of H5' (Fig. 2.6, Table 2.4). This upfield proton chemical shift is consistent with breaking the C–H5'···O=C interaction. In $[(L_1^1)Zn(Cl)](BPh_4)$ most aromatic resonances are shifted upfield by 0.1–0.3 ppm compared to those in $[(L_1^1)Zn](PF_6)_2$, a feature consistent with a more electron rich zinc(II) centre in $[(L_1^1)Zn(Cl)](BPh_4)$. The notable exceptions, however, are H6, H5' and the N–H, which undergo large downfield shifts of *ca.* 0.4–1.2 ppm (Fig. 2.6, Table 2.4). These downfield shifts can be rationalised in terms of the N–H7···Cl–Zn,

C–H6···Cl–Zn and C–H5'···O=C hydrogen bonding interactions found in the X-ray crystal structure of $[(\mathbf{L_1}^1)Zn(Cl)](BPh_4)$ being retained in solution. It is particularly remarkable that the C–H···Cl hydrogen bonding interactions are retained in solution as to our knowledge these interactions have only been previously claimed in the solid state. It is also interesting that, despite being considered very weak, C–H···Cl–Zn interactions seem to be responsible for quite large downfield shifts of the proton resonances, *ca.* 0.46 ppm. The C–H···Cl–Zn hydrogen bonding in $[(\mathbf{L_1}^1)Zn(Cl)](BPh_4)$ seems to be strong enough to be retained even at high temperatures as suggested by variable temperature (20–50 °C) ^{1}H NMR studies. Thus, the chemical shift of the two H6 protons of $[(\mathbf{L_1}^1)Zn](PF_6)_2$, which are equivalent in solution, does not change upon heating to 50 °C (See Appendix, Fig. A1.1). In addition, the ^{13}C NMR spectra of $[(\mathbf{L_1}^1)Zn](PF_6)_2$ and $[(\mathbf{L_1}^1)Zn(Cl)](BPh_4)$ show carbonyl resonances at 185.7 and 178.9 ppm, respectively, which is indicative of the carbonyl group being co-ordinated to the zinc(II) centre in $[(\mathbf{L_1}^1)Zn](PF_6)_2$ but not in $[(\mathbf{L_1}^1)Zn(Cl)](BPh_4)$.

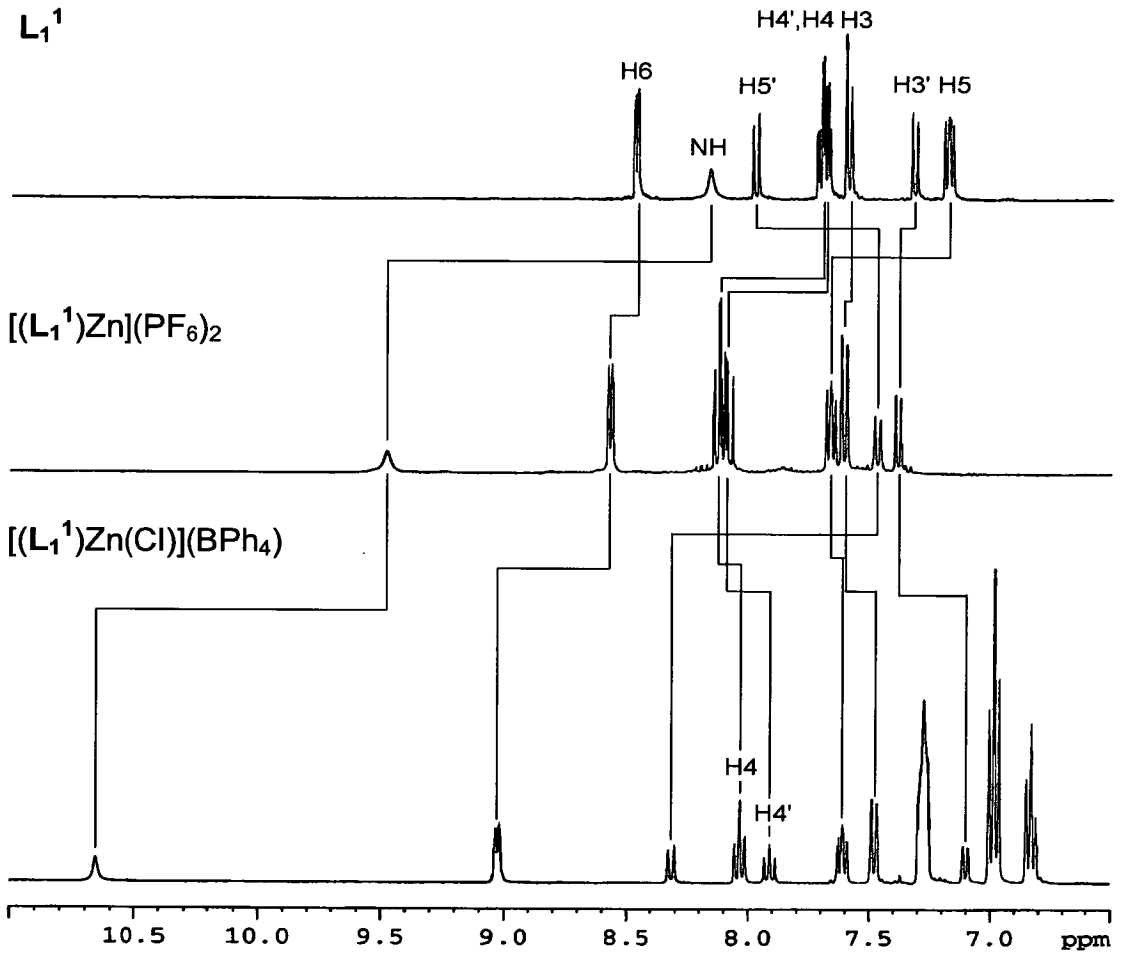

Fig. 2.6 Aromatic and NH region of the ^{1}H NMR spectrum (360.1 MHz, CD_3CN, 293 K) of $\mathbf{L_1}^1$ (top), $[(\mathbf{L_1}^1)Zn](PF_6)_2$ (middle) and $[(\mathbf{L_1}^1)Zn(Cl)](BPh_4)$ (bottom). See Table 2.4 for chemical shift values and Scheme 2.6 for labelling scheme explanation.

Table 2.4. Summary of ^{1}H NMR (360 MHz, CD_3CN, 293 K) chemical shift data for $\mathbf{L_1}^1$, $[(\mathbf{L_1}^1)Zn](PF_6)_2$ and $[(\mathbf{L_1}^1)Zn(Cl)](BPh_4)$.[a]

	$\mathbf{L_1}^1$	$[(\mathbf{L_1}^1)Zn](PF_6)_2$	$[(\mathbf{L_1}^1)Zn(Cl)](BPh_4)$
^{t}Bu			
H10	1.26	1.54 (+0.28)	1.37 (–0.17)
NH			
H7	8.16	9.48 (+1.32)	10.67 (+1.19)
$PyCH_2N$			
$H1'_{A,B}$	3.71	4.28 (+0.57)	4.03 (–0.25)
$H1_{A,B}$	3.79	4.32 (+0.53)	4.10 (–0.22)
py (aromatic)			
H3'	7.32	7.38 (+0.06)	7.12 (–0.26)
H4'	7.67	8.10 (+0.43)	7.92 (–0.18)
H5'	7.98	7.43 (–0.55)	8.32 (+0.89)
H3	7.60	7.61 (+0.01)	7.50 (–0.11)
H4	7.70	8.12 (+0.42)	8.05 (–0.07)
H5	7.18	7.67 (+0.49)	7.62 (–0.05)
H6	8.47	8.57 (+0.10)	9.03 (+0.46)

[a] Chemical shifts are in ppm relative to CH_3CN at 1.94 ppm. Values in parentheses denote chemical shifts downfield (positive) or upfield (negative) *versus* values in previous column. The symbol ' refers to the 2-pyridylmethyl with the 6-pivaloylamido group.

IR studies of $\mathbf{L_1}^1$, $[(\mathbf{L_1}^1)Zn](PF_6)_2$ and $[(\mathbf{L_1}^1)Zn(Cl)](BPh_4)$ are in total agreement with all the conclusions derived from NMR and X-ray studies. Thus, the IR spectra of $[(\mathbf{L_1}^1)Zn](PF_6)_2$ and $[(\mathbf{L_1}^1)Zn(Cl)](BPh_4)$ show $\nu_{C=O}$ bands shifted to higher wavenumbers by 75 ± 4 cm^{-1} in acetonitrile solutions and by 76 ± 4 cm^{-1} in the solid state on going from chloride co-ordination in $[(\mathbf{L_1}^1)Zn(Cl)](BPh_4)$ to amide co-ordination in $[(\mathbf{L_1}^1)Zn](PF_6)_2$ (Table 2.5). The N–H···Cl–Zn hydrogen bonding is reflected in the ν_{N-H} bands being shifted by 64 ± 4 cm^{-1} in acetonitrile solutions and by 135 ± 4 cm^{-1} in the solid state to lower wavenumbers. The difference between the strength of N–H···Cl–Zn hydrogen bonding in solution and the solid state may be due

to the balancing with C–H···O=C and C–H···Cl–Zn interactions, which would result from slight rotation of the amide group and adjustments in the position of the pyridine rings. Thus, the ν_{N-H} band in solution of the trigonal bipyramidal complex $[(\mathbf{L_1}^1)Zn(Cl)](BPh_4)$ is shifted to lower energy values by 174 ± 4 cm^{-1} relative to $\mathbf{L_1}^1$ (Table 2.6), which also indicates the formation of N-H···Cl-Zn interaction in solution. Hence, the magnitude of the downfield shifts experienced by the NH proton resonance (NMR), changes in the ν_{N-H} vibration (IR) and hydrogen bonding distances (X-ray diffraction) can be approximately correlated.

Table 2.5 Selected infrared vibrational data of $[(\mathbf{L_1}^1)Zn](PF_6)_2$ and $[(\mathbf{L_1}^1)Zn(Cl)](BPh_4)$.

	ν_{N-H} [a]/cm^{-1}	$\nu_{C=O}$ [a]/cm^{-1}
$[(\mathbf{L_1}^1)Zn](PF_6)_2$ (CH_3CN solution)	3328	1625
$[(\mathbf{L_1}^1)Zn(Cl)](BPh_4)$ (CH_3CN solution)	3264	1700
$([(\mathbf{L_1}^1)Zn(Cl)](BPh_4) - [(\mathbf{L_1}^1)Zn](PF_6)_2$	*(–64)*	*(75)*
$[(\mathbf{L_1}^1)Zn](PF_6)_2$ (solid state)	3390	1624
$[(\mathbf{L_1}^1)Zn(Cl)](BPh_4)$ (solid state)	3255	1700
$([(\mathbf{L_1}^1)Zn(Cl)](BPh_4) - [(\mathbf{L_1}^1)Zn](PF_6)_2$	*(–135)*	*(76)*

[a] ± 4 cm^{-1}.

Table 2.6. Selected infrared vibrational data of ligand $\mathbf{L_1}^1$ and complex $[(\mathbf{L_1}^1)Zn(Cl)](BPh_4)$ in acetonitrile solutions.

	ν_{N-H} [a]/cm^{-1}
$\mathbf{L_1}^1$	3438
$[(\mathbf{L_1}^1)Zn(Cl)](BPh_4)$	3264
(difference)	*(+174)*

[a] ± 4 cm^{-1}.

2.2.4.2 6-Amino-2-pyridylmethyl derivatives {L_1^2, [(L_1^2)Zn(Cl)](X) (X = BPh_4, Cl)}

The ^{1}H NMR spectra (360.1 MHz, CD_3CN, 293 K) of [($\mathbf{L_1}^2$)Zn(Cl)](BPh_4), [($\mathbf{L_1}^2$)Zn(Cl)](Cl) and $\mathbf{L_1}^2$ show broad singlets due to the NH_2 protons at 6.98, 7.02 and 4.80 ppm, respectively (Table 2.7 and Experimental Section). The large downfield shift experienced by the amine proton resonance of [($\mathbf{L_1}^2$)Zn(Cl)](BPh_4) or [($\mathbf{L_1}^2$)Zn(Cl)](Cl) relative to $\mathbf{L_1}^2$ of *ca.* 2.2 ppm is consistent with the formation of internal N–H···Cl–Zn hydrogen bonding in solution and it is comparable to the downfield shift experienced by the amide NH proton of [($\mathbf{L_1}^1$)Zn(Cl)](BPh_4) relative to $\mathbf{L_1}^1$ (2.51 ppm). The X-ray structure of [($\mathbf{L_1}^2$)Zn(Cl)](BPh_4) also shows a very short external N–H···π hydrogen bond with a phenyl group of the BPh_4^- anion (Fig. 2.5). Concentration-dependent experiments, however, suggest that this interaction is not formed in solution.[12]

Table 2.7. Summary of selected ^{1}H NMR (360 MHz, CD_3CN, 293 K) chemical shift data for ligands $\mathbf{L_1}^1$, $\mathbf{L_1}^2$ and complexes [($\mathbf{L_1}^1$)Zn(Cl)](BPh_4), [($\mathbf{L_1}^2$)Zn(Cl)](BPh_4).[a]

	$\mathbf{L_1}^1$	[($\mathbf{L_1}^1$)Zn(Cl)](BPh_4)	$\mathbf{L_1}^2$	[($\mathbf{L_1}^2$)Zn(Cl)](BPh_4)
tBu				
H10	1.26	1.37 (+0.11)	N/A	N/A
NH				
H7	8.16	10.67 (+2.51)	4.8	6.98 (+2.18)
PyCH_2N				
H1'A, B	3.71	4.03 (+0.32)	3.6	3.8 (+0.2)
Py (aromatic)				
H3'	7.32	7.12 (-0.20)	6.82	6.58 (+0.24)
H4'	7.67	7.92 (+0.25)	7.37	7.51 (+0.14)
H5'	7.98	8.32 (+0.34)	6.35	6.58 (+0.23)

[a] Chemical shifts are in ppm relative to CH_3CN at 1.94 ppm. Values in parentheses denote chemical shifts downfield (positive) or upfield (negative) versus values in the corresponding ligand. The symbol ' refers to the 2-pyridylmethyl with the 6-pivaloylamido or amino group.

2.3 CONCLUSIONS

This study has explored the use of N–H groups of the ligand unit (6-RNH-2-pyridylmethyl)amine as a strategy to induce internal hydrogen bonding to an adjacent metal-bound ligand in a trigonal bypiramidal geometry. The study involved a labile metal centre such as zinc(II), which is the most commonly used metal in natural metellonucleases.

Two ligands with a pivaloylamido group ($\mathbf{L_1}^1$) and an amino group ($\mathbf{L_1}^2$) were synthesised and fully characterised by ^{1}H and ^{13}C NMR, ESI-MS and elemental analysis. In addition, $\mathbf{L_1}^1$ was further characterised by X-ray crystallography.

$\mathbf{L_1}^1$ with the pivaloylamido group form zinc(II) complexes $[(\mathbf{L_1}^1)Zn(Cl)](Cl)$ and $[(\mathbf{L_1}^1)Zn(Cl)](BPh_4)$ with N4Cl coordination environment and internal N-H···Cl-Zn hydrogen bonding and $[(\mathbf{L_1}^1)Zn](PF_6)_2$, with N4O coordination environment. $\mathbf{L_1}^2$ with the amino group form zinc(II) complexes $[(\mathbf{L_1}^2)Zn(Cl)](Cl)$ and $[(\mathbf{L_1}^2)Zn(Cl)](BPh_4)$ with N4Cl coordination environment and internal N-H···Cl-Zn hydrogen bonding and a variety of external hydrogen bonding.

The X-ray diffraction crystal structures of trigonal bipyramidal zinc(II) complexes with N_4O coordination environment ($[(\mathbf{L_1}^1)Zn](PF_6)_2$) and N_4Cl coordination environment ($[(\mathbf{L_1}^1)Zn(Cl)](BPh_4)$ and $[(\mathbf{L_1}^2)Zn(Cl)](BPh_4)$) were reported. Thus, the molecular structure of $[(\mathbf{L_1}^1)Zn](PF_6)_2$ shows coordination of the amide oxygen to the metal centre. NMR and IR studies also confirm that this

interaction is retained in solution. This is obviously a disadvantage in our research as there will always be a competition between external ligand(s) coordination and the chelate effect-favoured amide oxygen coordination. However, $[(\mathbf{L_1}^1)Zn](PF_6)_2$ and related complexes are useful models for assessing the effectiveness of the carbonyl mechanism proposed for peptidases.[13-15]

Another important aspect was to correlate the information extracted from X-ray studies with structural and spectroscopic studies in solution. We have used $\mathbf{L_1}^1$, $\mathbf{L_1}^2$ and its complexes $[(\mathbf{L_1}^1)Zn](PF_6)_2$, $[(\mathbf{L_1}^1)Zn(Cl)](BPh_4)$, $[(\mathbf{L_1}^2)Zn(Cl)](BPh_4)$ and $[(\mathbf{L_1}^2)Zn(Cl)](Cl)$ as models to provide good evidence that all structural features found in the solid state structures, except a very short intermolecular external N-H···π (arene) hydrogen bonding in $[(\mathbf{L_1}^2)Zn(Cl)](BPh_4)$, are retained in solution and are clearly expressed in the ^1H, ^{13}C NMR and IR spectra of these compounds. This work reveals the characteristic ^1H NMR signatures of two possible arrangements of the pivaloylamido unit in $\mathbf{L_1}^1$ and its complexes $[(\mathbf{L_1}^1)Zn](PF_6)_2$ and $[(\mathbf{L_1}^1)Zn(Cl)](BPh_4)$, which can be used as a diagnostic tool for postulating the structures of ligands with a 6-(amidopyridinemethyl)amine unit. We also report that C–H···Cl–Zn hydrogen bonding in $[(\mathbf{L_1}^1)Zn](PF_6)_2$ results in large proton chemical shift changes. C–H···Cl–M (M = transition metal) hydrogen bonding has received considerable attention.[9, 16-18] This study provides what is to our knowledge the first experimental evidence that these interactions can be retained in solution.

There is considerable current interest in elucidating the role(s) of second-sphere hydrogen bonding to metal-bound species in metallohydrolases, oxidases and peroxidases using small-molecule models.[19] In this chapter we have shown that the use of the ligand unit (6-RNH-2-pyridylmethyl)amine in **tpa**-based ligands is a good strategy to induce internal hydrogen bonding to an adjacent metal-bound ligand in a trigonal bipyramidal geometry.

2.4 EXPERIMENTAL

2.4.1 MATERIALS AND METHODS

Reagents were obtained from commercial sources and used as received unless otherwise noted. Solvents were dried and purified under N_2 by using standard methods[20] and were distilled immediately before use. All compounds were prepared under N_2 unless otherwise mentioned. The tripodal ligands **tpa** and $\mathbf{L_1}$[1,2] were prepared adapting a literature procedure.[1, 3] The NMR spectra were obtained using a Bruker DPX 360 spectrometer at 20°C in CD_3CN unless otherwise noted. ^{13}C and ^1H chemical shifts are referenced with respect to the carbon (δ_C 1.32 and 118.26 ppm) and residual proton (δ_H 1.94 ppm) solvent peaks. Peak assignments are done with the aid of 2-D NMR spectroscopy. Mass spectra were performed on a Micromass Platform II system operating in flow injection analysis mode with the electrospray method. Elemental analyses were carried out by the microanalyses service provided by the School of Chemistry at the University of Edinburgh. Infrared spectra were recorded with a JASCO FTIR-410 spectrometer between 4000 and 250 cm^{-1} as KBr pellets (solid state) or as dry acetonitrile solutions in KBr cells.

2.4.2 SYNTHESIS OF LIGANDS

***N*,*N*-Bis(2-pyridylmethyl)-*N*-(6-pivaloylamido-2-pyridylmethyl)amine ($\mathbf{L_1}$[1]).**

2-(Pivaloylamido)-6-(aminomethyl)pyridine[3] (7 g, 34 mmol) and 2-picolyl chloride (11 g, 68 mmol) were dissolved in acetonitrile (100 cm^3) and stirred at room

temperature for 5 minutes. Then, sodium carbonate (36.4 g, 0.34 mol) was added and the temperature was raised to 44 °C. After 48 h the solution was cooled to room temperature and poured into 200 cm^3 of 1 M $NaOH_{(aq)}$. The crude product was then extracted with dichloromethane (3 × 80 cm^3) and the organic fractions were dried over Na_2SO_4. The solvent was evaporated under vacuum to yield the crude product as a brown oil. The crude material was recrystallised from diethyl ether (100 cm^3) to yield the pure product as a dark red solid (7.6 g, 59 %) (Found: C, 70.89; H, 6.95; N, 17.86. Calc. for $C_{23}H_{27}N_5O$: C, 70.92; H, 6.99; N, 17.89 %).

^{1}H NMR (CD_3CN, 360.1 MHz) δ_H (ppm) 8.47 (dd, J = 4.9, 1.9 Hz, 2H, py-*H*6), 8.16 (s, 1H, N*H*), 7.98 (t, J = 8.2 Hz, 1H, py'-*H*5), 7.70 (td, J = 7.7 and 1.8 Hz, 2H, py-*H*5), 7.69 (t, J = 7.8 Hz, 1H, py'-*H*4), 7.60 (d, J = 7.7 Hz, 2H, py-*H*3), 7.32 (d, J = 7.3 Hz, 1H, py'-*H*3), 7.18 (ddd, J = 7.5, 4.9, 1.1 Hz, 2H, py-*H*5), 3.79 (s, 4H, NCH_2-py), 3.71 (s, 2H, NCH_2-py'), 1.26 (s, 9H, C–(CH_3)$_3$). ^{13}C NMR (CD_3CN, 90.5 MHz) δ_C (ppm) 176.4 (*C*=O), 159.0 (py-*C*2), 157.7 and 150.6 (py'-*C*2 and py'-*C*6), 148.3 (py-*C*6), 138.0 (py'-*C*3), 135.8 (py-*C*3), 122.2 and 121.5 (py-*C*4 and py-*C*5), 117.8 and 111.0 (py'-*C*4 and py'-*C*5), 59.3 (N*C*H_2-py), 59.0 (N*C*H_2-py'), 38.8 (*C*–(CH$_3$)$_3$), 25.9 (C–(*C*H$_3$)$_3$). ESI-MS (+ion) Found 390.3 (100 %), Calcd. 390.23 (100 %) for [($\mathbf{L_1}^1$)H]$^+$, and matches theoretical isotope distribution. IR (KBr, cm^{-1}) ν(NH) 3438.

_N,N_-Bis(2-pyridylmethyl)-_N_-(6-amino-2-pyridylmethyl)amine $\mathbf{L_1}^2$.

$\mathbf{L_1}^1$ (4 g, 10.3 mmol) was dissolved in 2 M $HCl_{(aq)}$ (150 cm^3) and the solution was refluxed for 24 h. The solution was then poured into 1 M $NaOH_{(aq)}$. The product was

extracted with dichloromethane (3 × 100 cm^3) and the organic fractions were dried over Na_2SO_4. The solvent was evaporated under vacuum and washed with diethyl ether to yield the product as a brown oil (3 g, 96.3 %) (Found: C, 70.80; H, 6.29; N, 22.79. Calc. for $C_{18}H_{19}N_5$: C, 70.80; H, 6.27; N, 22.93%).

^{1}H NMR (CD_3CN, 360.1 MHz): δ_H (ppm) 8.46 (m, 2H, py-*H*6), 7.68 (td, J = 7.92, 1.8 Hz, 2H py-*H*4), 7.58 (d, J = 7.9 Hz, 2H, py-*H*3), 7.37 (dd, J = 8.2, 7.5 Hz, 1H, py'-*H*4), 7.16 (m, 2H, py-*H*5), 6.82 (d, J = 7.5 Hz, 1H, py'-*H*3), 6.35 (d, J = 8.2 Hz, 1H, py'-*H*5), 4.8 (br, 2H, py'-NH_2) 3.8 (s, 4H, NCH_2-py), 3.6 (s, 2H, NCH_2-py'). ^{13}C NMR (CD_3CN, 90.5 MHz): δ_C (ppm) 160.9 (py-C2), 160.0 and 159.0 (py'-C2 and py'-C6), 149.9 (py-C6), 138.8 (py'-C3), 137.3 (py-C3), 123.9 and 123.0 (py-C4 and py-C5), 112.9 and 107.3 (py'-C4 and py'-C5), 61.0 (N*C*H_2-py and N*C*H_2-py'). ESI-MS (+ ion): Found 306.1 (100 %). Calc. 306.0 (100 %) for $[(L_1^2)H]^+$, and matches theoretical isotope distribution.

2.4.3 SYNTHESIS OF Zn(II) COMPLEXES

$[(L_1^1)Zn](PF_6)_2$

$ZnCl_2$ (170 mg, 1.290 mmol) and $AgPF_6$ (650 mg, 2.580 mmol) were dissolved in dry acetonitrile (60 cm^3) and the solution was stirred for 1 h resulting in the appearance of a white precipitate, AgCl, which was removed by filtration. L_1^1 (500 mg, 1.290 mmol) was then added and the mixture was allowed to react for 12 h at room temperature. The solution was centrifuged and the solvent evaporated under

vacuum to yield the product as a yellow solid (770 mg, 80%) (Found: C, 36.83; H, 3.54; N, 9.21. Calc. for $C_{23}H_{27}N_5OZnP_2F_{12}$: C, 37.09; H, 3.65; N, 9.40 %).

^{1}H NMR (CD_3CN, 360.1 MHz) δ_H (ppm) 9.48 (br s, 1H, N*H*), 8.57 (dd, J = 5.4, 1.7 Hz, 2H, py-*H*6), 8.12 (td, *J* = 7.7, 1.7 Hz, 2H, py-*H*4), 8.10 (dd, *J* = 8.0, 7.7 Hz, 1H, py'-*H*4), 7.67 (dd, *J* = 8.0, 5.4 Hz, 2H, py-*H*5), 7.61 (d, *J* = 7.8 Hz, 2H, py-*H*3), 7.43 (d, *J* = 8.0 Hz, 1H, py'-*H*5), 7.38 (d, *J* = 7.7 Hz, 1H, py'-*H*3), 4.32 (s, 4H, NCH_2-py), 4.21 (s, 2H, NCH_2-py'), 1.54 (s, 9H, C–(CH_3)$_3$). ^{13}C NMR (CD_3CN, 90.5 MHz, 298 K) δ_C (ppm) 185.7 (*C*=O) 159.4 (py-*C*2) 158.5 and 157.5 (py'-*C*2 and py'-*C*6), 147.9 (py-*C*6), 143.1 (py'-*C*3), 141.5 (py-*C*3), 125.0 and 124.4 (py-*C*4 and py-*C*5), 120.8 and 115.7 (py'-*C*4 and py'-*C*5), 56.8 (N*C*H_2-py), 56.5 (N*C*H_2-py'), 41.2 (*C*–(CH$_3$)$_3$), 25.7 (C-(*C*H$_3$)$_3$). ESI-MS (+ ion) Found 226.6 (100 %), Calcd. 226.57 for $[(\mathbf{L_1}^1)Zn]^{2+}$, and matches theoretical isotope distribution. IR (KBr, cm^{-1}) ν(NH) 3390, ν(CO) 1624.

$[(\mathbf{L_1}^1)Zn(Cl)](Cl)$

$\mathbf{L_1}^1$ (0.25g, 0.6 mmol) and $ZnCl_2$ (0.08g, 0.6 mmol) were dissolved in dry acetonitrile (15 cm^3). The solution was stirred for 20 h at room temperature. The solvent was then evaporated under vacuum to yield a grey solid (0.27 g, 87 %) (Found: C, 52.00; H, 5.11; N, 13.20. Calc. for $C_{23}H_{27}N_5OZnCl_2$: C, 52.54; H, 5.18; N, 13.32 %).

^{1}H NMR (CD_3CN, 360.1 MHz) δ_H (ppm) 9.77 (s, 1H, N*H*), 8.93 (d, *J* = 5.4 Hz, 2H, py-*H*6), 7.85 (td, *J* = 7.6, 1.7 Hz, 1H, py-*H*4), 7.83 (d, *J* = 8.4 Hz, 2H, py'-*H*5), 7.44

(t, J = 7.7 Hz, 1H, py'-*H*4), 7.41 (dd, J = 7.1, 5 Hz, 2H, py-*H*5), 7.35 (d, J = 7.9 Hz, 2H, py-*H*3), 6.85 (d, 7.4 Hz, 1H, py'-*H*3), 4.5–4.2 (br, 4H, NCH_2-py), 3.8 (s, 2H, NCH_2-py'), 1.39 (s, 9H, C–(CH_3)$_3$); ^{13}C NMR (CD_3CN, 90.5 MHz, 298 K) δ_C (ppm) 178.1 (*C*=O), 154.7 (py-*C*2) 153.0 and 152.9 (py'-*C*2 and py'-*C*6), 147.7 (py-*C*6), 139.7 (py'-*C*3), 140.2 (py-*C*3), 124.5 and 124.4 (py-*C*4 and py-*C*5), 120.0 and 114.7 (py'-*C*4 and py'-*C*5), 59.3 (N*C*H_2-py), 59.3 (N*C*H_2-py'), 40.2 (*C*–(CH$_3$)$_3$), 27.0 (C–(*C*H$_3$)$_3$). ESI-MS (+ ion) Found 488.2 (100 %), Calcd. 488.12 (100 %) for [(**L$_1$**^{1})Zn(Cl)]$^+$, and matches theoretical isotope distribution.

[(L$_1$^{1})Zn(Cl)](BPh$_4$)

[(**L$_1$**^{1})Zn(Cl)](Cl) (0.10 g, 0.2 mmol) was dissolved in methanol (5 cm^3). $NaBPh_4$ (0.07 g, 0.2 mmol) was then added and the solution was stirred for 2 h. The white precipitate thus formed was collected by filtration, washed with diethyl ether (2 cm^3), and dried under vacuum (0.11 g, 69 %) (Found: C, 68.90; H, 5.80; N, 9.65. Calc. for $C_{48}H_{80}BClN_6OZnCl$, [(**L$_1$**^{1})Zn(Cl)](Cl)·CH_3CN: C, 69.19; H, 5.92; N, 9.88 %).

^{1}H NMR (CD_3CN, 360.1 MHz) δ_H (ppm) [(**L$_1$**^{1})Zn(Cl)]$^+$ 10.67 (s, 1H, N*H*), 9.03 (d, J = 4.9 Hz, 2H, py-*H*6), 8.32 (d, J = 8.5 Hz, 1H, py'-*H*5), 8.05 (td, J = 7.7 and 1.6 Hz, 2H, py-*H*4), 7.92 (t, J = 7.9 Hz, 1H, py'-*H*4), 7.62 (t, J = 6.3 Hz, 2H, py-*H*5), 7.50 (d, J = 7.8 Hz, 2H, py-*H*3), 7.12 (d, 7.5 Hz, 1H, py'-*H*3), 4.10 (s, 4H, NCH_2-py), 4.03 (s, 2H, NCH_2-py'), 1.37 (s, 9H, C–(CH_3)$_3$); BPh_4^- 7.28 (m, 8H, Ar-*H*2), 6.98 (t, J = 7.5 Hz, 8H, Ar-*H*3) and 6.83 (t, J = 7.2 Hz, Ar-*H*4). ^{13}C NMR (CD_3CN, 62.9 MHz, 298 K) δ_C (ppm); [(**L$_1$**^{1})Zn(Cl)]$^+$ 178.9 (*C*=O), 155.6 (py-*C*2), 154.9 (py'-

*C*2), 154.2 (py'-*C*6), 149.5 (py-*C*6), 143.0 (py'-*C*3), 142.4 (py-*C*3), 126.1 (py-*C*4), 125.6 (py-*C*5), 120.3 (py'-*C*4), 118.3 (py'-*C*5), 57.6 (N*C*H_2-py), 56.8 (N*C*H_2-py'), 41.2 (*C*–$(CH_3)_3$) and 27.3 (C-(CH_3)$_3$); BPh_4^- 164.7 (B-*C*1, J_{B-C} = 49.6 Hz), 136.7 (*C*2), 126.6 (*C*3), 122.7 (*C*4). ESI-MS (+ ion) Found 488.2 (100 %), Calcd. 488.12 (100 %) for $[(\mathbf{L_1}^1)Zn(Cl)]^+$, and matches theoretical isotope distribution. IR (KBr, cm^{-1}) ν(NH) 3255, ν(CO) 1700.

$[(\mathbf{L_1}^2)Zn(Cl)](Cl)$

$\mathbf{L_1}^2$ (0.25 g, 0.8 mmol) and $ZnCl_2$ (0.11 g, 0.8 mmol) were dissolved in dry acetonitrile (10 cm^3). The solution was stirred for 1 h at room temperature. The solution was filtered and the filtrate was evaporated under vacuum to yield the crude material as a yellow solid. Addition of dry diethyl ether (10 cm^3) to the crude material formed a white precipitate. The white precipitate was re-dissolved in dry acetonitrile (10 cm^3) and filtered through Celite. The solvent was removed under vacuum to yield a white solid (0.09 g, 26 %).

^{1}H NMR (CD_3CN, 360.1 MHz): δ_H (ppm) 9.03 (d, J = 5.1 Hz, 2H, py-*H*6), 7.96 (td, J = 8.0, 1.8 Hz, 2H py-*H*4), 7.52 (t, J = 6.8 Hz, 1H, py-*H*5), 7.44 (d, J = 7.9 Hz, 2*H*, py-*H*3), 7.39 (t, J = 7.9 Hz, 1H, py'-*H*4), 7.16 (br, 2H, py'-NH_2), 6.66 (d, J = 8.2 Hz, 1H, py'-*H*3), 6.55 (d, J = 7.2 Hz, 1H, py'-*H*5), 4.13 (s, 4H, N*C*H_2-py), 3.9 (s, 2H, N*C*H_2-py'). ^{13}C NMR (CD_3CN, 90.5 MHz): δ_C (ppm) 162.0 and 151.9 (py'-*C*2 and py'-*C*6), 155.7 and 149.4 (py-*C*2 and py-*C*6), 141.4 (py-*C*3), 141.0 (py'-*C*3), 125.5 and 125.1 (py-*C*4 and py-*C*5), 112.3 and 112.2 (py'-*C*4 and py'-*C*5), 58.4 (N*C*H_2-

py') and 57.4(NCH_2-py). ESI-MS (+ ion): Found 404.2 (100 %), Calc. 404.1 (100 %) for $[(\mathbf{L_1}^2)Zn(Cl)]^+$, and matches theoretical isotope distribution.

$[(\mathbf{L_1}^2)Zn(Cl)](BPh_4)$

$[(\mathbf{L_1}^2)Zn(Cl)](Cl)$ (0.09 g, 0.2 mmol) was dissolved in methanol (5 cm^3). $NaBPh_4$ (0.07 g, 0.2 mmol) was then added and the solution was stirred for 2 h. The white precipitate formed was collected by filtration, washed with ether (2 cm^3), and dried under vacuum (0.10 g, 69 %) (Found: C, 68.69; H, 5.41; N, 10.03. Calc. for $C_{44}H_{39}BClN_5Zn$, $[(\mathbf{L_1}^2)Zn(Cl)](BPh_4)\cdot 0.5CH_3CN$: C, 69.23; H, 5.47; N, 10.33 %).

^{1}H NMR (CD_3CN, 360.1 MHz): δ_H (ppm) $[(\mathbf{L_1}^2)Zn(Cl)]^+$ 9.08 (d, J = 5.4 Hz, 2H, py-*H*6), 8.03 (td, J = 7.6, 1.5 Hz, 2H py-*H*4), 7.61 (t, J = 6.1 Hz, 1H, py-*H*5), 7.51 (dd, J = 8.3, 7.2 Hz, 2H, py'-*H*4), 7.48 (d, J = 7.5 Hz, 1H, py-*H*3), 6.98 (br, py'-NH_2), 6.58 (t, J = 7.9 Hz, 2H, py'-*H*3 and py'-*H*5), 4.06 (s, 4H, NCH_2-py), 3.80 (s, 2H, NCH_2-py'); BPh_4^- 7.27 (m, 8H, Ar-*H*2), 6.98 (t, J = 7.5 Hz, 8H, Ar-*H*3) and 6.83 (t, J = 7.2 Hz, Ar-*H*4). ^{13}C NMR (CD_3CN, 90.5 MHz, 298 K): δ_C (ppm) $[(\mathbf{L_1}^2)Zn(Cl)]^+$ 162.1 and 152.1 (py'-*C*2 and py'-*C*6), 155.8 and 149.7 (py-*C*2 and py-*C*6), 142.1 (py-*C*3), 141.8 (py'-*C*3), 125.9 and 125.5 (py-*C*4 and py-*C*5), 112.8 and 112.6 (py'-*C*4 and py'-*C*5), 57.3 (NCH_2-py'), 56.5 (NCH_2-py); BPh_4^- 164.6 (B-C1, J_{B-C} = 34.2 Hz), 136.6 (*C*2), 126.5 (*C*3), 122.7 (*C*4). ESI-MS (+ ion): Found 404.0 (100 %), Calc. 404.1 (100 %) for $[(\mathbf{L_1}^2)Zn(Cl)]^+$, and matches theoretical isotope distribution.

2.4.4 X-RAY CRYSTALLOGRAPHY

Crystals suitable for X-ray diffraction studies were grown by slow evaporation of $\mathbf{L_1}^1$ in diethyl ether; $[(\mathbf{L_1}^1)Zn](PF_6)_2$ in methanol/chloroform (1:1); $[(\mathbf{L_1}^1)Zn(Cl)](BPh_4)$ and $[(\mathbf{L_1}^2)Zn(Cl)](BPh_4)$ in acetonitrile/water (1:1) at room temperature.

Intensity data for $\mathbf{L_1}^1$ and $[(\mathbf{L_1}^1)Zn(Cl)](BPh_4)\cdot CH_3CN$ were collected at 150 K using a Bruker AXS SMART APEX area detector diffractometer with graphite-monochromated Mo-Kα radiation (λ = 0.71073 Å). The structures were solved by direct methods and refined to convergence against F^2 data using the SHELXTL suite of programs.[21] Data were corrected for absorption applying empirical methods using the program SADABS,[22, 23] and the structures were checked for higher symmetry using the program PLATON.[24] All non-hydrogen atoms were refined anisotropically; hydrogen atoms were placed in idealised positions and treated using a riding model with fixed isotropic displacement parameters. In $[(\mathbf{L_1}^1)Zn(Cl)](BPh_4)\cdot CH_3CN$ the N–H hydrogen was located in the difference map and refined isotropically.
CCDC reference numbers 203672-203673

Intensity data for $[(\mathbf{L_1}^1)Zn](PF_6)_2\cdot 0.5CH_3OH$ was collected at 150 K on a Stoe Stadi-4 diffractometer operating with Cu-Kα radiation (λ = 1.54184 Å). A face-indexed absorption correction was applied following optimisation of the crystal habit against a set of Ψ-scans (Stoe XSHAPE).[25] The structure was solved by direct methods, and refined by full-matrix least squares against F^2. All non-hydrogen atoms were refined with anisotropic displacement parameters with hydrogen atoms placed in idealised

positions. Although the fluorine atoms which form part of the PF_6^- anions adopt rather large anisotropic displacement parameters, they are not unreasonably so, and an ordered model is presented here. It was clear from electron density difference maps that the structure contained a small region of disordered solvent, probably methanol, based around a crystallographic inversion centre. This region was treated in the manner described by Van der Sluis and Spek.[26] It comprises 9.25 e^- per formula unit, which equates to approximately 0.5 methanol molecules; the values of $F(000)$, μ, density, *etc.* have been calculated on the basis of this assumption.

CCDC reference number 203674.

Intensity data for $[(\mathbf{L_1}^2)Zn(Cl)](BPh_4)\cdot 0.5CH_3CN$ was collected at 150 K using a Bruker-AXS SMART APEX area detector diffractometer with graphite-monochromated Mo-Kα radiation (λ = 0.71073 Å). The structure was solved by Patterson methods using the program DIRDIF-99[27] and refined to convergence against F^2 data using the SHELXTL suite of programs.[21] Data were corrected for absorption applying empirical methods using the program SADABS,[22, 23] and the structures were checked for higher symmetry using the program PLATON.[24] All non-hydrogen atoms were refined anisotropically unless otherwise noted. Hydrogen atoms were placed in idealised positions and refined using a riding model with fixed isotropic displacement parameters. The N–H hydrogens were located in the difference map and refined isotropically. Difference maps of the crystal structure of revealed the presence of a region of disordered solvent, which was modelled as a molecule of acetonitrile disordered over an inversion centre.

CCDC reference number 205581.

2.5 REFERENCES

(1) G. Anderegg and F. Wenk, *Helv. Chim. Acta*, 1967, **50**, 2330.

(2) M. Harata, K. Jitsukawa, H. Masuda and H. Einaga, *J. Am. Chem. Soc.*, 1994, **116**, 10817.

(3) L. M. Berreau, S. Mahapatra, J. A. Halfen, V. G. Young, Jr. and W. B. Tolman, *Inorg. Chem.*, 1996, **35**, 6339.

(4) A. Wada, Y. Honda, S. Yamaguchi, S. Nagatomo, T. Kitagawa, K. Jitsukawa and H. Masuda, *Inorg. Chem.*, 2004, **43(18)**, 5725.

(5) C. K. Johnson, 'ORTEP II', Oak Ridge National Laboratory, Oak Ridge, TN, 1976.

(6) L. M. Berreau, M. M. Makowska-Grzyska and A. M. Arif, *Inorg. Chem.*, 2000, **39**, 4390.

(7) F. H. Allen, O. Kennard, D. G. Watson, L. Brammer, A. G. Orpen and R. Taylor, *Journal of the Chemical Society, Perkin Transactions 2: Physical Organic Chemistry (1972-1999)*, 1987, S1.

(8) H. Adams, N. A. Bailey, D. E. Fenton and Q.-Y. He, *J. Chem. Soc., Dalton Trans.*, 1997, 1533.

(9) J. C. Mareque Rivas and L. Brammer, *Inorg. Chem.*, 1998, **37**, 4756.

(10) J. C. Mareque Rivas and L. Brammer, *Coord. Chem. Rev.*, 1999, **183**, 43.

(11) C. S. Allen, C. L. Chuang, M. Cornebise and J. W. Canary, *Inorg. Chim. Acta*, 1995, **239**, 29.

(12) See next chapter and Appendix 1

(13) B. L. Vallee and D. S. Auld, *Proc. Natl. Acad. Sci. U. S. A.*, 1990, **87**, 220.

(14) J. C. Mareque Rivas, R. Torres Martín de Rosales and S. Parsons, *Dalton Trans.*, 2003, 2156.

(15) J. C. Mareque Rivas, E. Salvagni, R. Prabaharan, R. Torres Martín de Rosales and S. Parsons, *Dalton Trans.*, 2004, 172.

(16) G. Aullon, D. Bellamy, G. A. Orpen, L. Brammer and E. A. Bruton, *Chemical Communications*, 1998, 653.

(17) A. L. Gillon, G. R. Lewis, A. G. Orpen, S. Rotter, J. Starbuck, X. Wang, Y. Rodríguez-Martín and C. Ruiz-Perez, *Dalton Trans.*, 2000, 3897.

(18) L. Brammer, J. K. Swearingen, E. A. Bruton and P. Sherwood, *Proc. Natl. Acad. Sci. U. S. A.*, 2002, **99**, 4956.

(19) (*a*) R. Krämer, *Coord. Chem. Rev.*, 1999, **182**, 243; (*b*) D. K. Garner, S. B. Fitch, L. H. McAlexander, L. M. Bezold, A. M. Arif and L. M. Berreau, *J. Am. Chem. Soc.*, 2002, **124**, 9970; (*c*) M. Wall, B. Linkletter, D. Williams, A.-M. Lebuis, R. C. Hynes and J. Chin, *J. Am. Chem. Soc.*, 1999, **121**, 4710; (*d*) F. Mancin and J. Chin, *J. Am. Chem. Soc.*, 2002, **124**, 10496; (*e*) J. Chin, S. Chung and D. H. Kim, *J. Am. Chem. Soc.*, 2002, **124**, 10498; (*f*) C. E. MacBeth, A. P. Golombek, V. G. Young Jr., C. Yang, K. Kuczera, M. P. Hendrich and A. S. Borovik, *Science*, 2000, **289**, 938; (*g*) A. Wada, M. Harata, K. Hasegawa, K. Jitsukawa, H. Masuda, M. Mukai, T. Kitagawa and H. Einaga, *Angew. Chem., Int. Ed.*, 1998, **37**, 798.

(20) W. L. F. Armarego and D. D. Perrin, '*Purification of Laboratory Chemicals*', Butterworth-Heinemann, Oxford, 1997.

(21) G. M. Sheldrick, '*SHELXTL 97*', University of Göttingen, 1997.

(22) G. M. Sheldrick, '*SADABS, Empirical absorption correction program*', University of Göttingen, 1995, based upon the method of Blessing.

(23) R. H. Blessing, *Acta Crystallogr., Sect. A*, 1995, **51**, 33.

(24) A. L. Spek, *Acta Crystallogr., Sect. A.*, 1990, **46**, C34.

(25) Stoe and Cie, '*GmbH, IPDS, 2.87 Software Manual*', Darmstadt, Germany.

(26) P. v. d. Sluis and A. L. Spek, *Acta Crystallogr., Sect. A.*, 1990, **46**, 194.

(27) T. Beurskens, G. Admiraal, G. Beurskens, W. P. Bosman, S. García-Granada, R. O. Gould, J. M. M. Smits and C. Smykalla, '*The DIRDIF Program System, Technical Report of the Crystallography Laboratory*', University of Nijmegen, The Netherlands, 1997.

Chapter 3. Factors that affect the strength of internal N-H···X-Zn (X = Cl, ONO_2) hydrogen bonds in trigonal bipyramidal Zn(II) complexes of tpa-based ligands

3.1 INTRODUCTION

Despite the great potential of exploiting and modelling second-sphere hydrogen bonding features of metals centres, only a few studies have investigated factors affecting their strength.[1] Strategies to manipulate the strength of hydrogen bonding to metal-bound ligands, however, is a key aspect for any research concerned with exploiting or modelling the effects of these interactions.

In this chapter we investigate the geometry and strength of internal N-H···X-Zn (X = Cl, NO_3) hydrogen bonding in trigonal bipyramidal geometry as model interaction. Factors that affect the geometry and strength of the internal N-H···X-Zn hydrogen bond and how these changes are expressed spectroscopically are discussed. In addition we investigate strategies and principles to manipulate hydrogen bonding interactions in metal complexes.

3.2 RESULTS AND DISCUSSION

3.2.1 LIGAND DESIGN AND SYNTHESIS

In the previous chapter we have shown that the (6-NHR-2-pyridylmethyl)amine (R = CO^{t}Bu or H) ligand unit in **tpa**-based ligands ($\mathbf{L_1}^1$ and $\mathbf{L_1}^2$) has a suitable stereochemistry for the participation of the N-H group in internal hydrogen bonding to an adjacent metal-bound ligand. In order to make a systematic

study of the strength of this interaction(s) we decided to synthesise the ligands $\mathbf{L_1}^3$ and $\mathbf{L_2}^2$ (Scheme 3.1).

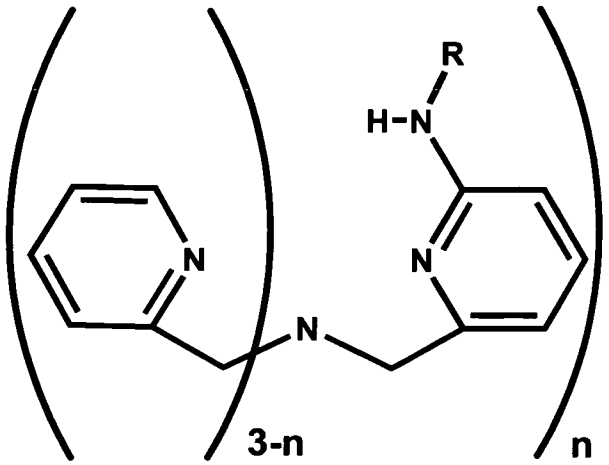

R = CO^{t}Bu; n = 1; $\mathbf{L_1}^1$
R = H; n = 1,2,3; $\mathbf{L_{1\text{-}3}}^2$
R = $CH_2{}^t$Bu; n = 1; $\mathbf{L_1}^3$

Scheme 3.1

Firstly, $\mathbf{L_1}^1$, $\mathbf{L_1}^2$ and $\mathbf{L_1}^3$, offer us the possibility of investigating the strength of internal hydrogen bonding exerted by three different types of RN-H hydrogen bond donors groups (R = CO^{t}Bu ($\mathbf{L_1}^1$), H ($\mathbf{L_1}^2$) and $CH_2{}^t$Bu ($\mathbf{L_1}^3$)) to a common hydrogen bond acceptor, Zn-Cl. Secondly, the ligand series $\mathbf{L_n}^2$ (n = 1-3) will be used to assess the effect of an increasing number of hydrogen bonding groups on the strength of N–H···Cl–Zn. Finally, $\mathbf{L_2}^2$ will be used to study the strength of internal hydrogen bonds as a function of the hydrogen bond acceptor, Zn-X (X = Cl, NO_3).

3.2.1.1 Synthesis of L_1^3

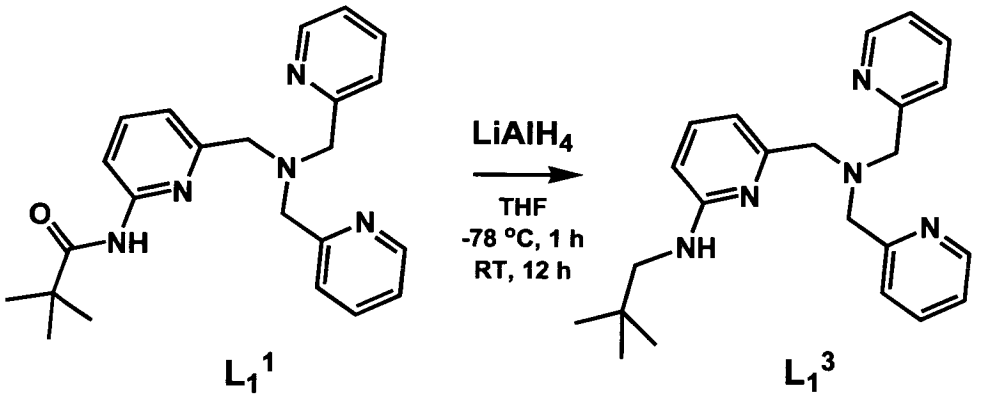

Scheme 3.2

The synthesis of *N*-(6-neopentylamino-2-pyridylmethyl)-*N*,*N*-bis-(2-pyridylmethyl)amine ($\mathbf{L_1}^3$) can be accomplished in 1 step (Scheme 3.2) starting from the corresponding tripodal ligand $\mathbf{L_1}^1$ with the 6-pivaloylamido-2-pyridylmethylamine fragment upon reduction, using $LiAlH_4$ as the reducing reagent. After quenching the reaction, filtration and extraction with dichloromethane, the crude product was purified by flash chromatography in neutral alumina using methanol:dichloromethane (2:98, v:v) as eluent.[2]

3.2.1.2 Synthesis of L_2^2

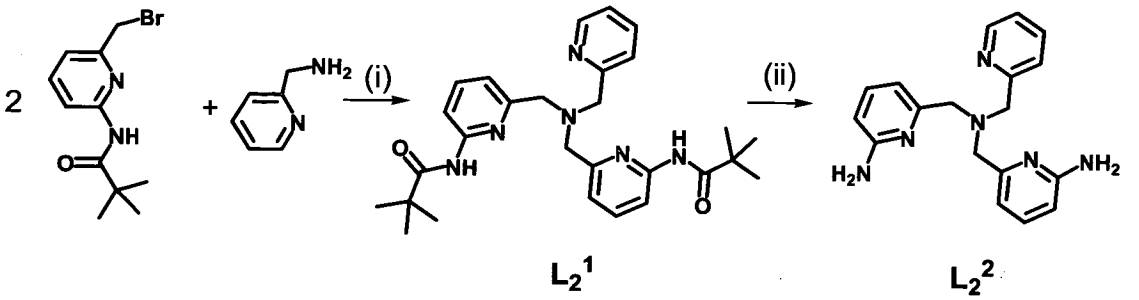

Scheme 3.3 Reagents and conditions used for the synthesis of compounds $\mathbf{L_2}^1$ and $\mathbf{L_2}^2$; (i) Na_2CO_3 (10 eq.), $BrNMe_4$ (0.1 eq.), CH_3CN, 44 °C; (ii) 2M $HCl_{aq.}$, reflux.

The synthesis of *N,N*-bis-(6-pivaloylamido-2-pyridylmethyl)-*N*-(2-pyridylmethyl)amine $\mathbf{L_2}^2$ can be accomplished in 2 steps (Scheme 3.3). Thus, the reaction in acetonitrile of two equivalents of 2-(pivaloylamido)-6-(bromomethyl)pyridine with 2-aminomethyl-pyridine in the presence of an excess of sodium carbonate and a catalytic amount of tetramethylammonium bromide as a phase-transfer catalyst yields the tripodal ligand $\mathbf{L_2}^1$. After filtration and evaporation of the solvent, the crude product was further purified by flash chromatography eluting the product using a 8:2 (v:v) ethyl acetate:dicholoromethane solution in neutral alumina and/or recrystallised from chloroform. $\mathbf{L_2}^1$ was then dissolved and refluxed in 2M $HCl_{(aq)}$ for 48 h to yield the unprotected amine $\mathbf{L_2}^2$ in the same way as described in Chapter 2 for $\mathbf{L_1}^2$.

3.2.2 SYNTHESIS OF Zn(II) COMPLEXES

The synthesis of $[(\mathbf{L_1}^3)Zn(Cl)](BPh_4)$ and $[(\mathbf{L_2}^2)Zn(Cl)](BPh_4)$ was accomplished following the same strategy as for $[(\mathbf{L_1}^1)Zn(Cl)](BPh_4)$ and $[(\mathbf{L_1}^2)Zn(Cl)](BPh_4)$, described in the previous chapter. The synthesis of $[(\mathbf{L_2}^2)Zn(ONO_2)](NO_3)$ was carried out by mixing equimolar amounts of $\mathbf{L_2}^2$ and $Zn(NO_3)_2{\cdot}6H_2O$ in H_2O:CH_3OH and refluxing for 1 h.

3.2.3 X-RAY CRYSTALLOGRAPHY

Crystal data for $[(\mathbf{L_1}^3)Zn(Cl)](BPh_4)$, $[(\mathbf{L_2}^2)Zn(Cl)](BPh_4)\cdot 0.5(CH_3CN\cdot H_2O)$, $[(\mathbf{L_2}^2)Zn(ONO_2)](NO_3)$ are listed in Table 3.1.

Table 3.1 Crystallographic data and structure refinement details for complexes $[(\mathbf{L_1}^3)Zn(Cl)](BPh_4)$, $[(\mathbf{L_2}^2)Zn(Cl)](BPh_4)\cdot 0.5(CH_3CN\cdot H_2O)$ and $[(\mathbf{L_2}^2)Zn(ONO_2)](NO_3)$.

	$[(\mathbf{L_1}^3)Zn(Cl)](BPh_4)$	$[(\mathbf{L_2}^2)Zn(Cl)](BPh_4)\cdot 0.5(CH_3CN\cdot H_2O)$	$[(\mathbf{L_2}^2)Zn(ONO_2)](NO_3)$
Empirical Formula	$C_{47}H_{49}BClN_5Zn$	$C_{43}H_{42.5}BClN_{6.5}O_{0.5}Zn$	$C_{18}H_{20}N_8O_6Zn$
M_r	795.54	769.97	509.79
T/ K	150(2)	150(2)	150(2)
Crystal system	Monoclinic	Monoclinic	Monoclinic
Space group	$P2_1/n$	$P2_1/c$	$I2/a$
a /Å	12.7167(3)	10.1460(4)	14.7313(12)
b /Å	14.3082(3)	16.5408(6)	13.7642(11)
c /Å	22.7135(5)	23.3955(10)	21.3172(2)
α / °	90	90	90
β / °	97.8740(10)	104.468(2)	104.670(4)
γ / °	90	90	90
V / Å^3	4093.83(16)	3801.8(3)	4192.1(6)
Z	4	4	1
D_c / g cm^{-3}	1.291	1.345	1.615
μ / mm–1	0.777	0.759	1.23
Reflections measured, unique	30807, 9952	29363, 6748	24789, 5146
R_{int}	0.0511	0.0486	0.0430
$R_1(F)^a$	0.0871	0.0755	0.0512
$wR_2(F^2)^a$ (all data)	0.1492	0.1174	0.1275
$S(F^2)^a$ (all data)	1.140	1.090	1.080
Largest difference peak, hole/e Å^3	1.047, -0.338	0.605, -0.281	1.997, -0.613

$^a R_1(F) = \Sigma(|F_o| - |F_c|)/ \Sigma(|F_o|$; $wR_2(F^2) = [\Sigma w(F_o^2 - F_c^2)^2/\Sigma wF_0^4]^{1/2}$; $S(F^2) = [\Sigma w(F_o^2 - F_c^2)^2/(n-p)]^{1/2}$.

3.2.3.1 Structure of $[(L_1^3)Zn(Cl)](BPh_4)$

A thermal ellipsoid plot of the X-ray crystal structure of $[(\mathbf{L_1}^3)Zn(Cl)](BPh_4)$ is shown in Fig. 3.1 and selected distances and angles are given in Tables 3.2 and 3.3.

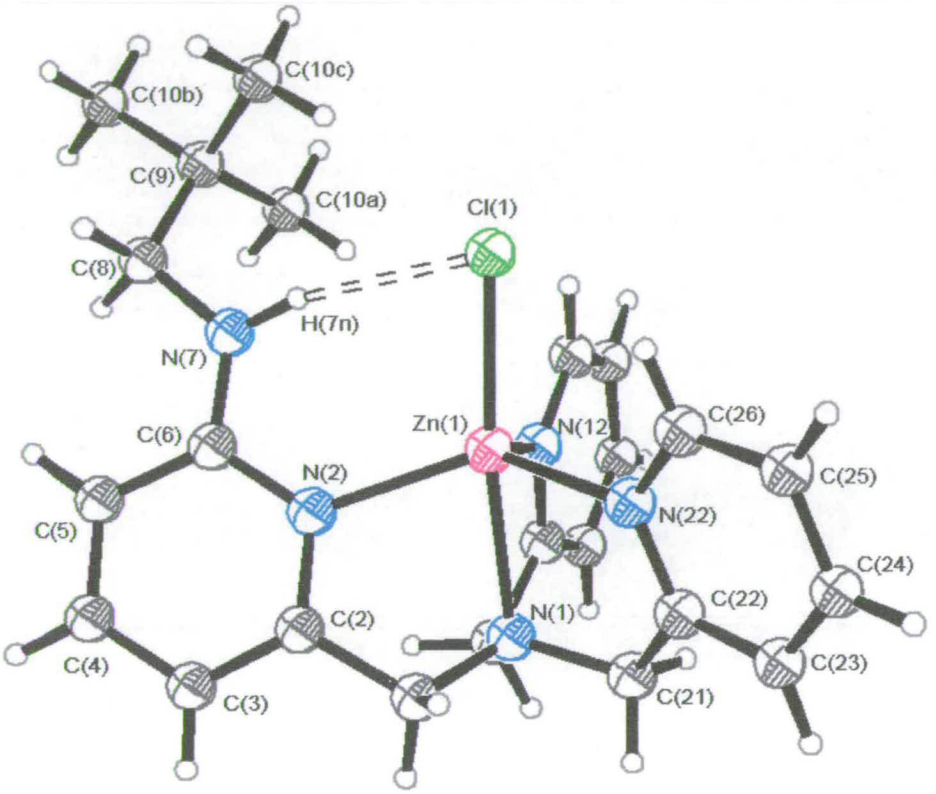

Fig. 3.1 Thermal ellipsoid plot drawn with 30% probability ellipsoids of the $[(\mathbf{L_1}^3)Zn(Cl)]^+$ cation of $[(\mathbf{L_1}^3)Zn(Cl)](BPh_4)$ showing the internal N–H···Cl–Zn hydrogen bonding. Only N–H hydrogens are shown for clarity.

As in $[(\mathbf{L_1}^1)Zn(Cl)](BPh_4)$ and $[(\mathbf{L_1}^2)Zn(Cl)](BPh_4)$, in $[(\mathbf{L_1}^3)Zn(Cl)](BPh_4)$ the zinc(II) centre is in a trigonal bipyramidal environment ligated to the three pyridine nitrogen atoms in the trigonal plane, and to the bridgehead nitrogen of the tripodal ligand and a chloride ion in the axial positions. The Zn–N distances are also in accordance with other $[(L)Zn(Cl)]^+$ cations.[3, 4] The longest Zn–N distance is to the bridgehead amino nitrogen (Zn(1)-N(1) 2.236(3) Å). The zinc(II) ion sits above the

trigonal plane resulting in acute N_{axial}–Zn–$N_{equatorial}$ angles of *ca.* 77.6 °. The Zn-$N_{equatorial}$ distances are in the range 2.100(2)-2.072(3) Å with the longest corresponding to the substituted pyridine. The N-H group of the neopentylamino group is involved in internal N-H···Cl-Zn hydrogen bonding (Table 3.2) (N(7)···Cl(1) 3.213(3) Å; H(7N)···Cl(1) 2.23 Å; N(7)–H(7N)···Cl(1) 164.4° for a N(7)–H(7N) bond extended to 1.01 Å[5])

3.2.3.2 Structure of $[(L_2^2)Zn(Cl)](BPh_4)\cdot 0.5(CH_3CN\cdot H_2O)$

A thermal ellipsoid plot of the X-ray crystal structure of $[(\mathbf{L_2}^2)Zn(Cl)](BPh_4)\cdot 0.5(CH_3CN\cdot H_2O)$ is shown in Fig. 3.2 and selected distances and angles are given in Tables 3.2 and 3.3.

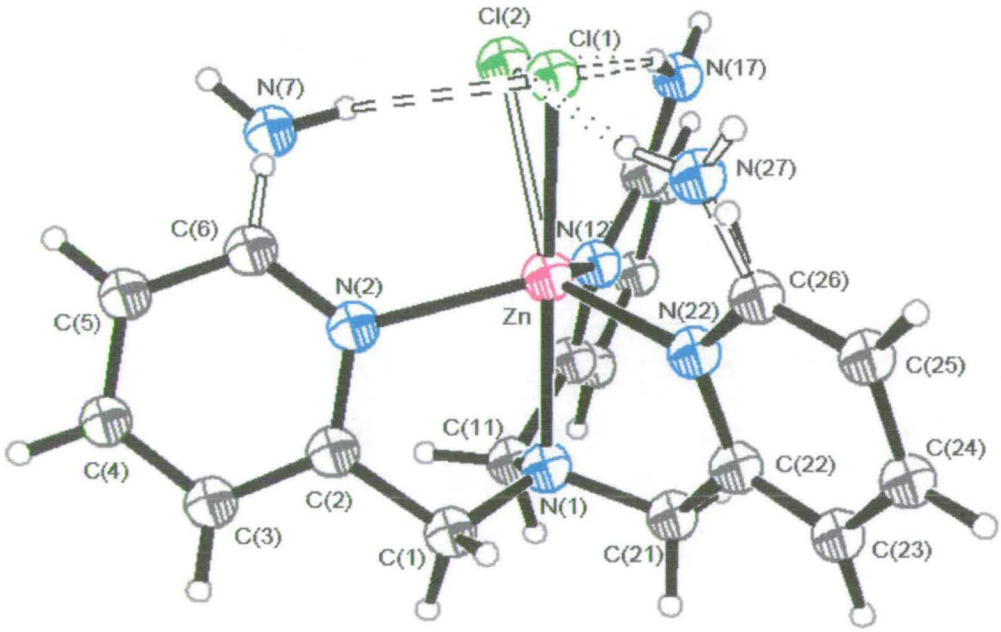

Fig. 3.2 Thermal ellipsoid plot drawn with 30% probability ellipsoids of the $[(\mathbf{L_2}^2)Zn(Cl)]^+$ cation of $[(\mathbf{L_2}^2)Zn(Cl)](BPh_4)\cdot 0.5(CH_3CN\cdot H_2O)$ showing the internal N–H···Cl–Zn hydrogen bonding. The positions of some atoms were disordered between two positions; empty-solid and dotted lines represent 33% site-occupancy (See text).

As in the structures reported previously the zinc(II) centre is in a trigonal bipyramidal environment ligated to the three pyridine nitrogen atoms in the trigonal plane, and to the bridgehead nitrogen of the tripodal ligand and a chloride ion in the axial positions. The Zn–N distances are also in accordance with other $[(L)Zn(Cl)]^+$ cations.[3, 4]

The $Zn\text{-}N_{equatorial}$ distances are in the range 2.120(3)-2.085(3) Å with the longest corresponding to Zn-N(2) and the shortest to Zn-N(12) distances. The X-ray crystal structure of $[(\mathbf{L_2}^2)Zn(Cl)](BPh_4)\cdot 0.5(CH_3CN\cdot H_2O)$ also shows the participation of the two NH_2 groups in internal N–H···Cl–Zn hydrogen bonds (Table 3.2). The position of one the NH_2 groups is disordered between two positions N(7) and N(27) with *ca.* 67 and 33% occupancies, respectively. Accordingly, the zinc-bound chloride is also disordered between two positions, Cl(1) (67% occupancy) and Cl(2) (33% occupancy) with distances to the zinc centre of 2.323(2) and 2.359(4) Å, respectively. It is important to note that the N-H···Cl-Zn hydrogen bonds to the longer Zn-Cl(2) are shorter than to Zn-Cl(1) (See Table 3.3). Like in $[(\mathbf{L_1}^2)Zn(Cl)](BPh_4)\cdot 0.5CH_3CN$ there is also a N-H···π interaction between one of the amino groups and a phenyl ring of the BPh_4 anion of a symmetry related molecule (not shown).

3.2.3.3 Structure of $[(L_2^2)Zn(ONO_2)](NO_3)$

A thermal ellipsoid plot of the X-ray crystal structure of $[(\mathbf{L_2^2})Zn(ONO_2)](NO_3)$ is shown in Fig. 3.3 and selected distances and angles are given in Tables 3.2 and 3.3.

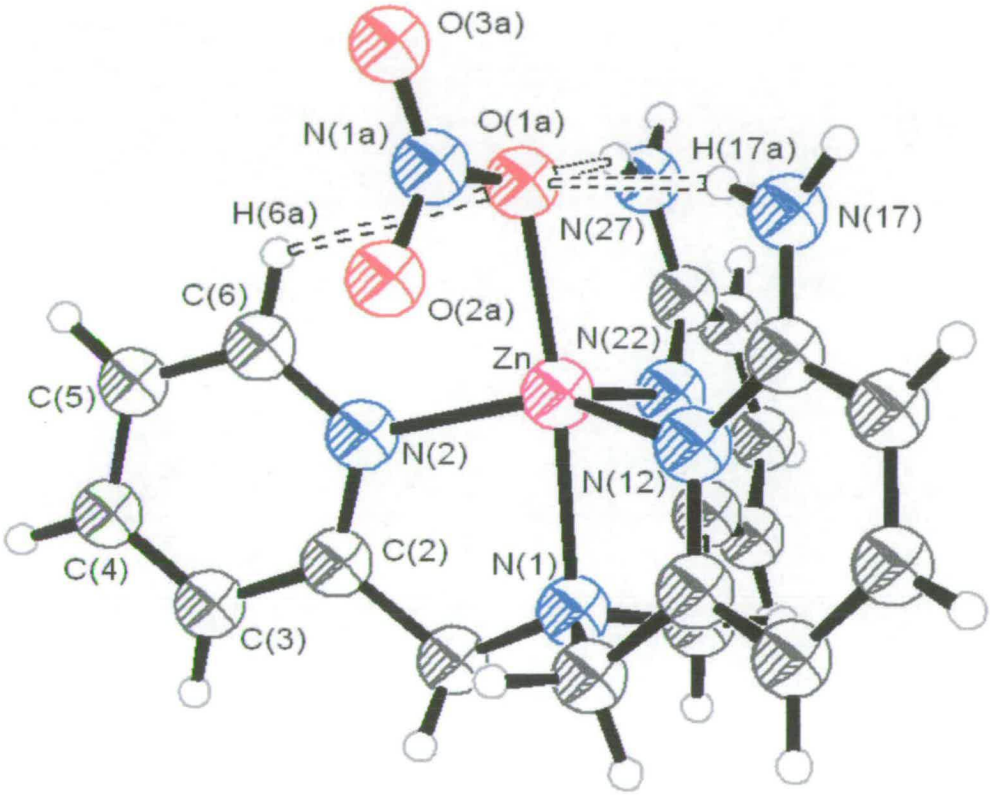

Fig. 3.3 Thermal ellipsoid plot drawn with 50% probability ellipsoids of the $[(\mathbf{L_2^2})Zn(ONO_2)]^+$ cation of $[(\mathbf{L_2^2})Zn(ONO_2)](NO_3)$ showing the internal N-H···O-Zn and C-H···O-Zn hydrogen bonding.

As in the structures reported previously the zinc(II) centre is in a trigonal bipyramidal environment ligated to the three pyridine nitrogen atoms in the trigonal plane, and to the bridgehead nitrogen of the tripodal ligand and an oxygen of the nitrate ion in the axial positions. The longest Zn–N distance is to the bridgehead amino nitrogen (Zn-N(1) 2.163(2) Å). The $Zn\text{-}N_{equatorial}$ distances are slightly shorter

than in $[(\mathbf{L_2}^2)Zn(Cl)](BPh_4)\cdot 0.5(CH_3CN\cdot H_2O)$ (2.120(3)-2.085(3) Å) and are in the range 2.093(3)-2.076(3) Å. The axial Zn-O(1A) distance (2.0993(19) Å), however, is considerably shorter than the corresponding Zn-Cl(1), Cl(2) distances in $[(\mathbf{L_2}^2)Zn(Cl)](BPh_4)\cdot 0.5(CH_3CN\cdot H_2O)$ (2.323(2), 2.359(4) Å).

The X-ray crystal structure of $[(\mathbf{L_2}^2)Zn(ONO_2)](NO_3)$ also shows the participation of the two amino groups in short internal hydrogen bonding with one oxygen of the metal-bound nitrate ion (See Table 3.2) The nitrate counter-ion is also involved in a short external hydrogen bond interaction (not shown) with one of the amino groups in a bifurcated mode (N(27)···O(5A) 3.24 Å, N(27)···O(6A) 2.94 Å, H(27B)···O(5A) 2.47 Å, H(27B)···O(6A) 2.09 Å, N(7)–H(27B)···O(5A) 144 °, N(7)–H(27B)···O(6A) 159 °).

Table 3.2 Geometric features of the main internal hydrogen bonding interactions in $[(\mathbf{L_1}^3)Zn(Cl)](BPh_4)$, $[(\mathbf{L_2}^2)Zn(Cl)](BPh_4)\cdot 0.5(CH_3CN\cdot H_2O)$ and $[(\mathbf{L_2}^2)Zn(ONO_2)](NO_3)$.

Interaction	D-H[a]/Å	D···A/Å	H···A/Å	D-H···A/ °
$[(\mathbf{L_1}^3)Zn(Cl)](BPh_4)$				
N(7)-H(7NA)···Cl(1)	1.01	3.213(3)	2.23	164.4
$[(\mathbf{L_2}^2)Zn(Cl)](BPh_4)\cdot 0.5(CH_3CN\cdot H_2O)$				
N(7)[b]-H(7A)[b]···Cl(1)[b]	1.01	3.169(6)	2.45	127.2
N(17)-H(17A)···Cl(1)[b]	1.01	3.277(5)	2.31	160.1
N(17)-H(17A)···Cl(2)[c]	1.01	3.183(12)	2.22	157.8
N(27)[c]-H(27A)[c]···Cl(2)[c]	1.01	3.076(6)	2.15	150.9
$[(\mathbf{L_2}^2)Zn(ONO_2)](NO_3)$				
N(17)-H(17A)···O(1A)	1.01	2.943(3)	2.17	158.8
N(27)-H(27A)···O(1A)	1.01	2.926(3)	2.13	159.5

[a] Extended distance. [b] 67% Occupancy. [c] 33% Occupancy

Table 3.3 Selected bond lengths (Å) and angles (°) for zinc(II) complexes $[(\mathbf{L_1}^3)Zn(Cl)](BPh_4)$, $[(\mathbf{L_2}^2)Zn(Cl)](BPh_4)\cdot 0.5(CH_3CN\cdot H_2O)$ and $[(\mathbf{L_2}^2)Zn(ONO_2)](NO_3)$.

	$[(\mathbf{L_1}^3)Zn(Cl)](BPh_4)$	$[(\mathbf{L_2}^2)Zn(Cl)](BPh_4)\cdot 0.5(CH_3CN\cdot H_2O)$	$[(\mathbf{L_2}^2)Zn(ONO_2)](NO_3)$
Zn^a–N(2)	2.100(2)	2.120(3)	2.090(2)
Zn^a–N(12)	2.072(3)	2.085(3)	2.093(2)
Zn^a–N(22)	2.093(2)	2.093(3)	2.076(2)
Zn^a–N(1)	2.236(3)	2.181(3)	2.163(2)
Zn^a–Cl^b	2.2806(9)	2.323(2)	2.0993(19)
N(2)–Zn^a–N(12)	106.71(10)	111.98(10)	140.10(8)
N(2)–Zn^a–N(22)	124.97(10)	121.06(10)	101.33(8)
N(12)–Zn^a–N(22)	114.71(10)	114.28(10)	109.71(8)
N(1)–Zn^a–N(2)	77.46(9)	76.85(10)	80.08(8)
N(1)–Zn^a–N(12)	77.72(11)	79.01(10)	79.85(8)
N(1)–Zn^a–N(22)	77.72(9)	78.23(11)	82.43(8)
N(1)–Zn^a–Cl^b	173.20(7)	169.20(12)	173.77(8)
Cl^b–Zn^a–N(2)	108.76(7)	101.62(10)	96.01(8)
Cl^b–Zn^a–N(12)	102.55(8)	111.18(10)	100.51(8)
Cl^b–Zn^a–N(22)	96.15(7)	93.81(13)	103.08(8)

[a] or Zn(1); [b] or Cl(1) or O(1A)

3.2.3.4 COMPARISON OF STRUCTURES: Strength/geometry of internal N-H···Cl-Zn hydrogen bonding and nature of the hydrogen bond donor.

The X-ray structures of $[(\mathbf{L_1}^1)Zn(Cl)](BPh_4)\cdot CH_3CN$, $[(\mathbf{L_1}^2)Zn(Cl)](BPh_4)\cdot 0.5(CH_3CN\cdot H_2O)$ and $[(\mathbf{L_1}^3)Zn(Cl)](BPh_4)$ allow us to investigate the strength of internal N-H···Cl-Zn hydrogen bond as a function of the nature of the hydrogen bond donor. Thus, in principle, since amide N-H groups are more acidic than those of amines, one might have expected stronger internal N-H···Cl-Zn hydrogen bonding in $[(\mathbf{L_1}^1)Zn(Cl)](BPh_4)\cdot CH_3CN$ than in

$[(\mathbf{L_1}^2)Zn(Cl)](BPh_4)\cdot 0.5(CH_3CN\cdot H_2O)$ and $[(\mathbf{L_1}^3)Zn(Cl)](BPh_4)$. The X-ray crystal structures of $[(\mathbf{L_1}^2)Zn(Cl)](BPh_4)\cdot 0.5(CH_3CN\cdot H_2O)$ and $[(\mathbf{L_1}^3)Zn(Cl)](BPh_4)$, however, shows internal N-H···Cl-Zn hydrogen bonds with geometric features which are essentially identical to in $[(\mathbf{L_1}^1)Zn(Cl)](BPh_4)\cdot CH_3CN$. For example, the hydrogen bond donor···acceptor distance, N(7)···Cl, is 3.2127(19) Å in $[(\mathbf{L_1}^1)Zn(Cl)](BPh_4)$, and 3.213(3) Å in $[(\mathbf{L_1}^2)Zn(Cl)](BPh_4)$ and $[(\mathbf{L_1}^3)Zn(Cl)](BPh_4)$.

An aspect that may partly account for this observation is the fact that whereas the pivaloylamide acts as an electron withdrawing group on the pyridine, the amine groups are electron donating. These effects are reflected in the $Zn\text{-}N_{py'}$ distances (py' = pyridine carrying the pivaloylamido, amino or neopentylamino group) and affects the distance between the hydrogen bonded atoms (Zn-N(2) 2.1351(15) Å, N(7)-H(7NA)···Cl–Zn 3.2127(19) Å $[(\mathbf{L_1}^1)Zn(Cl)](BPh_4)\cdot CH_3CN$; Zn-N(2) 2.0704(19) Å, N(7)-H(7NA)···Cl-Zn 3.213(3) Å $[(\mathbf{L_1}^2)Zn(Cl)](BPh_4)\cdot 0.5CH_3CN$; Zn-N(2) 2.100(2) Å, N(7)-H(7NA)···Cl–Zn 3.213(3) Å $[(\mathbf{L_1}^3)Zn(Cl)](BPh_4)$).

This could be a potentially important result in that it implies that even a poor hydrogen bond donor, if brought sufficiently close to the hydrogen bond acceptor as the result of short (strong) metal-ligand binding, should result in a short (strong) internal hydrogen bond to another ligand. Moreover, it could suggest that the same effect (the electron withdrawing nature) that makes the amide a better hydrogen bond donor than an amine, when part of a ligand, can cause it to be further away from the metal-bound hydrogen bond acceptor. Thus, it appears to us that an alternative

strategy to induce strong internal hydrogen bonding in coordination complexes could be to attach the hydrogen bonding group to a ligand that induces short metal-ligand distances.

The strength of the internal N–H···Cl–Zn hydrogen bonding can be approximately quantified from the equation proposed by Rozenberg *et al.*:[6]

$$-\Delta H = 0.134(r)^{-3.05} \quad (1)$$

Where $-\Delta H$ is in kJ·mol^{-1} and r is the D-H···A distance in nm (D = hydrogen bond donor, A = hydrogen bond acceptor). This equation is based on empirical data and allows an estimation of crystal hydrogen bond energies from the D-H···A distance of hydrogen bond interactions found in X-ray crystal structures. Thus, the N-H···Cl-Zn distances in $[(\mathbf{L_1}^1)Zn(Cl)](BPh_4)\cdot CH_3CN$ (0.222 nm), $[(\mathbf{L_1}^2)Zn(Cl)](BPh_4)\cdot 0.5CH_3CN$ (0.224 nm) and $[(\mathbf{L_1}^3)Zn(Cl)](BPh_4)$ (0.223 nm) correspond to very similar hydrogen bond energies of 13.2, 12.8 and 13.0 kJ·mol^{-1} respectively.

It is important to note that metal geometry also affects the geometry and strength of internal N-H···Cl-Zn hydrogen bonds. Thus, work in our group has shown that related tetrahedral structures (the most common geometry in nucleases) show similar metal-ligand effects in internal N-H···Cl-Zn hydrogen bond strength and corroborates this work.[7] Furthermore, the trigonal bipyramidal N_4ClZn complexes discussed above have shorter (stronger) internal N-H···Cl-Zn hydrogen bonds than

related tetrahedral N_2Cl_2Zn complexes even when Zn-$N_{Py'}$ distances (py' = pyridine carrying the N-H hydrogen bond donor) are longer in trigonal bipyramidal complexes (*ca.* 2.07 Å-2.13 Å in trigonal bipyramidal structures compared to 2.04-2.08 Å in tetrahedral structures). The main reason for the stronger internal N-H···Cl-Zn hydrogen bonding in the trigonal bipyramidal structures compared to the tetrahedral structures appears to be the smaller torsion angle between the ZnN(2)C(6)N(7) and ZnN(2)Cl planes, which is 25.1° in $[(\mathbf{L_1}^1)Zn(Cl)](BPh_4)\cdot CH_3CN$, 20.6° in $[(\mathbf{L_1}^2)Zn(Cl)](BPh_4)\cdot 0.5CH_3CN$ and 27.5° in $[(\mathbf{L_1}^3)Zn(Cl)](BPh_4)$ compared to 34.5°-43.9° in tetrahedral structures.[7]

3.2.3.5 COMPARISON OF STRUCTURES: Strength/geometry of internal N-H···X-Zn hydrogen bonding and nature of the hydrogen bond acceptor (X = Cl, NO_3).

The X-ray structures of $[(\mathbf{L_2}^2)Zn(Cl)](BPh_4)\cdot 0.5(CH_3CN\cdot H_2O)$ and $[(\mathbf{L_2}^2)Zn(ONO_2)](NO_3)$ allow us to investigate the strength of internal N-H···X-Zn hydrogen bond as a function of the nature of the hydrogen bond acceptor (X = Cl in $[(\mathbf{L_2}^2)Zn(Cl)](BPh_4)$, X = NO_3 in $[(\mathbf{L_2}^2)Zn(ONO_2)](NO_3)$). It may appear remarkable that despite the rigidity imposed by the Zn–L binding, the average hydrogen bond donor···acceptor distances are notoriously different (3.223 Å, X = Cl(1) at 67% occupancy and 3.120 Å, X = Cl(2) at 33% occupancy in $[(\mathbf{L_2}^2)Zn(Cl)](BPh_4)\cdot 0.5(CH_3CN\cdot H_2O)$ compared to 2.935 Å, X=O(1A) in $[(\mathbf{L_2}^2)Zn(ONO_2)](NO_3)$). However, the van der Waals radius of Cl is 0.23 Å bigger

than that of O,[8] which makes the average donor···acceptor interaction only shorter by ca. 0.03 Å in $[(\mathbf{L_2}^2)Zn(Cl)]BPh_4 \cdot 0.5(CH_3CN \cdot H_2O)$.

A structural feature that could account for the presumably slightly stronger internal N-H···X-Zn hydrogen bonding interactions in $[(\mathbf{L_2}^2)Zn(Cl)](BPh_4)$ may be the Zn-X,N distances/strengths. Thus, a weaker Zn-X bond should make X a better hydrogen bond acceptor. Whereas in $[(\mathbf{L_2}^2)Zn(Cl)](BPh_4) \cdot 0.5(CH_3CN \cdot H_2O)$ the axial average Zn-Cl distance is 2.335 Å, in $[(\mathbf{L_2}^2)Zn(ONO_2)](NO_3)$, the corresponding Zn-O(1A) distance is 2.0993(19) Å. However, if we take into consideration the difference in the van der Waals radii between Cl and O, the Zn-X bonds in both structures seems to have the same strength. Interestingly, the axial Zn-N(1) distances and average $Zn\text{-}N_{equatorial}$ distances in both structures have similar values (Zn-N(1) 2.181(3) Å, $Zn\text{-}N_{eq}$ 2.099 Å in $[(\mathbf{L_2}^2)Zn(Cl)](BPh_4) \cdot 0.5(CH_3CN \cdot H_2O)$ and Zn-N(1) 2.163(2) Å, $Zn\text{-}N_{eq}$ 2.086 Å in $[(\mathbf{L_2}^2)Zn(ONO_2)](NO_3)$).

Thus, it seems that the strength of N–H···X–Zn hydrogen bonds is slightly dependent on the nature of the hydrogen bond acceptor, and the strength order is $Cl^- > NO_3^-$. This result is in agreement with recent studies, which regard metal-bound chlorides as excellent hydrogen bond acceptors.[9]

3.2.3.6 COMPARISON OF STRUCTURES: Strength/Geometry of internal N-H···Cl-Zn hydrogen bonding and number of internal hydrogen bonding interactions.

The crystal structures of $[(\mathbf{L_1}^2)Zn(Cl)](BPh_4)\cdot 0.5CH_3CN$ described in Chapter 2 and $[(\mathbf{L_2}^2)Zn(Cl)](BPh_4)\cdot 0.5(CH_3CN\cdot H_2O)$, together with the structure of $[(\mathbf{L_3}^2)Zn(Cl)](BPh_4)\cdot CH_3CN$, recently characterised in our group which also shows the participation of all the amino groups in internal N-H···Cl-Zn hydrogen bonds,[10] allow the study of the strength of the internal N-H···Cl-Zn hydrogen bonding as a function of the number of interactions (Table 3.4).

Table 3.4 Comparison of average distances and angles of internal hydrogen bonding interactions in $[(\mathbf{L_1}^2)Zn(Cl)](BPh_4)\cdot 0.5CH_3CN$, $[(\mathbf{L_2}^2)Zn(Cl)](BPh_4)\cdot 0.5(CH_3CN\cdot H_2O)$ and $[(\mathbf{L_3}^2)Zn(Cl)](BPh_4)\cdot CH_3CN$[c].

	N···Cl/Å	H···Cl[a]/Å	N-H···Cl[a]/ °
$[(\mathbf{L_1}^2)Zn(Cl)](BPh_4)\cdot 0.5CH_3CN$	3.21	2.24	160.4
$[(\mathbf{L_2}^2)Zn(Cl)](BPh_4)\cdot 0.5(CH_3CN\cdot H_2O)$	3.19[b]	2.32[b]	147.2[b]
$[(\mathbf{L_3}^2)Zn(Cl)](BPh_4)\cdot CH_3CN$[c]	3.15[c]	2.18[c]	160.2[c]

[a] For a extended N-H distance of 1.01 Å; [b] Calculated using the equation: $[(measurement_{Av})_{67\%\ occupancy}\cdot 0.67 + (measurement_{Av})_{33\%\ occupancy}\cdot 0.33]\cdot 0.5$;
[c] From Ref. 10

Interestingly, as the number of N-H···Cl-Zn interactions increases from one in $[(\mathbf{L_1}^2)Zn(Cl)](BPh_4)\cdot 0.5CH_3CN$ to three in $[(\mathbf{L_3}^2)Zn(Cl)](BPh_4)\cdot CH_3CN$, the average N···Cl and N-H···Cl distances decrease by 0.06 Å, suggesting that the overall strength increases with the number of interactions.

In principle, a reason that could account for the observed strengthening of the overall N-H···Cl-Zn hydrogen bonding as the number of interactions increases could have been a shortening of equatorial N_{py}-Zn distances induced by the electron donating properties of the amino groups. However, based on the average equatorial N_{Py}-Zn distances of $[(\mathbf{L_1}^2)Zn(Cl)](BPh_4)\cdot 0.5CH_3CN$, $[(\mathbf{L_2}^2)Zn(Cl)](BPh_4)\cdot 0.5(CH_3CN\cdot H_2O)$ and $[(\mathbf{L_3}^2)Zn(Cl)](BPh_4)\cdot CH_3CN$ we can rule out this possibility. In fact, the amino groups have the completely opposite overall effect of lengthening average N_{Py}-Zn distances, presumably due to steric reasons.

Importantly, as the number of amino groups increases from $[(\mathbf{L_1}^2)Zn(Cl)](BPh_4)\cdot 0.5CH_3CN$ to $[(\mathbf{L_3}^2)Zn(Cl)](BPh_4)\cdot CH_3CN$, the axial Zn-Cl distance is progressively lengthened *ca.* 0.025 Å per amino group. Thus, the reason for the increasing strength observed seems to be the lengthening/weakening of the Zn-Cl bond which should make the zinc-bound Cl atom a better hydrogen bond acceptor. Structural changes induced by internal N-H···Cl-Zn hydrogen bonding in these and related complexes will be discussed in more detail in the next chapter.

3.2.3.7 EXTERNAL N-H···π HYDROGEN BONDING: Cambridge Structural Database Study.

Remarkably, the X-ray structure of $[(\mathbf{L_1}^2)Zn(Cl)](BPh_4)\cdot 0.5CH_3CN$ showed (Fig. 2.5 and Table 2.2) a very short external N-H···π hydrogen bond with a phenyl group of the BPh_4^- anion (N(7)···X(1A) 3.26 Å, H(7NB)···X(1A) 2.26 Å, N(7)-

H(7NB)···X(1A) 168°; Fig. 3.6). The structure of $[(\mathbf{L_2}^2)Zn(Cl)](BPh_4)\cdot 0.5(CH_3CN\cdot H_2O)$ (*vide supra*) also shows a similar interaction.

The generality of very short N-H···π (phenyl, centroid type) hydrogen bonds in the solid state was investigated by searching the Cambridge Structural Database (**CSD**).[11] A total of 41 crystal structures had very short (arbitrarily chosen to be <2.3 Å) H···X (X = phenyl centroid) H-bonds. These crystal structures were scrutinised and separated into organic (27 cases) and inorganic compounds (14 cases). Of the 27 organic structures with very short N-H···π hydrogen bonds only four involved a neutral N-H of which only one involved a primary amine, RNH_2, all the others involved $R_3N\text{-}H^+$ groups. In inorganic compounds, however, we found that 8 of the 14 cases involve metal-coordinated primary amines (RH_2N-M). This result could suggest that inductive effects arising from metal–ligand bonding interactions can be as effective at inducing strong hydrogen bonding as the nature of the hydrogen bonding groups themselves *e.g.* RH_2N-M as effective hydrogen bond donor as RNH_3^+. In fact, all 14 complexes contain strongly Lewis acidic metals. Further details including reference codes, parameters and histograms of the CSD search are provided in the Appendix.

3.2.4 IR STUDIES: Strength of internal N-H···Cl-Zn hydrogen bond in $[(L_1^1)Zn(Cl)](BPh_4)$

In the previous chapter it was shown that the formation of internal N-H···Cl-Zn hydrogen bonding in $[(\mathbf{L_1}^1)Zn(Cl)](BPh_4)$ is reflected in the ν_{N-H} vibration being shifted to lower wavenumbers on going from chloride coordination in $[(\mathbf{L_1}^1)Zn(Cl)](BPh_4)$ to amide coordination in $[(\mathbf{L_1}^1)Zn](PF_6)$ or the free ligand $\mathbf{L_1}^1$.

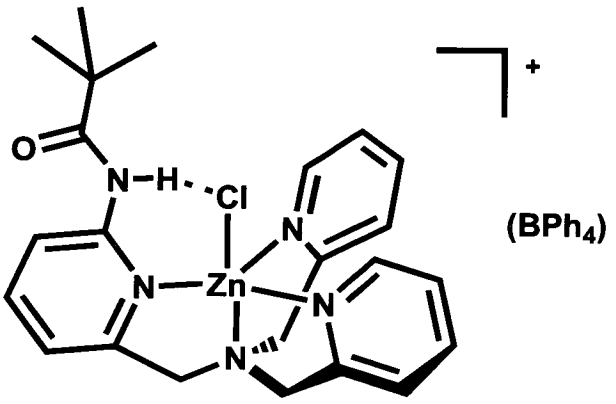

$[(L_1^1)Zn(Cl)]BPh_4$

The strength of the N-H···Cl-Zn hydrogen bonding can be approximately quantified from the positions of the N–H stretching vibration (ν_{N-H}) using Iogansen's equation:[12]

$$-\Delta H = 1.3(\Delta\nu)^{1/2} \qquad (2)$$

Where $-\Delta H$ is in $kJ \cdot mol^{-1}$ and $\Delta\nu$ is in cm^{-1}. This is a well-established *empirical* relationship that correlates the energy of the hydrogen bond ($-\Delta H$) and the red shift of the D–H stretching vibration ($\Delta\nu_{D-H}$), where D represents hydrogen bond

donor. This equation can be applied to any shift larger than 100 cm^{-1} and has been extensively used.[13, 14] Thus, in acetonitrile solution the ν_{N-H} band of the trigonal bipyramidal complex $[(\mathbf{L_1}^1)Zn(Cl)](BPh_4)$ is shifted to lower wavenumbers by 174 ± 4 cm^{-1} relative to $\mathbf{L_1}^1$. This shift corresponds to a hydrogen bond energy of 16.8 ± 0.6 $kJ{\cdot}mol^{-1}$ applying Iogansen's equation (Eq. 2).

It is important to note that this value for the strength of internal hydrogen bond energy calculated from IR studies differs slightly (3 $kJ{\cdot}mol^{-1}$ aprox.) from the value calculated using Rozenberg's equation (Eq. 1) using X-ray crystal structure distances (*vide supra*). A reason that may account for the different values determined by these methods is the inductive effect of the metal. Thus, Rozenberg's equation (Eq. 1) is derived from Iogansen's equation (Eq. 2) and empirical data from organic compounds, consequently the inductive effect of the metal might be largely omitted.

3.2.4.1 IR studies: Strength of internal N-H···X-Zn hydrogen bonding as a function of the hydrogen bond acceptor (X = Cl, NO_3)

Recent work in our group[10] allow us to compare the strength of internal N-H···X-Zn (X = Cl, NO_3) hydrogen bonding as a function of the hydrogen bond acceptor using solid state IR spectroscopy. Thus, the shift to lower wavenumbers of the ν_{N-H} bands of $[(\mathbf{L_2}^3)Zn(ONO_2)]^+$ (3361 cm^{-1}) and $[(\mathbf{L_2}^3)Zn(Cl)]^+$ (3305 cm^{-1}) compared to 3411 cm^{-1} in the 'free' $\mathbf{L_2}^3$ ligand suggests that the strength of internal N-H···X-Zn hydrogen bonding follows the order $Cl^- > NO_3^-$.

Thus, as suggested by the X-ray crystallographic studies (*vide supra*) the strength of N–H···X–Zn hydrogen bonds is dependent on the nature of the hydrogen bond acceptor.

3.2.5 ^{1}H NMR VARIABLE TEMPERATURE STUDIES: Strength of internal N-H···Cl-Zn hydrogen bond in [(L_1^2)Zn(Cl)](X) (X = Cl, BPh_4)

In the ^{1}H NMR spectrum of [($\mathbf{L_1}^2$)Zn(Cl)](X) (X = Cl, BPh_4) in CD_3CN at room temperature the NH_2 protons appear as broad resonances at 6.98 and 7.02 ppm respectively indicating that they are in rapid exchange between the two chemical environments.

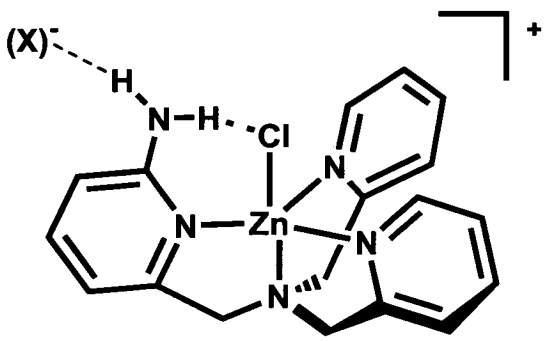

[(L_1^2)Zn(Cl)](X) (X = Cl, BPh_4)

At low temperatures, however, the NH_2 resonance flattens and then diverges into two broad signals (Fig. 3.4), of which the downfield resonance corresponds to the internal N–H, which is downfield shifted to *ca.* 7.94–7.98 ppm due to the N–H···Cl–Zn hydrogen bond. The external N-H is shifted upfield to *ca.* 7.03-6.03 ppm. The greater variability of the upfield of the external N-H is due to the possibility of hydrogen bonding to the counter ion (Cl^-) in solution (*vide infra*).

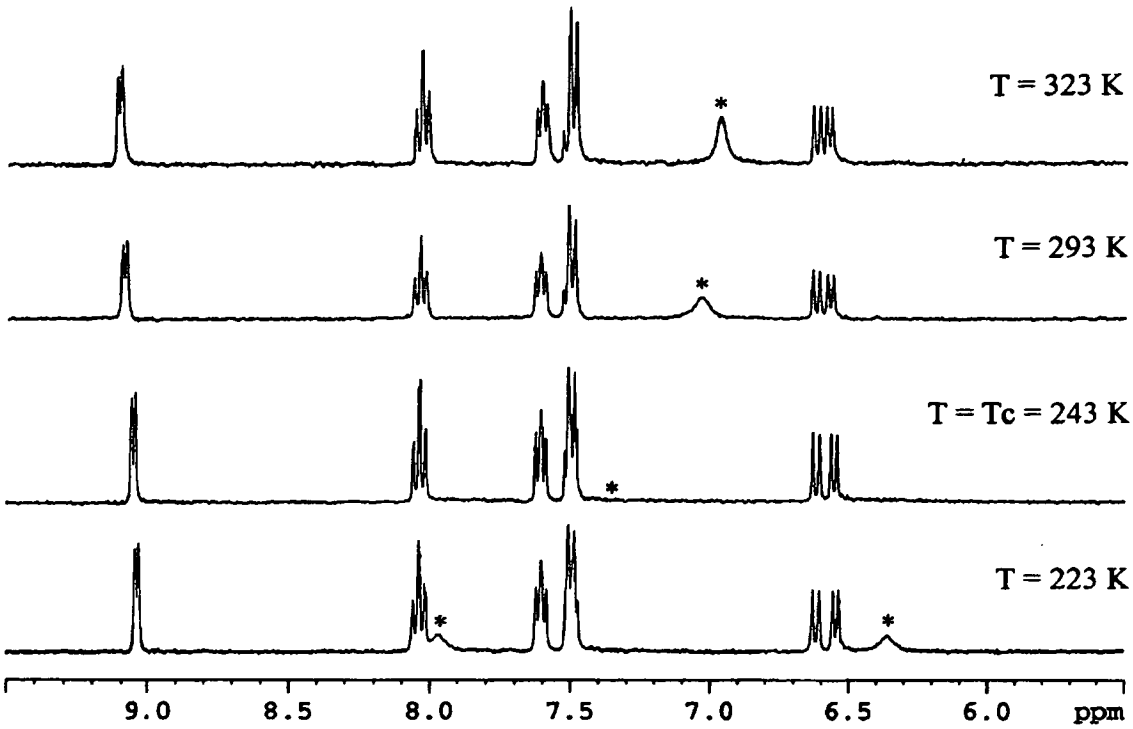

Fig. 3.4 ^{1}H VT NMR of $[(L_1^2)Zn(Cl)](Cl)$ in CD_3CN (1.8 mM) showing aromatic and NH_2(*) resonances.

The strength of the internal N–H···Cl–Zn hydrogen bond in the $[(L_1^2)Zn(Cl)]^+$ cation can be approximately determined by ^{1}H NMR spectroscopy variable temperature coalescence studies.[15] Thus, the rate constant of any reaction is described through the Eyring equation:

$$k = \frac{R \cdot T}{N \cdot h} \cdot e^{-\Delta G^{\#} / R \cdot T} \qquad (3)$$

Where $\Delta G^{\#}$ is the free activation energy, N is Avogadro's number, R is the gas constant and h is Planck's constant. As the temperature is lowered the exchange

between the two protons will slow down and hence the average signal will begin to split. The temperature at which this occurs is the coalescence temperature (T_c). H. S. Gutowsky showed that the rate of rotation k_c at T_c is given by:

$$k_c = \frac{\pi(\Delta\nu)}{\sqrt{2}} \tag{4}$$

Where $\Delta\nu$ is the separation of the two signals in Hz in the absence of exchange. This equation applies only if the exchange process is first-order kinetically, if the two singlets have equal intensity and if the exchanging nuclei are not coupled to each other.[16] Inserting this value for k_c into the Eyring equation (Eq. 3) and after numerical solution of all the constants, the Eyring equation can be expressed in the following form:

$$\Delta G^{\#} = 19 \cdot 10^{-3} \cdot T_c(9.97 + \log T_c - \log \Delta\nu) \tag{5}$$

This equation can be used to make an approximated measurement of the energy barriers ($\Delta G^{\#}$) of many exchange processes if we know the chemical shifts of two exchanging nuclei and the coalescence temperature. Applying Eq. (5) we were able to determine the barrier restricting the rotation of the NH_2 group by ^1H NMR spectroscopy variable temperature coalescence studies of $[(L_1{}^2)Zn(Cl)](X)$ (X = BPh_4, Cl) (Fig. 3.4, Table 3.5 and Appendix).

In order to calculate the energy of the N-H···Cl-Zn hydrogen we need to estimate first the barrier restricting the rotation of the NH_2 group of the metal complex in the absence of hydrogen bonding. The barrier restricting the rotation of the NH_2 in 2-aminopyridine is 16.6 kJ mol^{-1}.[17] We were unable to determine the barrier restricting the rotation of the complex $[(\mathbf{L_1}^2)Zn(NCCH3)](PF_6)_2$ because the coalescence temperature for the exchange of the internal and external NH was below the melting point of the solvent (CD_3CN or CD_2Cl_2), which means that this barrier is very low. The barrier restricting the rotation of the NH_2 of the metal complex $[IrH_2(X)(Y)(PPh_3)](BF_4)$ (X = CH_3CN; Y = 2-aminopyridine) with N–H···X hydrogen bonding, however, was estimated to be < 27.4 kJ mol–1.[17] In the absence of a better value, we have taken 27.4 $kJ{\cdot}mol^{-1}$ as an upper limit estimate of the intrinsic barrier restricting rotation of the NH_2 group in the absence of hydrogen bonding, from which we could at least determine the minimum energy of the N–H···Cl-Zn hydrogen bond in $[(\mathbf{L_1}^2)Zn(Cl)](BPh_4)$ and $[(\mathbf{L_1}^2)Zn(Cl)](Cl)$.

Thus, the barrier restricting the rotation of the NH_2 group of $[(\mathbf{L_1}^2)Zn(Cl)](BPh_4)$ was estimated to be *ca.* 44.2 $kJ{\cdot}mol^{-1}$ from the coalescence temperature (T_c) and amine proton resonances at low temperatures. From this barrier the energy of the N-H···Cl-Zn hydrogen bond was approximately calculated to be *ca.* 16.8 $kJ{\cdot}mol^{-1}$ by subtracting the activation barrier restricting rotation of the NH_2 group in the absence of hydrogen bonding (*vide supra*).

Concentration experiments suggest that the Cl^- counter-ion weakly hydrogen bonds to the external N–H in concentrated samples of $[(\mathbf{L_1}^2)Zn(Cl)](Cl)$ and that its

contribution to the rotational barrier is negligible at lower concentrations (Table 3.5 and Appendix). The proton resonance of the external N–H moves downfield and the barrier restricting rotation of the NH_2 increases slightly as the concentration increases, presumably due to some external N–H···Cl–Zn hydrogen bonding, which is very weak in concentrations < 7 mM (See Table 3.5 and Appendix, Figs. A3.8-9).

Thus, these ^{1}H NMR studies suggest that N–H···Cl–Zn hydrogen bonding in $[(\mathbf{L_1}^2)Zn(Cl)](BPh_4)$ is at least as strong as in $[(\mathbf{L_1}^1)Zn(Cl)](BPh_4)$, in excellent agreement with the crystallographic results, discussion and IR studies in solution. The X-ray structure of $[(\mathbf{L_1}^2)Zn(Cl)](BPh_4)$ shows a very short external N–H···π hydrogen bond with a phenyl group of the BPh_4^- anion (Fig. 2.5). The fact that the ^{1}H NMR spectra of 1.4–28 mM solutions of $[(\mathbf{L_1}^2)Zn(Cl)](BPh_4)$ in CD_3CN resembles that of 1.4 mM solutions of $[(\mathbf{L_1}^2)Zn(Cl)](Cl)$ suggests in this case that the external N–H···π hydrogen bond is not formed in solution (See Table 3.5 and Appendix, A3)

Table 3.5 Summary of temperature and concentration dependency of the NH_2 chemical shifts (δ, given in ppm) in the ^1H NMR (360.1 MHz, CD_3CN) of $[(\mathbf{L_1}^2)Zn(Cl)](Cl)$ (i), and $[(\mathbf{L_1}^2)Zn(Cl)](BPh_4)$ (ii), showing also the calculated rotational barriers of the NH_2 group and estimated H-bond energy of the internal N-H···Cl-Zn H-bond in these compounds.

(i) $[(\mathbf{L_1}^2)Zn(Cl)](Cl)$

	δNH_{av} (internal + external)/ppm	δNH_{av} (internal + external)/ppm	δNH_i (internal)/ppm	δNH_e (extenal)/ppm	$T_{coalescence}$/K	Rotational barrier/kJmol^{-1}	H-bond energy[a]/kJ mol^{-1}
28 mM	7.10	7.29	7.91	7.37	248	47.2	19.8
14 mM	7.04	7.20	7.93	7.08	243	45.9	18.5
7 mM	7.00	7.12	7.94	6.82	243	45.4	18
3.5 mM	6.97	7.07	7.95	6.56	243	44.9	17.5
1.8 mM	6.97	7.03	7.96	6.36	243	44.6	17.2
T/K	323	293	223	223			

[a]Assuming an intrinsic C–N rotational barrier of 27.4 kJ mol^{-1} (see text).

(ii) $[(\mathbf{L_1}^2)Zn(Cl)](BPh_4)$

	δNH_{av} (internal+ external)/ppm	δNH_{av} (internal+ external)/ppm	δNH_i (internal)/ppm	δNH_e (extenal)/ppm	$T_{coalescence}$/K	Rotional barrier/kJ mol^{-1}	H-bond energy[a]/kJ mol^{-1}
28 mM	6.92	6.94	7.98	6.03	243	44.2	16.8
7 mM	6.92	6.96	7.97	6.03	243	44.2	16.8
1.8 mM	6.92	6.96	7.98	6.03	243	44.2	16.8
T/K	323	293	223	223			

[a]Assuming an intrinsic C–N rotational barrier of 27.4 kJ mol^{-1} (see text).

3.3 CONCLUSION

In this Chapter we have investigated factors that affect the strength of internal N-H···X-Zn (X = Cl, NO_3) hydrogen bonding in complexes with trigonal bipyramidal geometry as a function of the hydrogen bond donor and acceptor.

From the point of view of the hydrogen bond donor, in principle, the amide N-H of $[(\mathbf{L_1}^1)Zn(Cl)](BPh_4)$ should have formed a stronger hydrogen bond than the less acidic amino groups of $[(\mathbf{L_1}^2)Zn(Cl)](BPh_4)$ and $[(\mathbf{L_1}^3)Zn(Cl)](BPh_4)$. In the solid state, however, the X-ray crystal structures of $[(\mathbf{L_1}^1)Zn(Cl)](BPh_4)\cdot CH_3CN$, $[(\mathbf{L_1}^2)Zn(Cl)](BPh_4)\cdot 0.5CH_3CN$ and $[(\mathbf{L_1}^3)Zn(Cl)](BPh_4)$ show that the strength and geometric features of this interaction are relatively insensitive to the nature of the hydrogen bond donor. We propose that a variety of structural parameters determine the geometry of the internal N–H···Cl–Zn hydrogen bond, including the $Zn–N_{py}$, distance and the angle between the planes containing the hydrogen bond donor and the Zn–Cl vector.

From the point of view of the hydrogen bond acceptor, the strength of internal N–H···X–Zn (X = Cl, NO_3) hydrogen bonds is dependent on the nature of the hydrogen bond acceptor and the strength order is $Cl^- > NO_3^-$.

Interestingly, the strength seems to be also dependent on the number of internal hydrogen bonds to the metal-bound ligand. Thus, as the number of internal

N–H···Cl–Zn increases, the average N···Cl distance shortens, indicating the strengthening of the internal N–H···Cl–Zn hydrogen bonds. We propose that the lengthening/weakening of the axial Zn-Cl bond induced by N–H···Cl–Zn hydrogen bonds is making the zinc-bound chloride a better hydrogen bond acceptor and hence the observed strengthening.

Thus, metal–ligand effects and geometry are clear examples of 'inorganic' factors that affect the strength of hydrogen bonding interactions involving coordination complexes.

Another objective was to correlate the information obtained from X-ray studies with spectroscopic studies in solution. This work provides an upper limit of the strength of the internal N–H···Cl–Zn hydrogen bonding in acetonitrile solution using IR and ^{1}H NMR variable temperature coalescence studies, which is ~ 16–17 kJ·mol^{-1} in complexes carrying different hydrogen bonding donors ([($\mathbf{L_1}^1$)Zn(Cl)](BPh$_4$) and [($\mathbf{L_1}^2$)Zn(Cl)](BPh$_4$) or [($\mathbf{L_1}^2$)Zn(Cl)](Cl). The magnitude of changes in the ^{1}H NMR and IR spectra can be correlated with the strength of the hydrogen bond in acetonitrile solutions and corroborates the conclusions derived from the X-ray crystallographic studies.

There is considerable current interest in elucidating the role(s) of second-sphere hydrogen bonding to metal-bound species in metallohydrolases, oxidases and peroxidases using small-molecule models.[18] Based on this work it is reasonable to suggest that strong internal hydrogen bonding in models of these metalloenzymes

could be effectively pursued with ligands that induce short metal-L distances (L = ligand carrying a hydrogen bonding group), by increasing the number of interactions and with good hydrogen bond acceptors.

3.4 EXPERIMENTAL

3.4.1 Materials and Methods

Reagents were obtained from commercial sources and used as received unless otherwise noted. Solvents were dried and purified under N_2 by using standard methods[19] and were distilled immediately before use. All compounds were prepared under N_2 unless otherwise mentioned. The synthesis and characterisation of $\mathbf{L_1}^1$, $\mathbf{L_1}^2$, $[(\mathbf{L_1}^1)Zn(Cl)](BPh_4)$, $[(\mathbf{L_1}^2)Zn(Cl)](BPh_4)$ and $[(\mathbf{L_1}^2)Zn(Cl)](Cl)$ were reported in Chapter 2. The NMR spectra were obtained using a Bruker DPX 360 at 20 °C in CD_3CN unless otherwise noted. ^1H chemical shifts are referenced with respect to the residual proton (δ_H 1.94 ppm) solvent peak. Peak assignments are done with the aid of 2-D NMR spectroscopy. Sample concentrations for the NMR studies were 1.4-28 mM. Mass spectra were performed on a Micromass Platform II system operating in Flow Injection Analysis mode with the electrospray method. Elemental analyses were carried out by the microanalyses service provided by the School of Chemistry at the University of Edinburgh. Infrared spectra were recorded with a JASCO FTIR-410 spectrometer between 4000 and 250 cm^{-1} as KBr pellets or as acetonitrile

solutions in KBr cells. The strength of N-H···Cl-Zn hydrogen bonding was estimated using solution FTIR studies applying Iogansen's equation[12] and variable temperature NMR coalescence methods[15]. The variable temperature ^{1}H NMR studies were repeated twice on freshly prepared samples and gave reproducible results.

3.4.2 Synthesis of ligands

***N*-(6-Neopentylamino-2-pyridylmethyl)-*N,N*-bis-(2-pyridylmethyl)amine L_1[3].**

A solution of *N*-(6-pivaloylamido-2-pyridylmethyl)-*N,N*-bis(2-pyridylmethyl)amine L_1[1] (1.0 g, 2.6 mmol) in 60 cm^3 of dry THF was added for 15 min to a solution of $LiAlH_4$ (1.0 g, 26.0 mmol) in 60 cm^3 of THF at -78 °C. The resulting solution was stirred for 1 h and then allowed to warm up to room temperature. After 12 h, the excess $LiAlH_4$ was quenched with dropwise addition of 10% aqueous THF. The precipitated inorganic salts were removed by filtration. Extraction of the filtrate with DCM (3 × 100 cm^3), followed by drying the combined organic fractions over anhydrous sodium sulphate, filltration, and removal of the solvent under reduced pressure, yielded a brown oil. The crude material was purified by column chromatography on neutral alumina by eluting with MeOH–DCM (2 : 98) to afford the ligand as a brown solid (0.65 g, 66%).

^{1}H NMR ($CDCl_3$, 250.1 MHz) δ_H (ppm) 8.50 (d, J = 6.2 Hz, 2H, py-H), 7.63 (m, 2H and 2H, py-*H*), 7.41 (t, J = 7.4 Hz, 1H, py-*H*), 7.11 (m, 2H, py-*H*), 6.79 (d, J = 7.3 Hz, 1H, py-*H*), 6.29 (d, J = 8.4 Hz, 1H, py-*H*), 4.60 (t, J = 6.0 Hz, 1H, N*H*CH_2), 3.90

(s, 4H, NC*H*$_2$py), 3.74 (s, 2H, NC*H*$_2$py), 3.02 (d, *J* = 6.0 Hz, 2H, NHC*H*$_2$C(CH$_3$)$_3$), 1.00 (s, 9H, CH$_2$(CH$_3$)$_3$). ^{13}C NMR (CDCl$_3$, 62.9 MHz) δ_C (ppm) 159.4, 158.6 and 156.4 (py-*C*), 148.9, 138.5, 136.4, 123.0, 122.0, 111.1 and 104.4 (py-*C*H), 60.1 and 59.6 (N*C*H$_2$py), 54.0 (N*C*H$_2$C-(CH$_3$)$_3$), 32.0 (CH$_2$*C*(CH$_3$)$_3$), 27.5 (C(*C*H$_3$)$_3$). ESI-MS (+ ion) m/z: found: 375.8 (100%), calc. 375.52 (100%) for [(**L$_1$**^{3})H]$^+$, and matches theoretical isotope distribution.

_N,N_-bis-(6-pivaloylamido-2-pyridylmethyl)-_N_-(2-pyridylmethyl)amine L$_2$[1].

2-(Aminomethyl)pyridine (0.37 g, 3.4 mmol) and 2-(pivaloylamido)-6-(bromomethyl)pyridine (2.0 g, 6.8 mmol) were dissolved in acetonitrile (80 cm^3) and stirred at room temperature for 5 minutes. Then, sodium carbonate (1.0 g, 9.43 mmol) and tetrabutylammonium bromide (10 mg, 0.03 mmol) were added and the temperature was raised to 44 °C. After 48 h the solution was cooled to room temperature and poured into 100 cm^3 of 1M NaOH$_{(aq)}$. The crude product was then extracted with dichloromethane (3 x 80 cm^3) and the organic fractions were dried over Na$_2$SO$_4$. The solvent was evaporated under vacuum to yield the product as a brown oil (2.2 g, 66%)

^{1}H NMR (CD$_3$Cl, 360.1 MHz) δ_H (ppm) 8.53 (m, 1H py-*H6*), 8.11 (d, J = 8.3 Hz, 2H, py'-*H5*), 8.01 (s, 2H, N*H*), 7.67 (t, J = 7.9 Hz, 2H, py'-*H4*), 7.60 (d, J = 7.7 Hz, 2H, py-*H3*), 7.57 (m, 1H, py-*H4*), 7.29 (d, J = 7.3 Hz, 2H, py'-*H3*), 7.15 (m, 1H, py-*H5*), 6.88 (d, J = 7.2 Hz, 1H, py-*H3*), 3.87 (s, 2H, NC*H*$_2$-py), 3.76 (s, 4H, NC*H*$_2$-py'), 1.33 (s, 6H, C-(C*H*$_3$)$_3$). ^{13}C NMR (CD$_3$Cl, 90.5 MHz) δ_C (ppm) 176.9 (*C*=O), 159.3 (py-*C2*), 157.7 and 151.0 (py'-C2 and py'-*C6*), 149.1 (py-*C6*), 138.8 (py'-*C3*), 136.5

(py-*C3*), 122.8 and 122.1 (py-*C4* and py-*C5*), 118.6 and 112.0 (py'-*C4* and py'-*C5*), 60.3 (N*C*H$_2$-py), 59.9 (N*C*H$_2$-py'), 39.8 (*C*-(CH$_3$)$_3$), 27.5 (C-(*C*H$_3$)$_3$). ESI-MS (+ion) Found 488.9 and 510.8, Calcd. 488.30 (100%) and 511.28 (100%) for $[(\mathbf{L_2}^1)H]^+$ and $[(\mathbf{L_2}^1)Na]^+$, and matches theoretical isotope distribution.

_N,N_-bis-(6-amino-2-pyridylmethyl)-_N_-(2-pyridylmethyl)amine $\mathbf{L_2}^2$.

$\mathbf{L_2}^1$ (1 g, 1.7 mmol) was dissolved in 2M $HCl_{(aq)}$ (100 cm^3) and the solution was refluxed for 24 h. The solution was then cooled to room temperature and poured into 1M $NaOH_{(aq)}$. The product was extracted with dichloromethane (3 x 100 cm^3) and the organic fractions were dried over Na_2SO_4. The solvent was evaporated under vacuum and washed with diethyl ether to yield the product as a brown solid (0.47 g, 71%). (Found: C, 64.04; H, 6.20; N, 24.17. Calc. for $C_{18}H_{20}N_5 \cdot H_2O$: C, 63.89; H, 6.55; N, 24.83%).

^{1}H NMR (DMSO-d_6, 360.1 MHz) δ_H (ppm) 8.47 (m, 1H, py-*H6*), 7.78 (t, J = 7.5 Hz, 1H py-*H4*), 7.59 (d, J = 7.6 Hz, 1H, py-*H3*), 7.34 (t, J = 7.6 Hz, 2H, py'-*H4*), 7.24 (m, 2H, py-*H5*), 6.72 (d, J = 7.2 Hz, 1H, py'-*H3*), 6.28 (d, J = 8.3 Hz, 1H, py'-*H5*), 5.86 (br, 4H, py'-N*H*$_2$) 3.71 (s, 2H, NC*H*$_2$-py), 3.48 (s, 4H, NC*H*$_2$-py'). ^{13}C NMR (DMSO-d_6, 90.5 MHz) δ_C (ppm) 159.2 (py-*C2*), 159.2 and 157.3 (py'-*C2* and py'-*C6*), 148.8 (py-*C6*), 137.5 (py'-*C3*), 136.6 (py-*C3*), 122.2 and 122.1 (py-*C4* and py-*C5*), 109.7 and 106.1 (py'-*C4* and py'-*C5*), 59.5 (N*C*H$_2$-py and N*C*H$_2$-py'). ESI-MS (+ ion) Found 321.0 (100%), Calcd. 321.18 (100%) for $[(\mathbf{L_2}^2)H]^+$, and matches theoretical isotope distribution.

3.4.3 Synthesis of Zn(II) complexes

$[(L_1^3)Zn(Cl)](BPh_4)$

$ZnCl_2$ (18.3 mg, 0.13 mmol) and L_1^3 (50 mg, 0.13 mmol) were dissolved in acetonitrile (15 cm^3) and the solution was stirred for 2 h at room temperature. The solvent was removed under vacuum. The crude product was re-dissolved in methanol (10 cm^3) and $NaBPh_4$ (39 mg, 0.13 mmol) was added. The solution was filtered and the residue was washed with methanol (2 × 2 cm^3) to yield a pure pale yellow solid (70 mg, 70%) (Found: C, 70.4; H, 6.2; N, 8.8. Calc. for $C_{47}H_{49}BClN_5Zn$, $[(L_1^3)Zn(Cl)](BPh_4)\cdot 1/3H_2O$: C, 70.42; H, 6.25; N, 8.74%).

^1H NMR (CD_3CN, 360.1 MHz): δ_H (ppm) $[(L_1^3)Zn(Cl)]^+$ 9.08 (d, J = 5.0 Hz, 2H, py–*H*), 8.20 (t, J = 5.4 Hz, 1H, N*H*CH_2–$C(CH_3)_3$), 8.01 (td, J = 7.9, 1.8 Hz, 2H py–*H*), 7.59–7.53 (m, 2H and 1H, py–*H*), 7.42 (d, J = 7.9 Hz, 2H, py–*H*), 6.64 (d, J = 9.0 Hz, 1H, py–*H*), 6.50 (d, J = 7.2 Hz, 1H, py–*H*), 3.98 (s, 4H, NC*H*$_2$–py), 3.74 (s, 2H, NC*H*$_2$–py), 3.00 (d, J = 5.4 Hz, 2H, C*H*$_2$–$C(CH_3)_3$), 1.03 (s, 9H, CH_2–$C(CH_3)_3$); BPh_4^- 7.28 (m, 8H, Ar–*H*2), 6.96 (t, J = 7.6 Hz, 8H, Ar–*H*3) and 6.82 (t, J = 7.2 Hz, Ar–*H*4). ^{13}C NMR (CD_3CN, 90.5 MHz, 298 K): δ_C (ppm); $[(L_1^3)Zn(Cl)]^+$ 161.7, 155.7 and 152.8 (py–*C*), 149.6, 142.1, 142.1, 125.9, 125.5, 112.4 and 108.6 (py–*C*H), 57.5, 56.4 and 55.3 (N*C*H$_2$–py and *C*H$_2$–$C(CH_3)_3$), 32.9 (CH_2–*C*$(CH_3)_3$) and 27.7 (CH_2–$C(CH_3)_3$); BPh_4^- 164.6 (B–*C*1, J_{B-C} = 49 Hz), 136.6 (*C*2), 126.5 (*C*3), 122.7 (*C*4). ESI-MS (+ion): found 474.0 (100%), calc. 474.1 (100%) for $[L_1^3)Zn(Cl)]^+$, and matches theoretical isotope distribution.

$[(L_2^2)Zn(Cl)](BPh_4)$

L_2^2 (200 mg, 0.63 mmol) and $ZnCl_2$ (90 mg, 0.63 mmol) were dissolved in dry acetonitrile (20 cm^3). The solution was stirred for 1 h at room temperature. The solution was filtered and the yellow precipitate was dried under vacuum. To a solution of this solid in methanol (5 cm^3) was added $NaBPh_4$ (80 mg, 0.23 mmol). The resulting mixture was stirred for 1 h. The white precipitate formed was collected by filtration, washed with an additional 2 cm^3 of methanol, and dried under vacuum to yield the title compound (120 mg, 26%) (Found: C, 67.7; H, 5.4; N, 12.1. Calc. for $C_{42}H_{40}BClN_6Zn$, $[(L_2^2)Zn(Cl)](BPh_4)\cdot 0.5CH_3CN$: C, 67.87; H, 5.50; N, 11.96%).

^1H NMR (CD_3CN, 360.1 MHz): δ_H (ppm) $[(L_2^2)Zn(Cl)]^+$ 9.18 (d, J = 5.4 Hz, 1H, py–*H*), 8.01 (td, J = 7.9, 1.5 Hz, 1H py–*H*), 7.61 (t, J = 6.5 Hz, 1H, py–*H*), 7.51 (t, J = 8.3 Hz, 2H, py–*H*), 7.45 (d, J = 7.9 Hz, 1H, py–*H*), 6.80 (br, 4H, N*H*$_2$–py), 6.60 (d, J = 8.5 Hz, 2H, py–*H*), 6.55 (d, J = 6.8 Hz, 2H, py–*H*), 3.99 (s, 2H, NC*H*$_2$–py), 3.74 (s, 4H, NC*H*$_2$–py); BPh_4^- 7.27 (m, 8H, Ar–*H*2), 6.98 (t, J = 7.5 Hz, 8H, Ar–*H*3) and 6.83 (t, J = 7.2 Hz, Ar–*H*4). ^{13}C NMR (CD_3CN, 90.5 MHz, 298 K): δ_C (ppm); $[(L_2^2)Zn(Cl)]^+$ 162.1, 155.4 and 152.0 (py–*C*), 149.8, 141.9, 141.7, 125.7, 125.3, 113.0 and 112.6 (py–*C*H), 56.4 and 55.9 (N*C*H$_2$–py); BPh_4^- 164.6 (B–*C*1, J_{B-C} = 34.2 Hz), 136.6 (*C*2), 126.5 (*C*3), 122.7 (*C*4). ESI-MS (+ion): found: 419.1 (100%), calc. 419.07 (100%) for $[(L_2^2)Zn(Cl)]^+$, and matches theoretical isotope distribution.

$[(L_2^2)Zn(ONO_2)](NO_3)$

L_2^2 (280 mg, 0.87 mmol) and $Zn(NO_3)\cdot 6H_2O$ (0.259 mg, 0.87 mg) were dissolved in a H_2O:CH_3OH solution (14:1 cm^3). The solution was refluxed for 1 h and then was

allowed to cool to room temperature. The solution was filtered through celite and the filtrate was evaporated to yield the compound as a yellow solid (400 mg, 87 %).

^{1}H NMR (D_2O, 360.1 MHz): δ_H (ppm) $[(\mathbf{L_2}^2)Zn(NO_3)]^+$ 8.56 (br, 1H, py–*H*), 7.83 (td, J = 7.9, 1.5 Hz, 1H py–*H*), 7.40 (t, J = 6.5 Hz, 2H, py–*H*), 7.32 (d, J = 7.9 Hz, 1H, py–*H*), 6.51 (m, 5H, py–*H*), 3.86 (s, 2H, NCH_2–py), 3.62 (s, 4H, NCH_2–py); ESI-MS (+ion): found: 446.1 (100%), calc. 446.09 (100%) for $[(\mathbf{L_2}^2)Zn(NO_3)]^+$, and matches theoretical isotope distribution.

3.4.4 X-ray Crystallography

Crystals suitable for X-ray diffraction studies were grown by slow evaporation of solutions of $[(\mathbf{L_1}^3)Zn(Cl)](BPh_4)$, $[(\mathbf{L_2}^2)Zn(Cl)](BPh_4)$ in CH_3CN/H_2O and $[(\mathbf{L_2}^2)Zn(ONO_2)](NO_3)$ in CH_3OH/H_2O.

Intensity data for of $[(\mathbf{L_1}^3)Zn(Cl)](BPh_4)$, $[(\mathbf{L_2}^2)Zn(Cl)](BPh_4)\cdot 0.5H_2O\cdot 0.5CH_3CN$ and $[(\mathbf{L_2}^2)Zn(ONO_2)](NO_3)$ were collected at 150 K using a Bruker-AXS SMART APEX area detector diffractometer with graphite-monochromated Mo-Kα radiation (λ = 0.71073 Å). The structures were solved by direct methods and refined to convergence against F^2 data using the SHELXTL suite of programs.[20] Data were corrected for absorption applying empirical methods using the program SADABS,[21] and the structures were checked for higher symmetry using the program PLATON.[22] All non-hydrogen atoms were refined anisotropically unless otherwise noted.

Hydrogen atoms were placed in idealised positions and refined using a riding model with fixed isotropic displacement parameters. The N-H hydrogens were located in the difference map and refined isotropically. Some *tert*-butyl groups showed elongated anisotropic displacement parameters. Attempts were made to model disorder in these regions. The fitting statistics, however, showed no improvement over the ordered models with large anisotropic displacement parameters. Difference maps of the crystal structure of $[(\mathbf{L_2}^2)Zn(Cl)](BPh_4)\cdot 0.5(H_2O\cdot CH_3CN)$ revealed disorder affecting the Zn–Cl, and the atoms in 6-position of two of the pyridine rings, which refined to 67 and 33% site-occupancies. A region of disordered solvent was also observed, which was modelled as a molecule of acetonitrile (half occupancy) disordered over two positions, and a water molecule (half occupancy).

CCDC reference numbers 239823, 239821 and 22743.

3.5 REFERENCES

(1) (a) E. Peris, J. C. Lee, Jr., J. R. Rambo, O. Eisenstein and R. H. Crabtree, J. Am. Chem. Soc., 1995, 117, 3485-3491.(*b*) J. C. Mareque Rivas and L. Brammer, *Coord. Chem. Rev.*, 1999, **183**, 43; (*c*) L. M. Epstein and E. S. Shubina, *Coord. Chem. Rev.*, 2002, **231**, 165; (*d*) R. H. Crabtree, P. E. M. Siegbahn, O. Eisenstein, A. Rheingold and T. F. Koetzle, *Acc. Chem. Res.*, 1996, **29**, 348; (*e*) A. J. Lough, S. Park, R. Ramachandran and R. H. Morris, *J. Am. Chem. Soc.*, 1994, **116**, 8356; (*f*) G. Aullón, D. Bellamy, L. Brammer, E. A. Bruton and A. G. Orpen, *Chem. Commun.*, 1998, 653; (*g*) D. Braga and F. Crepioni, *Acc. Chem. Res.*, 1997, **30**, 81.

(2) These compounds where first synthesised by Dr. R Prabaharan and were included with his consent in this study. See J. C. Mareque-Rivas, R. Prabaharan and S. Parsons, *Dalton Trans.*, 2004, 1648-1655 and references therein for experimental details.

(3) H. Adams, N. A. Bailey, D. E. Fenton and Q.-Y. He, *J. Chem. Soc., Dalton Trans.*, 1997, 1533.

(4) C. S. Allen, C. L. Chuang, M. Cornebise and J. W. Canary, *Inorg. Chim. Acta*, 1995, **239**, 29.

(5) F. H. Allen, O. Kennard, D. G. Watson, L. Brammer, A. G. Orpen and R. Taylor, *Journal of the Chemical Society, Perkin Transactions 2: Physical Organic Chemistry (1972-1999)*, 1987, S1.

(6) M. Rozenberg, A. Loewenschuss and Y. Marcus, *Phys. Chem. Chem. Phys.*, 2000, **2**, 2699.

(7) J. C. Mareque-Rivas, E. Salvagni, R. Torres Martin de Rosales and S. Parsons, *Dalton Trans.*, 2003, 3339.

(8) A. Bondi, *J. Phys. Chem.*, 1964, **68**, 441.

(9) G. Aullon, D. Bellamy, G. A. Orpen, L. Brammer and E. A. Bruton, *Chem. Commun.*, 1998, 653.

(10) J. C. Mareque Rivas, R. Prabaharan, R. Torres Martín de Rosales, L. Metteau and S. Parsons, *Dalton Trans.*, 2004, 2800.

(11) F. H. Allen, *Acta Crystallogr.*, 2002, **B58**, 380.

(12) A. V. Iogansen, G. A. Kurkchi, V. M. Furman, V. P. Glazunov and S. E. Odinokov, *Zh. Prikl. Spektrosk.*, 1980, **33**, 460.

(13) (a) A. V. Iogansen, in '*Vodorodnaya Svyaz (Hydrogen Bonding)*', ed. N. D. Sokolov. Nauka, Moscow, 1981, p. 112 (in Russian); (b) A. V. Iogansen, *Spectrochim. Acta A*, 1999, **55**, 1585.

(14) See for example: (*a*) E. I. Gutsul, N. V. Belkova, M. S. Sverdlov, L. M. Epstein, E. S. Shubina, V. I. Bakhmutov, T. N. Gribanova, R. M. Minyaev, C. Bianchini, M. Peruzzini and F. Zanobini, *Chem. Eur. J.*, 2003, **9**, 2219-2228; (*b*) S. G. Kazarian, P. A. Hamley and M. Poliakov, *J. Am. Chem. Soc.*, 1993, 115, 9069.

(15) J. Sandstrom, '*Dynamic NMR Spectroscopy*', Academic Press, New York, 1982.

(16) H. Frieboling, '*Basic One- and Two- Dimensional NMR Spectroscopy*', VCH, Weinheim, 1991.

(17) E. Peris, J. C. Lee, Jr., J. R. Rambo, O. Eisenstein and R. H. Crabtree, *J. Am. Chem. Soc.*, 1995, **117**, 3485.

(18) (*a*) R. Krämer, *Coord. Chem. Rev.*, 1999, **182**, 243; (*b*) D. K. Garner, S. B. Fitch, L. H. McAlexander, L. M. Bezold, A. M. Arif and L. M. Berreau, *J. Am. Chem. Soc.*, 2002, **124**, 9970; (*c*) M. Wall, B. Linkletter, D. Williams, A.-M. Lebuis, R. C. Hynes and J. Chin, *J. Am. Chem. Soc.*, 1999, **121**, 4710; (*d*) F. Mancin and J. Chin, *J. Am. Chem. Soc.*, 2002, **124**, 10496; (*e*) J. Chin, S. Chung and D. H. Kim, *J. Am. Chem. Soc.*, 2002, **124**, 10498; (*f*) C. E. MacBeth, A. P. Golombek, V. G. Young Jr., C. Yang, K. Kuczera, M. P. Hendrich and A. S. Borovik, *Science*, 2000, **289**, 938; (*g*) A. Wada, M. Harata, K. Hasegawa, K. Jitsukawa, H. Masuda, M. Mukai, T. Kitagawa and H. Einaga, *Angew. Chem., Int. Ed.*, 1998, **37**, 798.

(19) W. L. F. Armarego and D. D. Perrin, '*Purification of Laboratory Chemicals*', Butterworth-Heinemann, Oxford, 1997.

(20) G. M. Sheldrick, '*SHELXTL 97*', University of Göttingen, 1997.

(21) G. M. Sheldrick, '*SADABS, Empirical absorption correction program*', University of Göttingen, 1995, based upon the method of Blessing.

(22) A. L. Spek, *Acta Crystallogr., Sect. A.*, 1990, **46**, C34.

Chapter 4. Effects of internal N-H···X-Zn (X = Cl, $O(H)_{1-2}$, phosphate) hydrogen bonding

4.1 Effects of internal N-H···Cl-Zn hydrogen bonding in metal-ligand distances

4.1.1 INTRODUCTION

In order to assess the real potential of exploiting/designing microenvironments around metal(s) ion(s) as a novel approach in ligand design, it is important to investigate and contrast the magnitude of effects associated with non-coordinating and coordinating groups in structural and functional features of model coordination complexes.

Important properties of metal-bound ligands, including nucleophilicity, electrophilicity and acidity depend on the interaction with the metal. In addition, properties of the metal are modulated by the ligand environment. In all these aspects the metal–ligand distance(s) is an important parameter. Given the current intense interest in ligands that induce intramolecular hydrogen bonds to metal bound ligands,[1] we considered important to investigate the implications of the hydrogen bonding groups on metal–ligand distances. As a model, in this section we investigate the extent to which ligands **L** that create a hydrogen bonding cavity in trigonal bipyramidal $[(\mathbf{L})Zn(Cl)]^+$ cations affect the **L**–Zn and Zn–Cl distances. The changes observed are compared with those induced by changes in the first coordination sphere.

4.1.2 Ligand selection

The ligands used in this study are shown in Scheme 4.1. Thus, the (6-R-2-pyridylmethyl)amine (R = NH_2 ($\mathbf{L}_n^2$) or $NHCH_2{}^tBu$ ($\mathbf{L}_n^3$) (*n* = number of hydrogen bonding groups)) ligand unit in **tpa** based ligands has a suitable stereochemistry for the participation of the N-H group in internal hydrogen bonding to an adjacent metal-bound ligand.[2-5] As a series, these ligands offer a similar N_4 coordinating environment and a variable hydrogen bonding and hydrophobic microenvironment.

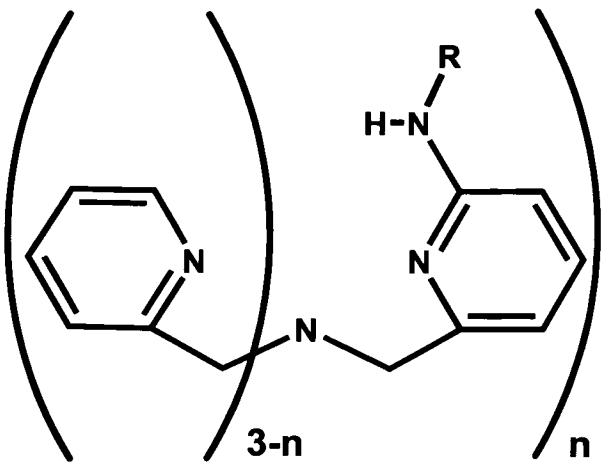

$R = H;\ n = 1, 2, 3;\ \mathbf{L}_{1\text{-}3}^2$

$R = CH_2{}^tBu;\ n = 1, 2, 3;\ \mathbf{L}_{1\text{-}3}^3$

Scheme 4.1

In [(**tpa**)Zn(Cl)](BPh_4)[6] the Zn-N distance to the axial bridgehead nitrogen is 2.271(3) Å. In [($\mathbf{L}_1^2$)Zn(Cl)](BPh_4) the same distance is 2.2247(18) Å, which means a decrease in the distance by *ca.* 0.05 Å. In contrast, the Zn-Cl bond is increased

from 2.2754(14) Å to 2.2959(7) Å. Since $[(\mathbf{L_1}^2)Zn(Cl)](BPh_4)$ exhibits an internal N-H···Cl-Zn hydrogen bond we considered interesting to compare with other $[(\mathbf{L})Zn(Cl)](BPh_4)$ complexes (**L** = ligand with two and three N–H hydrogen bond donors) to determine if there was a correlation between the number and geometries of N–H···Cl–Zn hydrogen bonding interactions and the length of the axial Zn–Cl bond.

4.1.3 RESULTS

4.1.3.1 Synthesis

The synthesis of the ligand tris[(6-neopentylamino-2-pyridyl)methyl]amine) $\mathbf{L_3}^3$ was accomplished from the corresponding tripodal ligand tris[(6-pivaloylamido--2-pyridyl)methyl]amine) $\mathbf{L_3}^1$ upon reduction.[7] The synthesis of the zinc(II) complex $[(\mathbf{L_3}^3)Zn(Cl)](BPh_4)$ was accomplished in the same way as described before for $[(\mathbf{L_1}^1)Zn(Cl)](BPh_4)$, $[(\mathbf{L_1}^2)Zn(Cl)](BPh_4)$ and $[(\mathbf{L_2}^2)Zn(Cl)](BPh_4)$.

4.1.3.2 X-ray Crystallography: Structure of $[(\mathbf{L_3}^3)Zn(Cl)](BPh_4)$

A thermal ellipsoid plot of the X-ray crystal structure of $[(\mathbf{L_3}^3)Zn(Cl)](BPh_4)$ is shown in Figure 4.1, crystallographic and refinement data are given in Table 4.1 and selected distances and angles are given in Table 4.2. As in $[(\mathbf{L_1}^1)Zn(Cl)](BPh_4)$,

$[(\mathbf{L_1}^2)Zn(Cl)](BPh_4)$ and $[(\mathbf{L_2}^2)Zn(Cl)](BPh_4)$, the zinc(II) ion in $[(\mathbf{L_3}^3)Zn(Cl)](BPh_4)$ is in a trigonal bipyramidal environment with the three pyridine units occupying the equatorial positions, and the bridgehead amine nitrogen and chloride in the axial positions. An interesting feature of the structure of $[(\mathbf{L_3}^3)Zn(Cl)](BPh_4)$ is the participation of all the N-H groups in internal N-H···Cl-Zn hydrogen bonding (N(7)···Cl(1) 3.205(3) Å; H(7N)···Cl(1) 2.26 Å; N(7)–H(7N)···Cl(1) 155.1°; N(17)···Cl(1) 3.187(3) Å; H(17N)···Cl(1) 2.23 Å; N(17)···H(17N)···Cl(1) 156.1°; N(27)···Cl(1) 3.115(3) Å; H(27N)···Cl(1) 2.12 Å; N(27)···H(27N)···Cl(1) 167.1°; for N–H bonds extended to 1.01 Å).[8]

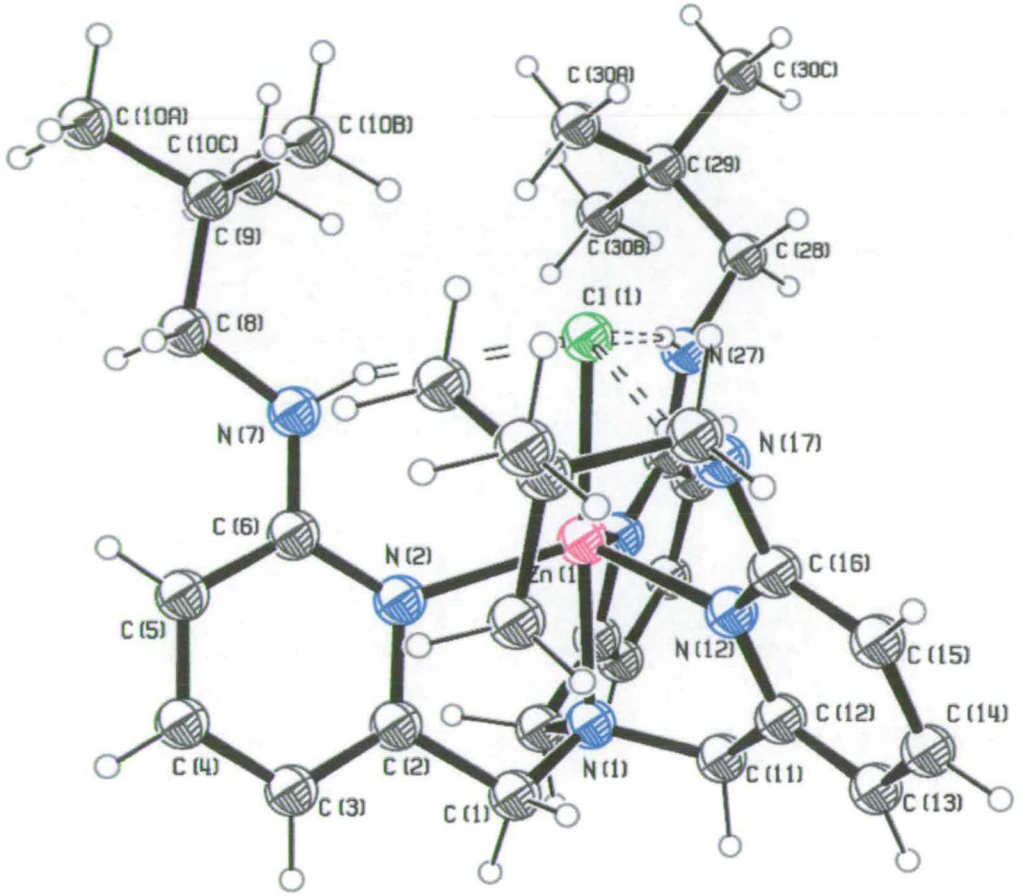

Fig. 4.1 Thermal ellipsoid plot drawn with 30% probability ellipsoids of the $[(L_3^3)Zn(Cl)]^+$ cation of $[(L_3^3)Zn(Cl)](BPh_4)$ showing three internal N–H···Cl–Zn hydrogen bonds. Only N–H hydrogens are shown for clarity

Table 4.1 Crystallographic data and structure refinement details for $[(\mathbf{L_3}^3)Zn(Cl)](BPh_4)$

Empirical Formula	$C_{57}H_{71}BClN_7Zn$
M_r	965.84
T/ K	150(2)
Crystal system	Triclinic
Space group	$P\bar{1}$
Crystal size/mm	0.43 × 0.34 × 0.21
a /Å	9.9472(3)
b /Å	16.1945(3)
c /Å	18.1206(6)
α / °	67.178(2)
β / °	76.584(2)
γ / °	79.533(2)
V / Å^3	2603.39(14)
Z	2
D_c / g cm^{-3}	1.232
μ / mm–1	0.773
R_{int}	0.0434
$R_1(F)^a$ (all data)	0.0633
$wR_2(F^2)^a$ (all data)	0.1205
$S(F^2)^a$ (all data)	1.041
Largest difference peak, hole/e Å^3	1.005, –0.469

$^aR_1(F) = \Sigma(|F_o| - |F_c|)/ \Sigma(|F_o|$; $wR_2(F^2) = [\Sigma w(F_o^2 - F_c^2)^2/\Sigma wF_0^4]^{1/2}$; $S(F^2) = [\Sigma w(F_o^2 - F_c^2)^2/(n-p)]^{1/2}$.

Table 4.2 Selected bond lengths (Å) and angles (°) for $[(\mathbf{L_3}^3)Zn(Cl)](BPh_4)$

Zn(1)–N(2)	2.152(2)
Zn(1)–N(12)	2.186(2)
Zn(1)–N(22)	2.211(2)
Zn(1)–N(1)	2.113(2)
Zn(1)–Cl(1)	2.2861(7)
N(2)–Zn(1)–N(12)	108.90(8)
N(2)–Zn(1)–N(22)	120.11(9)
N(12)–Zn(1)–N(22)	118.53(8)
N(1)–Zn(1)–N(2)	79.45(8)
N(1)–Zn(1)–N(12)	76.98(8)
N(1)–Zn(1)–N(22)	77.93(8)
N(1)–Zn(1)–Cl(1)	176.63(6)
Cl–Zn(1)–N(2)	103.76(6)
Cl–Zn(1)–N(12)	100.84(6)
Cl–Zn(1)–N(22)	101.08(6)

4.1.4 Discussion

The previously described molecular structures of $[(\mathbf{L_1}^2)Zn(Cl)](BPh_4)$, $[(\mathbf{L_2}^2)Zn(Cl)](BPh_4)$, $[(\mathbf{L_1}^3)Zn(Cl)](BPh_4)$ and $[(\mathbf{L_3}^3)Zn(Cl)](BPh_4)$ together with the structures of $[(\mathbf{L_3}^2)Zn(Cl)](BPh_4)$ and $[(\mathbf{L_2}^3)Zn(Cl)](BPh_4)$,[9] allow the study of the lengthening of the Zn–Cl bond by local N–H hydrogen bond donors.

Thus, the Zn–Cl distance follows the trend 2.275 Å in $[(\mathbf{tpa})Zn(Cl)](BPh_4)$, 2.296 Å in $[(\mathbf{L_1}^2)Zn(Cl)](BPh_4)$, 2.323 Å in $[(\mathbf{L_2}^2)Zn(Cl)](BPh_4)$, and 2.347 Å in $[(\mathbf{L_3}^2)Zn(Cl)](BPh_4)$ (Scheme 4.2). It is interesting to note that the lengthening of the axial Zn–Cl bond is accompanied by a progressive seemingly correlated shortening of the axial Zn–N(1) distance; 2.271 Å in $[(\mathbf{tpa})Zn(Cl)](BPh_4)$, 2.225 Å in $[(\mathbf{L_1}^2)Zn(Cl)](BPh_4)$, 2.181 Å in $[(\mathbf{L_2}^2)Zn(Cl)](BPh_4)$, to 2.115 Å in $[(\mathbf{L_3}^2)Zn(Cl)](BPh_4)$. As a result of the triply hydrogen bonding microenvironment the Zn–Cl distance of $[(\mathbf{L_3}^2)Zn(Cl)](BPh_4)$ is at the upper end of the range observed for axial Zn–Cl bonds, whereas the axial Zn–N(1) distance is one of shortest among N_4 ligands that induce a trigonal bipyramidal geometry (*vide infra*).

The Zn–Cl distances of the complexes with the neopentylamino groups $[(\mathbf{L_{1-3}}^3)Zn(Cl)](BPh_4)$ are also longer than in $[(\mathbf{tpa})Zn(Cl)](BPh_4)$, however, they are shorter than the amino analogues and follow a different trend, 2.281 Å in $[(\mathbf{L_1}^3)Zn(Cl)](BPh_4)$, 2.286 Å in $[(\mathbf{L_3}^3)Zn(Cl)](BPh_4)$ and 2.313 Å in $[(\mathbf{L_2}^3)Zn(Cl)](BPh_4)$. These structural differences could lead to functional differences between complexes with different internal hydrogen bonding groups. However, like

in $[(\mathbf{L_{1\text{-}3}}^2)Zn(Cl)](BPh_4)$, as the number of hydrogen bonding groups increases the axial Zn–N distance shortens; 2.236 Å in $[(\mathbf{L_1}^3)Zn(Cl)](BPh_4)$, 2.161 Å in $[(\mathbf{L_2}^3)Zn(Cl)](BPh_4)$ and 2.113 Å in $[(\mathbf{L_3}^3)Zn(Cl)](BPh_4)$.

Also noticeable are the changes induced by the amino and neopentylamino groups on the equatorial Zn–N_{py} distances. Thus, the average Zn–N_{py} distance is progressively lengthened from 2.069 Å in $[(\mathbf{tpa})Zn(Cl)](BPh_4)$ to 2.084 Å in $[(\mathbf{L_1}^2)Zn(Cl)](BPh_4)$, 2.099 Å in $[(\mathbf{L_2}^2)Zn(Cl)](BPh_4)$ and 2.159 Å in $[(\mathbf{L_3}^2)Zn(Cl)](BPh_4)$, despite the electron donating properties of the amino groups on the pyridine rings.

The zinc(II) complexes with the neopentylamino groups have average Zn–N_{py} distances of 2.088 Å in $[(\mathbf{L_1}^3)Zn(Cl)](BPh_4)$, 2.121 Å in $[(\mathbf{L_2}^3)Zn(Cl)](BPh_4)$ and 2.183 Å in $[(\mathbf{L_3}^3)Zn(Cl)](BPh_4)$, and hence are slightly longer than the corresponding amino analogues, presumably due to steric reasons. It should be noted that all these zinc(II) chloride complexes adopt a predominantly trigonal bipyramidal geometry. Thus, the degree of trigonality was evaluated by means of the angular structural parameter $\tau = (\beta - \alpha) / 60$ introduced by Addison *et al.*,[10] where α and β represent the two largest angles around the central atom with $\beta > \alpha$. A perfect trigonal bipyramidal geometry is associated with $\tau = 1$, while $\tau = 0$ is indicative of a perfect square pyramidal geometry; τ values in $[(\mathbf{L_{1\text{-}3}}^2)Zn(Cl)](BPh_4)$ and $[(\mathbf{L_{1\text{-}3}}^3)Zn(Cl)](BPh_4)$ are in the range 0.80–1.00.

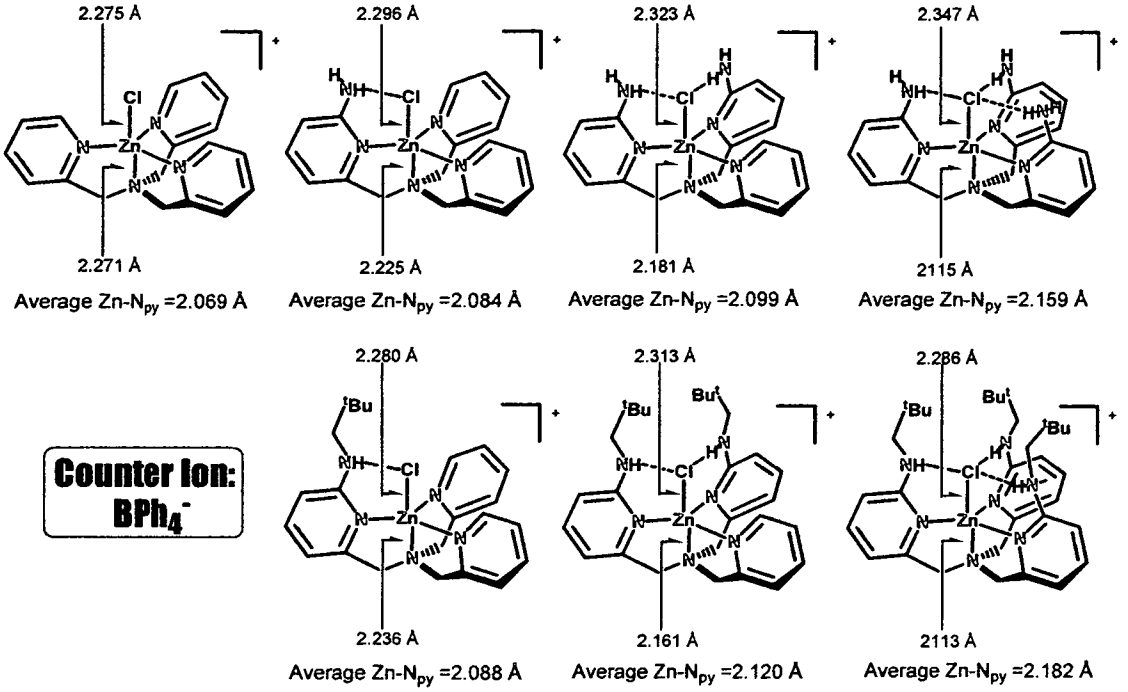

Scheme 4.2

The X-ray crystal structures of $[(\mathbf{L}_{1\text{-}3}^{2})Zn(Cl)](BPh_4)$ and $[(\mathbf{L}_{1\text{-}3}^{3})Zn(Cl)](BPh_4)$ show the participation of all the N–H groups in internal N–H···Cl–Zn hydrogen bonds. Thus, a possible reason for the weakening of Zn–Cl bonds could be the interaction with the local N–H groups. In that respect it is important to note that the influence of intramolecular N–H···S–Fe in Fe–S bond distances has been recently demonstrated, and it is important in relation with the functional importance of such a hydrogen bond in the active site of cytochromes P450.[11-13]

In order to compare the magnitude of the effects associated with the hydrogen bonding groups on axial Zn–Cl/N and equatorial Zn–N_{py} distances with those associated with changes in the first coordination sphere, we have examined the X-ray

structures of LZnCl complexes with predominantly trigonal bipyramidal geometries and different coordinating environments (Scheme 4.3).

Changes involving one of the N_{py} donating arms of N_4 tripodal tris-pyridine ligands by another N-donating group lead to axial Zn–Cl distances that range from 2.264 Å in $[(\alpha\text{-PhTPA})Zn(Cl)]^+$ to 2.289 Å in the mixed coordination/organometallic complex $[((CpMn(CO)_2(CH_2PzCH_2))N(CH_2Py)_2)Zn(Cl)]$ in which an anionic pyrazole unit (Pz) is simultaneously coordinated to the zinc(II) and manganese(I) centres (Scheme 4.3).[14, 15] Changes in the axial Zn–Cl distances are in this case accompanied by seemingly uncorrelated changes in the axial Zn–N distances of 2.271–2.297 Å.[6, 13-16] The average equatorial $Zn–N_{py}$ distances are in the 2.070–2.140 Å range, with the longer distances corresponding to the more donating and/or sterically hindered ligand environments. It is interesting to compare the axial Zn–N and Zn–Cl distances induced by a completely different tripodal N_4 ligand such as tris(2-aminoethyl)amine (tren); Zn–N 2.325 Å and Zn–Cl 2.308 Å.[17] Thus, N_4 tripodal ligands induce axial Zn–Cl distances of 2.264–2.308 Å, and axial Zn–N distances of 2.271–2.325 Å.

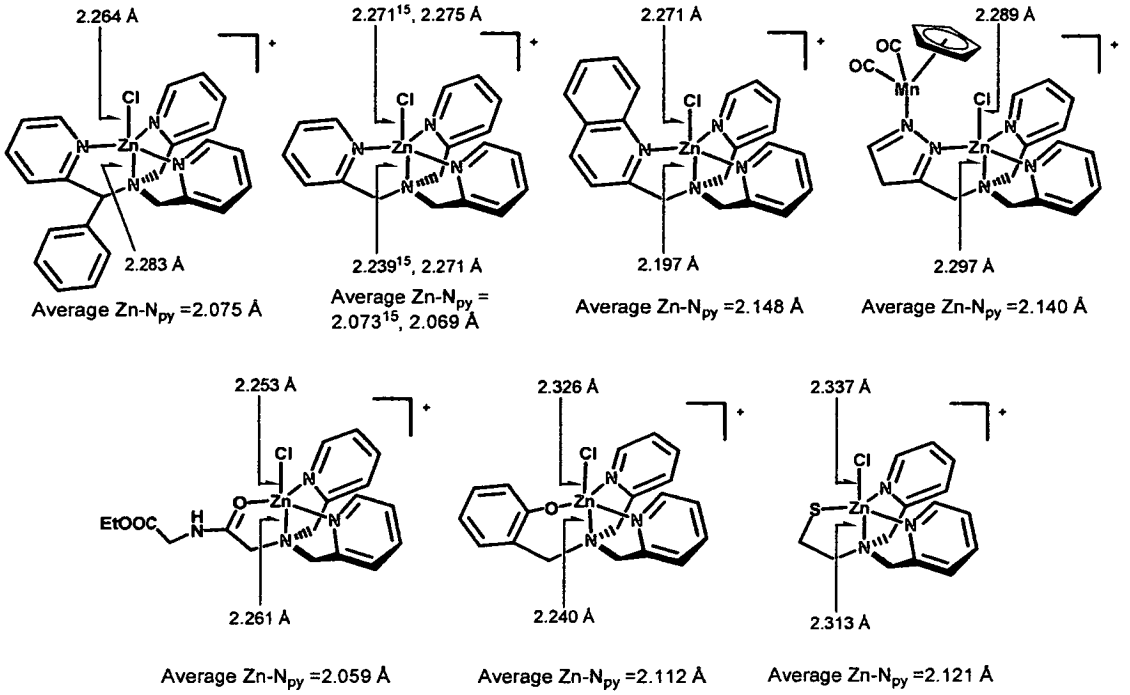

Scheme 4.3

The replacement of one of the N_{py} donating arms by an O or S donating one, leading to N_3O or N_3S tripodal ligands, results in axial Zn–Cl distances of 2.253–2.371 Å and Zn–N distances of 2.240–2.398 Å, and equatorial Zn–N_{py} distances of 2.059–2.121 Å (representative examples are shown in Scheme 3.9).[18-22] The greater variability of distances found in this case probably reflects the greater differences in the ligand environment, with the poorer donating groups inducing shorter Zn–Cl and Zn–N_{py} distances.

It seems significant that the local non-coordinating N–H hydrogen bonding groups can induce changes in the Zn–Cl distances of comparable magnitude to those induced by major changes in the first coordination sphere of the zinc(II) centre. Moreover, it is remarkable that despite the electron donating nature of the hydrogen

bonding groups the average equatorial Zn–N_{py} is lengthened to a greater extent than by replacing a neutral by an anionic coordinating group. These changes induced by the hydrogen bonding groups may prove significant in determining the properties of these metal complexes. Also, from this structural analysis it appears that hydrogen bonding to the Zn–Cl causes a much greater influence in the *trans* Zn–N distance than changes in the first coordination sphere. The '*trans influence*' caused by the hydrogen bonding groups could, like conventional *trans influence*, be important in determining binding, properties and substitution mechanisms of metal-bound species

4.2 Effect of hydrogen bonding and coordinating groups in modulating the zinc-water acidity

4.2.1 Introduction

In nucleases/hydrolases the catalytic metal, typically zinc(II), is coordinated to the protein backbone to three amino acid residues, of which histidine is by far the most common coordinating amino acid. A fourth coordination site is usually occupied by a catalytically important water molecule.[23] This motif is essential in the mechanism of action of hydrolases as the coordinated water molecule could be ionised or polarised generating a nucleophilic hydroxide that could attack the substrate (Scheme 4.4). Alternatively, the water molecule could be displaced by the substrate resulting in activation towards nucleophilic attack.

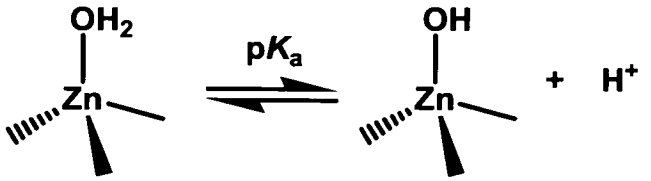

Scheme 4.4

Thus, the Zn(II)-bound water acidity is a key property in the function of catalytic zinc sites.[24] The Lewis acidic Zn(II) will aid in the activation of the coordinated water, lowering its pK_a compared to that of the bulk solvent and generating a relatively high concentration of coordinated hydroxide ion at the metal centre close to neutral pH. Therefore, zinc(II) complexes capable of generating a zinc(II)–hydroxide at neutral pH could be particularly suitable to effect hydrolysis reactions under biological conditions.

The identity of the ligands coordinated to the zinc(II) ion is known to play a critical role in the extent of polarisation and ionisation of the coordinated water molecule. For example, substitution of one of the three neutral histidine ligands in wild-type carbonic anhydrase (CA), a mononuclear zinc lyase that catalyses the reversible hydration of carbon dioxide into bicarbonate, by a negatively charged aspartate or glutamate led to an increase in the pK_a of the zinc-bound water from 6.8 to 8.6.[25] It is interesting, however, that the pK_a of carboxypeptidase A (CPA), is 9.5,[26]despite the zinc(II) ion being ligated also to two histidines and a glutamate. This may suggest that the active-site microenvironments are also important in determining the zinc-water acidity.

The role of the primary coordination sphere in the acidity of the metal-bound water has also been extensively investigated by both studies in model species[27-29] and theoretical calculations[30-37]. These studies show that the acidity of the zinc-bound water molecule indeed decreases with decreasing the coordination number and increasing the positive charge. The influence of hydrophobic microenvironments was demonstrated by Coates *et al.*[38] while investigating the acidity of the zinc-water unit in the model complexes $\{[N(CH_2CH_2NR_2)_3]Zn(OH_2)\}^{2+}$ (R= H, Me) (Figure 4.2).

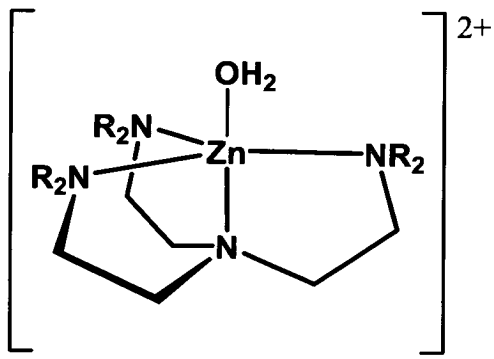

R = H, CH_3

Fig. 4.2 *$\{[N(CH_2CH_2NR_2)_3]Zn(OH_2)\}^{2+}$ (R= H, Me).*

Remarkably, it was found that the metal-bound water molecule in the substituted $\{[N(CH_2CH_2NMe_2)_3]Zn(OH_2)\}^{2+}$ complex was more acidic (pK_a= 9.0) than in the unsubstituted $\{[N(CH_2CH_2NH_2)_3]Zn(OH_2)\}^{2+}$ (pK_a = 10.3). This result was unexpected, as the methyl groups are electron-donating and hence should make the zinc centre less Lewis acidic. In this study it was suggested that second-sphere hydrophobic interactions with the coordinated water in $\{[N(CH_2CH_2NMe_2)_3]Zn(OH_2)\}^{2+}$ enhanced its acidity.

Thus, it seems that the active site microenvironment could also exert a substantial effect in the zinc–water acidity. In fact, in CA, a combination of hydrophobic and hydrogen bonding interactions are believed to account for the high zinc-water acidity (pK_a = 6.8) (Scheme 4.5).[39-41]

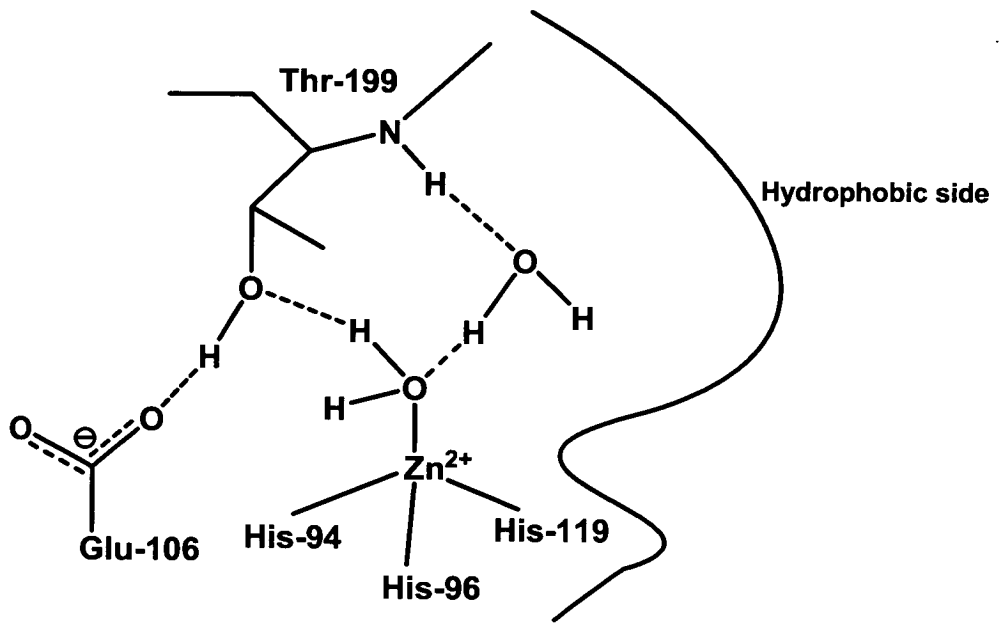

Scheme 4.5 *Proposed hydrophobic and hydrogen bonding interactions in the active site of CA.*

Site-directed mutagenesis studies also indicate that hydrogen bonding interactions between the zinc-bound water and second sphere XH groups (X = N, O) of arginine, lysine, histidine, tyrosine and/or serine residues can also have a large effect in the zinc water acidity.[42, 43] The extent to which the identity, number and position of these aminoacid residues affects the acidity of the zinc-water unit is not known. Furthermore, the relative contribution or importance of the first and second coordination sphere of the zinc(II) ion towards determining the pK_a of the zinc-bound water remains also to be elucidated.

In this section, we assess and compare the effects of the first and second coordination sphere of zinc(II)-aqua complexes towards the acidity of a zinc-water unit by using ligands that offer different coordinating and hydrogen bonding groups (Scheme 4.6).

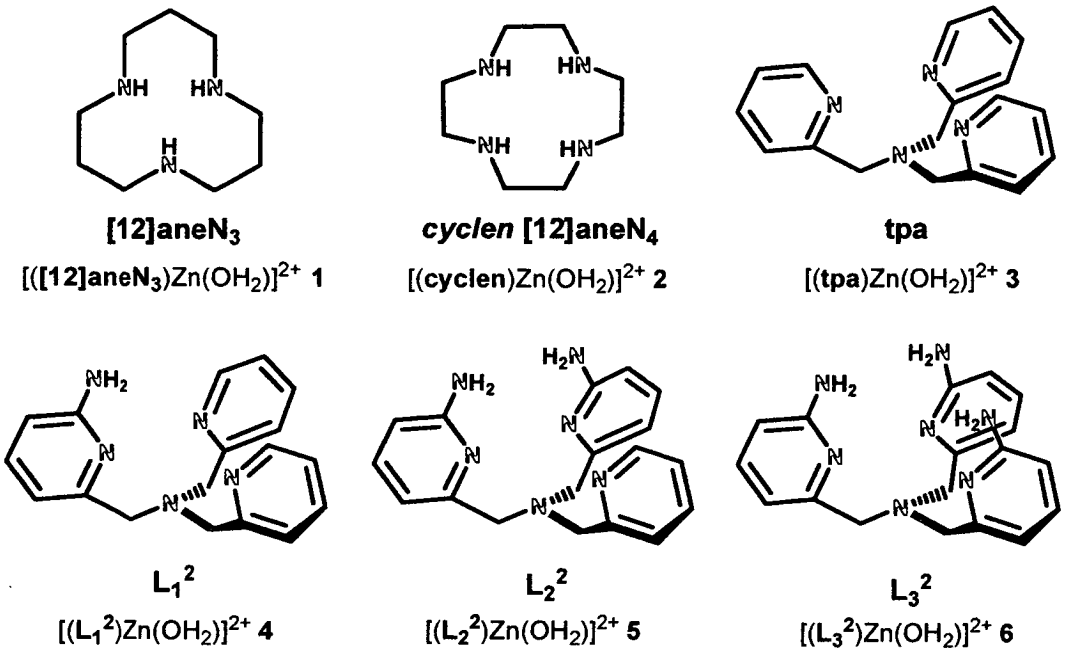

Scheme 4.6

4.2.2 Results and discussion

From potentiometric pH titrations performed in our group[44] of the ligands (1 mM) in the absence and presence of 1 mM Zn^{2+} at 25 °C with $I = 0.1$ ($NaNO_3$), the deprotonation constants for each of the acid species of each ligand, as well as the complexation constants (log K_{LZn}) and deprotonation constants (pK_a for Zn–OH_2 ↔

Zn–OH) of the zinc(II)-aqua complexes **3–6** were determined by the program HYPERQUAD[45] (Table 4.3).

Table 4.3 Protonation and Zn(II) complexation constants determined by potentiometric pH titrations at 25 °C

	LH_3			$[(L)Zn(OH_2)]^{2+}$	
	log K_1	log K_2	log K_3	log KZnL	pK_a
1[a]	(12.6 ± 0.1)	(7.5 ± 0.2)	(2.4 ± 0.1)	(8.41 ± 0.02)	(7.30 ± 0.02)
2[b]	(10.7)	(9.7)	—	(16.2 ± 0.2)	(8.02 ± 0.03)
3	6.28 ± 0.05	4.49 ± 0.05	2.73 ± 0.1	11.06 ± 0.04	8.08 ± 0.04
4	7.25 ± 0.01	4.94 ± 0.02	3.25 ± 0.02	10.36 ± 0.02	7.62 ± 0.09
5	7.52 ± 0.02	5.76 ± 0.03	3.61 ± 0.01	8.82 ± 0.01	6.68 ± 0.02
6	8.00 ± 0.08	6.33 ± 0.07	4.94 ± 0.03	8.09 ± 0.05	5.99 ± 0.05

[a] $I = 0.1$ ($NaClO_4$), from ref. 29, 46. [b] $I = 0.2$ ($NaClO_4$), from ref. 47.

These data together with the corresponding literature values for **1**[29, 46] and **2**[47] show that as the coordination number increases (**1** < **2** = **3**) the charge on the zinc(II) centre is reduced, thereby its capacity to polarise/ionise the bound water molecule is reduced (pK_a of the zinc-bound water molecule of **1** < **2** ≈ **3**), which demonstrates the importance of the first coordination sphere.

Given that amino groups are electron-donating it may have been reasonable to expect the pK_a of the zinc-bound water molecule to follow the trend **3** < **4** < **5** < **6**. The observed trend, however, was **3** > **4** > **5** > **6** (Table 4.3, Figure 4.3), which can be

rationalised as resulting from the effect of intramolecular N–H···O(H)$_n$–Zn hydrogen bonding.[48, 49]

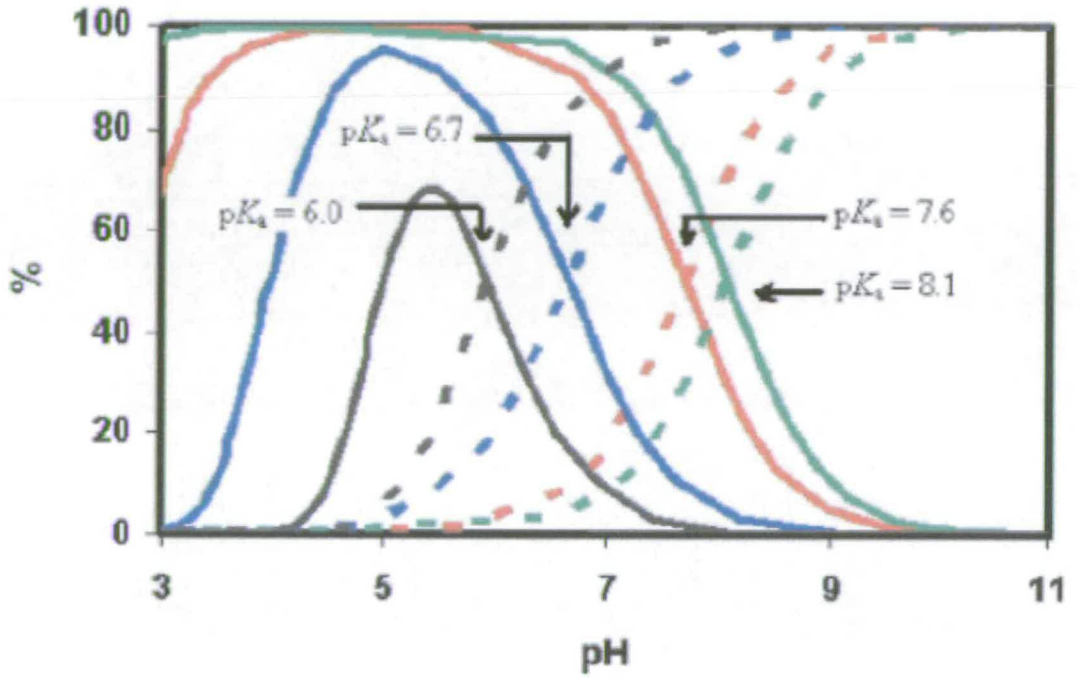

Fig. 4.3 Distribution of $LZnOH_2$ (solid lines) and LZnOH species (dashed lines) for **L** = **tpa** (green), L_1^2 (red), L_2^2 (blue) and L_3^2 (black).

Although we do not have crystallographic evidence of the formation of the intramolecular N–H···O(H)$_n$–Zn hydrogen bonding, there are a number of results which allow us to suggest that this is the case. For example, the ^{1}H NMR of **3-6** in D_2O is very similar to that of the corresponding chlorides (see Appendix, A4), which indicates that the zinc–aqua and zinc–chloride complexes adopt a similar structure in solution. Furthermore, the X-ray structures of $[(L_2^3)Zn(OH)](ClO_4)$ and $[(L_3^3)Zn(OH)](ClO_4)$ were determined in our group,[7] showing the participation of the N-H groups in short internal hydrogen bonding to the metal-bound hydroxide (Fig 4.4).

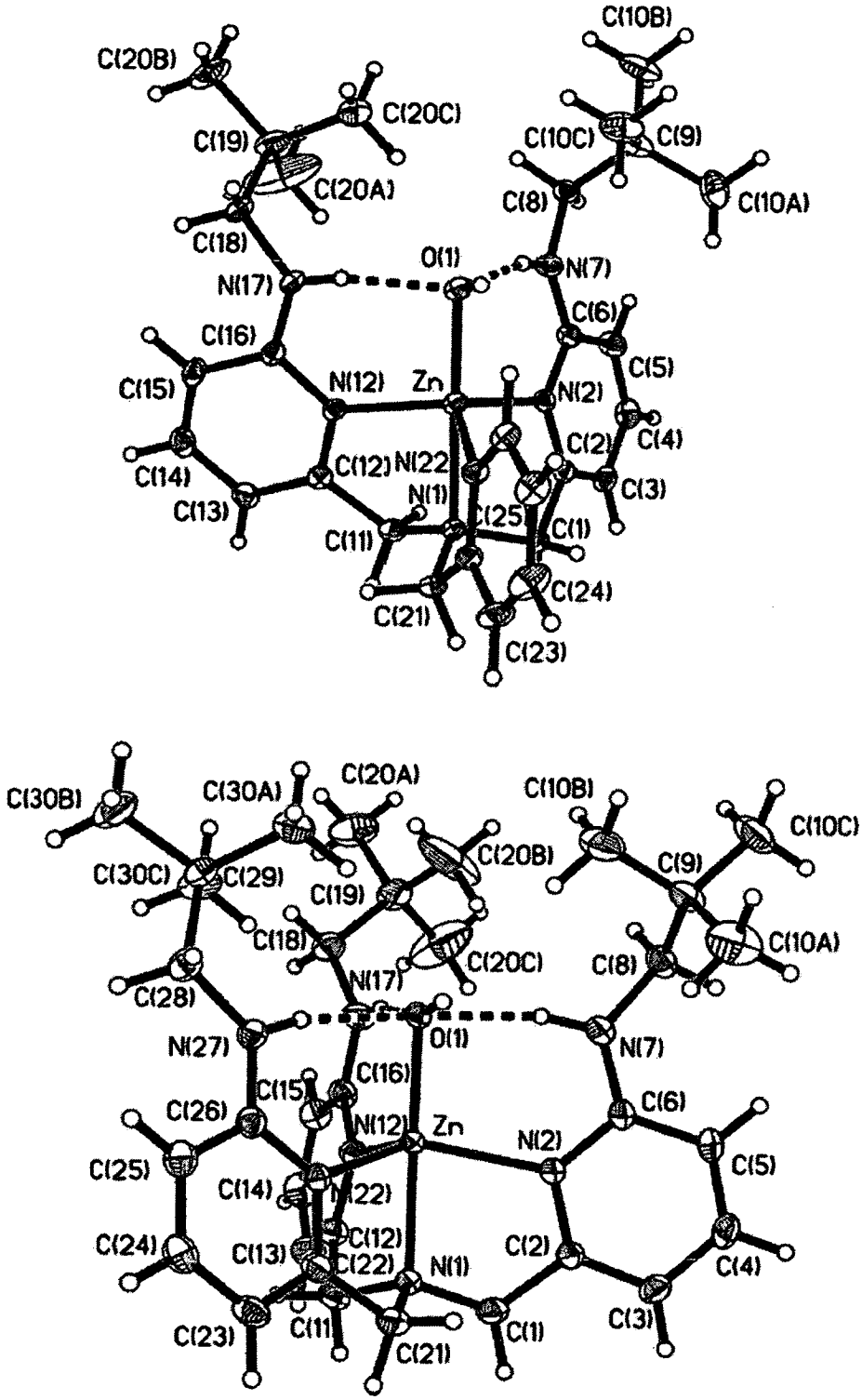

Fig 4.4 Thermal ellipsoid plot drawn with 30% probability ellipsoids of the molecular structure of the $[(\mathbf{L}_2^3)Zn(OH)]^+$ (top) and $[(\mathbf{L}_3^3)Zn(OH)]^+$ (bottom) cations of $[(\mathbf{L}_2^3)Zn(OH)](ClO_4)$ and $[(\mathbf{L}_3^3)Zn(OH)](ClO_4)$.[7]

From these structures it is interesting to note that the larger number of N–H···OH-Zn hydrogen bonds in $[(\mathbf{L_3}^3)Zn(OH)](ClO_4)$ than in $[(\mathbf{L_3}^3)Zn(OH)](ClO_4)$ seem to lengthen the Zn–O bond from 1.941(3) Å in $[(\mathbf{L_2}^3)Zn(OH)](ClO_4)$ to 1.957(2) Å in $[(\mathbf{L_3}^3)Zn(OH)](ClO_4)$.

In fact, the Zn-O distances in $[(\mathbf{L_2}^3)Zn(OH)](ClO_4)$ and $[(\mathbf{L_3}^3)Zn(OH)](ClO_4)$ are longer by *ca.* 0.1 Å than in other Zn(II)-OH complexes and similar to Zn(II)-OH_2 distances presumably due to N-H···OH-Zn hydrogen bonding.[50] It is also interesting that the Zn-O distances of $[(\mathbf{L_2}^3)Zn(OH)](ClO_4)$ (1.941(3) Å) and $[(\mathbf{L_3}^3)Zn(OH)](ClO_4)$ (1.957(2) Å) are similar to the shortest Zn-O distance in the dinuclear $[(\mathbf{tpa})Zn(\mu\text{-}OH)_2Zn(\mathbf{tpa})]^{2+}$ 1.962(1) Å.[51]

It is clear that the nature of the Zn-$O(H)_{1,2}$ bond is likely to influence the zinc-water acidity. From the above analysis it seems that the cooperation of a zinc(II) ion and multiple hydrogen bonding residues can lead to similar Zn-$OH_{1,2}$ distances than the interaction with a second zinc(II) ion. This is important because polynuclear zinc(II) complexes have more acidic zinc-water units than mononuclear zinc(II) complexes, presumably due to the cooperation of Lewis acidic zinc(II) ions towards polarising the O-H bond. Thus, in principle, hydrogen bond donors could cooperate with the Lewis acidic zinc(II) centre towards polarising the O–H bond. In addition, hydrogen bond donors should provide greater stabilisation of the zinc–hydroxide relative to the zinc–water unit as the former is a better hydrogen bond acceptor.

To explore further this idea, it is interesting to compare the Zn-OH unit of other structurally characterised complexes with Zn-$OH_{1,2}$ bonds. Monomeric [(**L**)Zn(OH)] complexes (**L** = N3 coordinating tris(pyrazolyl)hydroborate, $Tp^{R,R'}$ or tris[2-(1-isopropyl-4-*tert*-butylimidazolyl)]phosphine, $Pim^{t\text{-}Bu,i\text{-}Pr}$) constitute the best structurally characterised family and exhibit Zn-O distances of 1.847-1.860 Å,[50] whereas related dinuclear [$Tp^{R,R'}$-Zn-(μ-$OH)_2$-Zn-$Tp^{R,R'}$] complexes exhibit longer distances of 1.901-1.914 Å,[50] presumably due to the interaction of the hydroxide ligand with another zinc(II) ion. Correspondingly, in the trinuclear $[(\mathbf{L})Zn(OH)]_3^{3+}$ cation (**L** = 1,5,9-triazacyclododecane, [12]aneN_3) the Zn-O distance is 1.944 Å.[29] It should be noted that the solid state structure of $[([12]aneN_3)Zn(OH)]_3^{3+}$ contains Zn-OH units connected by a complex network of O-H···O hydrogen bonds within each trimer. The reaction of the acid $(C_6F_5)BOH_2$ with these monomeric [(**L**)Zn(OH)] complexes results sometimes in complexes that can be viewed as consisting of $\{[LZn]_2\text{-}(H_3O_2)\}^+$ cations and $[(C_6F_5)_2(H_3O_2)]^-$ anions with formally $[H_3O_2]^-$ anions in which the Zn-O distance has been lengthened to 1.873-1.916 Å.[52, 53] In other cases the hydroxide ligand is protonated to $[LZn(OH_2)]^+$ cations that are O-H···O hydrogen bonded to $[(C_6F_5)_3BOH]^-$ anions with correspondingly even longer Zn-O distances of ~1.94 Å.[50] Thus, a lengthening of the Zn-O distance by *ca.* 0.05-0.07 Å and 0.10 Å that seems to accompany the simultaneous interaction with two and three Zn(II) ions, respectively appears comparable with that of forming the Zn-bound $[H_3O_2]^-$ anion (0.02-0.05 Å) or H_2O (0.09 Å). In fact, Zn-O_2H_3-Zn and Zn-OH-Zn bridges were structurally characterised using pyrazolyl bridging ligands showing essentially identical Zn-O distances; 1.961-1.969 Å and 1.969 Å, respectively.[53, 54]

From the above analysis and this study, it seems that the interaction with hydrogen bonding groups leading to similar Zn-O distances than those of dinuclear zinc(II) complexes also leads to increased zinc-water acidities.

Moreover, we demonstrate that the presence of hydrogen bond donors around the Zn–O(H)$_n$ (n = 1, 2) unit substantially augments the magnitude of the overall effect (water acidity lowered by *ca.* 1.5 pK_a units), presumably due to their ability to provide additional stabilisation of the zinc–hydroxide species as these can act as double hydrogen bond acceptors.

Remarkably, the magnitude of the changes observed suggest that the second coordination sphere can be *at least* as important as the first coordination sphere in determining the zinc–water acidity. Thus, whereas the zinc–water acidity changes by less than a pK_a unit upon changing the coordination number of the zinc(II) centre and/or the nature of the coordinating groups, it changes by *ca.* 1 pK_a unit *per* hydrogen bond donor. Recently the effect of various coordination environments on the acidity of the zinc-bound water in model complexes of tetradentate tripodal ligands was systematically evaluated.[55] From this work it was concluded that although the zinc–water acidity is significantly influenced (1–2 pK_a units) by both the charge of the ligand and the binding energy of the tripod, environmental effects may have a modulating or even dominating effect. Herein we provide experimental evidence of the latter. The effect that hydrophobic groups in the proximity of a zinc-bound water molecule exert on its acidity was also investigated using model zinc(II) complexes and was shown to be quite significant (changes of 1–2 pK_a units).[15]

4.3 Effects of hydrogen bonding groups in phosphate ester binding to zinc(II) complexes

4.3.1 Introduction

Phosphate binding is an important factor in any research concerned with the design of synthetic nucleases. Thus, strong phosphate binding could provide a mechanism for the activation of phosphate esters towards nucleophilic attack. The design of efficient host molecules for phosphate anion guests has been attracting much current attention in biomimetic and supramolecular chemistry because of the many important biological roles of phosphates and potential applications in biotechnology.[56-60] For example, the phosphorylation/dephosphorylation of serine, tyrosine and threonine residues of proteins is an ubiquitous mechanism for the cellular control of metabolic pathways, cell growth and differentiation and apoptosis.[61] Protein phosphorylation can also induce conformational changes in the tertiary structure of enzymes, therefore regulating enzymatic activity.[62] Thus, small molecules that can directly interact with phosphate groups on protein surfaces may allow the sensing and even the regulation of the phosphorylation/dephosphorylation events.

Nature uses incredibly sophisticated mechanisms to bind phosphates. For example, phosphate transport proteins which are responsible for the transport of the essential nutrient phosphorus into cells and organelles bind phosphates with remarkable affinity. This is been illustrated in a significant study in which the X-ray

crystal structure at 1.7 Å resolution of a phosphate transport protein shows 12 strong hydrogen bonds with the phosphate.[63, 64]

Strong phosphate binding with small molecules, however, is generally very difficult to achieve. Organic receptors equipped with acidic hydrogens have been proved to be efficient hosts of phosphate anions due to strong complementary hydrogen bonding in *non-aqueous* solutions, such as $CHCl_3$, CH_3CN and DMSO, with 1:1 affinity constants (K_{aff} = [phosphate-host]/[phosphate][host] (M^{-1})) as high as 10^6 M^{-1}.[65-70] Hydrogen bonding has also been used to activate phosphate esters towards nucleophilic attack.[65, 71, 72] These hydrogen bonds, however, are typically disrupted in water and as a result it is generally difficult to achieve strong binding/activation of phosphates with organic hosts.[73-76] It should be noted that some studies have reported host-phosphate affinities in water as high as 10^5 M^{-1} using positively charged polyamine hosts (Scheme 4.7).[75, 77-79] However, the pH used in these studies is usually lower than 7 which prevents their use under physiological conditions

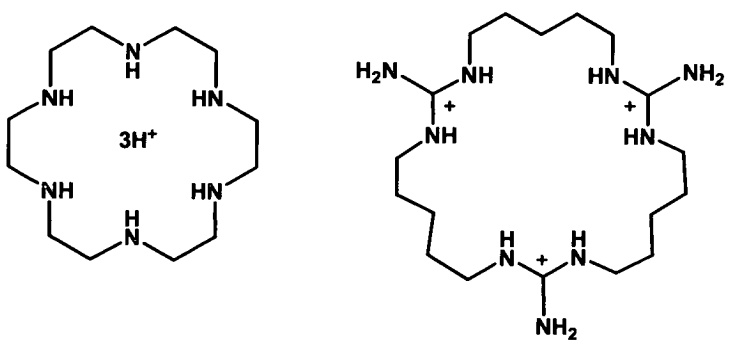

Scheme 4.7 *Illustration of some of the most efficient polyamine hosts used for phosphate binding and corresponding LogK_{aff} values for adenosine 5'-triphosphate (ATP) and phosphate anions in aqueous solution.*[75, 77-79]

In Nature, many of the chemical transformations of phosphates, including hydrolysis, are performed by metalloenzymes, and they are facilitated by the cooperative action of two or more metals, being Zn^{2+} one of the most frequently employed. As a result, the development of zinc(II) complexes as hosts for phosphate ions has received an increasing attention, but only a limited number of them show high phosphate affinities (*i.e.* $K_{aff} > 10^6$ M^{-1}, $\log K_{aff} > 7$) (Scheme 4.8) in aqueous solution and need the cooperation between two or more metal centres.[80-82]

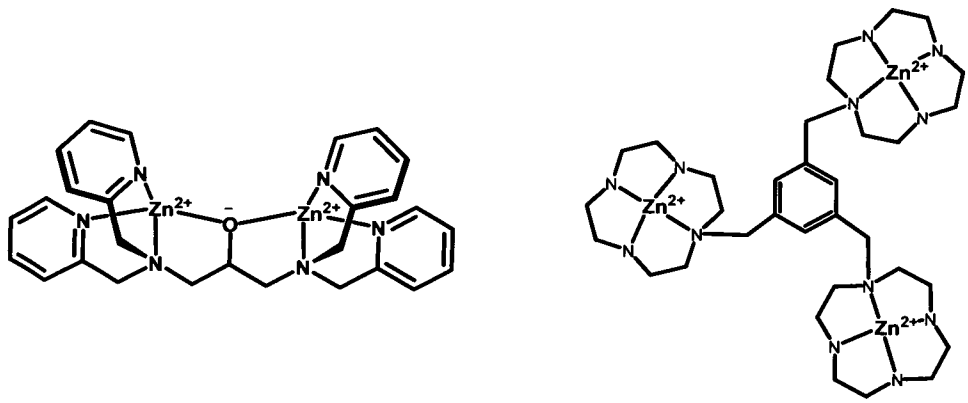

LogK_{Aff} = 8.4 for LZn_2-PP^{2-} **LogK_{Aff} = 7.0 for LZn_3-PP^{2-}**

Scheme 4.8 *Illustration of some of the most efficient metal-based hosts used for phosphate binding and corresponding $\log K_{aff}$ values for phenyl phosphate (PP^{2-}) in aqueous solution.*[82]

An interesting application of some of these synthetic hosts is their use as sensors. For example, an anthracene bis(zinc(II)-dipicolylamine) complex (Figure 4.5) has been shown to selectively bind monophosphorylated peptides in aqueous solution with remarkably high affinity constants ($K_{aff} = 1.8 \cdot 10^7$ M^{-1}; $\log K_{aff} = 7.3$).[81] This compound has also been reported very recently by another group to be an efficient fluorescent sensor for apoptotic cells.[83]

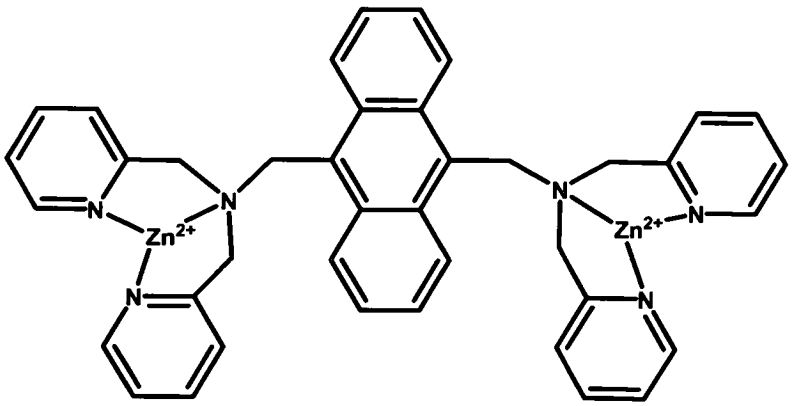

Fig. 4.5 *Fluorescent sensor anthracene bis(zinc(II)-dipicolylamine) for phosphorylated peptides and apoptotic cells.*[81,83]

The effect of second coordination sphere interactions in synthetic hosts for phosphates has received much less attention, perhaps due to the difficulty of designing such receptors. Very recently, the combination of metal binding, shape and hydrogen bonding complementarily appeared to improve the affinity and selectivity of phosphate anions to the host molecule in aqueous solution, showing binding affinities in the 10^2-10^6 M^{-1} range ($\log K_{aff}$ = 3-7) for different phosphates at pH 7 and 25 °C (Scheme 4.9a).[84] Also very recently, metal coordination and internal N–H···O–P hydrogen bonding have resulted in improved phosphodiester binding to a monometallic Co(III) complex (Scheme 4.9b), with an affinity constant for binding of dimethyl phosphate in water of $2 \cdot 10^2$ M^{-1}, at 80 °C.[85]

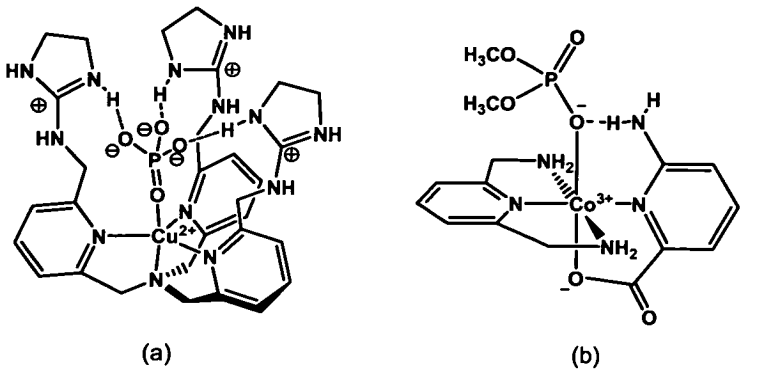

Scheme 4.9 Metal-based phosphate receptors that make use of second coordination sphere H-bonding interactions.[84-85]

The incorporation of second coordination sphere hydrogen bonding groups to monometallic complexes has also been used as a strategy to activate phosphodiesters towards hydrolysis.[49, 86, 87] For example, it has been shown that binding of a phosphate ester to two Cu^{2+} ions with simultaneous hydrogen bonding to one ammonium group can result in a remarkable acceleration, *ca.* 10^7-fold, of the hydrolysis of bis(*p*-nitrophenyl)phosphate (BNPP) (Figure 4.6).[86] The excellent reactivity of this dicopper(II) complex was explained in terms of the additional electrostatic activation provided by the N–H···O–P hydrogen bonding.

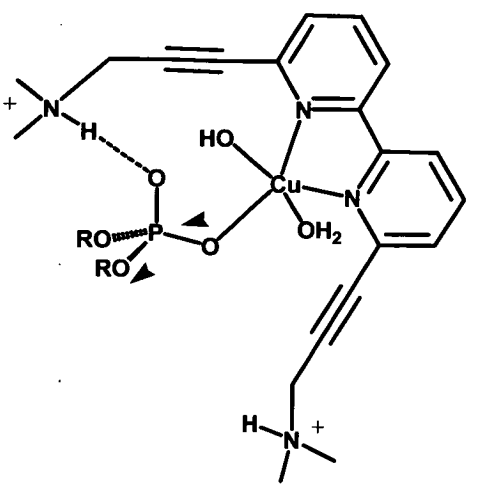

Fig 4.6 *Proposed reaction mechanism for the hydrolysis of BNPP by LCu(II) (L = bipy derivative).*[86]

Thus, the cooperation of metal ions and hydrogen bonding groups appears to be a promising novel strategy to improve both the binding of phosphates and the efficacy of their chemical transformations by bio-inspired metallohosts in water. These metal complexes can also provide new insights into the enzyme chemistry. The tripodal ligands $\mathbf{L_1}^2$ and $\mathbf{L_2}^2$ seemed suitable to study the biomimetic cooperation of zinc(II) ions and N-H groups as a way to improve binding and activation of phosphate anions at artificial receptor sites. In addition, zinc(II) complexes of the parent ligand without the hydrogen bonding group (**tpa**) were known to bind phosphates.[88] Herein we report the effect that amine hydrogen bond donors have on the binding of dibenzyl phosphate $\mathbf{DBP}^-$ to $(\mathbf{L_2}^1)$Zn **8** relative to (**tpa**)Zn **7** and of phenyl phosphate $\mathbf{PP}^{2-}$ to $(\mathbf{L_2}^2)$Zn **9** relative to (**tpa**)Zn **7** (Scheme 4.10).

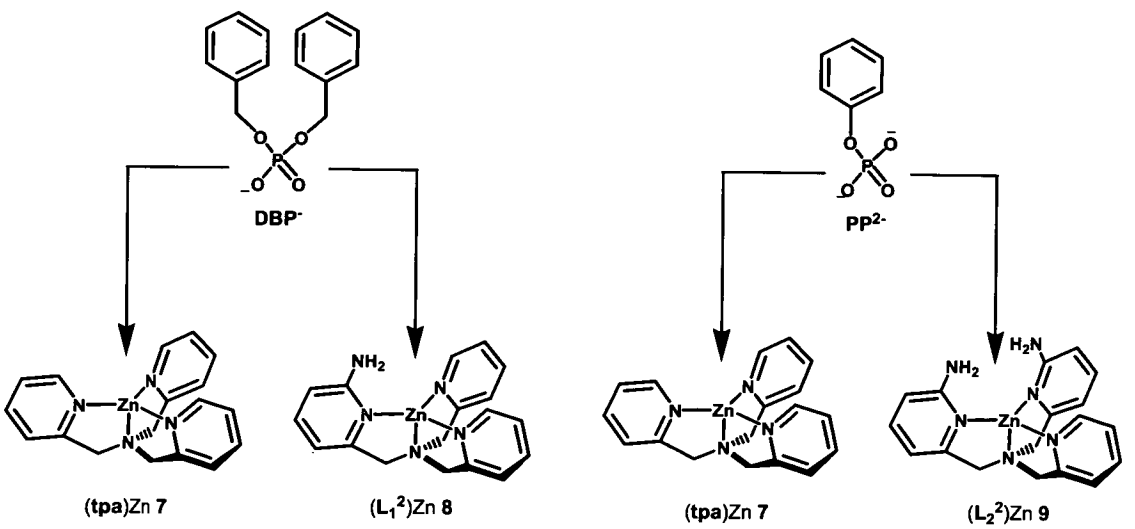

Scheme 4.10

4.3.2 Results and Discussion

4.3.2.1 Synthesis

The synthesis of the complexes $[(\mathbf{tpa})Zn(NCCH_3)](PF_6)_2$ **7**, $[(\mathbf{L_2}^1)Zn(NCCH_3)](PF_6)_2$ **8** and $[(\mathbf{L_2}^2)Zn(NCCH_3)](PF_6)_2$ **9** were accomplished following literature procedures.[89] The dizinc(II) complex $[(\mathbf{L_1}^2)Zn(\mu\text{-}\eta^2\text{-}DBP)_2Zn(\mathbf{L_1}^2)](PF_6)_2$ was assembled by reaction of equimolar amounts of $[Zn(NCCH_3)_4](PF_6)_2$, DBP and $\mathbf{L_1}^2$ in CH_3CN.

4.3.2.2 X-ray Crystallography

Crystal data for $[(\mathbf{L_1}^2)Zn(\mu\text{-}\eta^2\text{-}DBP)_2Zn(\mathbf{L_1}^2)](PF_6)_2\cdot 0.3CH_3OH$ are listed in Table 4.4. The structure of the $[(\mathbf{L_1}^2)Zn(\mu\text{-}\eta^2\text{-}DBP)_2Zn(\mathbf{L_1}^2)]^{2+}$ cation is shown in Figure 4.7; selected distances and angles are given in Table 4.5.

Table 4.4 Crystallographic data and structure refinement details for $[(\mathbf{L_1}^2)Zn(\mu\text{-}\eta^2\text{-}DBP)_2Zn(\mathbf{L_1}^2)](PF_6)_2\cdot 0.3CH_3OH$

Empirical Formula	$C_{64.30}H_{67.20}F_{12}N_{10}O_{8.30}P_4Zn_2$
M_r	1595.5
T/ K	150(2)
Crystal system	Monoclinic
Space group	$P2_1/c$
Crystal size/mm	0.40 × 0.34 × 0.32
a /Å	12.5627(7)
b /Å	12.7358(8)
c /Å	21.7676(13)
α / °	90.00
β / °	94.3790(10)
γ / °	90.00

V / Å^3	3472.6(4)
Z	2
D_c / g cm^{-3}	1.526
μ / mm–1	0.877
R_{int}	0.0318
$R_1(F)^a$ (all data)	0.0611
$wR_2(F^2)^a$ (all data)	0.1303
$S(F^2)^a$ (all data)	1.212
Largest difference peak, hole/e Å^3	0.755, -0.399

$^aR_1(F) = \Sigma(|F_o| - |F_c|)/ \Sigma(|F_o|$; $wR_2(F^2) = [\Sigma w(F_o^2 - F_c^2)^2/\Sigma wF_o^4]^{1/2}$; $S(F^2) = [\Sigma w(F_o^2 - F_c^2)^2/(n-p)]^{1/2}$.

Colourless crystals of $[(\mathbf{L_1}^2)Zn(\mu\text{-}\eta^2\text{-}DBP)_2Zn(\mathbf{L_1}^2)](PF_6)_2{\cdot}0.3CH_3OH$ suitable for X-ray diffraction studies were grown by slow evaporation of a CH_3OH solution. Each of the symmetry-related zinc(II) centres is six-coordinate, being ligated by the three pyridyl and single aliphatic nitrogens of $\mathbf{L_1}^2$ and two oxygens of DBP^- (Figure 4.7). The geometry about each of the zinc(II) centres is best described as distorted octahedral. The Zn···Zn distance of 4.91 Å is shorter than in flexible dizinc(II) complexes bridged by a single phosphate.[88, 90] The Zn···Zn distance in $[(\mathbf{L_1}^2)Zn(\mu\text{-}\eta^2\text{-}DBP)_2Zn(\mathbf{L_1}^2)](PF_6)_2{\cdot}0.3CH_3OH$ is also somewhat shorter than in dizinc(II) complexes bridged by two phosphates and a flexible dinucleating ligand framework such as [30]aneN_6O_4.[91]

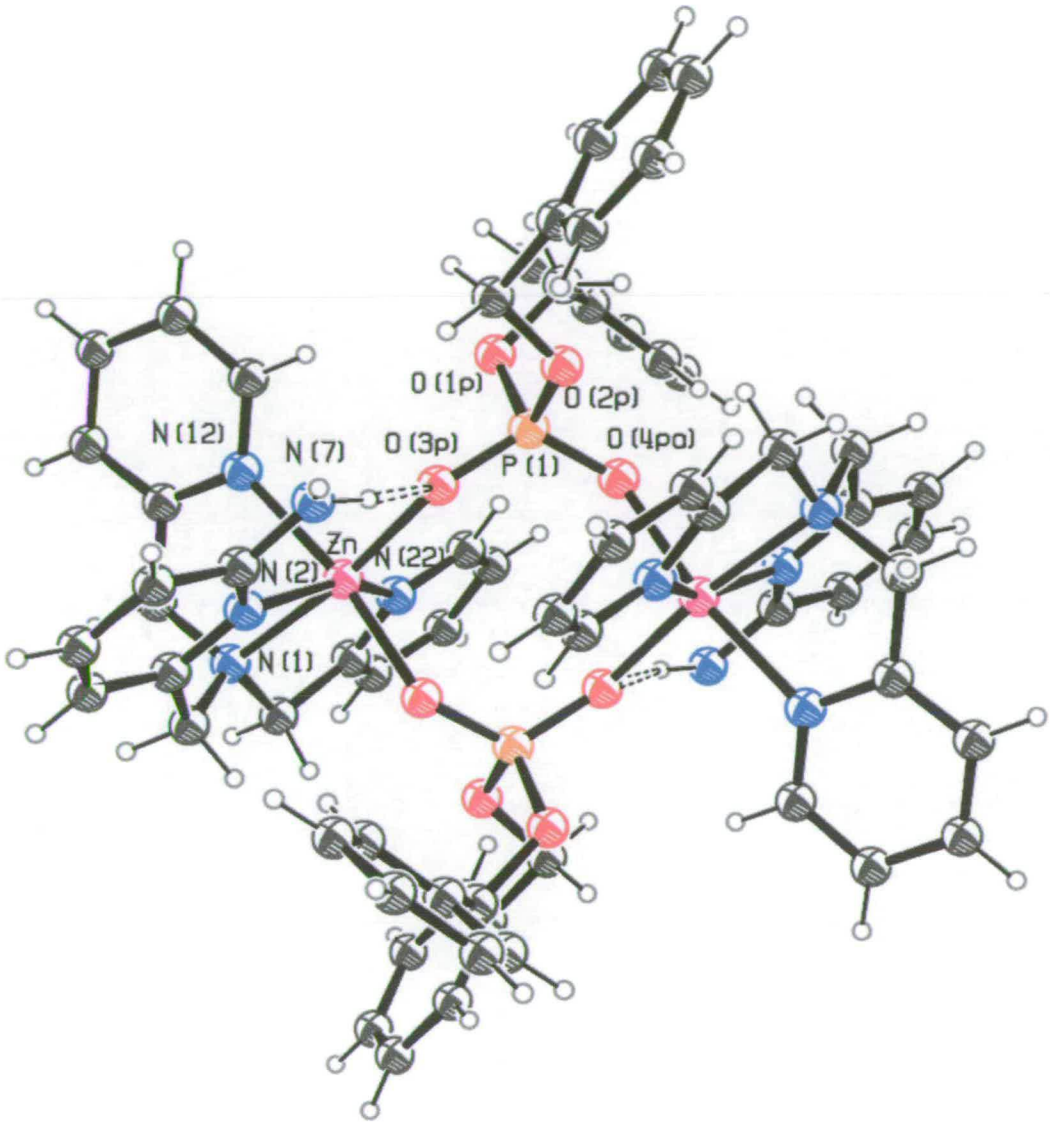

Fig. 4.7 A thermal ellipsoid plot of $[(\mathbf{L_1}^2)Zn(\mu\text{-}\eta^2\text{-}DBP)_2Zn(\mathbf{L_1}^2)]^{2+}$ drawn with 30% probability ellipsoids. Hydrogen atoms except those of N(7) are omitted for clarity.

A key feature present in the structure of $[(\mathbf{L_1}^2)Zn(\mu\text{-}\eta^2\text{-}DBP)_2Zn(\mathbf{L_1}^2)](PF_6)_2\cdot 0.3CH_3OH$, which is absent in any of the previously structurally characterised dinuclear metal complexes bridged by phosphate esters is the short intramolecular N-H···O-P hydrogen bond ((N(7)···O(3P) 2.9321(3) Å, H(7A)···O(3P) 2.00 Å, N(7)–H(7A)···O(3P) 151° (for the N(7)–H(7A) extended to

1.01 Å) (Figure 4.7). Recently, it was suggested that hydrogen bonding stabilises metal-bound phosphates.[85] It may also orient the zinc(II)-bound phosphate diester. Thus, whereas the P(1)–O(4P)–Zn angle of 136.57(12)° is similar (±1°) to the corresponding angles in other crystallographically characterised dizinc(II) phosphate-bridged complexes,[88, 90, 91] the P(1)–O(3P)–Zn angle has expanded to 143.60(13)°, presumably to optimise the N(7)–H(7A)···O(3P) hydrogen bond.

Table 4.5 Selected bond lengths (Å) and angles (°) for $[(\mathbf{L_1}^2)Zn(\mu\text{-}\eta^2\text{-}DBP)_2Zn(\mathbf{L_1}^2)](PF_6)_2$

Zn–N(2)	2.203(2)
Zn–N(12)	2.176(2)
Zn–N(22)	2.193(2)
Zn–N(1)	2.225(2)
Zn–O(3P)	2.0255(19)
Zn–O(4P)	2.0711(19)
N(2)–Zn–N(12)	86.89(9)
N(2)–Zn–N(22)	155.41(9)
N(12)–Zn–N(22)	93.43(9)
N(1)–Zn–N(2)	78.93(9)
N(1)–Zn–N(12)	79.18(9)
N(1)–Zn–N(22)	76.99(9)
N(1)–Zn–O(3P)	172.48(8)
N(1)–Zn–O(4P)	93.03(8)
O(3P)–Zn–N(12)	93.33(8)
O(3P)–Zn–N(22)	104.40(9)
O(3P)–Zn– O(4P)	94.34(8)

4.3.2.3 NMR studies

a) Binding of Dibenzyl Phosphate (DBP)

Binding of DBP^- to $[(\mathbf{tpa})Zn(NCCH_3)](PF_6)_2$ **7** and $[(\mathbf{L_1}^2)Zn(NCCH_3)](PF_6)_2$ **8** was investigated by $^{31}P\{^1H\}$ NMR titration experiments of 5 mM DBP in D_2O at pH 7 (50 mM HEPES) with varying amounts of **7** and **8** (50 mM in CD_3CN).

The addition of increasing amounts of these zinc(II) complexes to solutions of DBP causes a progressive upfield shift of the ^{31}P signal relative to free DBP (Figure 4.8). The upfield shift of the DBP signal for solutions containing less than 2 equiv. of Zn^{2+} relative to DBP^- is smaller than for solutions containing more than 2 equiv., and could be due to the formation of DBP:$(ZnL)_n$ complexes ($n > 1$). The rather large upfield shifts observed for the ^{31}P signal of the zinc-bound DBP, *ca.* 1.5–2.0 ppm, is also consistent with the occurrence of bridging coordination modes in solution. The fact that the upfield shifts can be more prominent by as much as 0.5 ppm, when $\mathbf{L_2}^1Zn$ **8** is added, indicates that this has higher binding affinity for DBP^- than **tpa**Zn **7**.

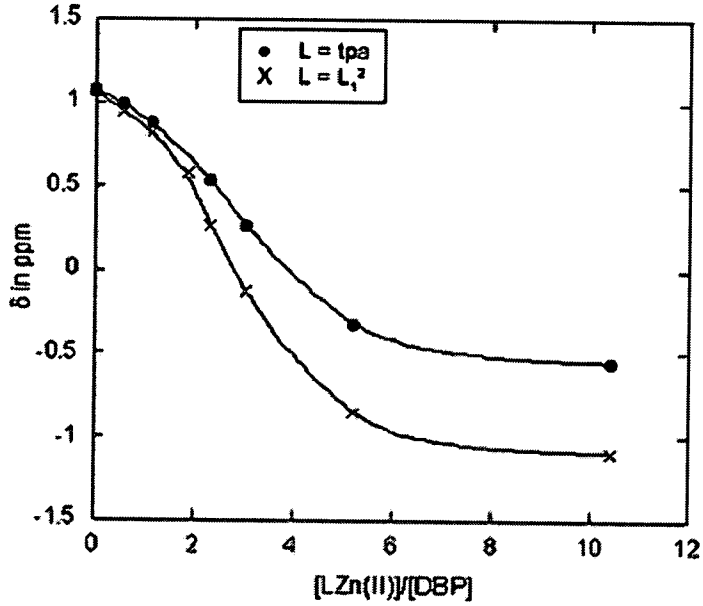

Fig. 4.8 Changes of the ^{31}P chemical shift of DBP at 20 °C (5 mM in D_2O, pH 7 upon addition of increasing amounts of **7** and **8** (50 mM in CD_3CN).

The same studies were carried out in the presence of $I = 1$ ($NaNO_3$) and $I = 0.1$ (NaCl). The titration data shows that in all cases DBP^- binds better to **8** than to **7** (Figure 4.8, 4.9 and 4.10). It also shows that the affinity of DBP^- >> Cl^- >> NO_3^- to these zinc(II) complexes (Figure 4.11 and 4.12) consistent with the zinc(II) co-ordinating abilities of these ligands. The fact that the ^{31}P chemical shift of DBP^- changes up to large $[Zn^{2+}]/[DBP]$ ratios could indicate that DBP^- does not bind very strongly to these zinc(II) complexes.

It is interesting, however, that binding of DBP^- to **8** is stronger than to **7** given that electronically the amino group in $\mathbf{L_2^1}$ of **8** is an electron-donating group and sterically it could hinder the approach of the external phosphate. The stronger binding of DBP^- to the $\mathbf{L_2^1}$Zn moiety could be explained if the amino group is acting

as a hydrogen bond donor to the metal-bound DBP^- anion, as it does in the crystal structure of $[(\mathbf{L_1}^2)Zn(\mu\text{-}\eta^2\text{-}DBP)_2Zn(\mathbf{L_1}^2)](PF_6)_2\cdot 0.3CH_3OH$. Recently, it was reported that the binding of dianionic (*p*-nitrophenyl) phosphate ester NPP^{2-} to [((2-guanidyl)ether-cyclen)$Zn(OH_2)$]$^{2+}$ was *ca.* 10 times stronger than to [(cyclen)$Zn(OH_2)$]$^{2+}$ due to phosphate-guanidinium double hydrogen bonding.[92] Interestingly, the maximum upfield shift observed for the ^{31}P signal of NPP^{2-} bound to {((2-guanidyl)ether-cyclen)Zn}$^{2+}$ relative to bound to {(cyclen)Zn}$^{2+}$ was also 0.5 ppm.

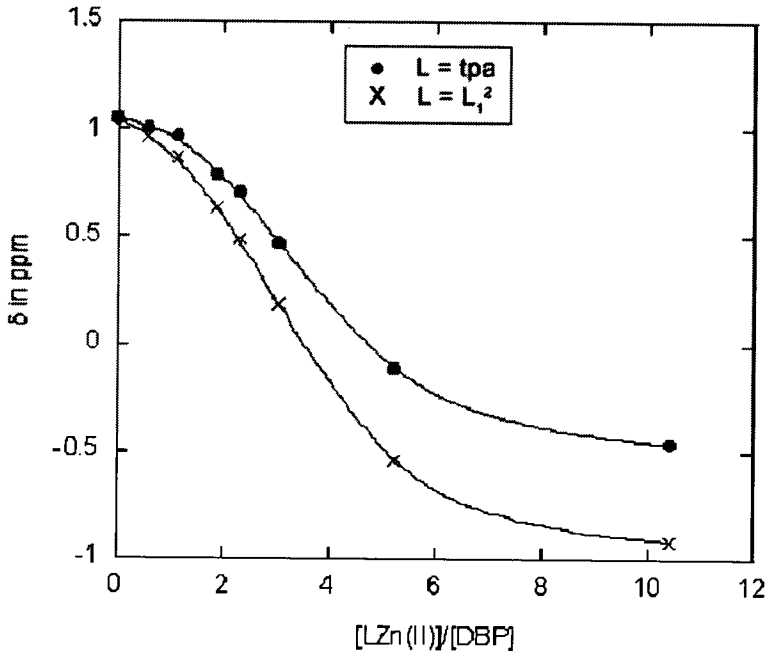

Fig. 4.9 Changes of the ^{31}P chemical shift of DBP at 20 °C (5 mM in D_2O, pH 7 with I = 1 ($NaNO_3$)) upon addition of increasing amounts of [(**tpa**)Zn(S)]$(PF_6)_2$ **7** and $[(\mathbf{L_1}^2)Zn(S)](PF_6)_2$ **8** (50 mM in S = CD_3CN).

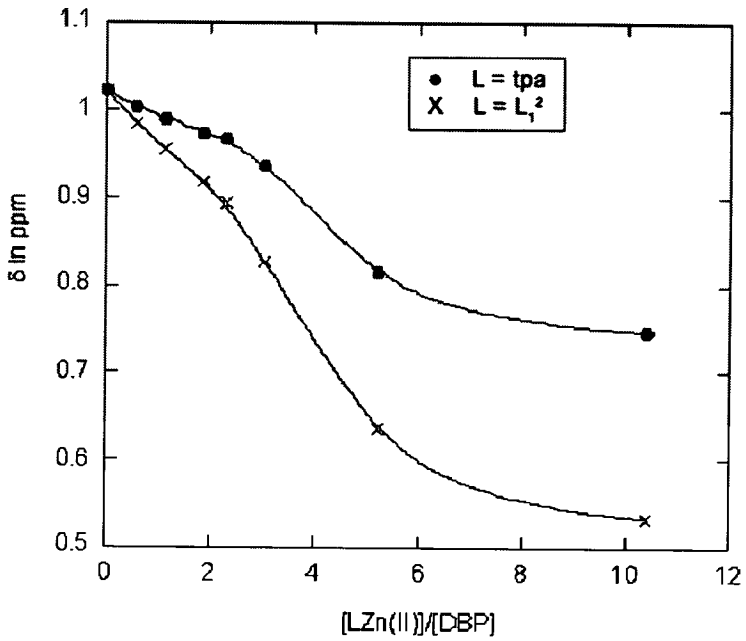

Fig. 4.10 Changes of the ^{31}P chemical shift of DBP at 20 °C (5 mM in D_2O, pH 7 with $I = 0.1$ (NaCl)) upon addition of increasing amounts of [(**tpa**)Zn(S)]$(PF_6)_2$ **7** and [($\mathbf{L_1}^2$)Zn(S)]$(PF_6)_2$ **8** (50 mM in S = CD_3CN)

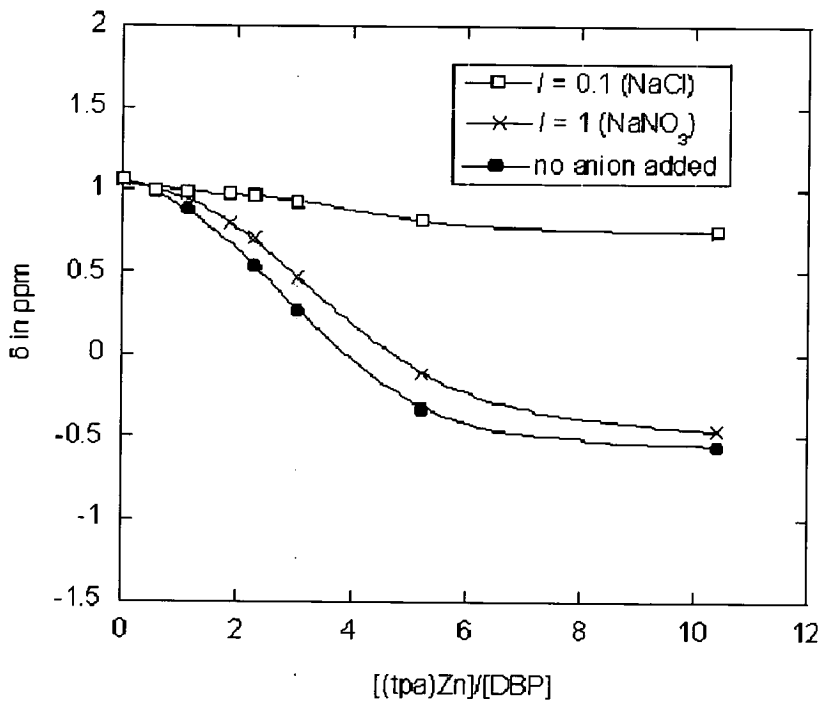

Fig. 4.11 Changes of the ^{31}P chemical shift of DBP at 20 °C (5 mM in D_2O, pH 7 upon addition of increasing amounts of [(**tpa**)Zn(S)]$(PF_6)_2$ **7** (50 mM in S = CD_3CN) in the absence and presence of different anions.

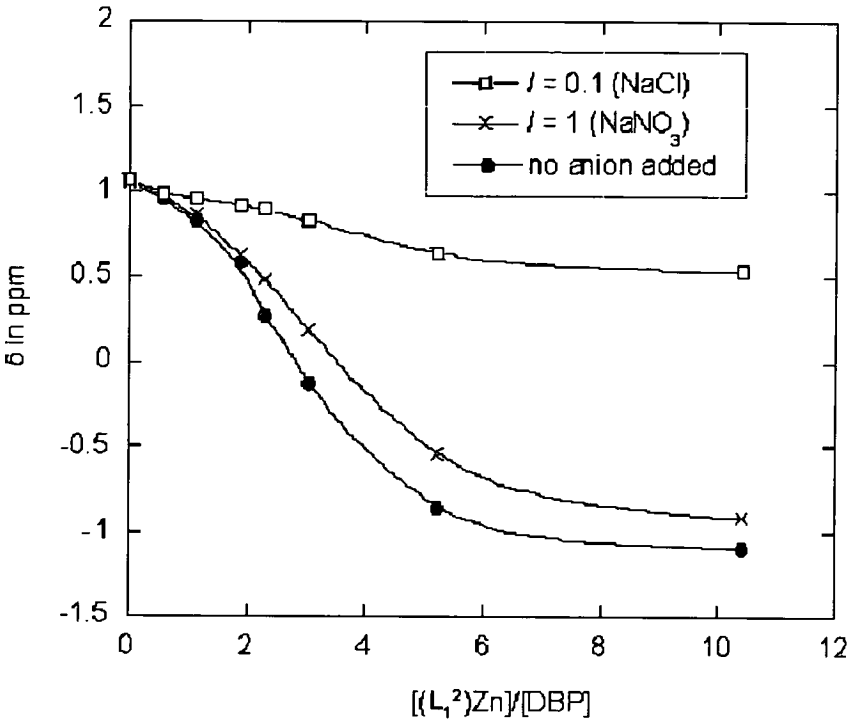

Fig. 4.12 Changes of the ^{31}P chemical shift of DBP at 20 °C (5 mM in D_2O, pH 7 upon addition of increasing amounts of $[(\mathbf{L_1}^2)Zn(S)](PF_6)_2$ **8** (50 mM in S = CD_3CN) in the absence and presence of different anions.

b) Binding of Phenyl Phosphate (PP)

Binding of PP^{2-} to $[(\mathbf{tpa})Zn(NCCH_3)](PF_6)_2$ **7** and $[(\mathbf{L_2}^2)Zn(NCCH_3)](PF_6)_2$ **9** was investigated by ^1H NMR titrations of 1 mM **7** and **9** with PP^{2-} (0–8 mM) in D_2O at 25 °C and pH 7 (50 mM HEPES). The proton resonance of **7** and **9** experiencing the largest shifts upon addition of PP^{2-} is H6, presumably because it is the proton closest to the binding pocket formed by the preorganisation of the ligands upon zinc(II)-binding (Scheme 4.11). This proton resonance experiences downfield shifts upon addition of PP^{2-} (Figure 4.13). NMR titration studies revealed that **7** and **9** bind to PP^{2-} in water at pH 7 to form 1:1 guest:host complexes.

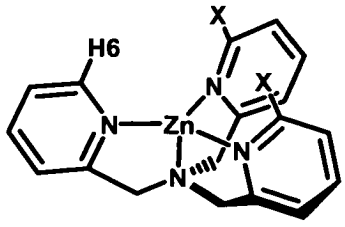

X= H, (**tpa**)Zn **7**
X= NH_2 ($\mathbf{L_2}^2$)Zn **9**

Scheme 4.11

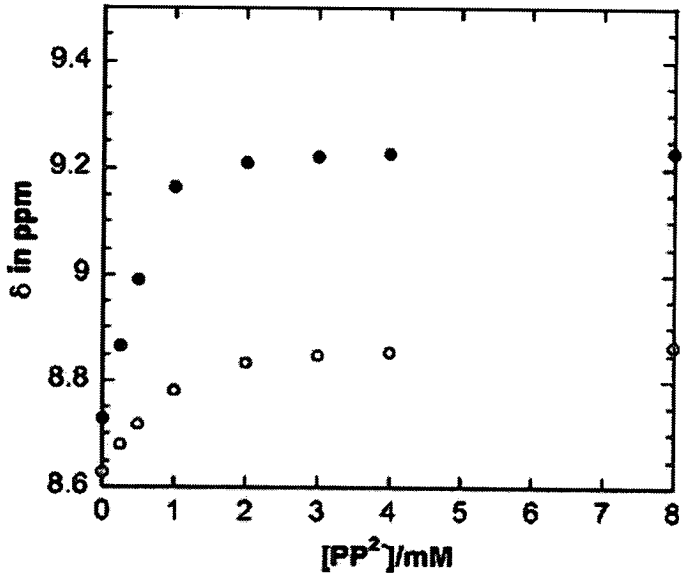

Fig. 4.13 Changes of the proton chemical shift of H6 of **7** (1 mM in D_2O) (○) and **9** (1 mM in D_2O) (●) upon addition of increasing amounts of PP at pH 7 ± 0.1 (50 mM HEPES).

The apparent complexation constants, log K_{app}(LZn-PP), calculated by using the program HYPNMR 2000[93] are 3.6 ± 0.1 for **7** and 4.4 ± 0.1 for **9** at pH 7. It is remarkable that PP^{2-} binds more strongly to **9** than to **7**. Thus, electronically, the 6-amino groups are electron donating, which presumably should make the zinc(II) centre of **9** more electron rich and therefore lower its affinity for phosphates. In addition, the 6-amino groups should sterically hinder the approach of the external phosphate ligand. Moreover, the amino groups of $\mathbf{L_2}^2$ increase the acidity of the zinc-

water unit of **9** relative to that of **7** to such an extent that the percentage of the zinc-hydroxo form of **9** is *ca.* 4 times higher than that of **7** at pH 7. Thus, for **7** (1 mM in water), the concentration of the zinc-water and zinc-hydroxo forms are 0.77 and 0.15 mM, respectively. For **9** (1 mM in water), however, the concentration of the zinc-water and zinc-hydroxo forms are 0.28 mM and 0.63 mM, respectively.[94] In principle, the zinc-bound hydroxide should be more difficult to replace by the external phosphate than the zinc(II)-bound water molecule.

It has been recently proposed, however, that N–H···O–P hydrogen bonding was responsible for the dramatic increase in the binding affinity of dimethyl phosphate to a monometallic Co(III) complex (*vide supra*).[85] Thus, the preference of PP^{2-} for **9** over **7** could be explained if the amino groups of $\mathbf{L_2}^2$ are acting as hydrogen bond donors to the zinc-bound phosphate.

The X-ray crystal structures of $[(\mathbf{L_2}^2)Zn(ONO_2)](NO_3)$ (Figure 3.3) and $[(\mathbf{L_2}^2)Zn(Cl)](BPh_4)$ (Figure 3.2) show that the two amino groups are engaged in internal hydrogen bonds with the zinc(II)-bound oxygen of the coordinated NO_3^- or the chloride anion. These structures demonstrate that the positioning of the amino groups is suitable for simultaneous hydrogen bonding to the bound PP^{2-}. Thus, we propose that the increased binding affinity of PP^{2-} to **9** may be due to the possibility of forming internal N–H···O–P hydrogen bonding. It is remarkable that the improved affinity of PP^{2-} for zinc(II) receptors with hydrogen bond donors is comparable in magnitude to that of dizinc(II) receptors relative to monozinc(II) receptors (Scheme 4.13).[82] Thus, this result highlights the great potential of exploiting the second

coordination sphere as strategy to improve the affinity of phosphates to zinc(II) complexes.

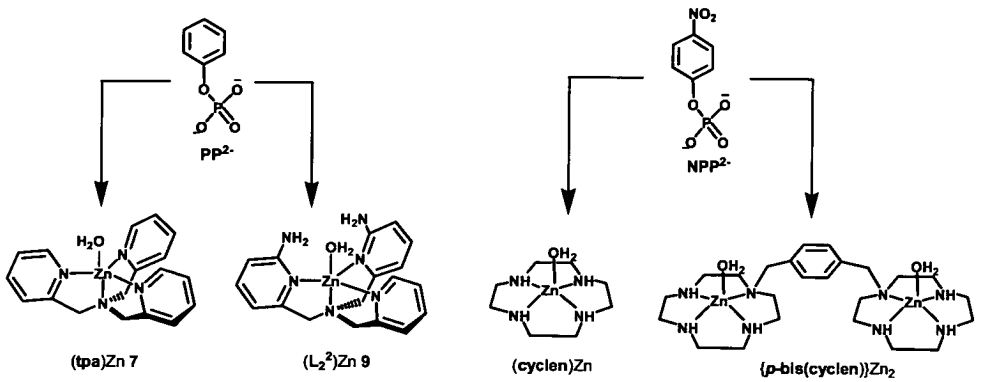

	(tpa)Zn 7	(L_2^2)Zn 9	(cyclen)Zn	{*p*-bis(cyclen)}Zn_2
pK_a ($LZn\text{-}OH_2$ -> $LZn\text{-}OH + H^+$)	**8.1**	**6.7**	**8.0**[a]	**7.2, 7.9**[a]
log K_{app}(LZn-P) at pH=7	**3.6**	**4.4**	**3.3**[a]	**4.0**[a]

[a] E. Kimura, S. Aoki, T. Koike and M. Shiro, *J. Am. Chem. Soc.*, 1997, **119**, 3068.

Scheme 4.13

4.4 CONCLUSIONS

This chapter has examined the effect that RN–H hydrogen bonding groups (R = H, $CH_2{}^tBu$) of $N(CH_2Py)_{3-n}(CH_2Py\text{-}6\text{-}NHR)_n$ ligands $\mathbf{L}_n{}^{2,3}$ (n = 1–3) have on **L**–Zn and Zn–Cl distances of trigonal bipyramidal $[(\mathbf{L})Zn(Cl)]^+$ cations. The magnitude of the structural changes exerted by the hydrogen bonding groups is compared with those arising from a range of $N(CH_2Py)_2(CH_2Y)$ (Y = coordinating group) ligands. Among the implications of introducing local RN-H hydrogen bonding groups is the shortening of the axial Zn–N, lengthening of the equatorial Zn–N_{py} by and lengthening of the axial Zn–Cl bonds by as much as 0.16, 0.12 and 0.07 Å, respectively. In general, the magnitude of these changes increases as the number of the hydrogen bonding groups increases, and these changes are comparable or greater in magnitude than those arising from significant changes in the zinc(II) first coordination sphere. In some cases differences between the changes induced by R = H and $CH_2{}^tBu$ were noted, which could lead to different chemistry. This structural study may facilitate future structure–function relationships.

We have also shown that the acidity of the catalytically important zinc–water unit can be increased with hydrogen bond donors around the metal-bound water by as much as one pK_a unit *per* hydrogen bond donor. As a result the zinc–water unit of **6** has the very low pK_a of 6.0. This is, to the best of our knowledge, the lowest pK_a value obtained using mononuclear zinc(II) synthetic analogues, [95] Moreover, the

zinc–water acidity of **3–6** is as low or even lower (in **6**) as that achieved by zinc(II) hydrolases despite the use of a tetradentate rather than tridentate ligand environment. The implication of this result for metalloenzymes is that although features of the primary coordination sphere such as a low coordination number and moderately donating ligands play a role in lowering the zinc–water acidity, the active site microenvironment, if capable of hydrogen bonding to the zinc–water unit, could exert the dominant effect.

In terms of phosphate binding, we have reported the X-ray crystal structure of a dizinc(II) complex with the unique feature of internal N–H···O–P hydrogen bonding to bridging η^2-dibenzyl phosphates. We have also shown that the affinity of phosphates to zinc(II) complexes in water solution and neutral pH can be increased with hydrogen bond donors adjacent to the metal centre with a magnitude comparable to that of dizinc(II) receptors. Thus, this improved affinity could provide a mechanism to activate phosphate esters towards nucleophilic attack.

We expect the use of ligands with internal hydrogen bond donors such as $\mathbf{L_{1\text{-}3}}^2$ will provide synthetic nucleases that resemble more faithfully the microenvironments and chemistry of phosphates in the active sites of nucleases, in which case they could allow the elucidation of the cooperative mechanisms between the metal(s) and the second co-ordination sphere. Hydrogen bonding features in synthetic nucleases could also improve the catalytic properties of metal complexes by further activating ground state molecules and preferentially stabilising the transition states of reactions.

4.5 EXPERIMENTAL

4.5.1 Materials and methods

Reagents were obtained from commercial sources and used as received unless otherwise noted. Solvents were dried and purified under N_2 by using standard methods[96] and were distilled immediately before use. All compounds were prepared under N_2 unless otherwise mentioned. The buffer solutions of HEPES (2-(4-(2-hydroxyethyl)-1-piperazinyl)ethanesulfonic acid, (50 mM in D_2O) pD 7.4 (20°C) were used for the phosphate binding studies and the ionic strength was adjusted to 0.1 N with $NaNO_3$ unless otherwise noted. The pD values in D_2O were corrected for a deuterium isotope effect using the expression pD = pH-meter reading + 0.4.[97] NMR spectra were obtained using a Bruker DPX 360 at 20 °C in CD_3CN unless otherwise noted. ^{13}C and ^{1}H chemical shifts are referenced with respect to the carbon (δ_C 1.32 and 118.26 ppm) and residual proton (δ_H 1.94 ppm (CD_3CN); 4.79 (D_2O)) solvent peaks. ^{31}P resonances were referenced to an external solution of 85% H_3PO_4 (δ_P 0 ppm). Mass spectra were performed on a Micromass Platform II system operating in Flow Injection Analysis mode with the electrospray method. Elemental analyses were carried out by the microanalyses service provided by the School of Chemistry at the University of Edinburgh.

4.5.2 Synthesis

$[(L_3^3)Zn(Cl)](BPh_4)$

$ZnCl_2$ (16 mg, 0.116 mmol) and L_3^3 (63 mg, 0.116 mmol) were dissolved in acetonitrile (15 cm^3) and the solution was stirred for 2 h at room temperature. The solvent was removed under vacuum. The crude product was re-dissolved in methanol (10 cm^3) and $NaBPh_4$ (40 mg, 0.116 mmol) was added. The solution was filtered and the residue was washed with methanol (2 × 2 cm^3) to yield the title compound as a pale yellow solid (32 mg, 29%) (Found: C, 70.5; H, 7.6; N, 9.7. Calc. for $C_{57}H_{71}BClN_7Zn{\cdot}0.5H_2O$: C, 70.22; H, 7.44; N, 10.06%).

^1H NMR (CD_3CN, 360.1 MHz): δ_H (ppm) $[(L_3^3)Zn(Cl)]^+$ 7.68 (t, J = 5.0 Hz, 3H, N*H*CH_2–$C(CH_3)_3$), 7.59 (dd, J = 7.6 and 8.3 Hz, 3H, py–*H*), 6.65 (d, J = 8.6 Hz, 3H, py–*H*), 6.52 (d, J = 6.8 Hz, 2H, py–*H*), 3.76 (s, 6H, NCH_2–py), 3.01 (d, J = 5.6 Hz, 6H, CH_2–$C(CH_3)_3$), 1.00 (s, 27H, CH_2–$C(CH_3)_3$); BPh_4^- 7.26 (m, 8H, Ar–*H*2), 7.00 (t, J = 7.2 Hz, 8H, Ar–*H*3) and 6.83 (t, J = 7.2 Hz, Ar–*H*4). ^{13}C NMR (CD_3CN, 90.5 MHz, 298 K): δ_C (ppm); $[(L_3^3)Zn(Cl)]^+$ 162.1 and 152.3 (py–*C*), 141.9, 112.4 and 108.2 (py–*C*H), 56.3 and 55.4 (NCH_2–py and CH_2–$C(CH_3)_3$), 32.8 (CH_2–$C(CH_3)_3$) and 27.7 (CH_2–$C(CH_3)_3$); BPh_4^- 163.9 (B–*C*1, J_{B-C} = 49 Hz), 136.6 (*C*2), 126.5 (*C*3), 122.7 (*C*4). ESI-MS (+ion): found: 644.4 (100%), calc. 644.32 (100%) for $[(L_3^3)Zn(Cl)]^+$, and matches theoretical isotope distribution.

$[(L_1^2)Zn(\mu\text{-}\eta^2\text{-DBP})_2Zn(L_1^2)](PF_6)_2$

$ZnCl_2$ (55 mg, 0.4 mmol) and $AgPF_6$ (202 mg, 0.8 mmol) were dissolved in dry acetronitrile (20 mL) and the solution was stirred for 1 h resulting in the appearance of a white precipitate, AgCl, which was removed by filtration. Dibenzyl phosphate (110 mg, 0.4 mmol) was then added to the solution. After stirring at room temperature overnight, $\mathbf{L_1}^2$ (122 mg, 0.4 mmol) was added and the reaction mixture was kept stirring at room temperature for 4 h after which time a grey precipitate was removed by centrifuge. The solution was evaporated under vacuum to give a yellow solid (203 mg). Re-crystallisation of the solid from CH_3OH at room temperature yielded crystals suitable for X-ray diffraction studies with the following spectroscopic and analytical data (Found: C, 48.27; H, 4.16; N, 8.78. Calc. for $C_{64}H_{66}N_{10}O_8P_4F_{12}Zn_2$: C, 48.47; H, 4.19; N, 8.83).

^{1}H NMR (CD_3CN, 360.1 MHz, 293 K) δ_H (ppm) 9.10 (d, J = 4.9 Hz, 2H, py-*H6*), 7.99 (td, J = 7.8, 1.7 Hz, 2H py-*H4*), 7.50 (m, 4H, py-*H5* and py-H3), 7.46 (t, J = 8.6 Hz, 1H, py'-*H4*), 7.36-7.31 (m, 10H, P-O-($CH_2C_6H_5$)$_2$), 6.59 (br, py'-NH_2), 6.56 (t, J = 8.8 Hz, 2H, py'-H_3 and py'-H_5), 5.04 (d, J = 7.6 Hz, 4H, P-O-($CH_2C_6H_5$)$_2$), 4.09 (s, 4H, NCH_2-py), 3.83 (s, 2H, NCH_2-py'). ^{13}C NMR (CD_3CN, 90.5 MHz, 293 K) δ_C (ppm); 161.7, 155.9 (py'-*C2* and py'-*C6*), 152.1 and 159.1 (py-*C2* and py-*C6*), 142.0 (py-*C3*), 141.8 (py'-*C3*), 129.4, 128.8 and 128.5 (P-O-CH_2-C_6H_5)$_2$, 125.8 and 125.5 (py-*C4* and py-*C5*), 112.6 and 112.3 (py'-*C4* and py'-*C5*), 68.6 (d, $^2J_{P\text{-}C}$ = 5 Hz, P-OCH_2-C_6H_5), 57.4 (NCH_2-py'), 56.8 (NCH_2-py). ^{31}P NMR (CD_3CN, 145.8 MHz, 293K) δ_P (ppm) 1.059. ESI-MS (+ ion) Found 646.2, Calcd. 646.16 (100%).

4.5.3 X-ray crystallography

Intensity data for $[(\mathbf{L_3}^3)Zn(Cl)](BPh_4)$ were collected at 150 K using a Bruker-AXS SMART APEX area detector diffractometer with graphite-monochromated Mo-Kα radiation (λ = 0.71073 Å). The structures were solved by direct methods and refined to convergence against F^2 data using the SHELXTL suite of programs.[98] Data were corrected for absorption applying empirical methods using the program SADABS,[99, 100] and the structures were checked for higher symmetry using the program PLATON.[101] All non-hydrogen atoms were refined anisotropically unless otherwise noted. Hydrogen atoms were placed in idealised positions and refined using a riding model with fixed isotropic displacement parameters. The N–H hydrogens were located in the difference map and refined isotropically. Some *tert*-butyl groups in $[(\mathbf{L_3}^3)Zn(Cl)](BPh_4)$ showed elongated anisotropic displacement parameters. Attempts were made to model disorder in these regions. The fitting statistics, however, showed no improvement over the ordered models with large anisotropic displacement parameters.

CCDC reference number 239825.

Intensity data for $[(\mathbf{L_1}^2)Zn(\mu\text{-}\eta^2\text{-DBP})_2Zn(\mathbf{L_1}^2)](PF_6)_2\cdot 0.3CH_3OH$ were collected at 150 K using a Bruker-AXS SMART APEX area detector diffractometer with graphite-monochromated Mo-Kα radiation (λ = 0.71073 Å). The structures were

solved by direct methods and refined to convergence against F^2 data using the SHELXTL suite of programs.[98] Data were corrected for absorption applying empirical methods using the program SADABS,[99, 100] and the structures were checked for higher symmetry using the program PLATON.[101] All non-hydrogen atoms were refined anisotropically unless otherwise noted. Hydrogen atoms were placed in idealized positions and refined using a riding model with fixed isotropic displacement parameters. The N-H hydrogens were located in the difference map and refined isotropically. One of the phenyl groups of DBP (C12C13C14C15C16C17) was disordered and modelled over two positions with 60% and 40% occupancy. Chemically equivalent bonds and angles in the disordered fragment were restrained to be similar. The $PF6^-$ anion was also disordered and modelled over two positions with 60% and 40% occupancy.

CCDC reference number 216363.

4.5.4 Potentiometric Titrations

The potentiometric studies were conducted with a Titrino 702 SM autotitrator (Brinkmann Instruments). A Metrohm combined pH glass electrode (Ag/AgCl) with 3M NaCl internal filling solution was used. The NaOH solution was standardised against potassium hydrogen phthalate with phenolphthalein as indicator. The stock Zn(II) solution (0.02 M) was prepared by dissolving $Zn(NO_3)_2 \cdot 6H_2O$ (5.95 g) in deionised water and standardized using a Dowex 50W X-8 Ion Exchange Resin (20-

50 mesh) in the H^+ form (10 cm^3 of the Zn(II) solution required 3.9 cm^3 of a standardized 0.1021 M NaOH solution). Solutions were prepared using doubly deionised freshly distilled water and kept under a stream of $N_{2(g)}$. The electrode was calibrated with dilute standard acid and alkali solutions, thus defining pH = - log $[H^+]$ (pK_w = -13.78).[102] The linearity of the electrode response and carbonate contamination of the standardised NaOH solution (0.1 N) was determined by the Gran's method[102] and was found to be less than 2%. In a typical pH metric determination an aqueous solution (50 cm^3) of the ligand (1 mM) with 4 equiv. of HNO_3 in the absence (for determination of ligand protonation constants log K_n (n =1-3)) or presence of equivalent Zn^{2+} ions (for determination of K_{ZnL} and deprotonation constants of the zinc-bound water in the zinc complexes) was titrated with NaOH (0.1 N). The temperature of solutions (25 °C) in the covered, water-jacketed cell was kept constant by a Julabo circulating bath. The ionic strength (I) was adjusted to 0.1 N with $NaNO_3$. The protonation and stability constants were calculated from the titration data using the program HYPERQUAD 2000 Version 2.1 NT.[45] The data reported represents the average of at least three different titrations. About 110 points were collected for each titration.

4.6 REFERENCES

(1) (*a*) R. Krämer, *Coord. Chem. Rev.*, 1999, **182**, 243; (*b*) D. K. Garner, S. B. Fitch, L. H. McAlexander, L. M. Bezold, A. M. Arif and L. M. Berreau, *J. Am. Chem. Soc.*, 2002, **124**, 9970; (*c*) M. Wall, B. Linkletter, D. Williams, A.-M. Lebuis, R. C. Hynes and J. Chin, *J. Am. Chem. Soc.*, 1999, **121**, 4710; (*d*) F. Mancin and J. Chin, *J. Am. Chem. Soc.*, 2002, **124**, 10496; (*e*) J. Chin, S. Chung and D. H. Kim, *J. Am. Chem. Soc.*, 2002, **124**, 10498; (*f*) C. E. MacBeth, A. P. Golombek, V. G. Young Jr., C. Yang, K. Kuczera, M. P. Hendrich and A. S. Borovik, *Science*, 2000, **289**, 938; (*g*) A. Wada, M. Harata, K. Hasegawa, K. Jitsukawa, H. Masuda, M. Mukai, T. Kitagawa and H. Einaga, *Angew. Chem., Int. Ed.*, 1998, **37**, 798.

(2) J. C. Mareque Rivas, R. Torres Martín de Rosales and S. Parsons, *Dalton Trans.*, 2003, 2156.

(3) D. K. Garner, R. A. Allred, K. J. Tubbs, A. M. Arif and L. M. Berreau, *Inorg. Chem.*, 2002, **41**, 3533.

(4) L. M. Berreau, M. M. Makowska-Grzyska and A. M. Arif, *Inorg. Chem.*, 2001, **40**, 2212.

(5) K. Jitsukawa, M. Harata, H. Arii, H. Sakurai and H. Masuda, *Inorg. Chim. Acta*, 2001, **324**, 108.

(6) H. Adams, N. A. Bailey, D. E. Fenton and Q.-Y. He, *J. Chem. Soc., Dalton Trans.*, 1997, 1533.

(7) J. C. Mareque-Rivas, R. Prabaharan and S. Parsons, *Dalton Transactions*, 2004, 1648.

(8) F. H. Allen, O. Kennard, D. G. Watson, L. Brammer, A. G. Orpen and R. Taylor, *Journal of the Chemical Society, Perkin Transactions 2: Physical Organic Chemistry (1972-1999)*, 1987, S1.

(9) $[(L_3^2)Zn(Cl)](BPh_4)\cdot CH_3CN$ was synthesised in our group by L. Metteau. $[(L_2^3)Zn(Cl)](BPh_4)$ was synthesised in our group by Dr. R. Prabaharan.

(10) A. W. Addison, T. N. Rao, J. Reedijk, J. v. Rijn and G. C. Verschoor, *Dalton Trans.*, 1984, 1349.

(11) N. Suzuki, T. Higuchi, Y. Urano, K. Kikuchi, H. Uekusa, Y. Ohashi, T. Uchida, T. Kitagawa and T. Nagano, *J. Am. Chem. Soc*, 1999, **121**, 11571.

(12) N. Ueyama, N. Nishikawa, Y. Yamada, T. Okamura, S. Oka, H. Sakurai and A. Nakamura, *Inorg. Chem.*, 1998, **27**, 2415.

(13) J. C. Roder, F. Meyer, R. F. Winter and E. Kaifer, *J. Organomet. Chem.*, 2002, **641**, 113.

(14) J. W. Canary, C. S. Allen, J. M. Castagnetto, Y.-H. Chiu, P. J. Toscano and Y. Wang, *Inorg. Chem.*, 1998, **37**, 6255.

(15) J. W. Canary, C. S. Allen, J. M. Castagnetto and Y. Wang, *J. Am. Chem. Soc.*, 1995, **117**, 8484.

(16) C. S. Allen, C. L. Chuang, M. Cornebise and J. W. Canary, *Inorg. Chim. Acta*, 1995, **239**, 29.

(17) R. J. Sime, R. L. Dodge, A. Zalkin and D. H. Tempelton, *Inorg. Chem.*, 1971, **10**, 537.

(18) N. Niklas, S. Wolf, G. Liehr, C. E. Anson, A. K. Powell and R. Alsfasser, *Inorg. Chim. Acta*, 2001, **314**, 126.

(19) N. Bag, S.-S. Chern, S.-M. Peng and C. K. Chang, *Inorg. Chem.*, 1995, **34**, 753.

(20) A. Trosch and H. Vahrenkamp, *Eur. J. Inorg. Chem.*, 1998, 827.

(21) H. Kurosaki, T. Tawada, S. Kawasoe, Y. Ohashi and M. Goto, *Biorg. Med. Chem. Lett.*, 2000, **10**, 1333.

(22) R. Burth, A. Stange, M. Schafer and H. Vahrenkamp, *Eur. J. Inorg. Chem.*, 1998, 1759.

(23) B. L. Vallee and D. S. Auld, *Biochemistry*, 1990, **29**, 5647.

(24) B. L. Vallee and D. S. Auld, *Acc. Chem. Res.*, 1993, **26**, 543.

(25) D. Christianson and C. A. Fierke, *Acc. Chem. Res.*, 1996, **29**, 331.

(26) K. Zhang and D. S. Auld, *Biochemistry*, 1993, **32**, 13844.

(27) H. Sigel and R. B. Martin, *Chem. Soc. Rev.*, 1994, **23**, 83.

(28) T. Itoh, Y. Fujii, T. Tada, Y. Yoshikawa and H. Hisada, *Bull. Chem. Soc. Jpn.*, 1996, **69**, 1265.

(29) E. Kimura, T. Shiota, T. Koike, M. Shiro and M. Kodama, *J. Am. Chem. Soc.*, 1990, **112**, 5805.

(30) I. Bertini, L. C., M. Rosi, A. Sgamellotti and F. Tarantelli, *Inorg. Chem.*, 1990, **29**, 1460.

(31) M. Sola, A. Lledos, M. Duran and J. Bertran, *Inorg. Chem.*, 1991, **30**, 2523.

(32) R. Cini, D. G. Musaev, L. G. Marzilli and K. Morokuma, *THEOCHEM (J. Mol. Struct.)*, 1997, **392**, 55.

(33) M. Sakurai, T. Furuki and Y. Inoue, *J. Phys. Chem.*, 1995, **99**, 17789.

(34) M. Trachtman, G. D. Markham, J. P. Glusker, P. George and C. W. Bock, *Inorg. Chem.*, 1998, **37**, 4421.

(35) D. R. Garmer and N. Gresh, *J. Am. Chem. Soc.*, 1994, **116**, 3556.

(36) M. Peschke, A. T. Blades and P. Kebarle, *J. Am. Chem. Soc.*, 2000, **122**, 1492.

(37) J. B. Cross, J. S. Duca, J. J. Kaminski and V. S. Madison, *J. Am. Chem. Soc.*, 2002, **124**, 11004.

(38) J. H. Coates, G. J. Gentle and S. F. Lincoln, *Nature*, 1974, **249**, 773.

(39) W. N. Lipscomb and N. Sträter, *Chem. Rev.*, 1996, **96**, 2375.

(40) W. N. Lipscomb, *Ann. Rev. Biochem*, 1983, **52**, 1983.

(41) J. E. Coleman, *Ann. Rev. Biochem.*, 1992, **61**, 897.

(42) J. F. Krebs, J. A. Ippolito, D. W. Christianson and C. A. Fierke, *J. Biol. Chem. Rev.*, 1993, **268**, 27458.

(43) X. Chen, C. Tu, P. V. LoGrasso, P. J. Laipis and D. N. Silverman., *Biochemistry*, 1993, **32**, 7861.

(44) Potentiometric titrations were performed in our group by Dr. R. Prabaharan.

(45) P. Gans, A. Sabatini and A. Vacca, *Talanta*, 1996, **43**, 1739.

(46) L. J. Zompa, *Inorg. Chem.*, 1978, **17**, 2531.

(47) M. Kodama and E. Kimura, *J. Chem. Soc., Dalton Trans.*, 1977, 2269.

(48) L. M. Berreau, S. Mahapatra, J. A. Halfen, V. G. Young, Jr. and W. B. Tolman, *Inorg. Chem.*, 1996, **35**, 6339.

(49) M. Wall, B. Linkletter, D. Williams, A.-M. Lebuis, R. C. Hynes and J. Chin, *J. Am. Chem. Soc.*, 1999, **121**, 4710.

(50) T. F. C. Bergquist, M. M. Morlok and G. Parkin, *J. Am. Chem. Soc*, 2003, **125**, 6189.

(51) N. N. Murthy and K. D. Karlin, *Chem. Commun.*, 1993, **1237**.

(52) M. Ruf, K. Weis and H. Vahrenkamp, *J. Am. Chem. Soc*, 1996, **118**, 9288.

(53) D. T. Puerta and S. M. Cohen, *Inorg. Chim. Acta*, 2002, **337**, 459.

(54) O. Seneque, M.-N. Rager, M. Giorgi and O. Reinaud, *J. Am. Chem. Soc.*, 2001, **123**, 8442.

(55) Y.-H. Chiu and J. W. Canary, *Inorg. Chem.*, 2003, **42**, 5107.

(56) B. N. Trawick, A. T. Dahiner and J. K. Bashkin, *Chem. Rev.*, 1998, **98**, 939.

(57) D. Magda, M. Wright, S. Crofts, A. Lin and J. L. Sessler, *J. Am. Chem. Soc.*, 1997, **119**, 6947.

(58) E. L. Hegg and J. N. Burstyn, *Coord. Chem. Rev.*, 1998, **173**, 133.

(59) P. D. Beer and P. A. Gale, *Angew. Chem. Int. Ed.*, 2001, **40**, 486.

(60) P. D. Beer, *Acc. Chem. Res.*, 1998, **31**, 71.

(61) B. M. Sefton and T. Hunter, '*Protein Phosphorylation*', Academic Press, New York, 1998.

(62) L. N. Johnson and R. J. Lewis, *Chem. Rev.*, 2001, **101**, 2209.

(63) H. Lueke and F. A. Quiocho, *Nature*, 1990, **347**, 402.

(64) J. J. He and F. A. Quiocho, *Science*, 1991, **251**, 1497.

(65) V. Jubian, A. Veronese, R. P. Dixon and A. D. Hamilton, *Angew. Chem., Int. Ed. Engl.*, 1995, **34**, 1237.

(66) J. O. Magrans, A. R. Ortiz, A. Mollins, P. H. P. Lebouille, J. Sánchez-Quesada, P. Prados, M. Pons, F. Gago and J. d. Mendoza, *Angew. Chem., Int. Ed. Engl.*, 1996, **35**, 1712.

(67) P. A. Gale, J. L. Sessler, V. Král and V. Lynch, *J. Am. Chem. Soc.*, 1996, **118**, 5140.

(68) D. M. Perreault, L. A. Cabell and E. V. Anslyn, *Bioorg. Med. Chem.*, 1997, **5**, 1209.

(69) J. P. Anzenbacher, A. C. Try, H. Miyaji, K. Jursikova, V. M. Lynch, M. Marquez and J. L. Sessler, *J. Am. Chem. Soc.*, 2000, **122**, 10268.

(70) F. P. Schmidtchen and M. Berger, *Chem. Rev.*, 1997, **97**, 1609.

(71) M. W. Hosseini, A. J. Blacker and J.-M. Lehn, *J. Am. Chem. Soc.*, 1990, **112**, 3896.

(72) D. A. Bell and E. V. Anslyn, '*Comprehensive Supramolecular Chemistry. Hydrogen-bonding Receptors: Open-chain Catalytic Systems*', Pergamon, New York, 1996.

(73) E. Kimura, *Top. Curr. Chem.*, 1985, **128**, 113.

(74) B. Dietrich, *Pure Appl. Chem.*, 1993, **65**, 1457.

(75) C. Bazzicalupi, A. Bencini, A. Bianchi, M. Cecchi, B. Escuder, V. Fusi, E. García-España, C. Giorgi, S. V. Luis, G. Maccagni, V. Marcelino, P. Paoletti and B. Valtancoli, *J. Am. Chem. Soc.*, 1999, **121**, 6807.

(76) P. D. Beer, J. Cadman, J. M. Lloris, R. Martinez-Manez, J. Soto, T. Pardo and M. D. Marcos, *J. Chem. Soc., Dalton Trans.*, 2000, 1805.

(77) B. Dieterich, D. L. Fyles, T. M. Fyles and J. M. Lehn, *Helv. Chim. Acta*, 1979, **62**, 2763.

(78) J. B. Cooper, M. G. B. Drew and P. D. Beer, *Dalton Trans.*, 2000, 2721.

(79) P. D. Beer and J. Cadman, *New J. Chem.*, 1999, **23**, 347.

(80) J. L. Sessler, J. M. Davis, V. Král, T. Kimbrough and V. Lynch, *Org. Biomol. Chem.*, 2003, **1**, 4113.

(81) A. Ojida, Y. Mito-oka, M. Inoue and I. Hamachi, *J. Am. Chem. Soc*, 2002, **124**, 6256.

(82) E. Kimura, S. Aoki, T. Koike and M. Shiro, *J. Am. Chem. Soc.*, 1997, **119**, 3068.

(83) A. V. Koulov, K. A. Stucker, C. Lakshmi, J. P. Robinson and B. D. Smith, *Cell Death and Diff.*, 2003, **10**, 1357.

(84) S. L. Tobey, B. D. Jones and E. V. Anslyn, *J. Am. Chem. Soc.*, 2003, **125**, 4026.

(85) J. Chin, S. Chung and D. H. Kim, *J. Am. Chem. Soc.*, 2002, **124**, 10948.

(86) E. Kövári and R. Krämer, *J. Am. Chem. Soc.*, 1996, **118**, 12704.

(87) H. Aït-Haddou, J. Sumaoka, S. L. Wiskur, J. F. Folmer-Andersen and E. V. Anslyn, *Angew. Chem. Int. Ed.*, 2002, **41**, 4014.

(88) H. Adams, N. A. Bailey, D. E. Fenton and Q.-Y. He, *J. Chem. Soc., Dalton Trans.*, 1995, 697.

(89) G. Anderegg and F. Wenk, *Helv. Chim. Acta*, 1967, **50**, 2330.

(90) Hikichi, M. Tanaka, Y. Moro-oka and N. Kitajima, *Chem. Commun.*, 1992, 814.

(91) C. Bazzicalupi, A. Bencini, A. Bianchi, V. Fusi, C. Giorgi, P. Paoletti, B. Valtancoli and D. Zanchi, *Inorg. Chem.*, 1997, **36**, 2784.

(92) S. Aoki, K. Iwaida, N. Hanamoto, M. Shiro and E. Kimura, *J. Am. Chem. Soc.*, 2002, **124**, 5257.

(93) (*a*) P. Gans, *HYPNMR 2000* (University of Leeds, Leeds, U.K.), 2000; (*b*) C. Frassineti, S. Ghelli, P. Gans, A. Sabatini, M. S. Moruzzi and A. Vacca, *Anal. Biochem.*, 1995, **231**, 374

(94) J. C. Mareque-Rivas, R. Prabaharan and R. Torres Martin de Rosales, *Chem. Commun.*, 2004, 76.

(95) The pK_a of the water molecule in the complex $[(THB)Zn(OH_2)]^{2+}$ using the tripodal pseudopeptide N3 ligand (THB) was determined to be 6.2; Gelinsky, M.; Vogler, R.; Vahrenkamp, H. *Inorg. Chem.* 2002, **41**, 2560.

(96) W. L. F. Armarego and D. D. Perrin, '*Purification of Laboratory Chemicals*', Butterworth-Heinemann, Oxford, 1997.

(97) P. K. Glasoe and F. A. Long, *J. Phys. Chem.*, 1960, **64**, 188.

(98) G. M. Sheldrick, '*SHELXTL 97*', University of Göttingen, 1997.

(99) G. M. Sheldrick, '*SADABS, Empirical absorption correction program*', University of Göttingen, 1995, based upon the method of Blessing.

(100) R. H. Blessing, *Acta Crystallogr., Sect. A*, 1995, **51**, 33.

(101) A. L. Spek, *Acta Crystallogr., Sect. A.*, 1990, **46**, C34.

(102) A. E. Martell and R. J. Motekaitis, '*Determination and Use of Stability Constants*', VCH-Publishing, 1992.

APPENDIX

A.1 Chapter 2: VT NMR Studies of [(L_1^1)Zn(Cl)](BPh_4)

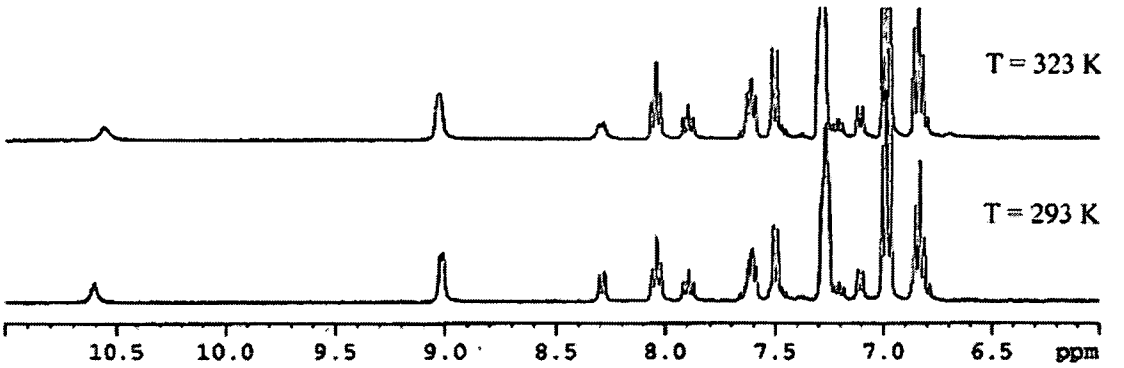

Fig. A1.1 Aromatic and NH region of the ^{1}H NMR spectra (360.1 MHz, CD_3CN) of [($\mathbf{L_1}^1$)Zn(Cl)](BPh_4) at 323 K (*top*) and 293 K (*bottom*).

A.2 Chapter 3: Cambridge Structural Database Search

Evidence of various types of O-H···C and N-H···C hydrogen bonding in crystalline alkynes, alkenes and aromatics has been reported elsewhere.[1] In this report the generality of only very short N-H···π (phenyl, centroid type) hydrogen bonds was investigated searching the 5.24 (November 2002) version of the Cambridge Structural Database (CSD). Only error-free, non-disordered structures with R < 0.1 were accepted. The N-H distance was normalised to 1.01 Å and the H···X (X = centroid of a phenyl ring) distance was specified to lay between 0 and 3 Å and the N-H···X angle to be calculated. A total of 41 structures satisfied our arbitrary criteria of very short NH···X hydrogen bond, H···X < 2.3 Å (Table A1.1). These crystal structures were scrutinised and separated into organic (27 structures) and inorganic (14 structures).

The focus of this search was on investigating what causes very short external N-H···π (phenyl, centroid type) hydrogen bonding in metal complexes compared to organic compounds. Thus, in organic compounds this structural feature is most commonly found (24 of 27 cases) when a R_3N-H^+ group is the hydrogen bond donor. By contrast, in metal complexes the majority (8 of 14) of short N-H···π (phenyl, centroid type) hydrogen bonds involved a RNH_2-M fragment as the H-bond donor (M = strongly Lewis acidic metal).

See Chapter 3 for interpretation of this CSD search. Histograms for the H···X distances (X = centroid of the phenyl ring) are given below (Figs. A2.1 and A2.2).

References:

(1) M. A. Viswamitra, R. Radhakrisham, J. Bandekar and G. R. Desiraju, *J. Am. Chem. Soc.*, 1993, **115**, 4868.

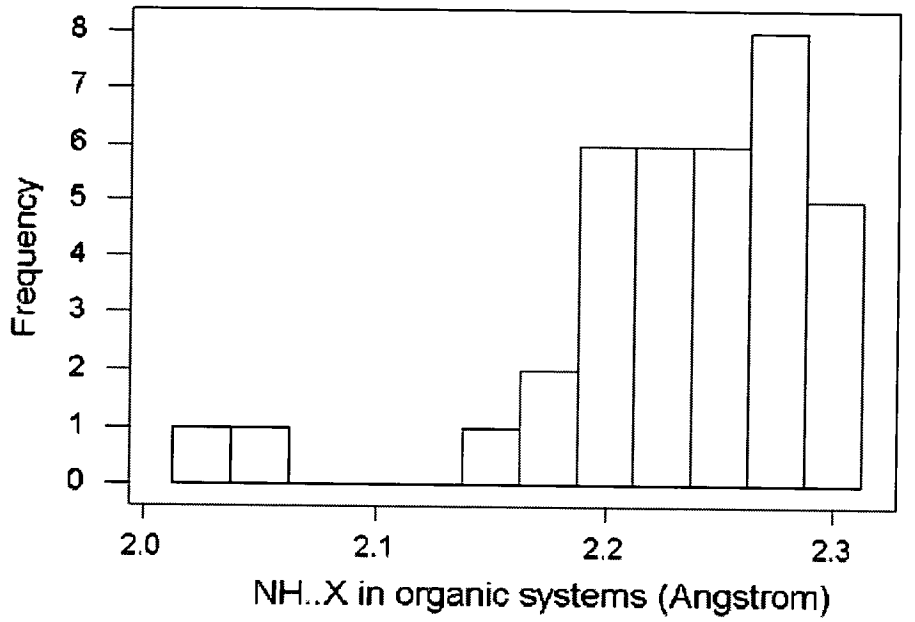

Fig. A2.1 Histogram of the H···X (X = centroid of a phenyl ring) distances found for very short N-H···X (X = centroid of a phenyl ring) H-bonds in organic systems.

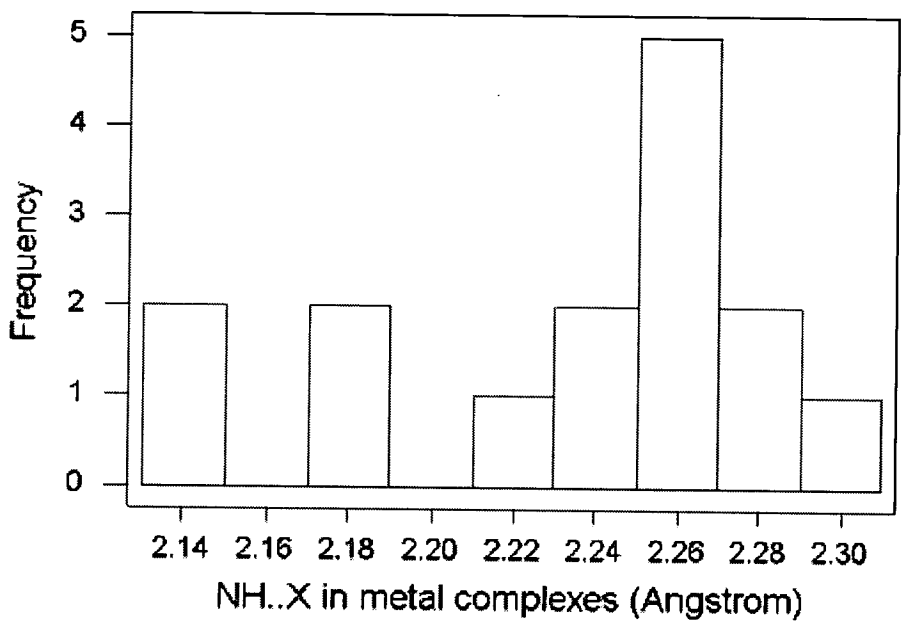

Fig. A2.2 Histogram of the H···X (X = centroid of a phenyl ring) distances found for very short N-H···X (X = centroid of a phenyl ring) H-bonds in metal complexes.

Table A2.1 Refcodes, distances and angles of (i) organic and (ii) inorganic crystal structures with very short N-H···X (X = centroid of a phenyl ring) H-bonds found searching the CSD (5.24 version).

(i)

	N-H···X/°	H···X/Å
ACINUV	165.308	2.233
ACIPOR	169.383	2.237
AMPHEB	141.292	2.181
AMPHEB01	140.994	2.198
AMPHEB02	174.041	2.022
AMPHEB03	171.391	2.046
BUWCAX	153.865	2.251
BUWCAX	154.217	2.273
CAVFOU	166.331	2.292
FIZWOA01	162.169	2.196
GOLDUG	162.694	2.276
GOLDUG	150.285	2.293
HENCIM	157.009	2.295
HENCUY	151.727	2.284
HENDAF	167.954	2.178
HENDIN	170.383	2.212
HENDOT	142.972	2.219
HENDUZ	164.189	2.280
HENFAH	172.703	2.254
HENFAH	149.028	2.251
HENFUB	137.581	2.271
HENGEM	151.859	2.218
HENGEM	158.245	2.142
HENGEM	152.755	2.229
KOVSIX	169.060	2.246
QIJXUC	173.649	2.271
ROHTIR	161.796	2.266
ROHTIR	154.316	2.212
ROHTIR	151.102	2.252
SUVHAS	171.859	2.200
ZOJFOT	166.206	2.197
QEWSEQ	159.518	2.299
SUQLOF	154.141	2.290
SUQLOF	156.504	2.282
SUQLOF	155.414	2.229
SUQLUL	172.268	2.238

(ii)

	N-H···X/°	H···X/Å
DANKEI	169.761	2.266
GEBHIE	160.004	2.173
KOZCAD	148.189	2.286
NEBHUX	137.270	2.296
NOCNEY	163.167	2.184
NOKBAQ	151.258	2.238
RELSOQ	149.619	2.218
REQTEM	167.109	2.230
SIBNAS	146.977	2.281
WODCEX	157.050	2.257
XIHSIQ	161.719	2.262
XIHSIQ	167.235	2.145
YBAENI	169.550	2.264
ZAXBOP	147.054	2.139
ZTANPB	166.595	2.258

A.3 Chapter 3: VT NMR Coalescence Studies and Concentration Experiments

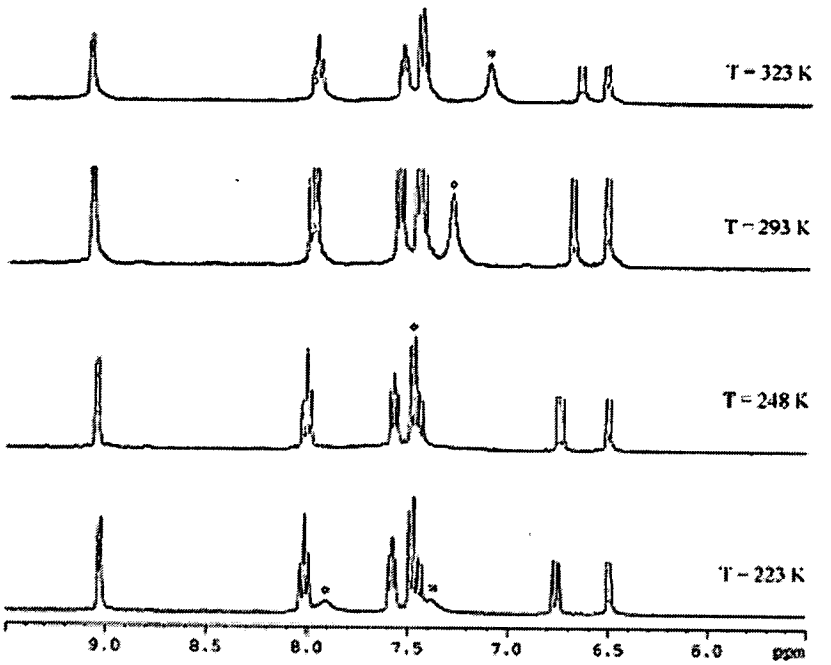

Fig. A3.1 ^{1}H VT NMR of $[(L_1^2)Zn(Cl)](Cl)$ in CD_3CN (28 mM) showing aromatic and NH_2 (*) resonances. See Table 3.5 and compare with Figs. 3.4, A3.2-A3.7.

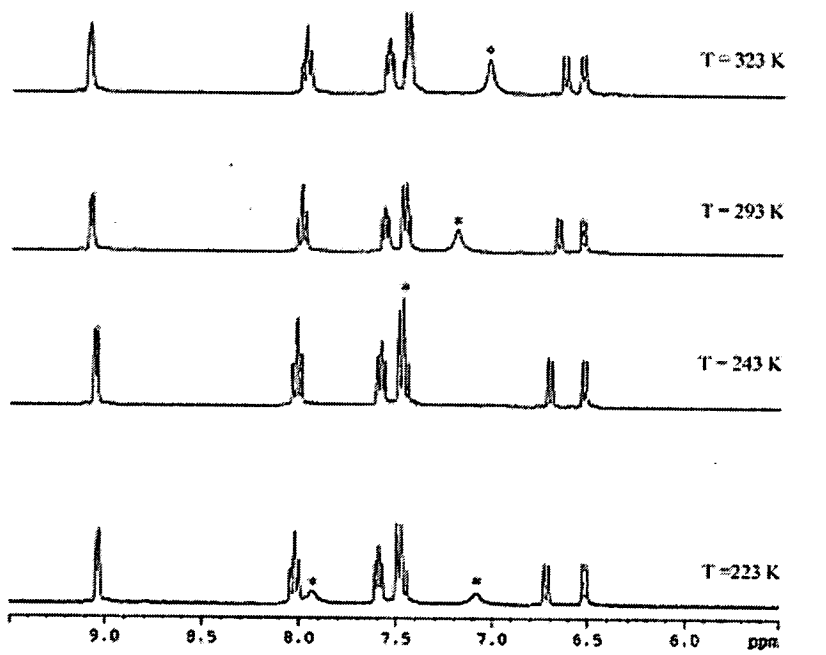

Fig. A3.2 ^{1}H VT NMR of $[(L_1^2)Zn(Cl)](Cl)$ in CD_3CN (14 mM) showing aromatic and NH_2 (*) resonances. See Table 3.5 and compare with Figs. 3.4, A3.1-A3.7.

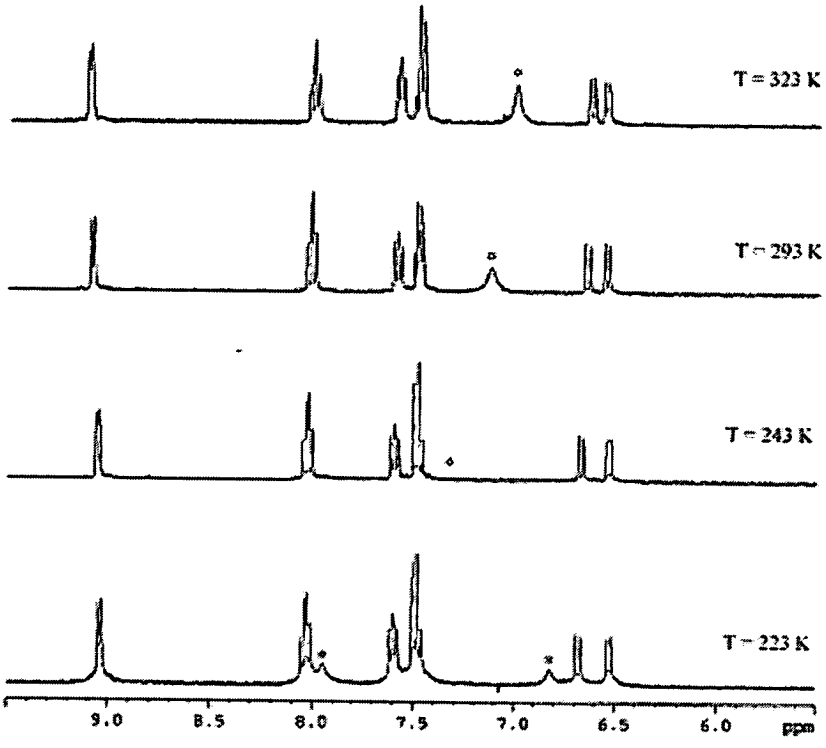

Fig. A3.3 ^{1}H VT NMR of $[(L_1{}^2)Zn(Cl)](Cl)$ in CD_3CN (7 mM) showing aromatic and NH_2 (*) resonances. See Table 3.5 and compare with Figs. 3.4, A3.1-A3.7.

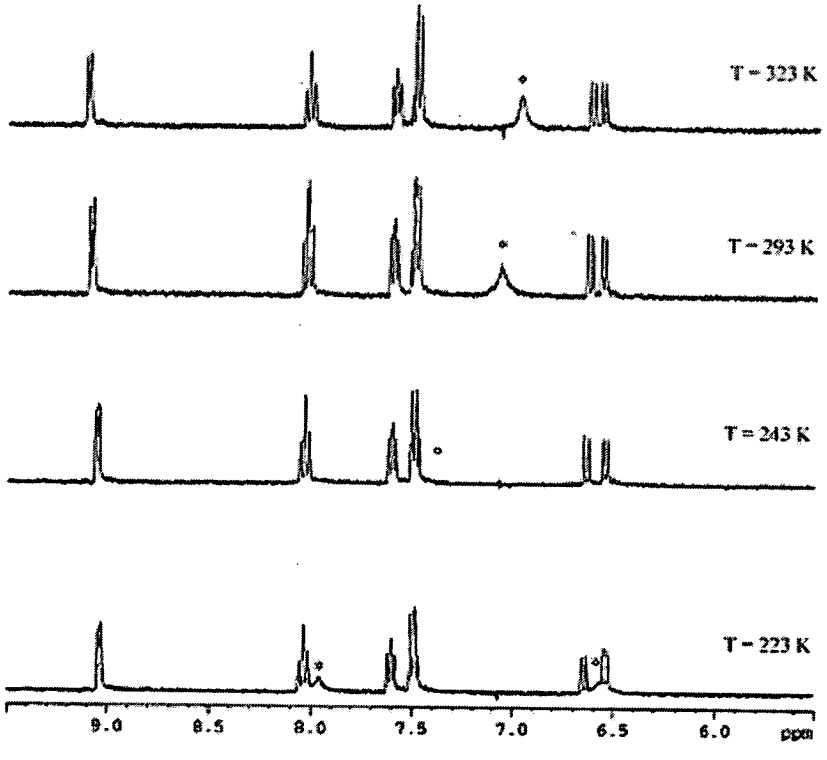

Fig. A3.4 ^{1}H VT NMR of $[(L_1{}^2)Zn(Cl)](Cl)$ in CD_3CN (3.5 mM) showing aromatic and NH_2 (*) resonances. See Table 3.5 and compare with Figs. 3.4, A3.1-A3.7.

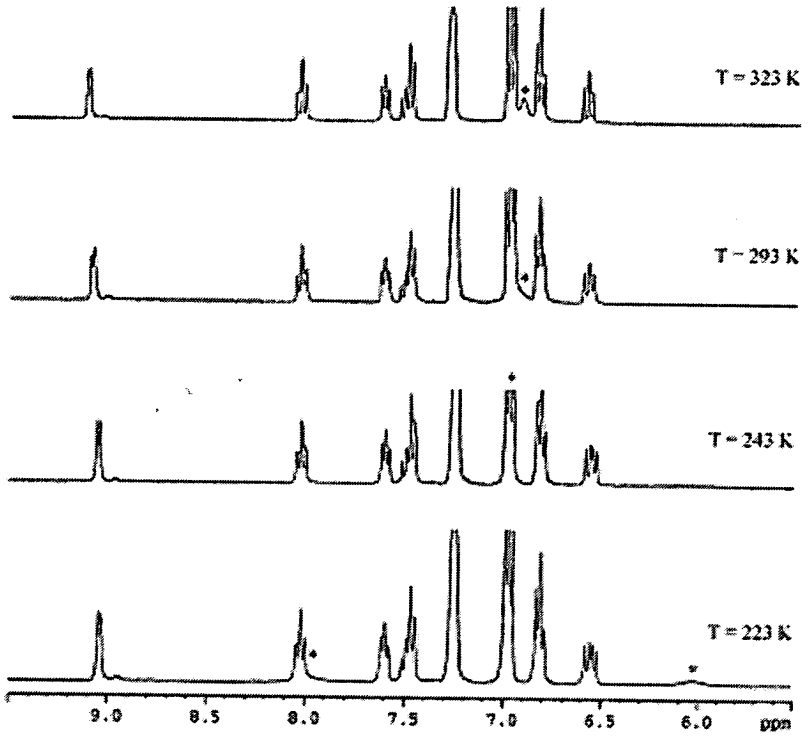

Fig. A3.5 ^{1}H VT NMR of $[(\mathbf{L_1}^2)Zn(Cl)](BPh_4)$ in CD_3CN (28 mM) showing aromatic and NH_2 (*) resonances. See Table 3.5 and compare with Figs. 3.4, A3.1-A3.7.

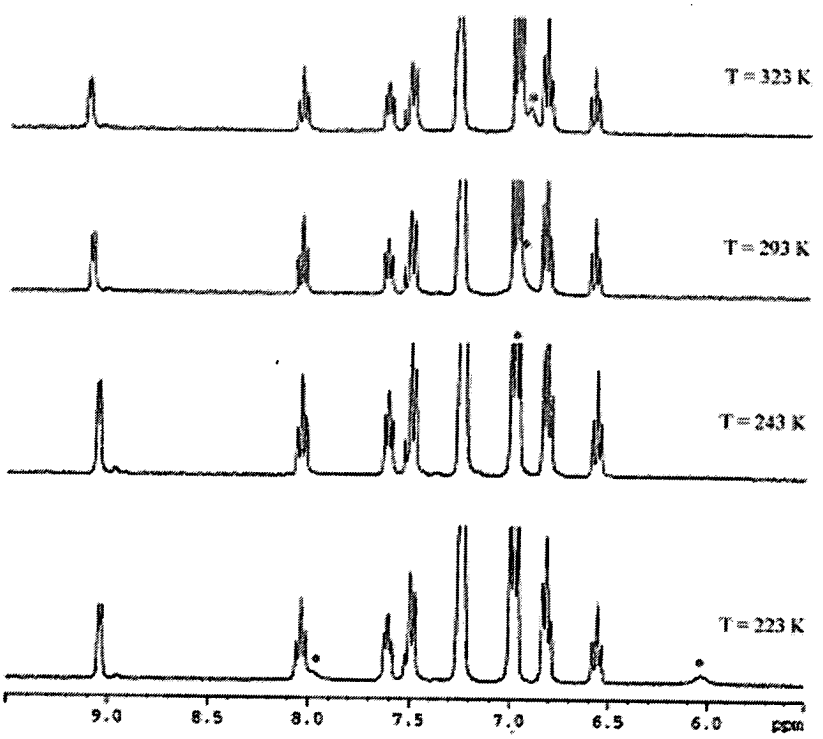

Fig. A3.6 1H VT NMR of $[(\mathbf{L_1}^2)Zn(Cl)](BPh_4)$ in CD_3CN (7 mM) showing aromatic and NH_2 (*) resonances. See Table 3.5 and compare with Figs. 3.4, A3.1-A3.7.

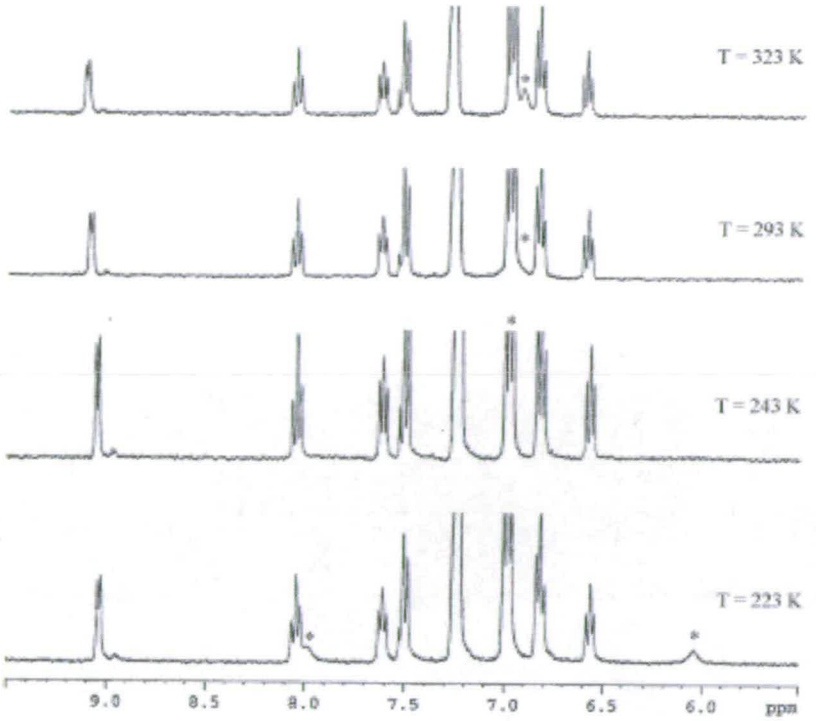

Fig. A3.7 ^{1}H VT NMR of [($\mathbf{L_1}^2$)Zn(Cl)](BPh$_4$) in CD$_3$CN (1.8 mM) showing aromatic and NH$_2$ (*) resonances. See Table 3.5 and compare with Figs. 3.4, A3.1-A3.6.

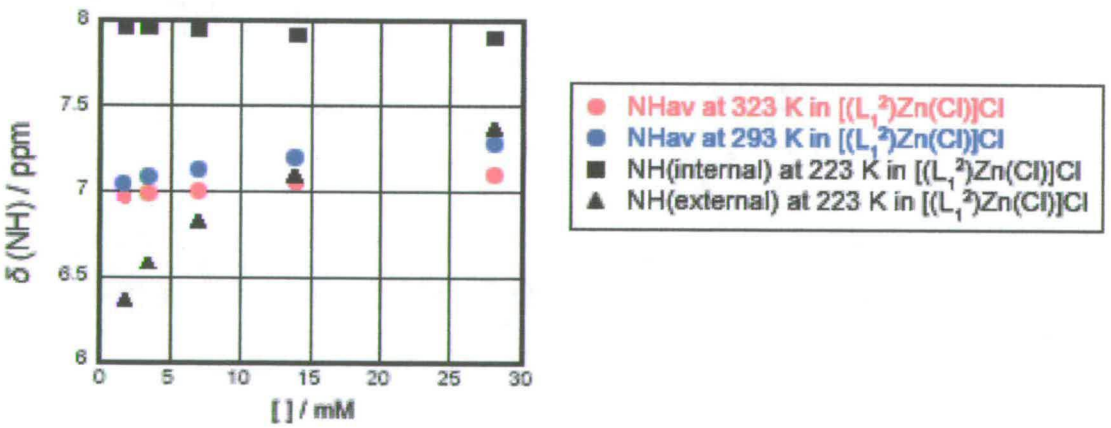

Fig. A3.8 Temperature and concentration dependency of the NH$_2$ chemical shift in the ^{1}H NMR spectra of [($\mathbf{L_1}^2$)Zn(Cl)](Cl). See Table 3.5 and compare with Fig. A3.9.

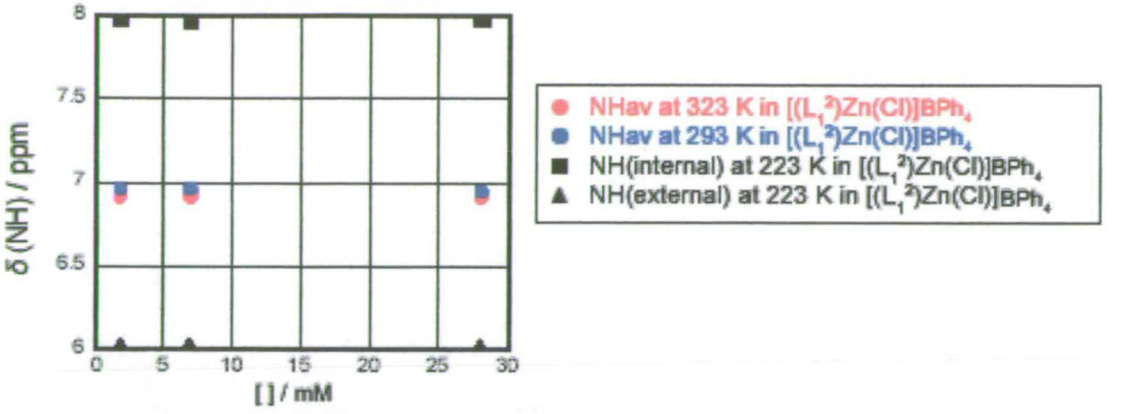

Fig. A3.9 Temperature and concentration dependency of the NH_2 chemical shift in the ^{1}H NMR spectra of [($\mathbf{L_1}^2$)Zn(Cl)](BPh$_4$). See Table 3.5 and compare with Fig A3.8.

A.4 Chapter 4: ^{1}H NMR Comparisons of [(L)Zn(OH$_2$)](NO$_3$)$_2$ and [(L)Zn(Cl)](Cl) complexes

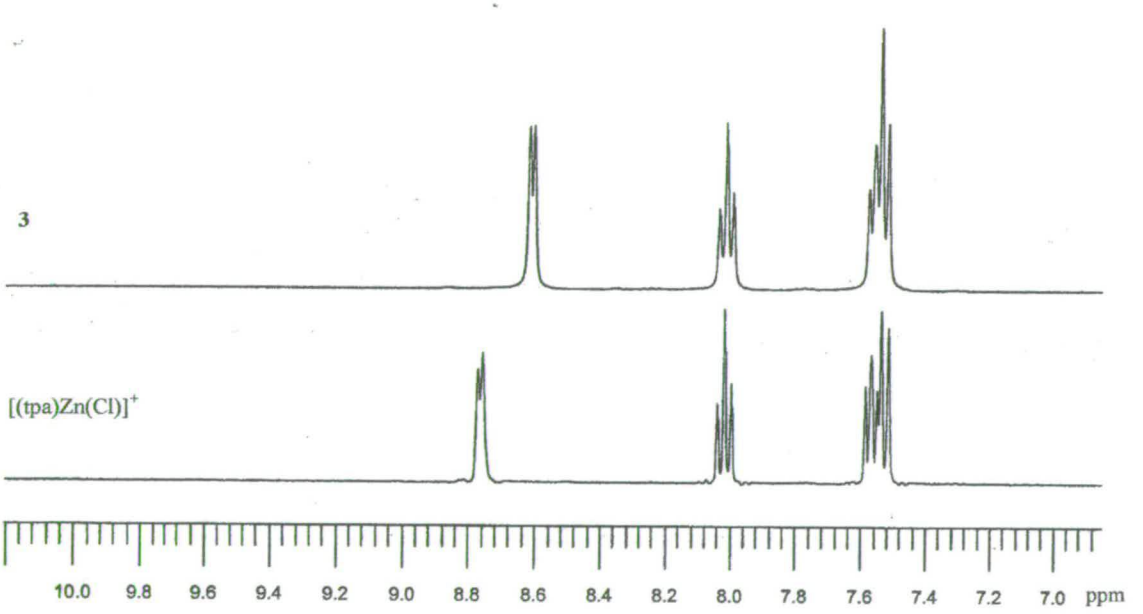

Fig. A4.1 Aromatic region of the ^{1}H NMR spectrum (360.1 MHz, D_2O, 293K) of **3** (*top*) and [(**tpa**)Zn(Cl)](Cl) (*bottom*).

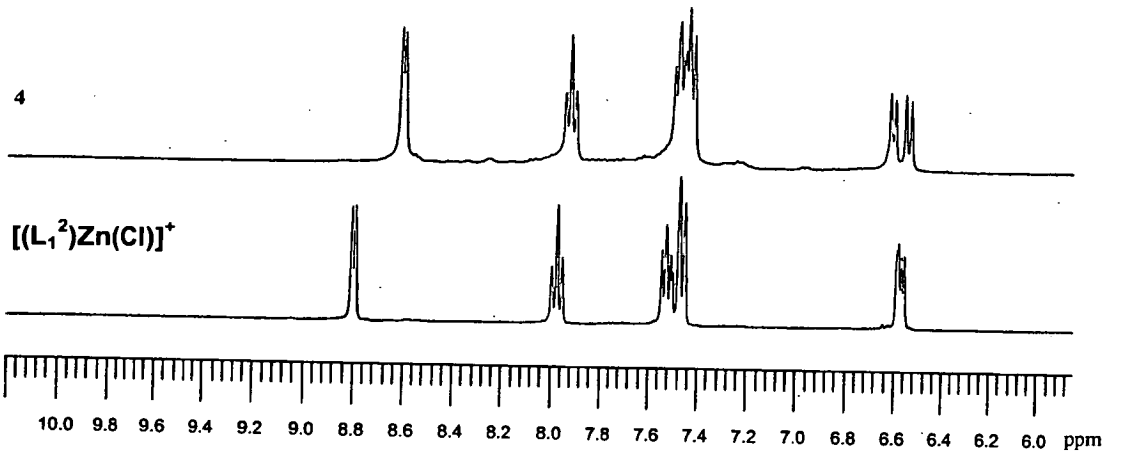

Fig. A4.2 Aromatic region of the ^{1}H NMR spectrum (360.1 MHz, D_2O, 293K) of **4** (*top*) and [($\mathbf{L_1}^2$)Zn(Cl)](Cl) (*bottom*).

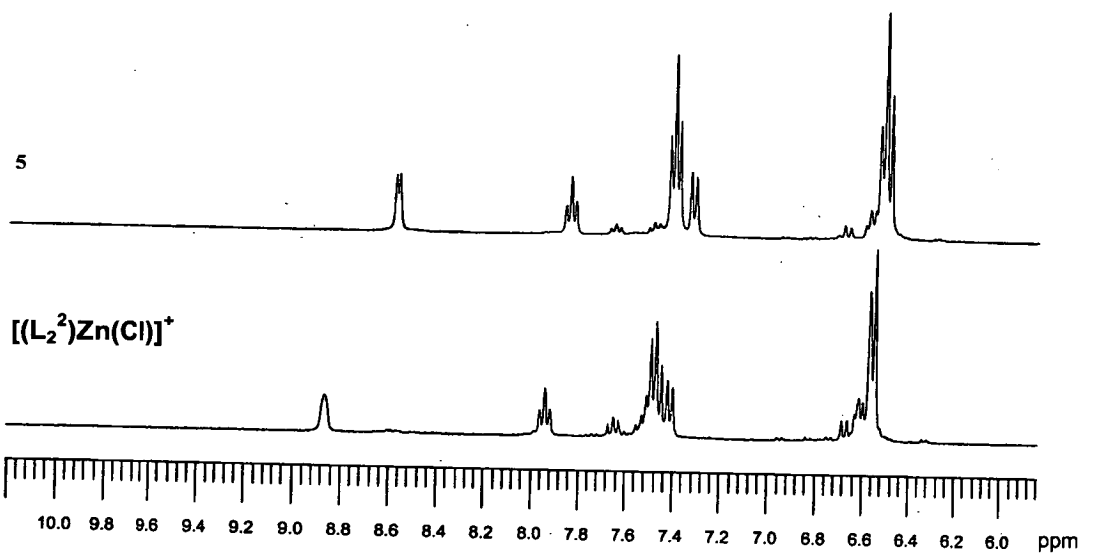

Fig. A4.3 Aromatic region of the ^{1}H NMR spectrum (360.1 MHz, D_2O, 293K) of **5** (*top*) and [($\mathbf{L_2}^2$)Zn(Cl)](Cl) (*bottom*).

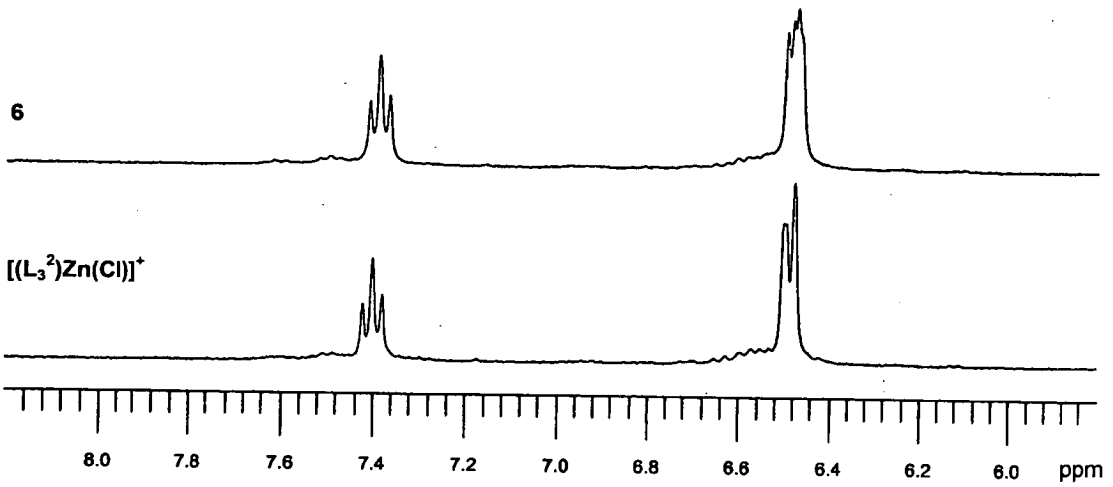

Fig. A4.4 Aromatic region of the ^{1}H NMR spectrum (360.1 MHz, D_2O, 293K) of **6** (*top*) and [($\mathbf{L_3}^2$)Zn(Cl)](Cl) (*bottom*).

Courses attended:

1. Weekly *Inorganic Section Seminars* during terms 2001-2004.
2. Weekly *School of Chemistry Colloquia* during terms 2001-2004.
3. *Induction Course for Laboratory Demonstrators in Chemistry*, Centre for Teaching, Learning and assessment, University of Edinburgh, October 2001.
4. *Postgraduate Course on X-Ray crystallography* by Dr. S. Parsons, School of Chemistry, University of Edinburgh, 19 November-10 December, 2001.
5. *Scientific Paper Production* by Prof. Bill Earnshaw (Institute of Cell & Molecular Biology), Transferable Skills Programme, University of Edinburgh. 8 May 2002.
6. *Transition Metal Chemistry I and II* by Dr. N. Robertson, undergraduate course, School of Chemistry, University of Edinburgh, 2002.
7. *Reaction Kinetics* by Dr. A.C Jones, undergraduate course, School of Chemistry, University of Edinburgh, 2002.
8. *Postgraduate Course on Nuclear Magnetic Resonance: Liquid and Solid State NMR Spectroscopy in Drug Discovery and Development*, School of Chemistry, University of Edinburgh, 19-20 March, 2003.

Publications

(1) J. C. Mareque Rivas, R. Prabaharan, R. Torres Martin de Rosales, L. Metteau and S. Parsons, LZnX complexes of tripodal ligands with intramolecular RN-H hydrogen bonding groups: structural implications of a hydrogen bonding cavity, and of X/R in the hydrogen bonding geometry/strength, *J. Chem. Soc., Dalton Trans.*, 2004, 2800-2807.

(2) J. C. Mareque-Rivas, R. Torres Martin de Rosales and S. Parsons, The affinity of phosphates to zinc(II) complexes can be increased with hydrogen bond donors, *Chem. Commun.*, 2004, 610-611.

(3) J. C. Mareque-Rivas, R. Prabaharan and R. Torres Martin de Rosales, Relative importance of hydrogen bonding and coordinating groups in modulating the zinc water acidity, *Chem. Commun.*, 2004, 76-77.

(4) J. C. Mareque Rivas, E. Salvagni, R. Prabaharan, R. Torres Martin de Rosales and S. Parsons, Zinc(II) complexes with intramolecular amide oxygen coordination as models of metalloamidases, *J. Chem. Soc., Dalton Trans.*, 2004, 172-177.

(5) J. C. Mareque Rivas, R. Torres Martin de Rosales and S. Parsons, Structural characterization of a dizinc(II) complex with bridging η^2-phosphate diesters and internal N-H···O-P hydrogen bonding, *J. Chem. Soc., Dalton Trans.*, 2003, 4385-4386.

(6) J. C. Mareque Rivas, E. Salvagni, R. Torres Martin de Rosales and S. Parsons, Internal hydrogen bonding in tetrahedral and trigonal bipyramidal zinc(II) complexes of pyridine-based ligands, *J. Chem. Soc., Dalton Trans.*, 2003, 3339-3349.

(7) J. C. Mareque Rivas, R. Torres Martin de Rosales and S. Parsons, Internal hydrogen bonding and amide co-ordination in zinc(II) complexes of a tripodal N4

ligand: structural, spectroscopic and reactivity studies, *J. Chem. Soc., Dalton Trans.*, 2003, 2156-2163.

Future Work

The acidity of a metal-bound water molecule is a key parameter of metallonucleases, as is the affinity of the scissile phosphate ester for the metal site.

This thesis work shows that amino hydrogen bonding groups adjacent to a zinc(II)-bound water molecule enhance the acidity of this water molecule as much as 1 pK_a unit per hydrogen bonding group. This study also shows that hydrogen bonding can increase the affinity of phosphates to zinc(II) centres in neutral aqueous solution. Considering these two important results, it is reasonable to suggest that the suitable positioning of hydrogen bonding groups local to a zinc(II) centre could emerge as a novel tactic for the generation of more effective synthetic nucleases.

Thus, a natural continuation of this work could be:

1) To carry out functional studies on the complexes prepared in this thesis work, and others providing different hydrogen bonding capabilities such as alkyl and aryl amines, guanidines and thioureas.

2) Considering that in general polymetallic complexes constitute more effective synthetic nucleases than the related mononuclear complexes, it should be interesting to investigate the effect of hydrogen bonding environments in polynuclear metal complexes.

Some of this work is already underway in this laboratory, and it should provide importance additional insights into the functional significance of hydrogen bonding groups in metallonucleaases, and the functional elements required for catalysing effectively the hydrolysis of phosphate ester with synthetic metallonucleases for applications in biotechnology.